

**ELECTROSPINNING OF CYCLODEXTRIN  
FUNCTIONALIZED NANOFIBERS AND THEIR  
APPLICATIONS**

A DISSERTATION SUBMITTED TO  
THE GRADUATE SCHOOL OF ENGINEERING AND SCIENCE  
OF BILKENT UNIVERSITY  
IN PARTIAL FULFILLMENT OF THE REQUIREMENTS FOR  
THE DEGREE OF  
DOCTOR OF PHILOSOPHY  
IN  
MATERIALS SCIENCE AND NANOTECHNOLOGY

By  
Zeynep Aytaç  
August 2016

ELECTROSPINNING OF CYCLODEXTRIN FUNCTIONALIZED  
NANOFIBERS AND THEIR APPLICATIONS

By Zeynep Aytaç

August 2016

We certify that we have read this dissertation and that in our opinion it is fully adequate, in scope and in quality, as a dissertation for the degree of Doctor of Philosophy.

---

Tamer Uyar (Advisor)

---

Hilal Türkođlu Şaşmazel

---

Engin Durgun

---

Gülüm Şumnu

---

Urartu Özgür Şafak Şeker

Approved for the Graduate School of Engineering and Science

---

Levent Onural

Director of the Graduate School

# ABSTRACT

## ELECTROSPINNING OF CYCLODEXTRIN FUNCTIONALIZED NANOFIBERS AND THEIR APPLICATIONS

Zeynep Aytaç

Ph.D. in Materials Science and Nanotechnology

Advisor: Tamer Uyar

August, 2016

Electrospinning is a widely used versatile method to produce nanofibers with high surface to volume ratio and porous structure. Owing to the unique properties, electrospun nanofibers are of great importance as a carrier matrix for drugs; antioxidant, and antibacterial agents, flavour/fragrances. Though polymers are material of choice for producing electrospun nanofibers, it is likely to obtain nanofibers from low molecular weight molecules. Cyclodextrin (CDs) are intriguing molecules having the capability of forming inclusion complex (IC) with numerous guest molecules such as drugs, food additives, flavour/fragrances, antioxidant and antibacterial agents. Therefore, CD-ICs enhance solubility, reduce volatility, and provide controlled release of the guest molecules. Integrating CD-ICs with electrospinning opens a new door to produce remarkable materials.

In this thesis, nanofibers containing CD-ICs of bioactive agents including antioxidant/antibacterial and flavour/fragrance molecules were produced via electrospinning technique. Firstly, CD-ICs of antioxidant/antibacterial compounds (gallic acid,  $\alpha$ -tocopherol, quercetin, and thymol) were synthesized and then, added into polylactic acid or zein solutions to produce CD-IC incorporated electrospun polymeric nanofibers. Afterwards, the release behavior, antioxidant and antibacterial activity of these nanofibers were

investigated. In addition, the potential use of these nanofibers as active food packaging and delivery material was revealed by packing meat samples by these nanofibers. Secondly, electrospun nanofibers were developed as a releasing material from CD-ICs of volatile flavour/fragrance molecules (geraniol, limonene, and linalool) without using polymeric matrix. The preservation of volatile compounds is shown to be possible to a great extent with antibacterial CD-IC nanofibers. Furthermore, the shelf life of flavour/fragrance molecules has been enhanced at least 50 days by CD-IC nanofibers. Finally, for the first time in the literature core-shell nanofibers were designed by using CD-IC of curcumin, an antioxidant molecule and polylactic acid solutions as core and shell, respectively. The ability of core-shell nanofibers as a drug delivery carrier was suggested by release and antioxidant activity tests. To conclude, CD-IC incorporated electrospun nanofibers produced by three different approach is shown to be used as efficient material for various applications particularly for food packaging and drug delivery.

*Keywords:* electrospinning, nanofiber, polylactic acid, zein, core-shell nanofibers, cyclodextrin, inclusion complex, antioxidant, antibacterial, flavour/fragrance, food packaging, drug delivery.

# ÖZET

## ELEKTROEĞİRME YÖNTEMİ İLE ÜRETİLEN SİKLODEKSTRİN FONKSİYONLU NANOLİFLER VE UYGULAMA ALANLARI

Zeynep Aytaç

Malzeme Bilimi ve Nanoteknoloji Programı, Doktora

Tez Danışmanı: Tamer Uyar

Ağustos, 2016

Elektroeğirme, yüksek yüzey alanına ve gözenekli yapıya sahip nanoliflerin üretimi için sıklıkla kullanılan verimli bir metottur. Bu teknik ile üretilen nanolifler eşsiz özellikleri nedeniyle ilaç; antioksidan ve antibakteriyel maddeler, tat/koku maddeleri için taşıyıcı matriks olarak büyük önem taşımaktadırlar. Bu metotla nanolif üretmek için genellikle polimerler kullanılsa da, polimerik olmayan moleküllerden de nanolifler üretilmektedir. Siklodekstrinler (CD'ler) ilaç, gıda katkı maddeleri, tat/koku maddeleri, antioksidan ve antibakteriyel maddeler gibi pek çok molekül ile inklüzyon kompleksi (IC) yapabilme özelliğine sahiptir. Dolayısıyla, CD-IC'ler bu moleküllerin çözünürlüklerinin artırılması, uçuculuklarının azaltılması ve kontrollü salımlarının sağlanması için kullanılmaktadır. CD-IC'lerin elektroeğirme tekniği ile birleştirilmesi dikkat çekici malzemelerin üretilmesinde yeni bir yol açmıştır.

Bu tez çalışması kapsamında, antioksidan/antibakteriyel ve tat/koku maddeler gibi bioaktif maddelerin CD-IC'lerini içeren nanolifler elektroeğirme tekniği ile üretilmiştir. İlk olarak, antioksidan/antibakteriyel moleküllerin (gallik asit,  $\alpha$ -tokoferol, kuersetin, timol) CD'ler ile IC'leri sentezlenmiştir. Daha sonra bu CD-IC'ler polilaktik asit ve zein solüsyonlarına eklenerek CD-IC'leri içeren

polimerik nanolifler elektroęirme yöntemi ile elde edilmiştir. Bu nanoliflerin salım davranışları, antioksidan ve antibakteriyel aktiviteleri de araştırılmıştır. Buna ek olarak, üretilen nanoliflerin aktif gıda paketleme ve ilaç salım malzemesi olarak kullanım potansiyeli, nanolifleri et örneklerine sararak yapılan testlerle gösterilmiştir. Bir sonraki aşamada; geraniyol, limonen, linalool gibi uçucu olan tat/koku moleküllerinin CD-IC'lerinden polimer kullanılmadan elektroęirme metodu ile nanolifler geliştirilmiştir. Oldukça uçucu bir yapıya sahip olan bu moleküllerin, korunmaları CD-IC nanolifleri ile büyük oranda sağlanmıştır. Ayrıca, tat/koku moleküllerinin raf ömrü en azından 50 güne kadar geliştirilmiştir. Daha sonraki çalışmamızda, antioksidan bir molekülün (kurkumin) CD-IC solüsyonu ve polilaktik asit solüsyonlarının sırasıyla çekirdek ve kabuk olarak kullanıldığı çekirdek-kabuk nanolifleri de elektroęirme teknięi yardımıyla ilk defa elde edilmiştir. Bu nanoliflerin ilaç taşıyıcı sistemlerdeki potansiyeli salım ve antioksidan aktivite testleri ile gösterilmiştir. Sonuç olarak, CD-IC'lerin katıldığı ve elektroęirme metodu kullanılarak üç farklı yaklaşımla üretilen nanoliflerin gıda paketlemesi ve ilaç salım sistemleri başta olmak üzere pek çok alanda uygulanabilecek etkili malzemeler oldukları gösterilmiştir.

*Anahtar kelimeler:* elektroęirme, nanolif, polilaktik asit, zein, öz-kabuk nanolifleri, siklodekstrin, inklüzyon kompleks, antioksidan, antibakteriyel, esans, tat/koku maddeleri, gıda paketlemesi, ilaç salımı.

## ACKNOWLEDGEMENTS

Firstly, I would like to express my deepest gratitude to my supervisor Prof. Tamer Uyar for his knowledge, invaluable guidance, encouragement and support during the course of this research. I would like to thank Prof. Turgay Tekinay and Prof. Engin Durgun for their guidance during my PhD studies, as well as to my jury members Prof. Gülüm Şumnu, Prof. Hilal Türkoğlu Şaşmazel, and Prof. Urartu Özgür Şafak Şeker for their contribution to my thesis.

I would like to give special thanks to Dr. Nalan Oya San Keskin and Dr. Semran İpek Küskü for their fruitful collaboration.

I would like to acknowledge to former and present members of Uyar Research Group Dr. Amaresh Chandra Pradhan, Dr. Ali Demirci, Dr. Anitha Senthamizhan, Dr. Aslı Çelebioğlu, Dr. Brabu Balusamy, Dr. Fatma Kayacı-Şenirmak, Dr. Kugalur Shanmugam Ranjith, Dr. Osman Arslan, Ömer Faruk Sarıoğlu, Dr. Serkan Demirci, Dr. Sesha Vempati, Şefika Eroğlu Özcan, Yelda Ertaş, Zehra İrem Yıldız.

I am also thankful to Fatih Büker, Dr. Gökçe Çelik, Mustafa Doğan, Mustafa Güler, and Zeynep Erdoğan for their technical assistance. I would also like to thank old and present UNAM members Gonca Ünal, Murat Biçici, Suna Temiz and Bilkent University member Nimet Kaya.

I owe special thanks to my friends, Dr. Gözde Uzunallı, Dr. Aslı Çelebioğlu and Özlem Bıkmaz. Thank you for encouragement and support through these years.

I would like to express my dearest gratitude to my mother, father and sister for their love, support and understanding.

I would like to thank The Scientific and Technological Research Council of Turkey (TUBITAK, project #111M459 and #213M185) for funding my research and BİDEB 2211-C for PhD scholarship.

*To My grandmothers,*

# CONTENTS

ABSTRACT .....	iii
ÖZET .....	v
ACKNOWLEDGEMENTS .....	vii
CONTENTS .....	x
LIST OF FIGURES .....	xvi
LIST OF TABLES .....	xxii
LIST OF ABBREVIATIONS .....	xxiii
<b>Chapter 1</b> .....	<b>1</b>
<b>INTRODUCTION</b> .....	<b>1</b>
1.1 Electrospinning .....	2
1.2 Cyclodextrins .....	7
1.3 Electrospun nanofibrous webs as carrier for bioactive compounds .....	11
<b>Chapter 2</b> .....	<b>17</b>
<b>ENCAPSULATION OF CYCLODEXTRIN INCLUSION COMPLEXES IN ELECTROSPUN POLYMERIC NANOFIBERS</b> .....	<b>17</b>
2. Encapsulation of gallic acid/cyclodextrin inclusion complex in electrospun polylactic acid nanofibers: Release behavior and antioxidant activity of gallic acid .....	18
2.1 Introduction .....	18
2.2 Experimental .....	21
2.2.1 Materials .....	21
2.2.2 Preparation of inclusion complex and physical mixture .....	21
2.2.3 Preparation of electrospinning solutions .....	22
2.2.4 Electrospinning .....	22
2.2.5 Characterizations and measurements .....	23
2.2.6 Computational method .....	26
2.3 Results and discussion .....	27
2.3.1 Phase solubility studies .....	27
2.3.2 Structural characterization of inclusion complex .....	28
2.3.3 Thermal analysis of inclusion complex .....	29
2.3.4 The molar ratio of inclusion complex .....	31

2.3.5 Molecular modeling of inclusion complex .....	33
2.3.6 Morphology analysis of nanofibers .....	35
2.3.7 In vitro release study.....	38
2.3.8 Antioxidant activity .....	41
2.4 Conclusion.....	42
3. Developing antioxidant food packaging using $\alpha$ -tocopherol/ $\gamma$ -cyclodextrin-inclusion complex incorporated polylactic acid nanofibers produced via electrospinning .....	44
3.1 Introduction .....	44
3.2 Experimental .....	46
3.2.1 Materials .....	46
3.2.2 Preparation of inclusion complex .....	47
3.2.3 Preparation of electrospinning solutions .....	47
3.2.4 Electrospinning.....	48
3.2.5 Characterizations and measurements.....	48
3.3 Results and discussion.....	51
3.3.1 Structural characterization of inclusion complex .....	51
3.3.2 Thermal analysis of inclusion complex .....	52
3.3.3 The molar ratio of inclusion complex.....	53
3.3.4 Morphology analysis of nanofibers .....	54
3.3.5 In vitro release study.....	55
3.3.6 Antioxidant activity .....	56
3.3.7 Lipid oxidation analysis (TBARS).....	57
3.4 Conclusion.....	59
4. Antioxidant electrospun zein nanofibers incorporating quercetin/ $\gamma$ -cyclodextrin-inclusion complex .....	61
4.1 Introduction .....	61
4.2 Experimental .....	63
4.2.1 Materials .....	63
4.2.2 Preparation of inclusion complex .....	63
4.2.3 Preparation of electrospinning solutions .....	63
4.2.4 Electrospinning.....	64
4.2.5 Characterizations and measurements.....	65

4.3 Results and discussion.....	66
4.3.1 Structural characterization of inclusion complex .....	66
4.3.2 Thermal analysis of inclusion complex .....	67
4.3.3 The molar ratio of inclusion complex.....	68
4.3.4 Morphology analysis of nanofibers .....	69
4.3.5 Antioxidant activity .....	70
4.4 Conclusion.....	71
5. Antibacterial packaging material designed by encapsulation of thymol/cyclodextrin-inclusion complex in electrospun zein nanofibers.....	72
5.1 Introduction .....	72
5.2 Experimental .....	74
5.2.1 Materials .....	74
5.2.2 Preparation of inclusion complex .....	74
5.2.3 Preparation of electrospinning solutions .....	74
5.2.4 Electrospinning.....	75
5.2.5 Characterizations and measurements.....	76
5.3 Results and discussion.....	79
5.3.1 Structural characterization of inclusion complex .....	79
5.3.2 Thermal analysis of inclusion complex .....	80
5.3.3 The molar ratio of inclusion complex.....	81
5.3.4 Morphology analysis of nanofibers .....	82
5.3.5 Release study .....	83
5.3.6 Antibacterial activity .....	85
5.4 Conclusion.....	88
<b>Chapter 3.....</b>	<b>89</b>
<b>ELECTROSPINNING OF POLYMER-FREE CYCLODEXTRIN INCLUSION COMPLEX NANOFIBERS.....</b>	<b>89</b>
6. Electrospinning of polymer-free cyclodextrin/geraniol-inclusion complex nanofibers: enhanced shelf-life of geraniol with antibacterial and antioxidant properties .....	90
6.1 Introduction .....	90
6.2 Experimental .....	93
6.2.1 Materials .....	93

6.2.2 Preparation of electrospinning solutions .....	94
6.2.3 Electrospinning .....	94
6.2.4 Characterizations and measurements.....	95
6.3 Results and discussion.....	100
6.3.1 Phase solubility studies.....	100
6.3.2 Morphology analysis of nanofibers .....	102
6.3.3 The molar ratio of inclusion complex.....	105
6.3.4 Thermal analysis of nanofibers.....	107
6.3.5 Structural characterization of nanofibers.....	111
6.3.6 Release study .....	113
6.3.7 Antibacterial activity .....	118
6.3.8 Antioxidant activity .....	120
6.4 Conclusion.....	123
7. Fast-dissolving, prolonged release and antibacterial cyclodextrin/limonene- inclusion complex nanofibrous webs via polymer-free electrospinning.....	125
7.1 Introduction .....	125
7.2 Experimental .....	127
7.2.1 Materials .....	127
7.2.2 Preparation of electrospinning solutions .....	127
7.2.3 Electrospinning .....	128
7.2.4 Characterizations and measurements.....	128
7.2.5 Computational method .....	132
7.3 Results and discussion.....	133
7.3.1 Phase solubility studies.....	133
7.3.2 Molecular modeling of inclusion complex .....	134
7.3.3 Morphology analysis of nanofibers .....	137
7.3.4 The molar ratio of inclusion complex.....	140
7.3.5 Thermal analysis of nanofibers.....	143
7.3.6 Structural characterization of nanofibers.....	148
7.3.7 Release study .....	149
7.3.8 Antibacterial activity .....	152
7.4 Conclusion.....	153

8. Fast-dissolving delivery membranes produced from electrospun polymer-free cyclodextrin/linalool-inclusion complex nanofibers with prolonged release and antibacterial activity .....	155
8.1 Introduction .....	155
8.2 Experimental .....	157
8.2.1 Materials .....	157
8.2.2 Preparation of electrospinning solutions .....	157
8.2.3 Electrospinning .....	158
8.2.4 Characterizations and measurements.....	158
8.3 Results and discussion.....	161
8.3.1 Morphology analysis of nanofibers .....	161
8.3.2 The molar ratio of inclusion complex.....	164
8.3.3 Thermal analysis of nanofibers.....	167
8.3.4 Structural characterization of nanofibers.....	171
8.3.5 Release study .....	171
8.3.6 Antibacterial activity .....	175
8.4 Conclusion.....	176
<b>Chapter 4.....</b>	<b>177</b>
<b>ELECTROSPINNING OF CORE-SHELL NANOFIBERS FROM CYCLODEXTRIN INCLUSION COMPLEXES .....</b>	<b>177</b>
9. Core-shell nanofibers via electrospinning for drug delivery application .....	178
9.1 Introduction .....	178
9.2 Experimental .....	180
9.2.1 Materials .....	180
9.2.2 Preparation of electrospinning solutions .....	180
9.2.3 Electrospinning .....	181
9.2.4 Characterizations and measurements.....	182
9.3 Results and discussion.....	184
9.3.1 Morphology analysis of nanofibers .....	184
9.3.2 Structural characterization of nanofibers.....	185
9.3.3 Thermal analysis of nanofibers.....	186
9.3.4 Antioxidant activity .....	188
9.3.5 In vitro release study.....	190

9.3.6 In vitro degradation test .....	190
9.4 Conclusion.....	191
<b>Chapter 5.....</b>	<b>193</b>
<b>CONCLUSION AND FUTURE PERSPECTIVES.....</b>	<b>193</b>
LIST OF PUBLICATIONS.....	198
<b>BIBLIOGRAPHY .....</b>	<b>201</b>

## LIST OF FIGURES

Figure 1. Schematic view of the electrospinning set-up. ....	3
Figure 2. Electrospinning set-up at UNAM. ....	3
Figure 3. The photograph of core-shell nozzle and schematic representation of electrospinning of core-shell nanofibers. ....	5
Figure 4. Application areas of electrospun nanofibers. ....	7
Figure 5. Chemical structure and schematic view of $\alpha$ -CD, $\beta$ -CD, and $\gamma$ -CD [56]. ....	9
Figure 6. (a) Chemical structure of HP $\beta$ CD, M $\beta$ CD, and HP $\gamma$ CD, (b) schematic representation of the primary and secondary rim of CD molecules. ....	10
Figure 7. Schematic view of IC formation between guest and CD molecule. ...	11
Figure 8. Chemical structure of (a) GA, (b) HP $\beta$ CD; schematic representation of (c) HP $\beta$ CD, (d) formation of GA/HP $\beta$ CD-IC, and (e) electrospinning of nanofibers from PLA/GA/HP $\beta$ CD-IC solution. (Copyright © 2016, Elsevier. Reprinted with permission from Ref. [117]) ....	20
Figure 9. Phase solubility diagram of GA/HP $\beta$ CD system in water. (Copyright © 2016, Elsevier. Reprinted with permission from Ref. [117]) ....	28
Figure 10. XRD patterns of GA, HP $\beta$ CD, GA/HP $\beta$ CD-IC, and GA/HP $\beta$ CD-PM. (Copyright © 2016, Elsevier. Reprinted with permission from Ref. [117]) .....	29
Figure 11. TGA thermograms of GA, HP $\beta$ CD, GA/HP $\beta$ CD-IC and GA/HP $\beta$ CD-PM. (Copyright © 2016, Elsevier. Reprinted with permission from Ref. [117]) .....	30
Figure 12. $^1\text{H-NMR}$ spectra of GA, HP $\beta$ CD and GA/HP $\beta$ CD-IC. (Copyright © 2016, Elsevier. Reprinted with permission from Ref. [117]) .....	32
Figure 13. Top and side view of GA/HP $\beta$ CD-IC for (a)-(b) head and (c)-(d) tail orientation of GA. Gray, red, and yellow spheres represent carbon, oxygen, and hydrogen atoms, respectively. (Copyright © 2016, Elsevier. Reprinted with permission from Ref. [117]) .....	34
Figure 14. SEM images and fiber diameter distributions with average fiber diameter (AFD) of electrospun nanofibers obtained from solutions of (a) PLA, (b) PLA/GA, and (c) PLA/GA/HP $\beta$ CD-IC. (Copyright © 2016, Elsevier. Reprinted with permission from Ref. [117]) .....	36
Figure 15. The cumulative release of GA from PLA/GA-NF and PLA/GA/HP $\beta$ CD-IC-NF into (a) water, (b) 10% ethanol, and (c) 95% ethanol ( $n = 3$ ). The error bars in the figure represent the standard deviation (SD). (Copyright © 2016, Elsevier. Reprinted with permission from Ref. [117]) .....	40
Figure 16. The photographs of (a) DPPH solution (before reaction); DPPH solutions in which (b) PLA-NF, (c) PLA/GA-NF and (d) PLA/GA/HP $\beta$ CD-IC-NF was immersed (after reaction). (Copyright © 2016, Elsevier. Reprinted with permission from Ref. [117]) .....	42

Figure 17. Chemical structure of (a) $\alpha$ -TC, (b) $\gamma$ -CD; schematic representation of (c) $\gamma$ -CD, (d) formation of $\alpha$ -TC/ $\gamma$ -CD-IC, and (e) electrospinning of nanofibers from PLA/ $\alpha$ -TC/ $\gamma$ -CD-IC solution. ....	45
Figure 18. The photographs of raw beef samples and raw beef samples packed with nanofibers in polyethylene zip bags. ....	51
Figure 19. XRD patterns of $\gamma$ -CD and $\alpha$ -TC/ $\gamma$ -CD-IC. ....	52
Figure 20. TGA thermograms of $\alpha$ -TC, $\gamma$ -CD, and $\alpha$ -TC/ $\gamma$ -CD-IC. ....	53
Figure 21. $^1\text{H-NMR}$ spectra of $\alpha$ -TC/ $\gamma$ -CD-IC. ....	54
Figure 22. SEM images of PLA-NF, PLA/ $\alpha$ -TC-NF, and PLA/ $\alpha$ -TC/ $\gamma$ -CD-IC-NF. ....	55
Figure 23. The cumulative release of $\alpha$ -TC from PLA/ $\alpha$ -TC-NF and PLA/ $\alpha$ -TC/ $\gamma$ -CD-IC-NF. ....	56
Figure 24. The photographs of (a) DPPH solution; DPPH solutions in which (b) PLA/ $\alpha$ -TC/ $\gamma$ -CD-IC-NF, (c) PLA/ $\alpha$ -TC-NF was immersed (after reaction). ....	57
Figure 25. Change of TBARS overtime during storage for raw beef meat sample (control), PLA/ $\alpha$ -TC/ $\gamma$ -CD-IC-NF and PLA/ $\alpha$ -TC-NF packed raw beef meat. .	58
Figure 26. The photographs of raw beef meat samples (control), raw beef meatsamples packed with PLA/ $\alpha$ -TC/ $\gamma$ -CD-IC-NF and PLA/ $\alpha$ -TC-NF for 28 days. ....	59
Figure 27. Chemical structure of (a) QU, (b) $\gamma$ -CD; schematic representation of (c) $\gamma$ -CD, (d) formation of QU/ $\gamma$ -CD-IC, and (e) electrospinning of nanofibers from zein/QU/ $\gamma$ -CD-IC solution. ....	62
Figure 28. XRD patterns of QU, $\gamma$ -CD, and QU/ $\gamma$ -CD-IC. ....	67
Figure 29. TGA thermograms of QU, $\gamma$ -CD, and QU/ $\gamma$ -CD-IC. ....	68
Figure 30. $^1\text{H-NMR}$ spectra of QU/ $\gamma$ -CD-IC. ....	69
Figure 31. SEM images of zein-NF, zein/QU-NF, and zein/QU/ $\gamma$ -CD-IC-NF. .	70
Figure 32. The photographs of (a) DPPH solution; DPPH solutions in which (b) zein/QU-NF, (c) zein/QU/ $\gamma$ -CD-IC-NF was immersed (after reaction). ....	71
Figure 33. Chemical structure of (a) THY; (b) $\gamma$ -CD; schematic representation of $\gamma$ -CD, (d) formation of THY/ $\gamma$ -CD-IC (1:1), and (b) electrospinning of nanofibers from zein/THY/ $\gamma$ -CD-IC (1:1) solution. ....	73
Figure 34. XRD patterns of THY, $\gamma$ -CD, THY/ $\gamma$ -CD-IC (1:1), and THY/ $\gamma$ -CD-IC (2:1). ....	79
Figure 35. TGA thermograms of THY, $\gamma$ -CD, THY/ $\gamma$ -CD-IC (1:1), and THY/ $\gamma$ -CD-IC (2:1). ....	81
Figure 36. $^1\text{H-NMR}$ spectra of THY/ $\gamma$ -CD-IC (1:1) and (d) THY/ $\gamma$ -CD-IC (2:1). ....	82
Figure 37. SEM images of electrospun nanofibers obtained from the solutions of (a) zein, (b) zein/THY, (c) zein/THY/ $\gamma$ -CD-IC (1:1), (d) zein/THY/ $\gamma$ -CD-IC (2:1). ....	83
Figure 38. The cumulative release of thymol from (a) zein/THY-NF, (b) zein/THY/ $\gamma$ -CD-IC-NF (1:1), and (c) zein/THY/ $\gamma$ -CD-IC-NF (2:1) at 37°C,	

50°C, 75°C (n = 3). The error bars in the figure represent the standard deviation (SD). .....	84
Figure 39. The growth inhibition rate (%) of <i>E. coli</i> and <i>S. aureus</i> colonies in zein/THY-NF, zein/THY/γ-CD-IC-NF (1:1), and zein/THY/γ-CD-IC-NF (2:1) (n = 3). The error bars in the figure represent the standard deviation (SD). .....	86
Figure 40. The photographs of the raw meat samples; raw meat samples packed with zein/THY-NF, zein/THY/γ-CD-IC-NF (1:1), and zein/THY/γ-CD-IC-NF (2:1) and the photographs of petri dishes at the end of 1, 2 and 5 days of storage at 4°C.....	87
Figure 41. The chemical structure of (a) HPβCD, (b) MβCD, (c) HPγCD; the schematic representation of (d) CD/geraniol-IC formation, and (e) electrospinning of nanofibers from CD/geraniol-IC aqueous solution. (Copyright © 2016, Royal Society of Chemistry. Reprinted with permission from Ref. [127]).....	92
Figure 42. Phase solubility diagram of (a) HPβCD/geraniol, (b) MβCD/geraniol, (c) HPγCD/geraniol systems in water (n = 3). (Copyright © 2016, Royal Society of Chemistry. Reprinted with permission from Ref. [127]) .....	101
Figure 43. SEM images of electrospun nanofibers obtained from the aqueous solutions of (a) HPβCD, (b) MβCD, (c) HPγCD, (d) HPβCD/geraniol-IC, (e) MβCD/geraniol-IC, and (f) HPγCD/geraniol-IC; the photographs of (g) HPβCD-NF, (h) MβCD-NF, (i) HPγCD-NF, (j) HPβCD/geraniol-IC-NF, (k) MβCD/geraniol-IC-NF, and (l) HPγCD/geraniol-IC-NF webs. (Copyright © 2016, Royal Society of Chemistry. Reprinted with permission from Ref. [127]) .....	102
Figure 44. SEM image of PVA/geraniol-NF. (Copyright © 2016, Royal Society of Chemistry. Reprinted with permission from Ref. [127]) .....	103
Figure 45. <sup>1</sup> H-NMR spectra of (a) HPβCD/geraniol-IC-NF, (b) MβCD/geraniol-IC-NF, and (c) HPγCD/geraniol-IC-NF dissolved in d6-DMSO. (Copyright © 2016, Royal Society of Chemistry. Reprinted with permission from Ref. [127]) .....	106
Figure 46. TGA thermograms of (a) geraniol, HPβCD-NF, HPβCD/geraniol-IC-NF; (b) geraniol, MβCD-NF, MβCD/geraniol-IC-NF; (c) geraniol, HPγCD-NF, HPγCD/geraniol-IC-NF. (Copyright © 2016, Royal Society of Chemistry. Reprinted with permission from Ref. [127]) .....	109
Figure 47. DSC thermograms of HPβCD-NF, HPβCD/geraniol-IC-NF, MβCD-NF, MβCD/geraniol-IC-NF, HPγCD-NF, and HPγCD/geraniol-IC-NF; (Copyright © 2016, Royal Society of Chemistry. Reprinted with permission from Ref. [127]) .....	110
Figure 48. XRD patterns of HPβCD-NF, MβCD-NF, HPγCD-NF, HPβCD/geraniol-IC-NF, MβCD/geraniol-IC-NF, and HPγCD/geraniol-IC-NF. (Copyright © 2016, Royal Society of Chemistry. Reprinted with permission from Ref. [127]) .....	111

Figure 49. FTIR spectra of geraniol, HP $\beta$ CD-NF, M $\beta$ CD-NF, HP $\gamma$ CD-NF, HP $\beta$ CD/geraniol-IC-NF, M $\beta$ CD/geraniol-IC-NF, and HP $\gamma$ CD/geraniol-IC-NF. (a) Exemplary images of *Escherichia coli* (*E. coli*), *Staphylococcus aureus* (*S. aureus*) colonies. (Copyright © 2016, Royal Society of Chemistry. Reprinted with permission from Ref. [127])..... 112

Figure 50. The cumulative release of geraniol from (a) HP $\beta$ CD/geraniol-IC-NF, (b) M $\beta$ CD/geraniol-IC-NF, and (c) HP $\gamma$ CD/geraniol-IC-NF at 37°C, 50°C, 75°C (n = 3). The error bars in the figure represent the standard deviation (SD). (Copyright © 2016, Royal Society of Chemistry. Reprinted with permission from Ref. [127]) ..... 114

Figure 51. TGA of geraniol, PVA-NF, PVA/geraniol-NF-1day, PVA/geraniol-NF-25day, and PVA/geraniol-NF-50day. (Copyright © 2016, Royal Society of Chemistry. Reprinted with permission from Ref. [127]) ..... 116

Figure 52. (a) Exemplary images of *Escherichia coli* (*E. coli*), *Staphylococcus aureus* (*S. aureus*) colonies. The growth inhibition rate (%) and exemplary images of *E. coli* and *S. aureus* colonies treated by (b) HP $\beta$ CD/geraniol-IC-NF, (c) M $\beta$ CD/geraniol-IC-NF, and (d) HP $\gamma$ CD/geraniol-IC-NF (n = 3). (Copyright © 2016, Royal Society of Chemistry. Reprinted with permission from Ref. [127])..... 119

Figure 53. The antioxidant activity (%) of geraniol, HP $\beta$ CD-NF, M $\beta$ CD-NF, HP $\gamma$ CD-NF, HP $\beta$ CD/geraniol-IC-NF, M $\beta$ CD/geraniol-IC-NF, and HP $\gamma$ CD/geraniol-IC-NF and the photographs of DPPH solutions in which geraniol, HP $\beta$ CD-NF, M $\beta$ CD-NF, HP $\gamma$ CD-NF, HP $\beta$ CD/geraniol-IC-NF, M $\beta$ CD/geraniol-IC-NF, HP $\gamma$ CD/geraniol-IC-NF were immersed, respectively. (n = 3). The error bars in the figure represent the standard deviation (SD). (Copyright © 2016, Royal Society of Chemistry. Reprinted with permission from Ref. [127]) ..... 123

Figure 54. The chemical structure of (a) HP $\beta$ CD, M $\beta$ CD, and HP $\gamma$ CD, (b) the chemical structure of limonene, the schematic representation of CD and CD/limonene-IC, (c) the schematic representation of electrospinning of nanofibers from CD/limonene-IC solution..... 126

Figure 55. Phase solubility diagram of (a) HP $\beta$ CD/limonene, (b) M $\beta$ CD/limonene, (c) HP $\gamma$ CD/limonene systems in water (n = 3). ..... 134

Figure 56. (a) The chemical structure of limonene; top view of ICs of (b) HP $\beta$ CD, (c) M $\beta$ CD, (d) HP $\gamma$ CD; side view of ICs of (e) HP $\beta$ CD, (f) M $\beta$ CD, and (g) HP $\gamma$ CD with limonene in aqueous medium. Gray and yellow spheres represent carbon and hydrogen atoms, respectively..... 136

Figure 57. SEM images of electrospun nanofibers obtained from the solutions of (a) HP $\beta$ CD/limonene-IC, (b) M $\beta$ CD/limonene-IC (c) HP $\gamma$ CD/limonene-IC; the photographs of (d) HP $\beta$ CD/limonene-IC-NF, (e) M $\beta$ CD/limonene-IC-NF, (f) HP $\gamma$ CD/limonene-IC-NF..... 138

Figure 58. The presentation of the solubility behaviour of pure limonene and HP $\beta$ CD/limonene-IC-NF, M $\beta$ CD/limonene-IC-NF, and HP $\gamma$ CD/limonene-IC-NF in water.....	140
Figure 59. <sup>1</sup> H-NMR spectra of (a) HP $\beta$ CD/limonene-IC-NF, (b) M $\beta$ CD/limonene-IC-NF, and (c) HP $\gamma$ CD/limonene-IC-NF.....	142
Figure 60. TGA thermograms of (a) limonene, HP $\beta$ CD-NF, HP $\beta$ CD/limonene-IC-NF; (b) limonene, M $\beta$ CD-NF, M $\beta$ CD/limonene-IC-NF; (c) limonene, HP $\gamma$ CD-NF, HP $\gamma$ CD/limonene-IC-NF.....	146
Figure 61. DSC thermograms of HP $\beta$ CD-NF, HP $\beta$ CD/limonene-IC-NF, M $\beta$ CD-NF, M $\beta$ CD/limonene-IC-NF, HP $\gamma$ CD-NF, and HP $\gamma$ CD/limonene-IC-NF.....	147
Figure 62. XRD patterns of HP $\beta$ CD-NF, M $\beta$ CD-NF, HP $\gamma$ CD-NF, HP $\beta$ CD/limonene-IC-NF, M $\beta$ CD/limonene-IC-NF, and HP $\gamma$ CD/limonene-IC-NF.....	148
Figure 63. The cumulative release of limonene from (a) HP $\beta$ CD/limonene-IC-NF, (b) M $\beta$ CD/limonene-IC-NF, and (c) HP $\gamma$ CD/limonene-IC-NF at 37°C, 50°C, and 75°C (n = 3). The error bars in the figure represent the standard deviation.....	150
Figure 64. The amount of limonene in HP $\beta$ CD/limonene-IC-NF, M $\beta$ CD/limonene-IC-NF, and HP $\gamma$ CD/limonene-IC-NF at RT for 100 days...	151
Figure 65. Exemplary images of <i>E. coli</i> , <i>S. aureus</i> colonies. The growth inhibition rate (%) and exemplary images of <i>E. coli</i> and <i>S. aureus</i> colonies treated by limonene, HP $\beta$ CD/limonene-IC-NF, M $\beta$ CD/limonene-IC-NF, and HP $\gamma$ CD/limonene-IC-NF (n = 3).....	153
Figure 66. (a) The chemical structure of HP $\beta$ CD, M $\beta$ CD, HP $\gamma$ CD; (b) the schematic representation of CD/linalool-IC formation, and (c) electrospinning of nanofibers from CD/linalool-IC aqueous solution.....	156
Figure 67. SEM images of electrospun nanofibers obtained from the aqueous solutions of (a) HP $\beta$ CD/linalool-IC, (b) M $\beta$ CD/linalool-IC, and (c) HP $\gamma$ CD/linalool-IC; the photographs of (d) HP $\beta$ CD/linalool-IC-NF, (e) M $\beta$ CD/linalool-IC-NF, and (f) HP $\gamma$ CD/linalool-IC-NF webs.....	162
Figure 68. The presentation of the solubility behaviour of pure linalool and HP $\beta$ CD/linalool-IC-NF, M $\beta$ CD/linalool-IC-NF, and HP $\gamma$ CD/linalool-IC-NF in water.....	164
Figure 69. <sup>1</sup> H-NMR spectra of (a) HP $\beta$ CD/linalool-IC-NF, (b) M $\beta$ CD/linalool-IC-NF, and (c) HP $\gamma$ CD/linalool-IC-NF dissolved in d6-DMSO.....	166
Figure 70. TGA thermograms of (a) linalool, HP $\beta$ CD-NF, HP $\beta$ CD/linalool-IC-NF; (b) linalool, M $\beta$ CD-NF, M $\beta$ CD/linalool-IC-NF; (c) linalool, HP $\gamma$ CD-NF, HP $\gamma$ CD/linalool-IC-NF.....	169
Figure 71. DSC thermograms of HP $\beta$ CD-NF, HP $\beta$ CD/linalool-IC-NF, M $\beta$ CD-NF, M $\beta$ CD/linalool-IC-NF, HP $\gamma$ CD-NF, and HP $\gamma$ CD/linalool-IC-NF.....	170
Figure 72. XRD patterns of HP $\beta$ CD-NF, M $\beta$ CD-NF, HP $\gamma$ CD-NF, HP $\beta$ CD/linalool-IC-NF, M $\beta$ CD/linalool-IC-NF, and HP $\gamma$ CD/linalool-IC-NF.....	171

Figure 73. The cumulative release of linalool from (a) HP $\beta$ CD/linalool-IC-NF, (b) M $\beta$ CD/linalool-IC-NF, and (c) HP $\gamma$ CD/linalool-IC-NF at 37°C, 50°C, 75°C (n = 3). The error bars in the figure represent the standard deviation (SD). .... 173

Figure 74. The amount of linalool in HP $\beta$ CD/linalool-IC-NF, M $\beta$ CD/linalool-IC-NF, and HP $\gamma$ CD/linalool-IC-NF at RT for 50 days. .... 174

Figure 75. Exemplary images of *E. coli*, *S. aureus* colonies. The growth inhibition rate (%) and exemplary images of *E. coli* and *S. aureus* colonies treated by HP $\beta$ CD/linalool-IC-NF, M $\beta$ CD/linalool-IC-NF, and HP $\gamma$ CD/linalool-IC-NF (n = 3). .... 175

Figure 76. Chemical structure of (a) curcumin; schematic representation of (b) HP $\beta$ CD, (c) formation of CUR/HP $\beta$ CD-IC, and (d) electrospinning of nanofibers from cCUR/HP $\beta$ CD-IC-sPLA solution. .... 179

Figure 77. SEM images of electrospun nanofibers obtained from solutions of (a) PLA-CUR, (b) PLA/CUR-HP $\beta$ CD-IC, (c) cCUR/HP $\beta$ CD-IC-sPLA-CS; the photographs of PLA-CUR-NF, (b) PLA/CUR-HP $\beta$ CD-IC-NF, (c) cCUR/HP $\beta$ CD-IC-sPLA-CSNF. .... 185

Figure 78. (a) TEM and (b) CLSM images of cCUR/HP $\beta$ CD-IC-sPLA-CSNF. .... 185

Figure 79. XRD patterns of CUR, HP $\beta$ CD, PLA-NF, PLA-CUR-NF, PLA/CUR-HP $\beta$ CD-IC-NF, and cCUR/HP $\beta$ CD-IC-sPLA-CSNF. .... 186

Figure 80. TGA thermograms of CUR, HP $\beta$ CD, PLA-NF, PLA-CUR-NF, PLA/CUR-HP $\beta$ CD-IC-NF, and cCUR/HP $\beta$ CD-IC-sPLA-CSNF. .... 187

Figure 81. Time dependent antioxidant activity of PLA-CUR-NF, PLA/CUR-HP $\beta$ CD-IC-NF, cCUR/HP $\beta$ CD-IC-sPLA-CSNF and the release of CUR from PLA-CUR-NF, PLA/CUR-HP $\beta$ CD-IC-NF, cCUR/HP $\beta$ CD-IC-sPLA-CSNF. 189

Figure 82. Concentration dependent antioxidant activity of PLA-CUR-NF, PLA/CUR-HP $\beta$ CD-IC-NF, cCUR/HP $\beta$ CD-IC-sPLA-CSNF. .... 190

Figure 83. SEM images of (a, d) PLA-CUR-NF, (b, e) PLA/CUR-HP $\beta$ CD-IC-NF, (c, f) cCUR/HP $\beta$ CD-IC-sPLA-CSNF after 4 (a-c) and 28 (d-f) days in vitro degradation in PBS. .... 191

## LIST OF TABLES

Table 1. General properties of native CDs [56].....	9
Table 2. The properties of the solutions used for electrospinning and morphological characteristics of the resulting nanofibers. (Copyright © 2016, Elsevier. Reprinted with permission from Ref. [117]).....	37
Table 3. The composition of the solutions used for electrospinning.....	48
Table 4. The composition of the solutions used for electrospinning.....	64
Table 5. The composition of the solutions used for electrospinning.....	75
Table 6. The properties of the solutions used for electrospinning and morphological characteristics of the resulting nanofibers. (Copyright © 2016, Royal Society of Chemistry. Reprinted with permission from Ref. [127]).....	104
Table 7. The amount of geraniol in CD/geraniol-IC-NFs and PVA/geraniol-NF at room temperature for 50 days. (Copyright © 2016, Royal Society of Chemistry. Reprinted with permission from Ref. [127]).....	117
Table 8. Complexation and solvation energies of limonene within HP $\beta$ CD, M $\beta$ CD, and HP $\gamma$ CD.....	137
Table 9. The properties of the solutions used for electrospinning and morphological characteristics of the resulting nanofibers.....	139
Table 10. The properties of the solutions used for electrospinning and morphological characteristics of the resulting nanofibers.....	163

## LIST OF ABBREVIATIONS

$^1\text{H}$ NMR	Proton nuclear magnetic resonance
ACN	Acetonitrile
CD	Cyclodextrin
$\text{CHCl}_3$	Chloroform
CLSM	Confocal laser scanning microscopy
CUR	Curcumin
d6-DMSO	Deuterated dimethylsulfoxide
DCM	Dichloromethane
DMF	Dimethylformamide
DPPH	2,2-diphenyl-1-picrylhydrazyl
DSC	Differential scanning calorimetry
E.coli	Escherichia coli
FTIR	Fourier transform infrared spectrometer
GA	Gallic acid
HPLC	High performance liquid chromatography
HP $\beta$ CD	Hydroxypropyl- $\beta$ -cyclodextrin
HP $\gamma$ CD	Hydroxypropyl- $\gamma$ -cyclodextrin
HS GC-MS	Head space gas chromatography-mass spectroscopy
IC	Inclusion complex
MeOH	Methanol
M $\beta$ CD	Methyl- $\beta$ -cyclodextrin
NF	Nanofiber
PBS	Phosphate buffered saline
PLA	Polylactic acid
QU	Quercetin

RT	Room temperature
S.aureus	Staphylococcus aureus
SEM	Scanning electron microscopy
TEM	Transmission electron microscopy
TGA	Thermal gravimetric analysis
THY	Thymol
XRD	X-ray diffraction
$\alpha$ -TC	$\alpha$ -Tocopherol

# **Chapter 1**

---

## **INTRODUCTION**

## 1.1 Electrospinning

Electrospinning has attracted considerable attention in recent years after Reneker revived attraction in 1990s [1] as a versatile method to produce nanofibers having high surface to volume ratio and highly porous structure [2, 3]. Unlike other fiber production methods it is not limited with a particular material range, thus electrospinning approach has been acknowledged universally to produce fibers from variety of materials including polymers, inorganic materials, and composites [4]. Electrospinning is capable of forming fibers in nanoscale diameters in contrast to other spinning methods including wet spinning, dry spinning, melt spinning, and gel spinning [5]. Moreover, it is also superior to other fiber production techniques in terms of cost, simplicity of set-up and production rate [6]. In addition to these features, design flexibility is of great significance for electrospun nanofibers [4].

Syringe pump, high voltage power supply, and grounded collector are the three main components of electrospinning set-up. The schematic view of electrospinning and our electrospinning set-up in our laboratory at UNAM is shown in Figure 1 and Figure 2, respectively. Polymer solution or melt is fed through the grounded collector at a constant rate via syringe pump. After applying high voltage from high voltage power supply, the drop in the outlet of the syringe is electrified. Due to the electrostatic repulsion and Coulombic force, the drop is transformed into a cone-shaped distortion called Taylor cone. When the electrostatic forces are high enough to overcome the surface tension of the polymer solution, jet is ejected. While jet elongates towards the grounded collector, stretching and whipping processes causes the formation of thin and

long fiber. As the solvent evaporates, fibers are produced in random fashion as a nanofibrous web on the collector [2, 3, 7].

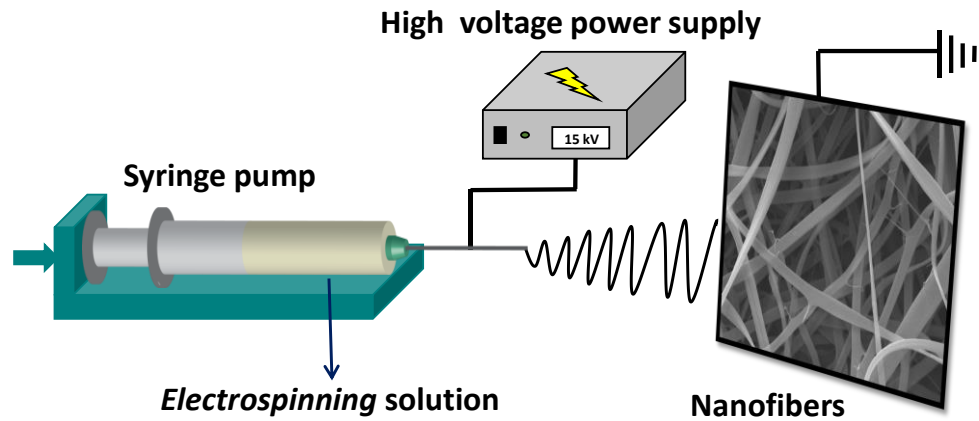


**Figure 1.** Schematic view of the electrospinning set-up.



**Figure 2.** Electrospinning set-up at UNAM.

In order to obtain bead-free and uniform electrospun nanofibers, the parameters need to be optimized are divided into three groups: *polymer solution parameters*

(type and molecular weight of the polymer; conductivity, viscosity and surface tension of polymer solution), *process parameters* (feed rate, applied voltage, distance between syringe and collector, diameter of the needle, collector type) and *environmental conditions* (temperature and humidity) [2, 5, 8]. First of all, molecular weight and concentration of the polymer solution must provide high enough viscosity to form the chain entanglement [3]. So, if the viscosity is not sufficient to produce bead-free nanofibers, increasing the concentration may help to produce bead-free nanofibers due to the increment in the viscosity. Conductivity is another significant parameter affecting the system. If the conductivity of the polymer solution is not enough, the stretching of the solution will not be at required level to obtain nanofibers [3, 9]. Process parameters like voltage, distance, and feed rate has also an effect on the electrospinning system. High voltage is necessary for the process. Applying higher voltage results in greater stretching of the solution owing to the higher coulombic forces and electric field. Therefore, thinner diameter of fibers are obtained. Optimizing the feed rate is a critical issue for solvents to evaporate. If the feed rate is too high, solvent will remain in the nanofibers because of the lack of time. Distance between the syringe and collector has an influence on the flight time and electric field applied. Thus, when the distance is not long enough solvent will remain and cause nanofibers to merge. If the distance is too long electric field might not be enough to accelerate the jet. Lastly, temperature and humidity is of vital importance for some of the solutions. Since they are known to affect the evaporation rate of the solvent. Additionally, temperature also reduce the viscosity of the polymer solution which is a critical parameter having

importance for electrospinning process. On the other hand, humidity is used to achieve porous nanofibers via electrospinning [3].

In addition to basic electrospinning, it is also possible to obtain nanofibers with different morphology such as aligned, core-shell, hollow and porous nanofibers. In an electrospinning set-up, nanofibers are collected randomly on a fixed grounded collector. However, using a cylindrical rotating collector instead of a fixed one enables to yield aligned nanofibers [10, 11]. Employing core-shell nozzle (Figure 3) will result in formation of core-shell nanofibers [12, 13]. Furthermore, it was also reported the production of core-shell nanofibers by using electrospinning and atomic layer deposition [14]. In order to obtain hollow nanofibers, the core part of the core-shell nanofibers is removed [15, 16]. Electrospun nanofibers have intra-fiber pores, however achieving the nanofibers having pores on the nanofiber is also possible via electrospinning [17, 18].

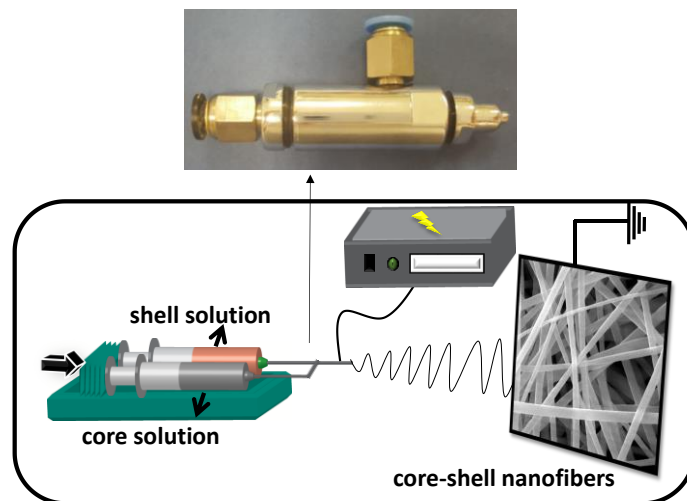


**Figure 3.** The photograph of core-shell nozzle and schematic representation of electrospinning of core-shell nanofibers.

Electrospun nanofibers can be used in many areas in which high surface to volume ratio is a significant characteristic desired. Highly porous structure is another advantage of electrospun nanofibers which makes them excellent candidate for many other applications. As mentioned above, flexibility of the system is also important for universality since nanofibers having different morphology might be obtained using electrospinning with slight modifications [19, 20]. Other than the exceptional characteristics of electrospun nanofibers, its ease of functionalization with number of molecules further extends its application areas [4]. For example, nanoparticles [21, 22], inorganic precursors [23, 24], drugs [25, 26], antioxidant [27, 28] and antibacterial agents [29, 30], food additives (essential oils, flavour/fragrance) [31-33] can be incorporated in electrospun nanofibers in one step. Consequently, electrospun nanofibers find application in filtration [34-36], biomedical [29, 37-41], food and agriculture [42-45], enzyme and catalyst [46-49], sensor [50-52], energy and electronics [53-55] (Figure 4).

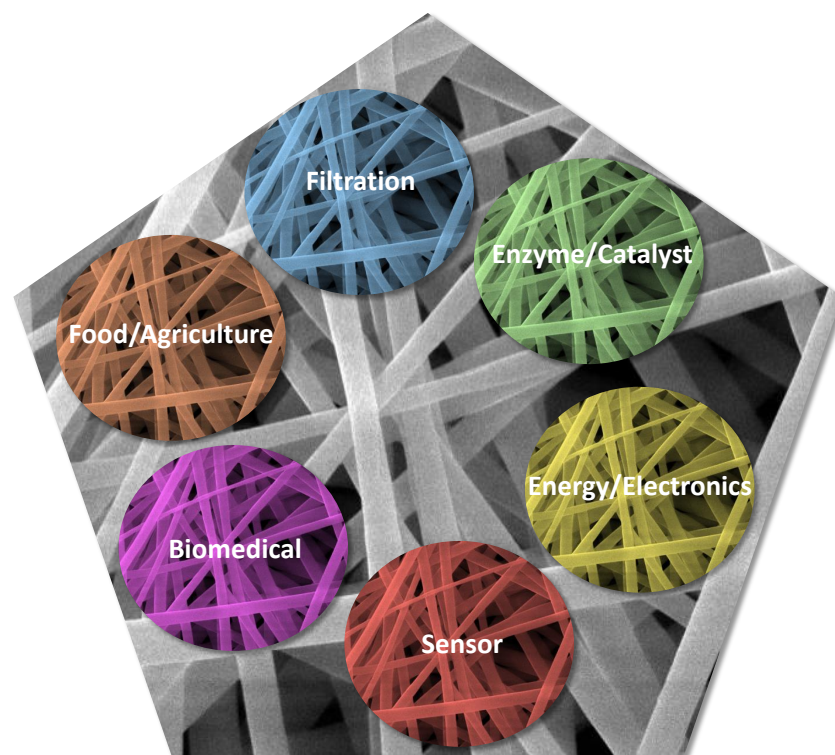


**Figure 4.** Application areas of electrospun nanofibers.

## 1. 2 Cyclodextrins

Cyclodextrins (CDs) are nontoxic cyclic oligosaccharides composed of six, seven, eight or more glucopyranose units and linked by  $\alpha$ -(1,4) bonds [56, 57]. When Villiers first discovered CDs in 1891, he named them as “cellulosine” due to their structural resemblance to cellulose [56]. Since Schardinger has a significant role to elucidate the chemistry of CDs in the early 1900s, CDs are also called as Schardinger dextrins [56, 57]. CDs are produced from starch or its derivatives by using CD glycosyltransferase (CGTase) of various microorganisms including *Bacillus macerans*, *Klebsiella oxytoca*, *Bacillus circulans*, and *Alkalophylic bacillus* [56]. However, isolation needs to be done to obtain each CD from the mixture obtained at the end of the enzymatic degradation. For

instance, if toluene is used  $\beta$ -CD is produced due to the formation of inclusion complex (IC) between toluene and  $\beta$ -CD [56]. The three major and most widely used CDs are  $\alpha$ -CD,  $\beta$ -CD,  $\gamma$ -CD and consist of 6, 7, and 8 glucopyranose units, respectively (Figure 5) [56-58]. The properties of native CDs are summarized in Table 1. The volume of the cavity is increasing from  $\alpha$ -CD to  $\gamma$ -CD. The solubility of  $\beta$ -CD is quite low compared to  $\alpha$ -CD and  $\gamma$ -CD, due to the complete secondary belt formation via hydrogen bonds.  $\alpha$ -CD can only form four hydrogen bond instead of six because of the distorted position of one glucopyranose unit. The higher solubility of  $\gamma$ -CD is most likely owing to its noncoplanar and more flexible structure [56]. Native CDs ( $\alpha$ -CD,  $\beta$ -CD, and  $\gamma$ -CD) can also be modified to obtain CD derivatives. According to the type of functional group substituted to hydroxyl groups in native CDs, hydrophilic or hydrophobic derivatives are achieved. While producing CD derivatives, the main purpose is increasing the solubility, complexation ability and stability against light or oxygen compared to native CDs [56, 57]. In addition to the changes in the solubility, the cavity volume of native CDs are also being modified in CD derivatives [57].

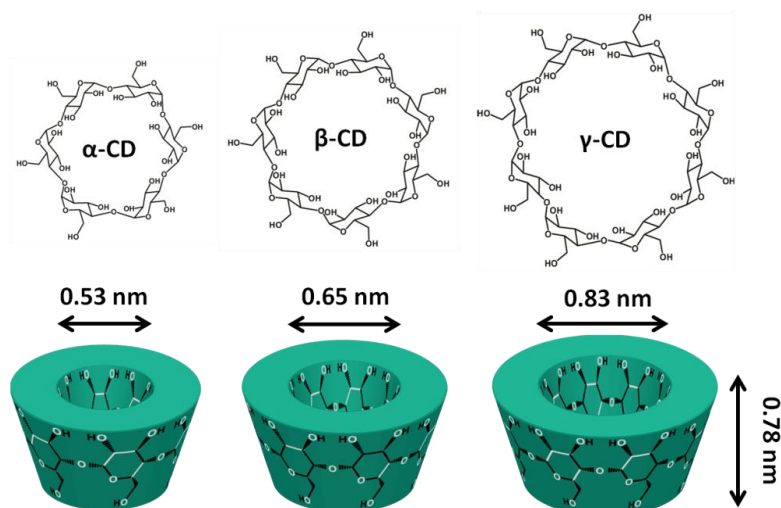


**Figure 5.** Chemical structure and schematic view of  $\alpha$ -CD,  $\beta$ -CD, and  $\gamma$ -CD [56].

**Table 1.** General properties of native CDs [56].

Properties	$\alpha$ -CD	$\beta$ -CD	$\gamma$ -CD
Number of glucopyranose units	6	7	8
Molecular weight (g/mol)	972	1135	1297
Outer diameter (Å)	14.6	15.4	17.5
Cavity diameter (Å)	4.7-5.3	6.0-6.5	7.5-8.3
Height of torus (Å)	7.9	7.9	7.9
Approximate cavity volume (Å <sup>3</sup> )	174	262	427
Solubility in water at 25 °C (g/100 mL)	14.5	1.85	23.2

As seen from the chemical structure of CDs in Figure 6, there exist two types of hydroxyl groups (primary and secondary) in the structure. Primary hydroxyl

groups (C6) are in the narrower edge, whereas secondary hydroxyl groups (C2 and C3) are located in the wider edge of CDs. Due to the steric arrangement CDs has truncated-cone shape structure with hydrophilic outside surface and relatively hydrophobic cavity in which apolar C3 and C5 hydrogens and ether-like oxygens are present [56-58]. The distinct character of CDs is related with their relatively hydrophobic cavity residing various types of molecules in appropriate polarity and dimension [56-58]. Thus, they are capable of making non-covalent host-guest ICs with solid, liquid, and gaseous compounds [56-58].

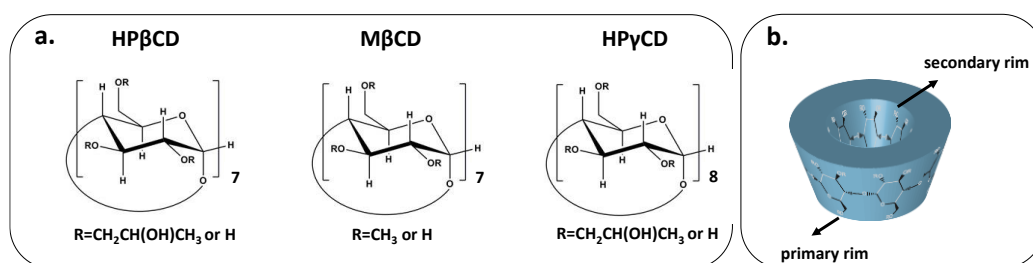


**Figure 6.** (a) Chemical structure of HPβCD, MβCD, and HPγCD, (b) schematic representation of the primary and secondary rim of CD molecules.

Complex formation is occurred when there is a dimensional and polarity fit between host and guest molecules (Figure 7). The main driving force of this phenomena is the replacement of enthalpy-rich water molecules from cavity by the apolar guest molecules. So, repulsive forces between water molecules and cavity and bulk water and guest molecule are main components of the driving force. So, CD-ICs decrease the ring strain of CDs and more stable lower energy state is obtained. Weak forces, such as van der Waals interactions, dipole-dipole interactions, hydrophobic interactions and hydrogen bonding play role in the formation of the complexes. Among several methods of producing CD-ICs co-

precipitation, slurry, paste, and dry mixing are the most widely used methods. However, co-precipitation is a common technique in laboratory scale [58]. In the simplest case, one guest molecule is held by one host (CD) molecule. However, two or more CD molecules might host one guest molecule or one CD molecule might reside two or more guest molecules [56, 57].

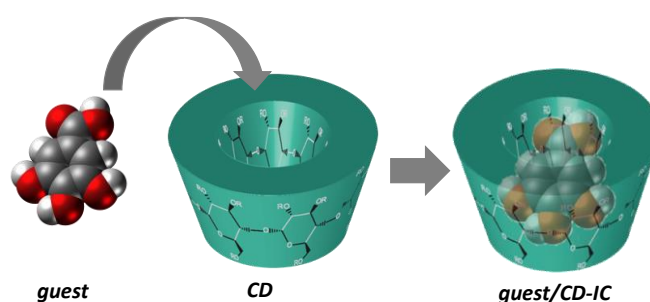


**Figure 7.** Schematic view of IC formation between guest and CD molecule.

Inclusion complexation leads to various modifications in the properties of the guest molecule such as converting liquid molecules to powder form [59-61], enhancement the solubility [62-64], stabilization against light [65, 66], oxygen [67], etc., reducing the volatility [68-71], controlling fluorescence and light absorption [72, 73]. Therefore, CDs find a broad application areas in filtration [74-78], pharmaceutical [79-82], food [83-88], cosmetic [89, 90], and personal care [91] industries.

### **1.3 Electrospun nanofibrous webs as carrier for bioactive compounds**

Bioactive compounds used in pharmaceutical and food industry have some limitations. The majority of these substances is problematic in terms of their low aqueous solubility, poor bioavailability, and sensitivity against various means

such as light, oxygen, temperature etc. These limitations increase the required dose and reduce the shelf life of these molecules [92, 93]. In addition, degradation of these products might produce off-flavors, off-colors, or carcinogenic compounds that is also not a desired feature of the products [92]. Therefore, encapsulation methods are used to overcome the limitations of these active agents with maintaining their biological activity [92]. Among several encapsulation methods, complexation with CDs is an effective approach. Since CD-ICs improve the solubility of bioactive molecules to reduce the required concentration for showing the biological effect and protect them from light, oxygen, temperature to prolong the shelf life of products [93].

On the other hand, electrospinning has gained interest as a universal method to produce functional nanofibers for applications in food packaging and drug delivery as mentioned previously. Since electrospun nanofibers offer advantages over films, they are superior to films. First, electrospinning system enables to produce nanofibers at room temperature in contrary to polymeric films which are usually produced at high temperatures. Therefore, encapsulation of essential oils and flavour/fragrances which are mostly volatile into electrospun nanofibers are a better alternative [31]. Secondly, nanofibers are responsive to changes such as relative humidity and temperature which enables tunable release of the active agents incorporated. Additionally, various compounds including drugs [25, 26], antioxidant [27, 28] and antibacterial agents [29, 30], and food additives [31-33] might be incorporated into electrospun nanofibers in one step.

Combining the synergetic effect of CD-ICs of bioactive agents with electrospun nanofibers is a new approach [94]. This approach has been applied

by our group in order to use several bioactive agents in a more efficient way [95-105]. There are also other studies in the literature following our approach in which IC of various molecules and CD types are included in many types of polymeric nanofibers [106-116]. Contribution of this thesis (Chapter 2) in “CD-IC incorporated polymeric nanofibers” area is the investigation of application of these nanofibers as packaging and delivery material [117].

In general, polymers have been taken as a material/matrix for the fabrication of nanofibers owing to the chain entanglement and overlapping between the polymer chains [118]. However, Celebioglu and Uyar successfully demonstrated the electrospinning of polymer-free nanofibers from various native and modified CDs without using any polymeric carrier matrix [119-123]. The self-assembly and aggregation characteristics of CD molecules in concentrated solutions via the formation of intermolecular hydrogen bonding enables the production of nanofibers in the absence of polymer matrix. Further, CD-IC nanofibers of triclosan was produced by our group [124, 125]. But, these studies were mostly focused on the production of CD-IC nanofibers except investigating antibacterial activity. Our research group also produced CD-IC incorporated polymeric nanofibers successfully as mentioned above [95-105, 117]. Yet, sometimes the necessity of using organic solvents which generally have environmental hazards might not suitable for applications including pharmaceutical and food packaging. However, usage of organic solvents might be unavoidable in the fabrication of some nanofibers. Therefore, water soluble molecules like CDs could be an alternative molecule to produce nanofibers. In addition, electrospinning of polymer-free CD-IC nanofibers having much higher

loading capacity of guest molecules (up to ~ 10-15%, w/w) as compared to CD-IC incorporated polymeric nanofibers were quite successfully and electrospinning was performed in aqueous solution [124, 125]. Therefore, polymer-free CD-IC nanofibers may open up new possibilities for various applications including cosmetic, biomedical, food packaging, and flavour/fragrance releasing. Recently, CD-IC nanofibers of vanillin was also produced by electrospinning [126]. Contribution of this thesis (Chapter 3) in “Electrospinning of CD-IC nanofibers” research is the application of these concept to flavour/fragrances and investigating of these nanofibers as a releasing nanoweb [127].

Production of core-shell nanofibers can be done in two step [14, 128]. However, core-shell nanofibers obtained via electrospinning system having a special nozzle (Figure 3) is a one step process and it is one of the most interesting structure which can be produced by using electrospinning. Core and shell solutions could be both miscible and immiscible depending on the solvents used [129]. The solution can be fed through to collector by two separate syringe pumps or pressurized gas [129]. The parameters which affect the monoaxial electrospinning is of importance for coaxial electrospinning as well. But in this case, the miscibility of the solvents used in core and shell solutions is a critical issue that must be considered. For example, using chloroform and water may result in formation of pendant droplets in the edge of the nozzle. However, using an intermediate solvent like methanol or ethanol might be helpful due to their miscibility with both of the solvents and low surface energy [129]. Flow rate ratio of core and shell solutions is of significance as well. Thus, if the flow rate

ratio less than 1:2 (core:shell) shell solution might not encapsulate the core solution; whereas if the ratio is high there will be a risk of producing nanofibers composed of only shell solution [129]. Core-shell nanofibers is of particular interest for non-spinnable systems, if one uses non-spinnable solution or even a powder and polymer solution in the core and shell, respectively. This is regarding with the internal (viscous and viscoelastic) stresses and Maxwell stresses present in such kind of a system [12, 130]. It was reported that core-shell nanofibers can be employed in order to protect sensitive bioactive agents against light and organic solvents caused by the direct contact with these means, and produce electrospun nanofibers which has unique properties such as high surface to volume ratio and porous structure. Furthermore, core-shell nanofibers developed for drug delivery might provide a better control over the release of the drug. Since the shell acts as an additional barrier for the release of drugs. It is also facile to play with the type of the polymer used, thickness of the shell and core fibers, encapsulated drug which can be both hydrophilic and hydrophobic. Lastly, the system is also available for encapsulation of more than one drug to the nanofibers for in-situ applications. On the other hand, there exist some limitations about the coaxial electrospinning. Common drawbacks of the system can be the difficulty in concentricity of the core and shell parts of the nanofibers and production of hollow nanofibers due to the non-continuous core entrainment [131]. In the literature, coaxial electrospinning is used in many application areas including delivery of growth factors [132], gene [133], protein [134], living organisms such as cell [135], virus [136], bacteria [137] in biomedical; food packaging [138, 139], enzyme/catalyst [140, 141], filtration [142, 143], sensor

[144, 145], and lithium-ion batteries [146], supercapacitors [147], [148] in energy/electronics. However, there is no study on the fabrication of core-shell nanofibers by using CD-IC solution in the shell. So, core-shell nanofibers obtained by CD-IC and polylactic acid serve as a leading study for the electrospinning literature. Contribution of this thesis (Chapter 4) to “core-shell nanofibers“ area is the production of new generation of core-shell nanofibers from CD-ICs for the first time.

In this thesis, electrospinning of cyclodextrin functionalized nanofibers were produced according to three different methods. Firstly, the studies are focused on the incorporation of CD-ICs of bioactive compounds (antioxidant/antibacterial agents) into electrospun polylactic acid or zein nanofibers for packaging and delivery applications (Chapter 2). Then, the production of electrospun nanofibers from CD-ICs of flavour/fragrances without using a polymer matrix was achieved and the release and shelf life of these molecules were investigated (Chapter 3), and finally, core-shell nanofibers were obtained by using CD-IC solution of an antioxidant (curcumin) in the core and polylactic acid solution in the shell for the first time (Chapter 4).

## Chapter 2

---

# **ENCAPSULATION OF CYCLODEXTRIN INCLUSION COMPLEXES IN ELECTROSPUN POLYMERIC NANOFIBERS**

(Parts of this study was published as “Encapsulation of gallic acid/cyclodextrin inclusion complex in electrospun polylactic acid nanofibers: Release behavior and antioxidant activity of gallic acid”, Zeynep Aytac, Semran Ipek Kusku, Engin Durgun, Tamer Uyar\*, Materials Science and Engineering C, June 1, 2016 (Web), Reproduced (or 'Reproduced in part') from Ref. [117] with permission from Elsevier doi:10.1016/j.msec.2016.02.063)

## **2. Encapsulation of gallic acid/cyclodextrin inclusion complex in electrospun polylactic acid nanofibers: Release behavior and antioxidant activity of gallic acid**

### **2.1 Introduction**

Phenolic compounds are the most common primary antioxidants to readily scavenge free radicals by donating hydrogen atom or an electron [149]. Gallic acid (GA) (Figure 8a) is a hydroxybenzoic acid and considered as a natural phenolic antioxidant and antimicrobial agent. GA and its derivatives including tannins and catechin are especially found in berries, citrus fruits, cereals, tea, wine and herbs [150]. Since it has antioxidant and antimicrobial activity, it is used as an additive in food, cosmetics and pharmaceutical industry [151-154]. However, it might easily oxidize which further leads to degradation. In order to protect GA against degradation and maintain its bioactivity against external and environmental factors, cyclodextrin (CD) (Figure 8b-c) inclusion complex (CD-IC) has been synthesized and considered to be an efficient system in recent years [155, 156]. Therefore stabilization of GA might be improved by an encapsulation technique, inclusion complexation.

Flexibility of electrospinning process enables to obtain nanofibers containing active agents which have potential to be used in diverse application areas. Therefore, active agent encapsulated polymeric films and electrospun nanofibers have been studied previously [151, 153, 157]. CD-ICs can be incorporated into polymeric films and then CD-IC functionalized polymeric films might be used in food packaging and pharmaceutical applications [158, 159]. However, designing delivery systems for food packaging and drug delivery applications by

using nanofibers is advantageous over films owing to the high surface area and highly porous structure. In one of our previous study, sulfisoxazole (SFS)/CD-IC incorporated hydroxypropyl cellulose (HPC) nanofibers (HPC/SFS/CD-IC-NF) and films (HPC/SFS/CD-IC-film) were produced. The release of SFS was much more but slower from HPC/SFS/CD-IC-NF as compared to HPC/SFS/CD-IC-film. Low surface area of HPC/SFS/CD-IC-film and close location of SFS to the surface in HPC/SFS/CD-IC-film was stated the reason of less amount and quick release of SFS from HPC/SFS/CD-IC-film [103].

Poly(lactic acid) (PLA) is biodegradable aliphatic polyester produced from lactic acid and well suited for food packaging and drug delivery applications owing to its biocompatibility, biodegradability; carbon dioxide, oxygen and water permeability, and light barrier properties [160]. Leading studies related to incorporation of CD-IC of various guest molecules into electrospun nanofibers were reported by our research group [95-105, 117].

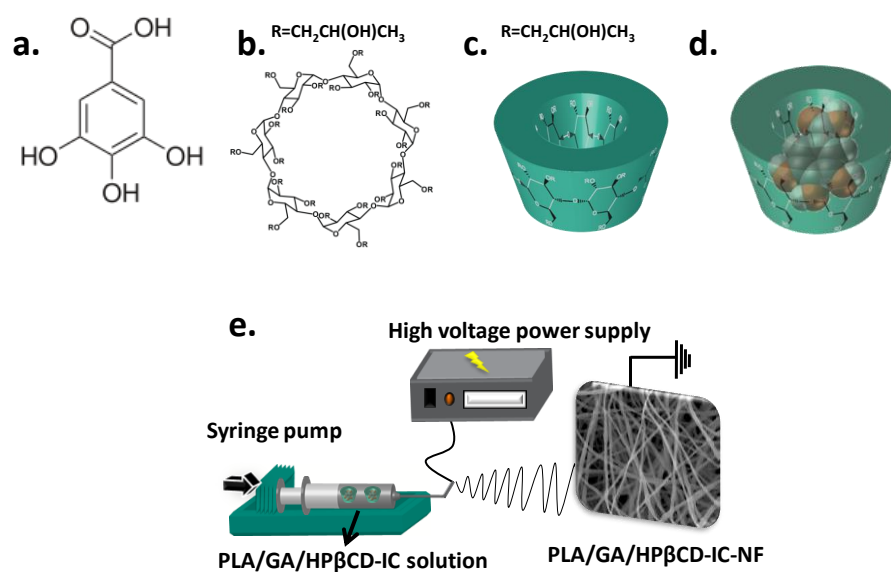


**Figure 8.** Chemical structure of (a) GA, (b) HPβCD; schematic representation of (c) HPβCD, (d) formation of GA/HPβCD-IC, and (e) electrospinning of nanofibers from PLA/GA/HPβCD-IC solution. (Copyright © 2016, Elsevier. Reprinted with permission from Ref. [117])

In this part, inclusion complex of GA and HPβCD (GA/HPβCD-IC) (Figure 8d) was formed and then it was incorporated into PLA nanofibers (PLA/GA/HPβCD-IC-NF) by electrospinning technique (Figure 8e). The prepared GA/HPβCD-IC was characterized by using phase solubility, X-ray diffraction (XRD), thermal gravimetric analysis (TGA), and proton nuclear magnetic resonance (<sup>1</sup>H-NMR). Computational modeling studies were also performed to investigate complexation in vacuum and in aqueous system. GA incorporated PLA nanofibers without HPβCD (PLA/GA-NF) were taken as a control sample. The morphological characterization of PLA/GA-NF and PLA/GA/HPβCD-IC-NF were carried out by scanning electron microscope (SEM). The release of GA from PLA/GA/HPβCD-IC-NF and PLA/GA-NF was determined in aqueous solution, 10% ethanol, and 95% ethanol by high

performance liquid chromatography (HPLC). The antioxidant activity of the GA present in PLA/GA/HP $\beta$ CD-IC-NF and PLA/GA-NF was evaluated using 2,2-diphenyl-1-picrylhydrazyl (DPPH) radical scavenging method.

## **2.2 Experimental**

### **2.2.1 Materials**

Polylactic acid (PLA) was donated by Natureworks (product code 6252D). Gallic acid (GA,  $\geq 97.5$ -102.5%, Sigma Aldrich), hydroxypropyl-beta-cyclodextrin (HP $\beta$ CD, Wacker Chemie AG, Germany), methanol (extra pure, Sigma Aldrich), ethanol (99.8%, Sigma Aldrich), dichloromethane (DCM, extra pure, Sigma Aldrich), N,N-dimethylformamide (DMF,  $\geq 99\%$ , Sigma Aldrich), acetonitrile (ACN, chromasol, Sigma Aldrich), deuterated dimethylsulfoxide (DMSO-d<sub>6</sub>, deuteration degree min 99.8% for NMR spectroscopy, Merck), 2,2-diphenyl-1-picrylhydrazyl (DPPH, Sigma Aldrich) were purchased and used as received without any further purification. Distilled-deionized water was supplied from Millipore milli-Q ultrapure water system.

### **2.2.2 Preparation of inclusion complex and physical mixture**

The formation of solid GA/HP $\beta$ CD-IC was prepared according to slurry method. Initially, GA was dissolved in aqueous solution; then HP $\beta$ CD was added and the mixture was stirred for 2 hours at 70°C. The mixture was kept in hood for 2 days and the resulting white powder was crashed in agate mortar. The molar ratio of GA:HP $\beta$ CD was used as 1:1. GA/HP $\beta$ CD-PM was obtained by mixing GA and HP $\beta$ CD in a glass mortar at a molar ratio of 1:1.

### **2.2.3 Preparation of electrospinning solutions**

Free GA and GA/HP $\beta$ CD-IC incorporated PLA nanofibers (PLA/GA-NF and PLA/GA/HP $\beta$ CD-IC-NF) were produced via electrospinning technique. For this purpose, Free GA (5%, w/w, with respect to polymer) was dissolved in DCM:DMF (7:3) at room temperature (RT). Then, 10% PLA (w/v) was added and PLA/GA solution was stirred for 2 hours before electrospinning. With regards to PLA/GA/HP $\beta$ CD-IC-NF; GA/HP $\beta$ CD-IC (5% GA, w/w, with respect to polymer) was dispersed in DCM:DMF (7:3) at RT. Afterwards, 10% PLA (w/v) was added, PLA/GA/HP $\beta$ CD-IC solution was stirred 2 hours prior to electrospinning. The vials were covered with a piece of aluminum foil during stirring to avoid any potential light effect for GA. As a reference sample, we have also electrospun 10% PLA solution (w/v) prepared in DCM:DMF (7:3). Table 2 summarizes the composition of the PLA, PLA/GA and PLA/GA/HP $\beta$ CD-IC solutions and the morphological findings of PLA-NF, PLA/GA-NF and PLA/GA/HP $\beta$ CD-IC-NF.

### **2.2.4 Electrospinning**

PLA, PLA/GA and PLA/GA/HP $\beta$ CD-IC solutions loaded into 3 ml plastic syringe with a needle inner diameter of 0.8 mm were placed horizontally on the pump. The solutions were sent towards to the collector at 1 ml/h rate by syringe pump (KD Scientific, KDS101). 15 kV was applied from a high voltage power supply (AU Series, Matsusada Precision Inc.). Cylindrical metal covered with aluminum foil was used as a collector. Distance between needle tip and collector was 10 cm. Experiments were performed at 24-25°C, 17-18% humidity.

## 2.2.5 Characterizations and measurements

Phase solubility measurements were performed in aqueous solution according to the method of Higuchi and Connors [161]. Excess amount of GA was added to 10 mL of water containing HP $\beta$ CD (ranging from 0 to 0.016 M). The equilibrium was achieved by stirring the solutions for 12 hours at RT, the suspensions were filtered through 0.45  $\mu$ m membrane filter to remove undissolved solid. GA concentration was determined spectrophotometrically at 259 nm (Varian, Cary 100). The stability constant ( $K_s$ ) of the complex was calculated from the phase solubility diagram according to the following equation:

$$K_s = \text{slope} / S_0(1 - \text{slope}) \quad (\text{Equation 1})$$

where  $S_0$  is the solubility of GA in the absence of HP $\beta$ CD. The phase diagram is a plot of the molar concentration of GA versus molar concentration of HP $\beta$ CD.

The crystalline structure of powder of GA, HP $\beta$ CD, GA/HP $\beta$ CD-IC and GA/HP $\beta$ CD-PM were recorded via X-ray diffraction (XRD, PANalytical X'Pert powder diffractometer) applying Cu K $\alpha$  radiation in a  $2\theta$  range 5 $^\circ$ -30 $^\circ$ .

Thermal gravimetric analysis (TGA, TA Q500, USA) was used to investigate the thermal properties of GA, HP $\beta$ CD, GA/HP $\beta$ CD-IC and GA/HP $\beta$ CD-PM in high resolution TGA mode (dynamic rate). The measurements were carried out under nitrogen atmosphere, and the samples were heated up to 500 $^\circ$ C at a constant heating rate of 20 $^\circ$ C/min.

The proton nuclear magnetic resonance ( $^1\text{H-NMR}$ ) spectra were recorded on Bruker DPX-400 at 400 MHz. 10 mg of GA, HP $\beta$ CD and GA/HP $\beta$ CD-IC was dissolved in 0.5 mL of d<sub>6</sub>-DMSO to evaluate the molar ratio of GA/HP $\beta$ CD-IC. Integration of the chemical shifts ( $\delta$ ) given in parts per million (ppm) was calculated by using Mestrenova software.

In order to investigate how the solution parameters affect the diameter of nanofibers, viscosity and conductivity measurements were done at RT. The viscosity of PLA, PLA/GA and PLA/GA/HP $\beta$ CD-IC solutions were analyzed via Anton Paar Physica MCR 301 rheometer equipped with a cone/plate accessory (spindle type CP40-2) at a constant shear rate of 100 1/sec and the conductivity of the above-mentioned solutions was measured with Inolab 720-WTW.

The morphology of PLA-NF, PLA/GA-NF and PLA/GA/HP $\beta$ CD-IC-NF was investigated by scanning electron microscopy (SEM, FEI-Quanta 200 FEG). Samples were mounted on metal stubs with double-sided adhesive copper tape and coated with 5 nm Au/Pd (PECS-682). Average fiber diameter (AFD) of the nanofibers was calculated from the SEM micrographs. At least 100 fibers were measured for each sample, and their averages and standard deviations were reported.

The cumulative amount of released GA from PLA/GA-NF and PLA/GA/HP $\beta$ CD-IC-NF were measured via high performance liquid chromatography (HPLC, Agilent, 1200 series) equipped with VWD UV detector and the detection was accomplished at 259 nm. Nanofibers (20 mg)

were individually immersed in 30 ml of aqueous solution, 10% ethanol and 95% ethanol and the solutions were stirred at RT at 50 rpm for 4 hours. The three medium were used to observe the release of GA in mediums having different polarity. 0.5 ml of sample solution was withdrawn at specified time intervals and an equal amount of fresh medium was refilled. The diol column (250 mm x 4.6 mm i.d., 5 $\mu$ m, Inertisil GL Sciences Inc.) operating at 1 ml/min with ACN:water (50:50) eluent was used for chromatographic separation. The calibration curves were obtained by dissolving GA in aqueous solution, 10% ethanol and 95% ethanol. The cumulative amount of GA released from nanofibers was converted to concentration (ppm) according to the calibration curves. The experiments were performed in triplicate and the results were reported as average values $\pm$ standard deviation. The loading efficiency (LE) (%) of PLA/GA-NF and PLA/GA/HP $\beta$ CD-IC-NF were determined by dissolving certain amount of nanofiber in DCM:DMF (7:3) and the amount of GA in the nanofiber was determined by HPLC using the calibration curve obtained in DCM:DMF (7:3) in triplicate. Finally, loading efficiency (%) was calculated according to the following equation:

$$\text{Loading efficiency (LE) (\%)} = C_e/C_t \times 100 \quad (\text{Equation 2})$$

where  $C_e$  is the concentration of encapsulated active compound and  $C_t$  is the total concentration of active compound.

Antioxidant tests for PLA-NF, PLA/GA-NF and PLA/GA/HP $\beta$ CD-IC-NF were performed via 2,2-diphenyl-1-picrylhydrazyl (DPPH) radical scavenging assay.

The nanofibers having equivalent amount of GA were immersed in 3 ml of  $10^{-4}$  M DPPH solution prepared in methanol in dark for 30 minutes at RT. The

mixtures were incubated in the dark at RT for 15 minutes. The absorbance of the solutions was measured by UV-Vis NIR spectroscopy (Varian, Cary 5000) at 517 nm. The absorbance of DPPH was defined as 100% and the antioxidant activities (%) were calculated according to the following equation:

$$\text{Antioxidant activity (\%)} = (A_{\text{control}} - A_{\text{sample}}) / A_{\text{control}} * 100 \quad (\text{Equation 3})$$

where  $A_{\text{control}}$  and  $A_{\text{sample}}$  represent the absorbance values of control DPPH solution and DPPH solution with nanofibers, respectively. The experiments were carried out in triplicate and the results were given as average values  $\pm$  standard deviation.

## 2.2.6 Computational method

We have performed ab initio calculations [162, 163] within the generalized gradient approximation [164] including Van der Waals correction [165], as implemented in the Vienna Ab initio simulation package [166, 167]. The pseudopotentials of all elements were described by projector augmented-wave method (PAW) [168] using a plane-wave basis set with a kinetic energy cutoff of 520 eV. The initial structure of HP $\beta$ CD was obtained from Cambridge Structural Database [169]. The guest molecule (GA), bare HP $\beta$ CD, and their IC were relaxed in vacuum using the conjugate gradient algorithm without any constraints by setting convergence criteria on the total energy and force to  $10^{-4}$  eV and  $10^{-2}$  eV/Å, respectively. In addition, as the existence of solvent could alter the inclusion complex formation dynamics by effecting intermolecular interactions, we also considered the solvent (water in this case) effect which is entirely based on implicit solvent model [170]. Combined with ab initio methods, this model splits the system into an explicit part for solute which is treated

quantum mechanically and an implicit part for solvent treated as a continuum. This solvent model takes into account dispersive interactions [171] and implemented in VASPsol as a patch of VASP [172, 173].

## **2.3 Results and discussion**

### **2.3.1 Phase solubility studies**

Phase solubility diagram obtained for GA/HP $\beta$ CD complex within the concentration range studied displayed typical A<sub>L</sub> type diagram (i.e. linear increment in the solubility of GA as a function of CD concentration), consistent with 1:1 molecular complex formation (Figure 9).

The stability constant ( $K_c$ ) is an important index associated with the drug release and represents the binding strength between guest and host (CD) [174].  $K_c$  determined according to equation 1 for GA/HP $\beta$ CD complex was 100 M<sup>-1</sup>, suggesting a weak interaction between GA and HP $\beta$ CD. This weak interaction might be because of the electrostatic interaction between solvent and GA nearby HP $\beta$ CD cavity as explained in modeling study.

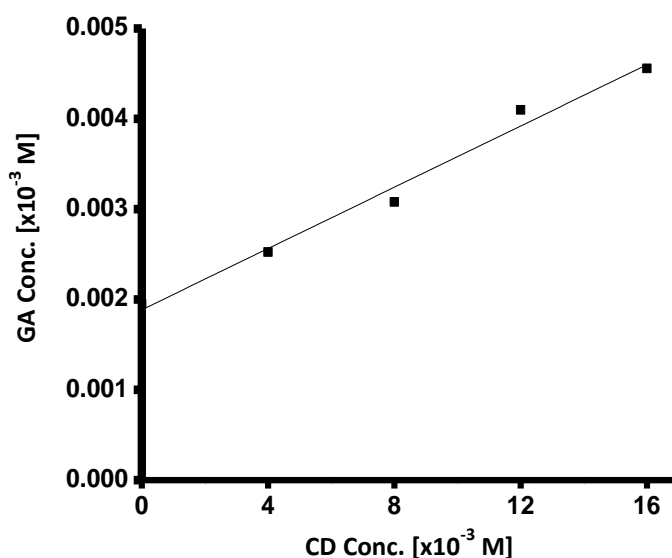


**Figure 9.** Phase solubility diagram of GA/HP $\beta$ CD system in water. (Copyright © 2016, Elsevier. Reprinted with permission from Ref. [117])

### 2.3.2 Structural characterization of inclusion complex

XRD analysis is used for the detection of inclusion complex formation between guest and host (CD) molecules. In case of inclusion complexation, the guest molecules are separated from each other due to the presence of CD cavities; so it is not possible to detect the crystalline peaks of guest molecules [175]. XRD patterns of GA, HP $\beta$ CD, GA/HP $\beta$ CD-IC and GA/HP $\beta$ CD-PM are shown in Figure 10. Several intense and sharp diffraction peaks at  $2\theta$  values of  $16.68^\circ$ ,  $25.54^\circ$  and  $27.85^\circ$  were observed in the diffraction pattern of GA. In contrast, no sharp peaks were observed in the diffraction pattern of HP $\beta$ CD; instead halo-pattern was recorded which is characteristic for amorphous compounds. We observed the characteristic crystalline peaks of GA with less intensity in the diffraction pattern of GA/HP $\beta$ CD-PM whereas no such peaks were observed in the case of GA/HP $\beta$ CD-IC. Therefore, the disappearance of characteristic peaks

of GA confirms the interaction between GA and HP $\beta$ CD and further leads to a conclusion that GA was probably included in the cavity of HP $\beta$ CD [176].

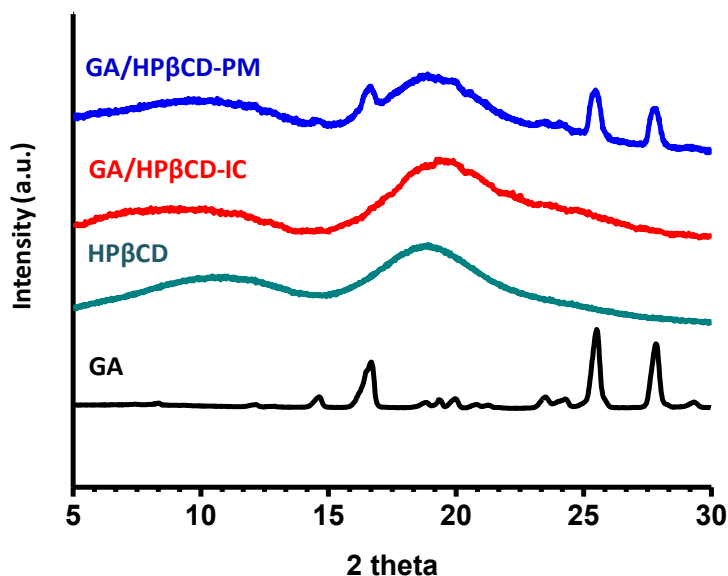


**Figure 10.** XRD patterns of GA, HP $\beta$ CD, GA/HP $\beta$ CD-IC, and GA/HP $\beta$ CD-PM. (Copyright © 2016, Elsevier. Reprinted with permission from Ref. [117])

### 2.3.3 Thermal analysis of inclusion complex

GA/HP $\beta$ CD-IC was further investigated by Hi-Res TGA to determine the thermal stability (Figure 11). Hi-Res TGA of GA, HP $\beta$ CD and GA/HP $\beta$ CD-PM was also shown for reference. GA exhibited two steps of weight loss, between 210°C and 325°C which correspond to the decomposition of GA. HP $\beta$ CD lost weight in two distinct steps, the former was loss of water molecules those are in the cavity; the latter that is after 295°C was the main decomposition of HP $\beta$ CD. In case of GA/HP $\beta$ CD-PM, there exist three weight losses which can be attributed to water, GA; GA and HP $\beta$ CD, respectively. The first weight loss occurred at temperatures below 100°C; the second and third weight losses range between 200°C to 250°C and 270°C to 400°C. So, the onset of thermal

degradation of GA has decreased slightly. GA/HP $\beta$ CD-IC exhibited weight losses in three stages. The first weight loss occurred at temperatures below 100°C can be ascribed to the water loss; the second and third weight losses range from 210°C to 250°C and 265°C to 400°C might correspond to GA and HP $\beta$ CD, respectively. So, it is concluded that the thermal stability of GA did not alter by complexation in contrast to GA/HP $\beta$ CD-PM. The observed results further confirm the complex formation [177]. In addition, the amount of GA in GA/HP $\beta$ CD-IC and GA/HP $\beta$ CD-PM were determined as ~10.2% and ~9.4% from TGA thermogram, respectively. The calculated amount of GA in GA/HP $\beta$ CD-IC correlates well with the initial amount of GA used for the preparation of complexation. Therefore, the initial amount of GA was preserved during the formation and storage in GA/HP $\beta$ CD-IC.

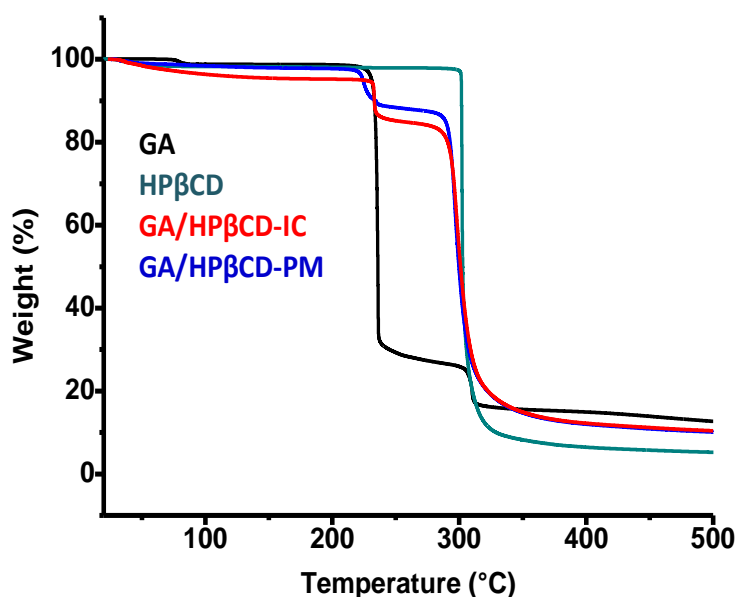


**Figure 11.** TGA thermograms of GA, HP $\beta$ CD, GA/HP $\beta$ CD-IC and GA/HP $\beta$ CD-PM. (Copyright © 2016, Elsevier. Reprinted with permission from Ref. [117])

### **2.3.4 The molar ratio of inclusion complex**

$^1\text{H-NMR}$  was used in order to determine the molar ratio of GA to HP $\beta$ CD. We have shown  $^1\text{H-NMR}$  spectra of GA, HP $\beta$ CD and GA/HP $\beta$ CD-IC in Figure 12. Firstly,  $^1\text{H-NMR}$  analysis was carried out for GA and HP $\beta$ CD to determine the characteristic peaks of their protons. The molar ratio of GA/HP $\beta$ CD-IC was decided as 0.64:1.00 (GA:HP $\beta$ CD) by taking integration the peak ratio of the characteristic chemical shifts of GA (6.9 ppm) and HP $\beta$ CD (1.0 ppm). Shortly, we revealed from  $^1\text{H-NMR}$  study that the initial molar ratio of GA:HP $\beta$ CD (1:1) was preserved to a great extent by complexation.

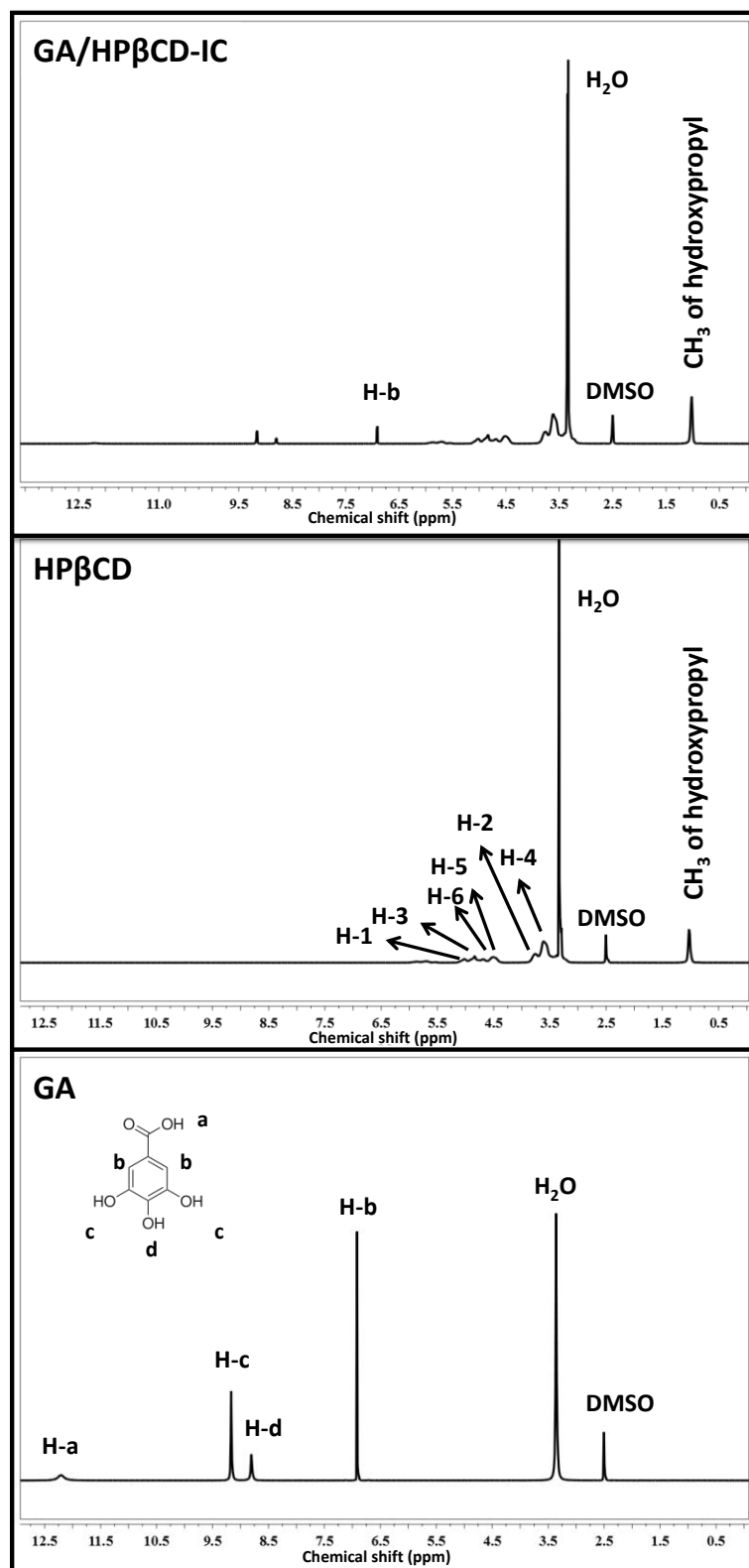


**Figure 12.**  $^1\text{H-NMR}$  spectra of GA, HP $\beta$ CD and GA/HP $\beta$ CD-IC. (Copyright © 2016, Elsevier. Reprinted with permission from Ref. [117])

### 2.3.5 Molecular modeling of inclusion complex

Since the inclusion process of the guest molecule within HP $\beta$ CD is driven by the energetics of inclusion process, we first fully optimized the initial structures of HP $\beta$ CD and GA separately in vacuum. HP $\beta$ CD is constructed manually by adding four 2-hydroxypropyl groups on the primary groups of  $\beta$ -CD corresponding to a substitution degree per anhydroglucose unit of 0.6 which was compatible with the experiments. To form IC, the guest molecule (single GA) is introduced into the cavity of a HP $\beta$ CD with tail and head orientations as shown in Figure 13. The complexation energy ( $E_{\text{comp}} = E_{\text{CD}} + E_{\text{guest}} - E_{\text{IC}}$ ), which is the difference between the total energies of HP $\beta$ CD ( $E_{\text{HP}\beta\text{CD}}$ ), the guest molecule ( $E_{\text{guest}}$ ), and the inclusion complex ( $E_{\text{IC}}$ ) has been calculated at various possible locations. Notably, GA prefers to stay at the center of the HP $\beta$ CD cavity due to better size match. Our calculations suggest that with tail orientation stronger complexation can be formed. When compared,  $E_{\text{comp}}$  is 24.67 kcal/mol in tail orientation, thus  $\sim 15.34$  kcal/mol higher than head orientation (9.33 kcal/mol). This result can be expected due to increasing polar interactions between hydroxyl groups with tail orientation. In either case, the complexation is driven by non-covalent interactions with no chemical bond formation between the guest molecule and the host (CD).

Having determined the lowest energy conformation of IC both in tail and head orientation in vacuum, we also envisaged solvent effect on complexation formation of these structures. Accordingly, water is implicitly taken into consideration as solvent. The structures are reoptimized in water and  $E_{\text{comp}}$  is calculated. Our analysis suggested that IC can also be formed in water for both

orientations. Lower  $E_{\text{comp}}$  in water when compared to vacuum can be explained by hydrophobic nature of HP $\beta$ CD cavity. A considerable electrostatic interaction occurs between solvent and GA nearby HP $\beta$ CD cavity. This results in weakening of van der Waals interaction between HP $\beta$ CD and GA which in turn decreases  $E_{\text{comp}}$ . Tail orientation is energetically still 12.69 kcal/mol more favorable (15.22 kcal/mol) than head orientation (2.53 kcal/mol) in solvent. In addition, the contribution of van der Waals interaction to the total energy of the inclusion complex do not show any significant difference for different orientations (-196.71 kcal/mol for tail orientation, -194.86 kcal/mol for head orientation) in water, suggesting more pronounced role for electrostatic interaction imposed by solvent effect of water in forming IC.

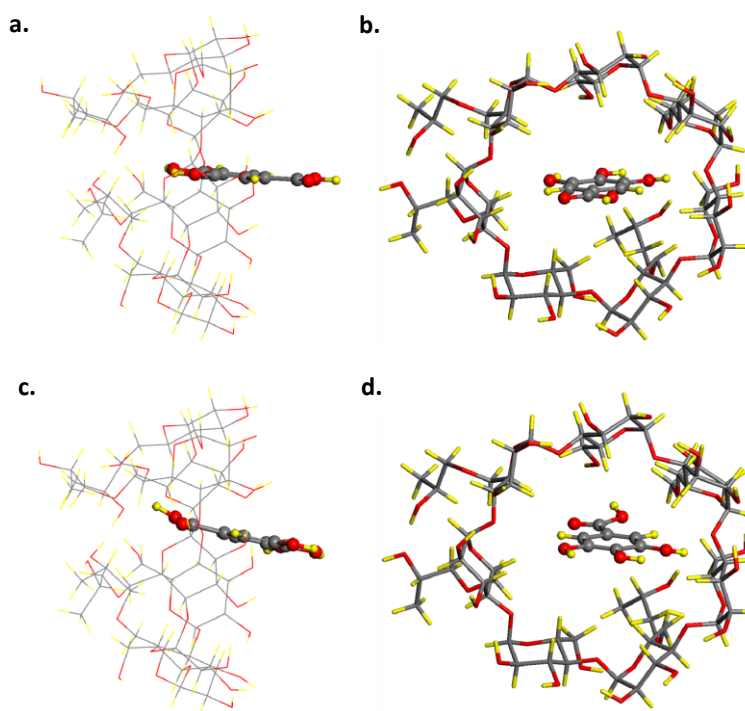


**Figure 13.** Top and side view of GA/HP $\beta$ CD-IC for (a)-(b) head and (c)-(d) tail orientation of GA. Gray, red, and yellow spheres represent carbon, oxygen, and hydrogen atoms, respectively. (Copyright © 2016, Elsevier. Reprinted with permission from Ref. [117])

### 2.3.6 Morphology analysis of nanofibers

SEM images and AFD distributions of PLA-NF, PLA/GA-NF and PLA/GA/HP $\beta$ CD-IC-NF are shown in Figure 14. AFD of PLA-NF, PLA/GA-NF and PLA/GA/HP $\beta$ CD-IC-NF were calculated to be  $320\pm 115$  nm,  $495\pm 105$  nm and  $235\pm 65$ , respectively. The difference in the AFD of nanofibers might be related with the viscosity and conductivity of the solutions. The solution properties of PLA, PLA/GA and PLA/GA/HP $\beta$ CD-IC, and the resulting electrospun nanofibers are shown in Table 2. The observed higher diameter of PLA/GA-NF as compared to PLA-NF is correlated with difference in the viscosity of solution. At the same time, it should be noted that higher conductivity might suppressed the increment in the diameter of PLA/GA-NF. It is obvious that the diameter of the fiber increases upon increasing the viscosity of a solution due to the higher chain entanglement in the polymer solution [3]. On the other hand, as the conductivity of a solution increases the diameter of the nanofibers decreases owing to the increment in the number of charges leading greater stretching of the polymer jet [3]. With respect to PLA/GA/HP $\beta$ CD-IC solution, the viscosity of solution was slightly higher than PLA/GA solution; so, the diameter of PLA/GA/HP $\beta$ CD-IC-NF was expected to be slightly higher than PLA/GA-NF. But considerably higher conductivity of PLA/GA/HP $\beta$ CD-IC solution as compared to PLA/GA solution leads to lower diameter of PLA/GA/HP $\beta$ CD-IC-NF. Moreover, encapsulation of both free GA and GA/HP $\beta$ CD-IC into PLA solution did not change the morphology of nanofibers other than the increment in the AFD of nanofibers.

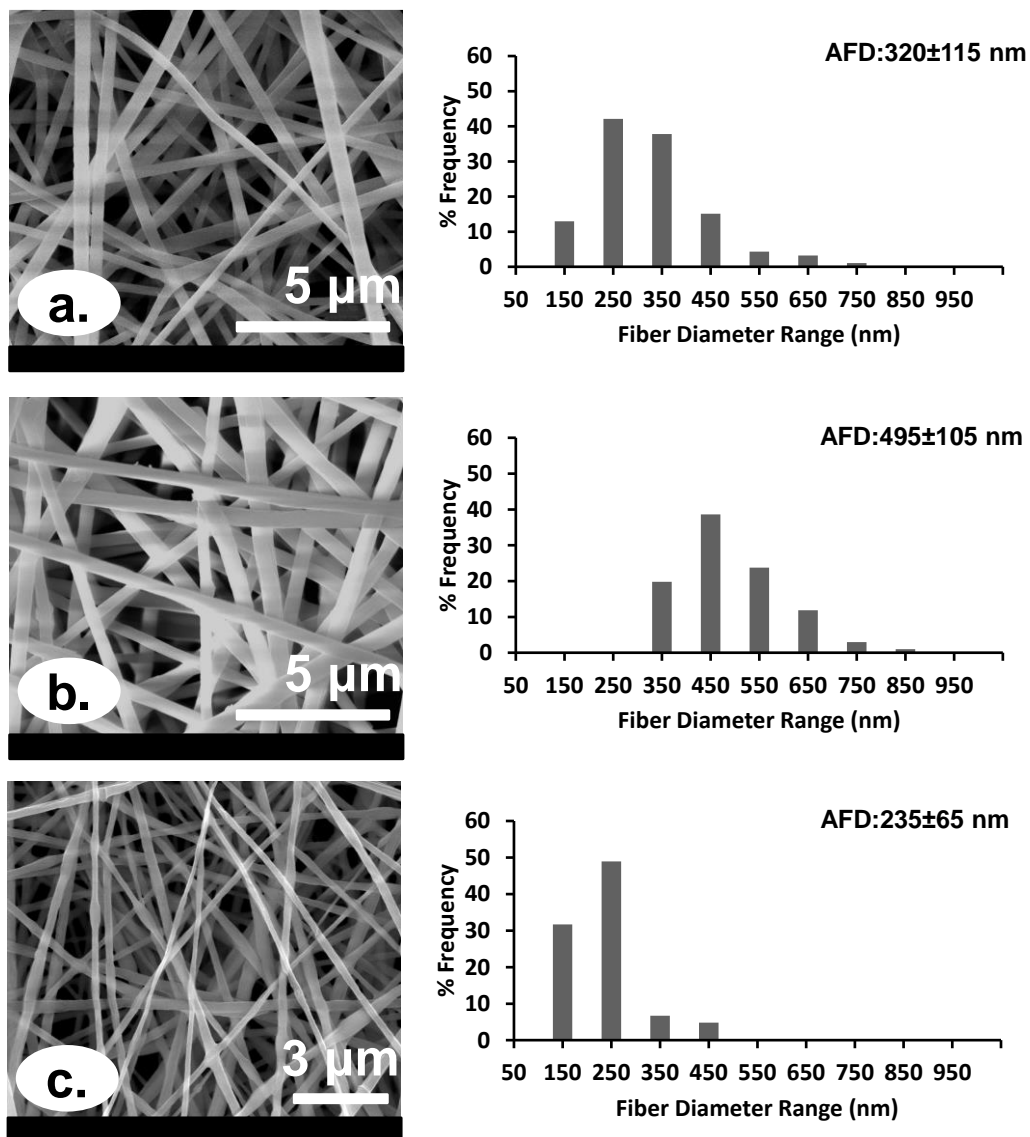


**Figure 14.** SEM images and fiber diameter distributions with average fiber diameter (AFD) of electrospun nanofibers obtained from solutions of (a) PLA, (b) PLA/GA, and (c) PLA/GA/HP $\beta$ CD-IC. (Copyright © 2016, Elsevier. Reprinted with permission from Ref. [117])

**Table 2.** The properties of the solutions used for electrospinning and morphological characteristics of the resulting nanofibers. (Copyright © 2016, Elsevier. Reprinted with permission from Ref. [117])

Solutions	% PLA <sup>a</sup> (w/v)	% HPβCD <sup>b</sup> (w/w)	% GA <sup>b</sup> (w/w)	Viscosity (Pa·s)	Conductivity (μS/cm)	Average fiber diameter (nm)	Fiber morphology
PLA	10	-	-	0.15	0.16	320±115	Bead free nanofibers
PLA/GA	10	-	5	0.18	0.30	495±105	Bead free nanofibers
PLA/GA/HPβCD-IC	10	43	5	0.22	14.13	235±65	Bead free nanofibers

<sup>a</sup> with respect to solvent (DCM:DME, 7:3)

<sup>b</sup> with respect to polymer (PLA).

### 2.3.7 In vitro release study

The release of GA from PLA/GA-NF and PLA/GA/HP $\beta$ CD-IC-NF into three different mediums (aqueous solution, 10% ethanol and 95% ethanol which are aqueous, alcoholic and fatty food simulants, respectively) was measured at RT via HPLC and the results are shown concentration (ppm) versus of time in Figure 15. Loading efficiency (LE) (%) of nanofibers was determined as  $80\pm 0.7\%$  and  $75\pm 0.7\%$  for PLA/GA-NF and PLA/GA/HP $\beta$ CD-IC-NF, respectively by using equation 2. The release of GA from PLA/GA-NF and PLA/GA/HP $\beta$ CD-IC-NF shows similar behavior in all three mediums. The release of GA has reached steady state followed by fast release at the initial stage. In general, the surface area and the type of the medium are of great significance for the total amount of compound released and its release rate. In aqueous solution and 10% ethanol, higher amount of GA was released in total from PLA/GA/HP $\beta$ CD-IC-NF compared to PLA/GA-NF, since CDs increase the solubility of guests and the concentration of diffusible species from polymeric systems in aqueous solutions [178]. In addition, the surface area of PLA/GA/HP $\beta$ CD-IC-NF was most likely higher than PLA/GA-NF due to the lower AFD of PLA/GA/HP $\beta$ CD-IC-NF. Therefore, the other reason of higher amount of GA released from PLA/GA/HP $\beta$ CD-IC-NF could be the higher surface area of PLA/GA/HP $\beta$ CD-IC-NF compared to PLA/GA-NF that provides more contact with the medium. On the other hand, the solubility of GA in ethanol is quite high [179]; therefore, PLA/GA-NF released more amount of GA in total into 95% ethanol when compared with PLA/GA/HP $\beta$ CD-IC-NF.

Moreover, GA released from PLA/GA-NF is the highest into 95% ethanol among three systems.

The rate of GA released into aqueous solution and 10% ethanol was slower from PLA/GA-NF compared to PLA/GA/HP $\beta$ CD-IC-NF; whereas GA released slower into 95% ethanol from PLA/GA/HP $\beta$ CD-IC-NF compared with PLA/GA-NF. The difference in the rate of GA released from nanofibers was most likely due to the solubility variance of GA in different mediums. Additionally, accelerated release rate of drug was also related with the dissolution of CD-IC upon contact with water that increases the porosity of the matrix [178]. In addition, CDs not only enhance the aqueous solubility of hydrophobic guests but also act as a hydrating agent that promotes the diffusion of water into the matrix [178]. As a result, PLA/GA/HP $\beta$ CD-IC-NF could be used to provide quick release into aqueous solution and 10% ethanol. At the same time this material might prevent initial oxidation and reduce the required amount of antioxidant agent due to the considerably high solubility of GA. On the contrary, PLA/GA/HP $\beta$ CD-IC-NF could serve as a slow release material for 95% ethanol system.

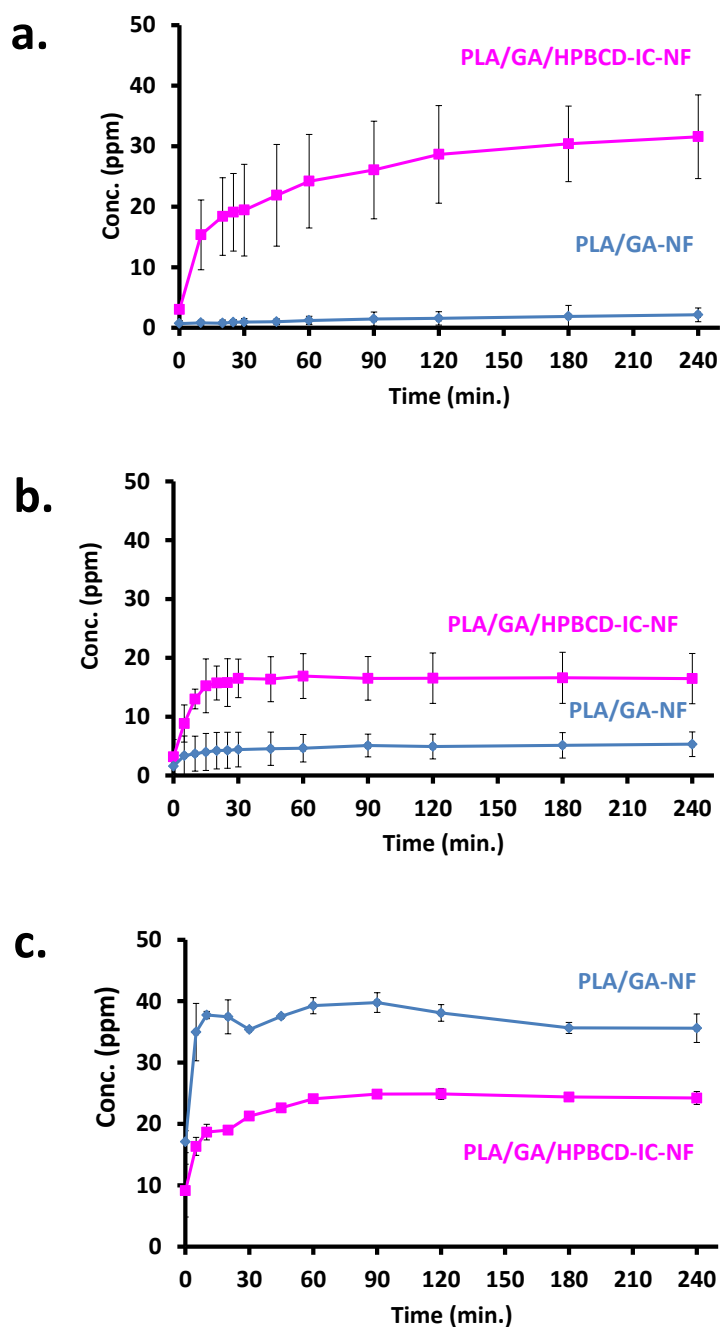


**Figure 15.** The cumulative release of GA from PLA/GA-NF and PLA/GA/HPβCD-IC-NF into (a) water, (b) 10% ethanol, and (c) 95% ethanol (n = 3). The error bars in the figure represent the standard deviation (SD). (Copyright © 2016, Elsevier. Reprinted with permission from Ref. [117])

### 2.3.8 Antioxidant activity

Phenolic compounds possess electron and/or hydrogen donor ability; therefore, they exhibit antioxidant activity. Molecules having hydroxyl groups in ortho position like GA, catechin with three hydroxyl groups bound to the aromatic ring is known to be effective phenolic compounds [180]. Here, we investigated the antioxidant capacity of GA in PLA/GA-NF and PLA/GA/HP $\beta$ CD-IC-NF using DPPH radical scavenging assay. The assay is based on the reduction and neutralization of DPPH which is a stable free radical in the presence of hydrogen donating antioxidants. Furthermore, the color of DPPH solution turns into yellow with the addition of antioxidant molecule into the solution [181]. The antioxidant activity of PLA-NF, PLA/GA-NF and PLA/GA/HP $\beta$ CD-IC-NF was calculated according to equation 3 as  $4\pm 0.014\%$ ,  $95\pm 0.006\%$  and  $96\pm 0.002\%$ , respectively. The photographs of the DPPH solution before reaction; PLA-NF, PLA/GA-NF and PLA/GA/HP $\beta$ CD-IC-NF after the reaction are shown in Figure 16. As expected, PLA-NF had quite low amount of antioxidant activity which might be related with the absorption of DPPH solution due to the high surface area of the nanofibers providing more contact with medium [182]. The color of the solution was still purple as shown in Figure 16. The antioxidant activity of PLA/GA/HP $\beta$ CD-IC-NF was slightly higher than PLA/GA-NF and the color of both of the solutions was pale yellow which means that there was no more DPPH molecule to deactivate in solutions. The almost same antioxidant activity of nanofibers might be explained by the quite high solubility of GA in alcohols [179] and position of GA in the cavity of CDs. According to modeling study insertion of GA into cavity from the tail

orientation is energetically more favorable, so hydroxyl groups might not be in the cavity of CD. Otherwise, it is not possible for antioxidants to donate hydrogen from their hydroxyl groups to DPPH molecule and the reaction would not take place. Moreover, electrospinning had no negative effect on the antioxidant property of GA since PLA/GA-NF and PLA/GA/HP $\beta$ CD-IC-NF still had quite high amount of antioxidant activity.

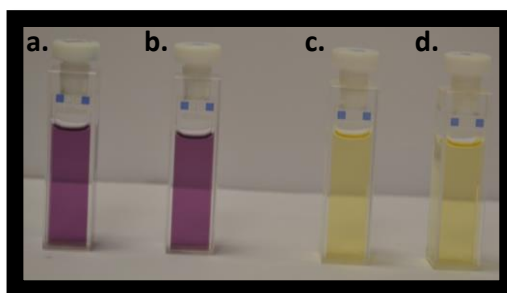


**Figure 16.** The photographs of (a) DPPH solution (before reaction); DPPH solutions in which (b) PLA-NF, (c) PLA/GA-NF and (d) PLA/GA/HP $\beta$ CD-IC-NF was immersed (after reaction). (Copyright © 2016, Elsevier. Reprinted with permission from Ref. [117])

## 2.4 Conclusion

Here, functional electrospun PLA nanofibers incorporating naturally occurring antioxidant compound; GA, was produced by electrospinning. The release of PLA/GA-NF and PLA/GA/HP $\beta$ CD-IC-NF was evaluated in three different medium: aqueous solution, 10% ethanol, and 95% ethanol. PLA/GA/HP $\beta$ CD-IC-NF exhibited fast release of GA in aqueous solution and 10% ethanol; however, PLA/GA/HP $\beta$ CD-IC-NF had shown slow release of GA in 95% ethanol. In addition, higher amount of GA release was achieved from PLA/GA/HP $\beta$ CD-IC-NF in aqueous solution and 10% ethanol compared to PLA/GA-NF due to the higher solubility of GA in aqueous based systems by

complexation with HP $\beta$ CD. Finally, high antioxidant activity was seen for both PLA/GA/HP $\beta$ CD-IC-NF and PLA/GA-NF. In brief, PLA/GA/HP $\beta$ CD-IC-NF having controlled release in three different mediums and quite high antioxidant activity was successfully produced. The observed results strongly suggested that PLA/GA/HP $\beta$ CD-IC-NF having antioxidant property which might be applicable as a food packaging material to increase the shelf life of food products and improve the overall food quality.

### **3. Developing antioxidant food packaging using $\alpha$ -tocopherol/ $\gamma$ -cyclodextrin-inclusion complex incorporated polylactic acid nanofibers produced via electrospinning**

#### **3.1 Introduction**

Oxidative reactions are a great problem for both natural and processed food products and presence of lipids in the products are the main reason of food spoilage as a result of lipid oxidation [183]. Once the food is deteriorated, its quality is reducing due to the release of off-odours and off-flavours, color and texture change and nutrition losses [183, 184]. Finally, the shelf life of the product becomes too short. That's why, active packaging systems are being used to prevent the lipid oxidation in food products [183, 184]. One of the most widely used strategy to do this is incorporating antioxidant agents into packaging material due to its sustained release ability of antioxidant agents during the storage as well [183, 184].

Polylactic acid (PLA) is a type of aliphatic polyester that is widely used in biological applications owing to its biocompatible and biodegradable nature [25, 39, 40, 185, 186]. In addition to these advantages, its carbon dioxide, oxygen and water permeability, and light barrier properties make it ideal candidate for packaging applications [160]. Furthermore, it has also some advantages like possibility to be produced by a renewable source (corn) [187], consumption of high amount of carbon dioxide during production, and recyclability [160].

$\gamma$ -CD (Figure 17b-c) is a kind of native CD constituted by 8 glucopyranose unit. When compared to two other native CDs ( $\alpha$ -CD and  $\beta$ -CD),  $\gamma$ -CD its size is bigger, solubility is higher and bioavailability is more pronounced. It was declared that it has no side effects on the absorption of nutrients in food products and nutraceutical applications [188].

$\alpha$ -Tocopherol ( $\alpha$ -TC) (Figure 17a) is the main component of vitamin E and find broad application in drug delivery and wound dressing [28, 189]. The main limitation of  $\alpha$ -TC is its poor solubility in aqueous solution and it is also sensitive to oxygen, light, alkali pH, trace of transition metal ions [190]. CDs arise much interest recently in order to eliminate the drawbacks of  $\alpha$ -TC by complexation. Therefore, CD-ICs of  $\alpha$ -TC were employed to enhance the solubility [191, 192] and protect against oxidation of food products [61]. Moreover, CD-ICs of  $\alpha$ -TC were incorporated into polymeric films to reduce the diffusion rate of  $\alpha$ -TC [193], retard the oxidation of the packaged food during the storage period [194], and prolong the shelf life of food products [158].

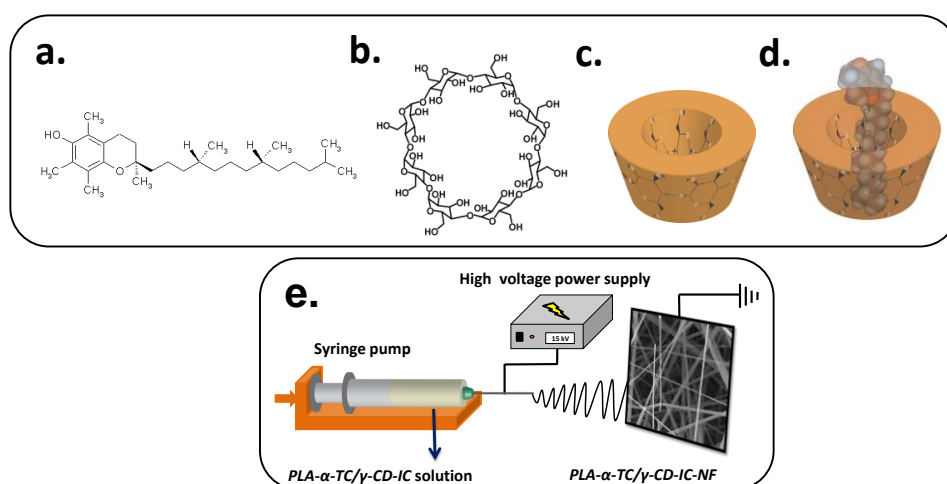


**Figure 17.** Chemical structure of (a)  $\alpha$ -TC, (b)  $\gamma$ -CD; schematic representation of (c)  $\gamma$ -CD, (d) formation of  $\alpha$ -TC/ $\gamma$ -CD-IC, and (e) electrospinning of nanofibers from PLA/ $\alpha$ -TC/ $\gamma$ -CD-IC solution.

In the present study, inclusion complex of  $\alpha$ -TC and  $\gamma$ -CD (Figure 17d) was synthesized ( $\alpha$ -TC/ $\gamma$ -CD-IC) and then added to PLA solution to produce nanofibers by electrospinning (PLA/ $\alpha$ -TC/ $\gamma$ -CD-IC-NF) (Figure 17e). The characterization of  $\alpha$ -TC/ $\gamma$ -CD-IC was done by X-ray diffraction (XRD), thermal gravimetric analysis (TGA), and proton nuclear magnetic resonance ( $^1\text{H-NMR}$ ) techniques. The morphological characterization of PLA/ $\alpha$ -TC/ $\gamma$ -CD-IC-NF and PLA/ $\alpha$ -TC-NF which was produced as reference sample were performed by scanning electron microscope (SEM). In vitro release of  $\alpha$ -TC from PLA/ $\alpha$ -TC/ $\gamma$ -CD-IC-NF and PLA/ $\alpha$ -TC-NF was decided in 95% ethanol by high performance liquid chromatography (HPLC). The antioxidant activity in PLA/ $\alpha$ -TC/ $\gamma$ -CD-IC-NF and PLA/ $\alpha$ -TC-NF was determined using 2,2-diphenyl-1-picrylhydrazyl (DPPH) radical scavenging method. Finally, PLA/ $\alpha$ -TC/ $\gamma$ -CD-IC-NF and PLA/ $\alpha$ -TC-NF were applied to raw beef samples to investigate their prevention on lipid oxidation via thiobarbituric acid reactive substance determination.

## **3.2 Experimental**

### **3.2.1 Materials**

Polylactic acid (PLA) was donated by Natureworks (product code 6252D).  $\alpha$ -Tocopherol ( $\alpha$ -TC,  $\geq 96\%$ , Sigma Aldrich), gamma-cyclodextrin ( $\gamma$ -CD, Wacker Chemie AG, Germany), thiobarbituric acid ( $\geq 98\%$ , Sigma Aldrich), methanol (extra pure, Sigma Aldrich), ethanol (99.8%, Sigma Aldrich), dichloromethane (DCM, extra pure, Sigma Aldrich), N,N-dimethylformamide (DMF,  $\geq 99\%$ , Sigma Aldrich), trichloroacetic acid (TCA, 99.5%, VWR), deuterated

dimethylsulfoxide (DMSO-d<sub>6</sub>, deuteration degree min 99.8% for NMR spectroscopy, Merck), 2,2-diphenyl-1-picrylhydrazyl (DPPH, Sigma Aldrich) were purchased and used as-received without any further purification. Distilled-deionized water was supplied from Millipore milli-Q ultrapure water system.

### **3.2.2 Preparation of inclusion complex**

The formation of solid  $\alpha$ -TC/ $\gamma$ -CD-IC at 1:1 molar ratio was done according to freeze-drying method. Initially,  $\gamma$ -CD was dissolved in aqueous solution; then  $\alpha$ -TC was added to that solution while keeping the solution stirred. After mixing the solution overnight, it was freeze-dried at -80°C for 24 hours. Afterwards, the mixture was kept in lyophilizer for 48 hours.

### **3.2.3 Preparation of electrospinning solutions**

$\alpha$ -TC and  $\alpha$ -TC/ $\gamma$ -CD-IC encapsulated PLA nanofibers (PLA/ $\alpha$ -TC-NF and PLA/ $\alpha$ -TC/ $\gamma$ -CD-IC-NF) were obtained through electrospinning.  $\alpha$ -TC (5%, w/w, with respect to polymer) was dissolved in DCM:DMF (7:3) solvent system at room temperature (RT). Then, 10% PLA (w/v) was added and the solution was stirred for 2 hours prior to electrospinning process. PLA/ $\alpha$ -TC/ $\gamma$ -CD-IC-NF,  $\alpha$ -TC/ $\gamma$ -CD-IC (5%  $\alpha$ -TC, w/w, with respect to polymer) was dispersed in DCM:DMF (7:3) at RT. Then, 10% PLA (w/v) was added to  $\alpha$ -TC/ $\gamma$ -CD-IC solution (PLA/ $\alpha$ -TC/ $\gamma$ -CD-IC) and the resulting solution was stirred 2 hours before electrospinning. The vials were covered with aluminum foil during stirring period to avoid any potential light effect. As another reference sample, we also electrospun 10% PLA solution (w/v) in DCM:DMF

(7:3). Table 3 summarizes the composition of the PLA, PLA/ $\alpha$ -TC and PLA/ $\alpha$ -TC/ $\gamma$ -CD-IC solutions.

**Table 3.** The composition of the solutions used for electrospinning.

Solutions	% PLA <sup>a</sup> (w/v)	% $\gamma$ -CD <sup>b</sup> (w/w)	% $\alpha$ -TC <sup>b</sup> (w/w)
PLA	10	-	-
PLA/ $\alpha$ -TC	10	-	5
PLA/ $\alpha$ -TC/ $\gamma$ -CD-IC	10	15	5

<sup>a</sup> with respect to solvent (DCM:DMF, 7:3)

<sup>b</sup> with respect to polymer (PLA).

### 3.2.4 Electrospinning

PLA, PLA/ $\alpha$ -TC and PLA/ $\alpha$ -TC/ $\gamma$ -CD-IC solutions in 3 ml plastic syringe (needle inner diameter: 0.8 mm) were loaded horizontally on the syringe pump. The solutions were fed through the collector at 1 ml/h rate by syringe pump (KD Scientific, KDS101). 15 kV was applied from a high voltage power supply (AU Series, Matsusada Precision Inc.). Metal covered with a piece of aluminum foil was used as a collector. Distance between needle tip and collector was 10 cm. Experiments were performed at 25°C, 18% humidity.

### 3.2.5 Characterizations and measurements

The crystalline structure of powder of  $\gamma$ -CD and  $\alpha$ -TC/ $\gamma$ -CD-IC were decided by X-ray diffraction (XRD, PANalytical X'Pert powder diffractometer) applying Cu K $\alpha$  radiation in a  $2\theta$  range 5°-30°. Since  $\alpha$ -TC is a liquid compound at RT, XRD analysis was not run for pure  $\alpha$ -TC.

Thermal stability of  $\alpha$ -TC,  $\gamma$ -CD, and  $\alpha$ -TC/ $\gamma$ -CD-IC was investigated via thermal gravimetric analysis (TGA, TA Q500, USA). The measurements were carried out under nitrogen atmosphere, and the samples were heated up to 500°C at a constant heating rate of 20°C/min.

The proton nuclear magnetic resonance ( $^1\text{H-NMR}$ ) spectra were recorded on Bruker DPX-400 at 400 MHz. In order to determine the molar ratio of  $\alpha$ -TC/ $\gamma$ -CD-IC, 20 mg/mL of  $\alpha$ -TC,  $\gamma$ -CD, and  $\alpha$ -TC/ $\gamma$ -CD-IC were dissolved in  $d_6$ -DMSO. Integration of the chemical shifts ( $\delta$ ) given in parts per million (ppm) was calculated by using Mestrenova software.

The morphological characterization of PLA-NF, PLA/ $\alpha$ -TC-NF and PLA/ $\alpha$ -TC/ $\gamma$ -CD-IC-NF was carried out using scanning electron microscopy (SEM, FEI-Quanta 200 FEG). Samples were stucked on metal stubs with double-sided adhesive copper tape and then coated with 5 nm Au/Pd (PECS-682). The calculation of average fiber diameter (AFD) of each nanofiber was made from the SEM micrographs taken. At least 100 fibers were measured for each sample, and their averages and standard deviations were reported.

In order to determine  $\alpha$ -TC released from PLA/ $\alpha$ -TC-NF and PLA/ $\alpha$ -TC/ $\gamma$ -CD-IC-NF, 20 mg of nanofibers were individually immersed in 30 ml of 95% ethanol and the solutions were stirred at RT at 50 rpm for 6 hours. 0.5 ml of sample solution was withdrawn at specified time intervals and equal amount of fresh medium was refilled. Then, the amount was decided by high performance liquid chromatography (HPLC, Agilent, 1200 series) equipped with VWD UV detector. C18 column (Agilent, column dimension: 4.6 mm 150 mm, particle

size: 5  $\mu\text{m}$ .) operating at 1 ml/min with 98:2 methanol:water (v/v) eluent was used for chromatographic separation. The detection was accomplished at 292 nm. The calibration curve was prepared to convert area values to concentration (ppm). The experiments were performed in triplicate and the results were reported as average values  $\pm$  standard deviation.

Antioxidant tests for PLA/ $\alpha$ -TC-NF and PLA/ $\alpha$ -TC/ $\gamma$ -CD-IC-NF were performed according to 2,2-diphenyl-1-picrylhydrazyl (DPPH) radical scavenging assay. For this purpose, nanofibers having equivalent amount of  $\alpha$ -TC were immersed in 3 ml of  $10^{-4}$  M DPPH solution prepared in methanol and then the mixtures were kept in dark at RT for 15 minutes. Lastly, the absorbance of the solutions was measured by UV-Vis spectroscopy (Varian, Cary 100) at 517 nm. In order to calculate antioxidant activity (%), the absorbance of DPPH was defined as 100% and the antioxidant activities (%) were calculated based on the following equation:

$$\text{Antioxidant activity (\%)} = (A_{\text{control}} - A_{\text{sample}}) / A_{\text{control}} * 100 \quad (\text{Equation 4})$$

where  $A_{\text{control}}$  and  $A_{\text{sample}}$  represent the absorbance values of control DPPH solution and DPPH solution with nanofibers, respectively.

Oxidative stability was evaluated by changes in thiobarbituric acid reactive substances (TBARS). Lipid oxidation was analyzed in raw beef samples (control) which was purchased from local market and raw beef samples packed with PLA/ $\alpha$ -TC-NF and PLA/ $\alpha$ -TC/ $\gamma$ -CD-IC-NF put into polyethylene zip bags (Figure 18) subjected to refrigerated storage for 4, 7, 10, 14, 21 and 28 days. At certain time intervals the meat samples were taken out and TBARS were calculated based on the method of Nisa et al. [195].



**Figure 18.** The photographs of raw beef samples and raw beef samples packed with nanofibers in polyethylene zip bags.

The procedure is as follows: 5 g of meat sample was homogenized in 35 ml of 7.5% trichloroacetic acid. The homogenized sample was centrifuged ( $3000\times g$ , 2 min) and 5 ml of the supernatant was mixed with 5 ml of 20 mM thiobarbituric acid; finally the solution was mixed and kept in the dark for 20 h at  $24^{\circ}\text{C}$ . The pink color that formed was measured spectrophotometrically (UV-Spectrophotometer, Shimadzu, Japan) at 532 nm. Results were expressed as mg malonaldehyde (MDA) per kg (mg MDA/kg) of sample. TBARS determinations for each sample were performed in triplicate.

### **3.3 Results and discussion**

#### **3.3.1 Structural characterization of inclusion complex**

XRD was used to prove whether the complexation is formed or not between  $\alpha$ -TC/ $\gamma$ -CD-IC. But, since  $\alpha$ -TC has a liquid nature at RT we could not run XRD for this molecule. XRD patterns of  $\gamma$ -CD and  $\alpha$ -TC/ $\gamma$ -CD-IC is shown in Figure 19. It is a known fact that cage-type packing crystal structure of native CDs turn into channel-type, once they form an IC with a guest molecule [196]. As seen from the graph, the crystalline peaks of  $\gamma$ -CD disappeared in  $\alpha$ -TC/ $\gamma$ -CD-IC and

new peaks are observed corresponding to hexagonal channel-type packing of  $\gamma$ -CD. Therefore, we can deduce that the formation between  $\alpha$ -TC and  $\gamma$ -CD was achieved.

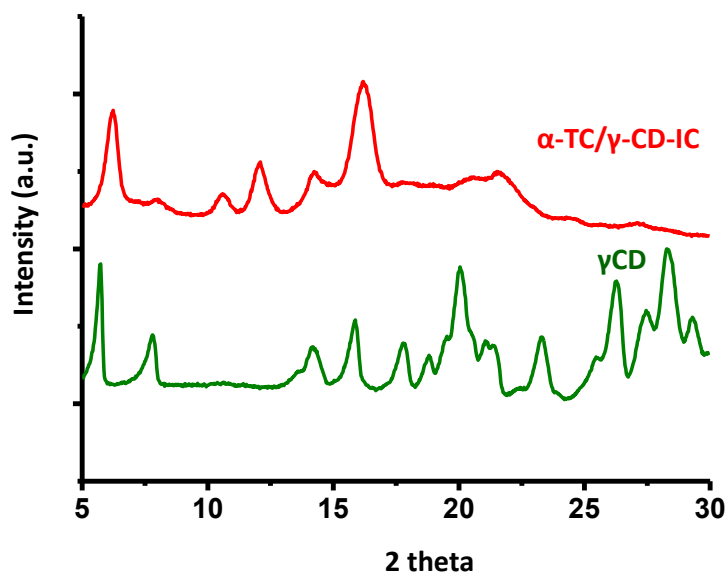


**Figure 19.** XRD patterns of  $\gamma$ -CD and  $\alpha$ -TC/ $\gamma$ -CD-IC.

### 3.3.2 Thermal analysis of inclusion complex

The thermal stability of  $\alpha$ -TC/ $\gamma$ -CD-IC was further investigated by TGA (Figure 20). TGA measurement of  $\alpha$ -TC and  $\gamma$ -CD was done as well for reference.  $\alpha$ -TC has a weight loss from 175°C to 385°C and this weight loss belongs to the thermal degradation of  $\alpha$ -TC. The weight loss of  $\gamma$ -CD is occurred in two steps, first corresponding to water loss and the second one attributed to the main decomposition of CD.  $\alpha$ -TC/ $\gamma$ -CD-IC exhibited three weight loss steps. These weight losses ascribed to water, thermal degradation of  $\alpha$ -TC, decomposition of CD, respectively. As seen from the graph, thermal stability of  $\alpha$ -TC did not reduce or improve by complexation [61]. TGA data was also used to determine

the amount of  $\alpha$ -TC in  $\alpha$ -TC/ $\gamma$ -CD-IC and it was found as 22.3% which is quite close to the theoretic amount used (24.9%).

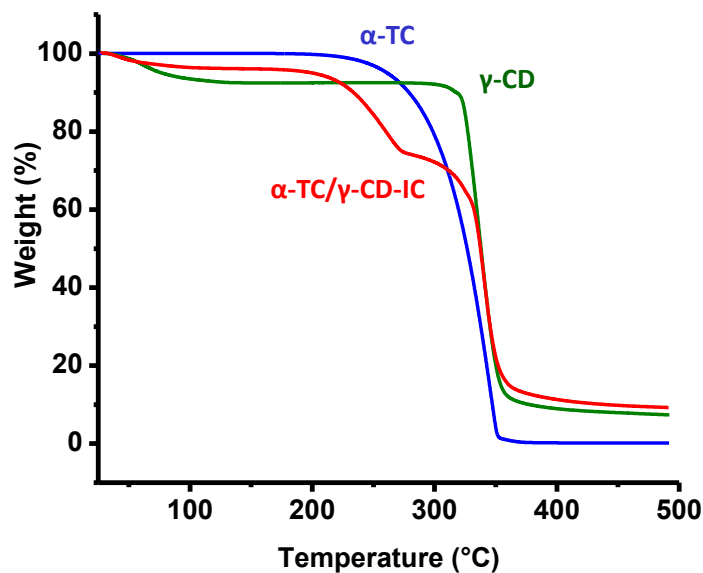


**Figure 20.** TGA thermograms of  $\alpha$ -TC,  $\gamma$ -CD, and  $\alpha$ -TC/ $\gamma$ -CD-IC.

### 3.3.3 The molar ratio of inclusion complex

The molar ratio in  $\alpha$ -TC/ $\gamma$ -CD-IC was calculated by  $^1\text{H-NMR}$  and the results are given in Figure 21. First of all,  $^1\text{H-NMR}$  spectra were recorded for  $\alpha$ -TC and  $\gamma$ -CD molecules to decide the peaks of the protons. Then, while calculating the molar ratio the peak at 2.0 ppm and 4.9 ppm were used for  $\alpha$ -TC and  $\gamma$ -CD, respectively. So, the molar ratio of  $\alpha$ -TC/ $\gamma$ -CD-IC was determined as 0.89:1.00 from  $^1\text{H-NMR}$  calculations.

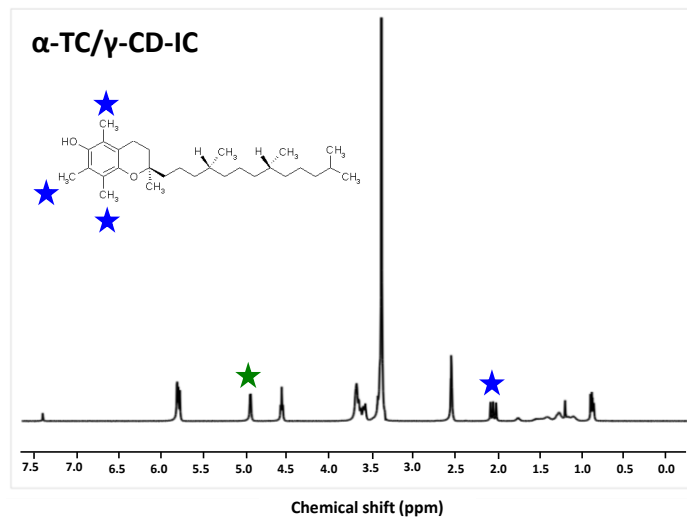


**Figure 21.**  $^1\text{H-NMR}$  spectra of  $\alpha$ -TC/ $\gamma$ -CD-IC.

### 3.3.4 Morphology analysis of nanofibers

The morphology of PLA-NF, PLA/ $\alpha$ -TC-NF and PLA/ $\alpha$ -TC/ $\gamma$ -CD-IC-NF was investigated by SEM. SEM images and AFD distributions are shown in Figure 22. As seen from the images, bead-free nanofibers were successfully obtained at 10% PLA (w/v) concentration. The diameter of PLA-NF, PLA/ $\alpha$ -TC-NF and PLA/ $\alpha$ -TC/ $\gamma$ -CD-IC-NF were calculated as  $300\pm 90$  nm,  $320\pm 120$  nm and  $265\pm 120$  nm, respectively. The difference in the AFD of nanofibers might be related with the viscosity and conductivity of the solutions [3]. In addition, encapsulation of  $\alpha$ -TC and  $\alpha$ -TC/ $\gamma$ -CD-IC into PLA solution did not change the morphology of nanofibers; thus, we could obtain bead-free nanofibers by using same concentration of PLA.

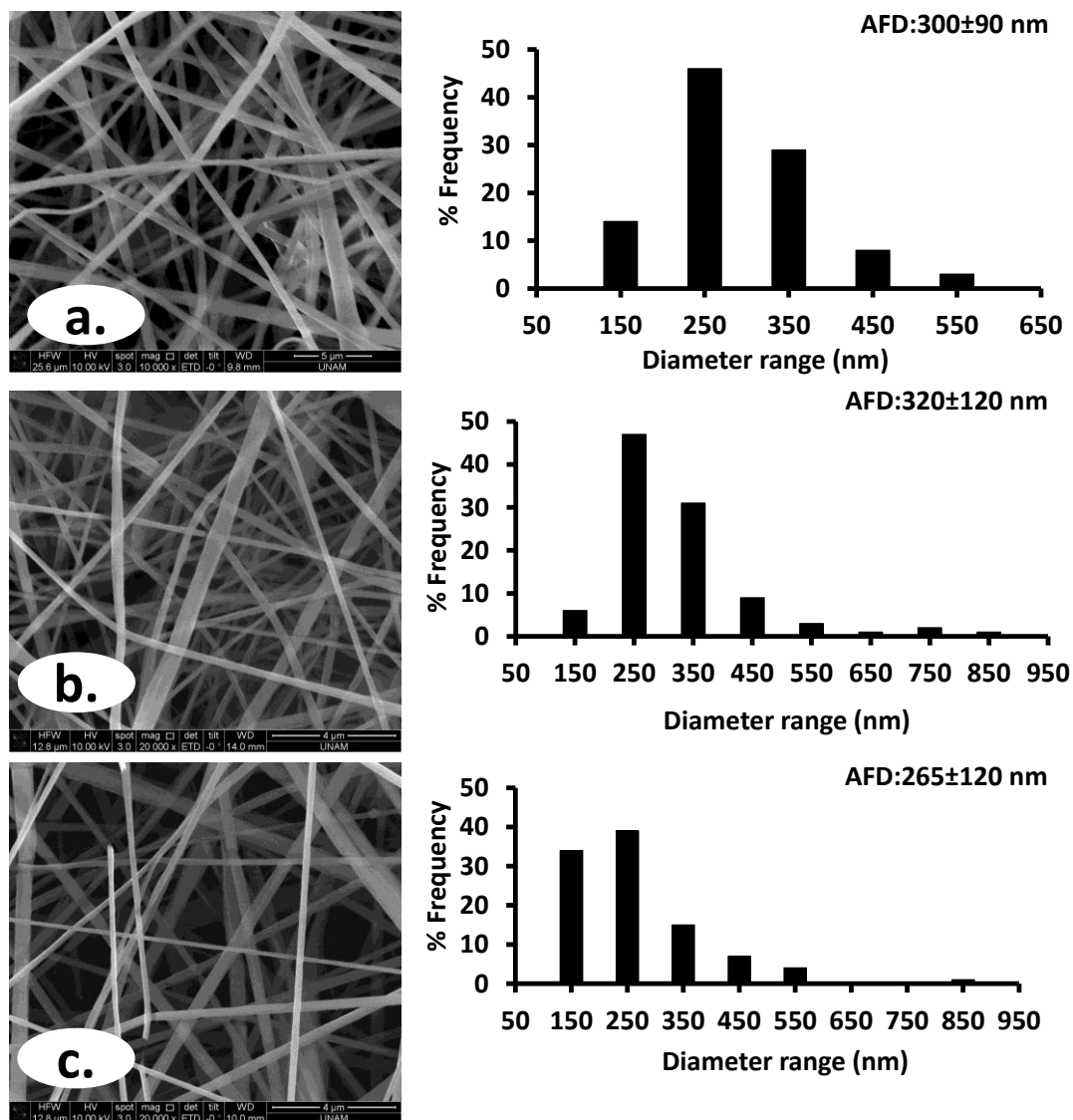


**Figure 22.** SEM images of PLA-NF, PLA/α-TC-NF, and PLA/α-TC/γ-CD-IC-NF.

### 3.3.5 In vitro release study

The release studies of α-TC from PLA/α-TC-NF and PLA/α-TC/γ-CD-IC-NF into 95% ethanol were performed and released amount of α-TC was evaluated by HPLC (Figure 23). PLA/α-TC/γ-CD-IC-NF released much more amount of α-TC in total and its release rate were slower than PLA/α-TC-NF, these were

probably due to the increment in the solubility and lower diffusion of  $\alpha$ -TC when it is in the cavity of  $\gamma$ -CD, respectively [197].

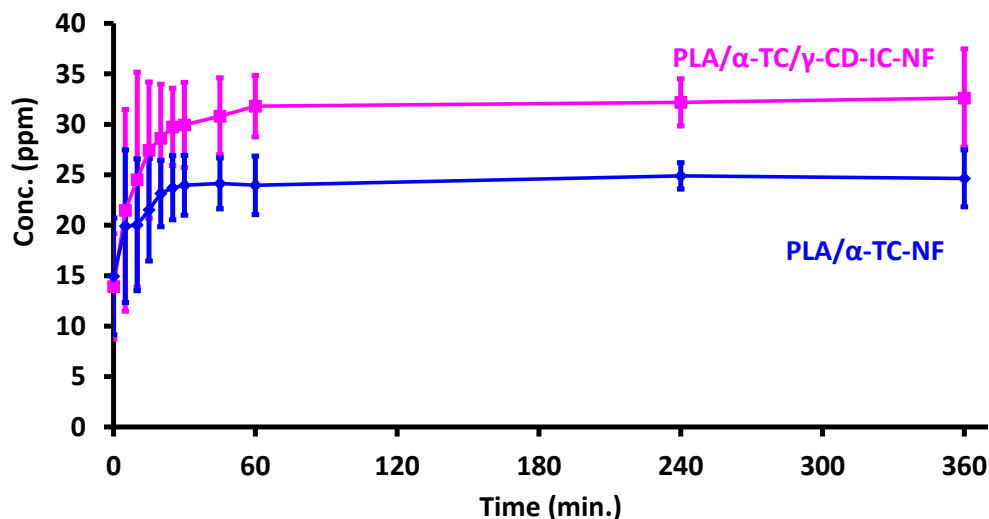


**Figure 23.** The cumulative release of  $\alpha$ -TC from PLA/ $\alpha$ -TC-NF and PLA/ $\alpha$ -TC/ $\gamma$ -CD-IC-NF.

### 3.3.6 Antioxidant activity

The antioxidant activities (%) were determined according to DPPH radical scavenging assay and the absorbance of the solutions were measured via UV-Vis spectroscopy. The antioxidant activities (%) of PLA/ $\alpha$ -TC/ $\gamma$ -CD-IC-NF and PLA/ $\alpha$ -TC-NF were quite high (93.3% and 92.9%) in spite of the high voltage applied during electrospinning process. Additionally, the antioxidant activity of the nanofibers were slightly different from each other. The photographs of the DPPH solution and PLA/ $\alpha$ -TC/ $\gamma$ -CD-IC-NF and PLA/ $\alpha$ -TC-NF immersed DPPH solution at the end of the reaction are shown in Figure 24. The color of the solutions in which nanofibers immersed were both yellow. So, it can be deduced that there is no more DPPH in the solution to deactivate.

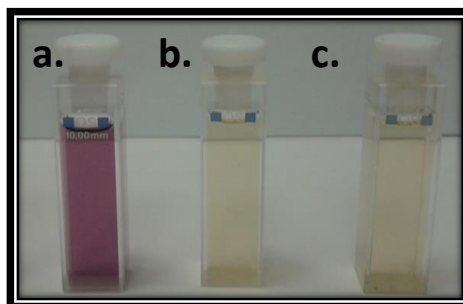


**Figure 24.** The photographs of (a) DPPH solution; DPPH solutions in which (b) PLA/ $\alpha$ -TC/ $\gamma$ -CD-IC-NF, (c) PLA/ $\alpha$ -TC-NF was immersed (after reaction).

### 3.3.7 Lipid oxidation analysis (TBARS)

Thiobarbituric acid reactive substances (TBARS) method has been widely used to determine the degree of lipid oxidation. TBARS are produced through second stage autooxidation during which peroxides are oxidized to aldehydes and ketones (e.g., MDA). The results and photographs are given in Figure 25 and Figure 26, respectively. After 4 days of storage, TBARS values of control (unpacked raw beef meat), PLA/ $\alpha$ -TC/ $\gamma$ -CD-IC-NF and PLA/ $\alpha$ -TC-NF packed raw beef were  $0.38 \pm 0.07$ ,  $0.28 \pm 0.08$  and  $0.38 \pm 0.16$  mg MDA/kg beef, respectively. TBARS values of all experimental groups continued to increase consistently throughout the storage. At the end of 28 days, TBARS values of control reached  $2.77 \pm 1.04$  mg MDA/kg beef. However, TBARS values of PLA/ $\alpha$ -TC/ $\gamma$ -CD-IC-NF and PLA/ $\alpha$ -TC-NF increased only up to  $1.37 \pm 0.39$  and  $1.39 \pm 0.23$  mg MDA/kg beef, respectively. Therefore, both PLA/ $\alpha$ -TC/ $\gamma$ -CD-IC-NF and PLA/ $\alpha$ -TC-NF are very effective for preservation of the beef meat against oxidation.

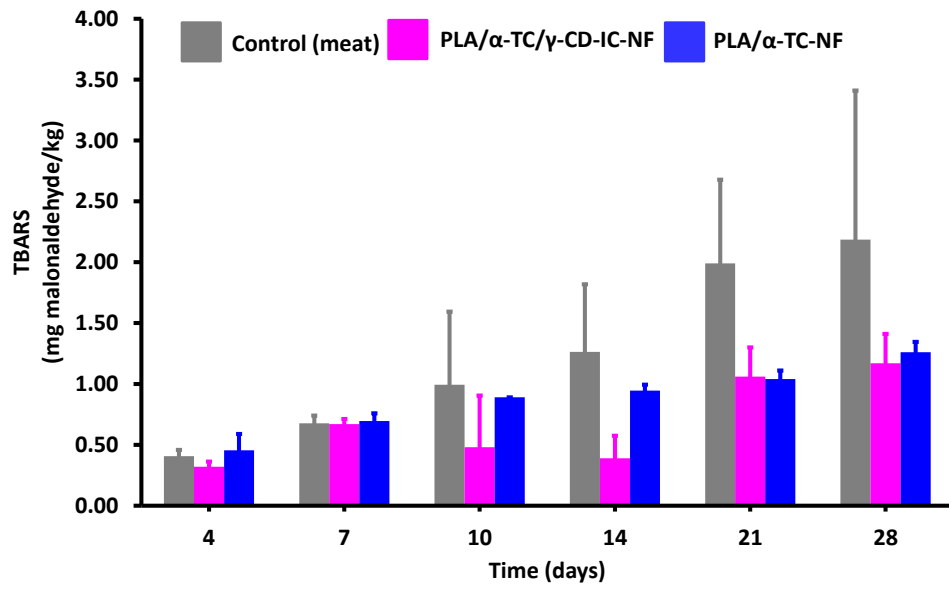


**Figure 25.** Change of TBARS overtime during storage for raw beef meat sample (control), PLA/α-TC/γ-CD-IC-NF and PLA/α-TC-NF packed raw beef meat.

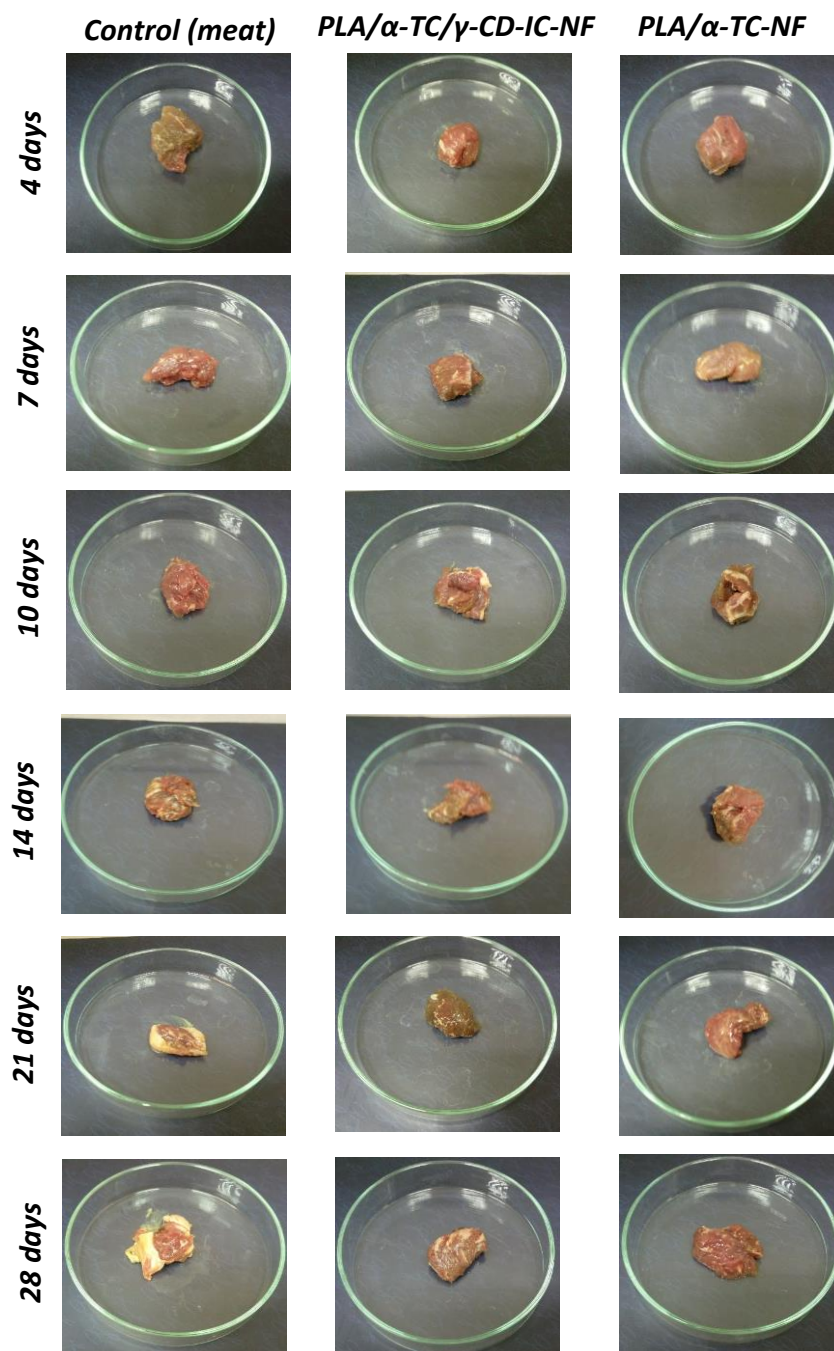


**Figure 26.** The photographs of raw beef meat samples (control), raw beef meatsamples packed with PLA/α-TC/γ-CD-IC-NF and PLA/α-TC-NF for 28 days.

### 3.4 Conclusion

As a result, the formation of IC between α-TC and γ-CD were confirmed by XRD, TGA, and <sup>1</sup>H-NMR. SEM images shows the bead-free morphology of

PLA/ $\alpha$ -TC/ $\gamma$ -CD-IC-NF and PLA/ $\alpha$ -TC-NF. The release rate of  $\alpha$ -TC from PLA/ $\alpha$ -TC/ $\gamma$ -CD-IC-NF were slower than PLA/ $\alpha$ -TC-NF due to the presence of CD-IC; however, total released amount was more in PLA/ $\alpha$ -TC/ $\gamma$ -CD-IC-NF. Both of the nanofibers exhibited quite high antioxidant activity. The potential of PLA/ $\alpha$ -TC/ $\gamma$ -CD-IC-NF and PLA/ $\alpha$ -TC-NF as packaging material for raw beef meat samples has been proven by TBARS method.

## **4. Antioxidant electrospun zein nanofibers incorporating quercetin/ $\gamma$ -cyclodextrin-inclusion complex**

### **4.1 Introduction**

Zein is a biocompatible and biodegradable polymer and produced from renewable sources, mostly corn [198, 199]. It is an amphiphilic protein composed of hydrophobic and hydrophilic amino acid residues, but the majority of the amino acids in its complex structure are hydrophobic non-polar amino acids [200]. Due to its inherent biocompatibility and biodegradability [198] it is applied to biomedical [201] and pharmaceutical [202] areas. In addition to the aforementioned inherent properties that make zein to be used in biomedical and pharmaceutical fields, its carbon dioxide and oxygen permeability [199] are of importance for food packaging applications [42, 203, 204].

$\gamma$ -CD (Figure 27b-c) is one of the most widely used CD types which is composed of 8 glucopyranose units. Its cavity volume, solubility and bioavailability is higher in contrast to  $\alpha$ -CD and  $\beta$ -CD. It was also stated that it has no side effects on the absorption of nutrients in food products and nutraceutical applications [188].

Quercetin (QU) (Figure 27a) has been used in pharmaceutical and food industries owing to antioxidant [205], antitumour [206] activities. QU is found in onion, apple, green tea and black tea in nature. Since it possesses low oral bioavailability and aqueous solubility, quick photodegradation; carrier systems are needed to reduce the required level of dose and extend its application areas. It was previously reported that electrospun nanofibers can be ideal candidates for QU delivery [207, 208]. There are studies concerning CD-IC of QU as well

[209, 210]. Furthermore, Koontz et al. incorporated CD-ICs of QU into polymeric films [61, 194]. In our previous studies, polyacrylic acid nanofibers was designed incorporating IC of QU with  $\beta$ -CD via electrospinning [104].

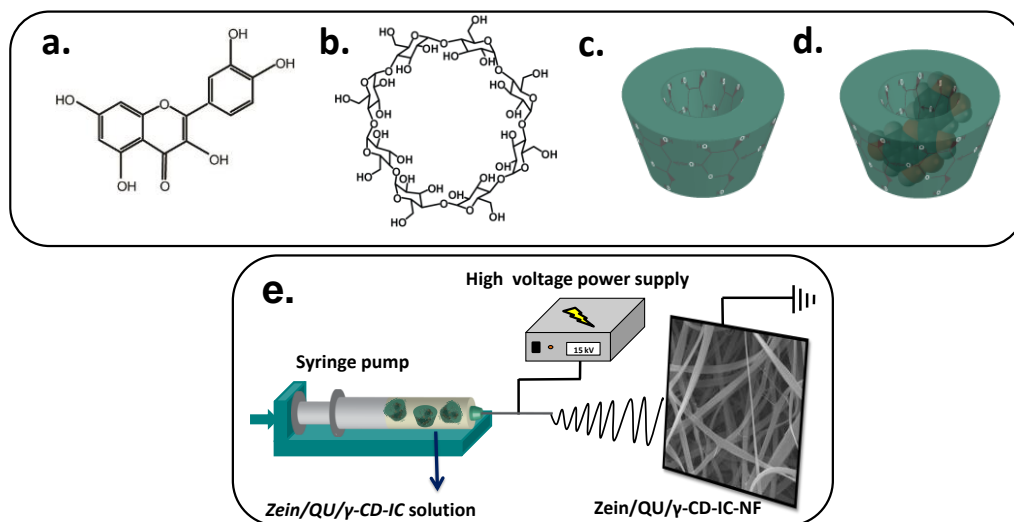


**Figure 27.** Chemical structure of (a) QU, (b)  $\gamma$ -CD; schematic representation of (c)  $\gamma$ -CD, (d) formation of QU/ $\gamma$ -CD-IC, and (e) electrospinning of nanofibers from zein/QU/ $\gamma$ -CD-IC solution.

In this study, inclusion complex of QU and  $\gamma$ -CD (Figure 27d) was prepared (QU/ $\gamma$ -CD-IC) and incorporated into to zein solution in order to obtain antioxidant nanofibers using electrospinning (zein/QU/ $\gamma$ -CD-IC-NF) (Figure 27e). X-ray diffraction (XRD), thermal gravimetric analysis (TGA), and proton nuclear magnetic resonance ( $^1\text{H-NMR}$ ) techniques were employed to characterize QU/ $\gamma$ -CD-IC. The morphological characterization of zein/QU/ $\gamma$ -CD-IC-NF and zein/QU-NF (reference sample) were performed via scanning electron microscope (SEM). The antioxidant activity in zein/QU/ $\gamma$ -CD-IC-NF and zein/QU-NF was investigated according to 2,2-diphenyl-1-picrylhydrazyl (DPPH) radical scavenging method.

## **4.2 Experimental**

### **4.2.1 Materials**

Zein from maize (Sigma–Aldrich), quercetin (QU,  $\geq 95\%$ , Sigma Aldrich), gamma-cyclodextrin ( $\gamma$ -CD, Wacker Chemie AG, Germany), methanol (extra pure, Sigma Aldrich), ethanol (99.8%, Sigma Aldrich), deuterated dimethylsulfoxide (DMSO-d<sub>6</sub>, deuteration degree min 99.8% for NMR spectroscopy, Merck), 2,2-diphenyl-1-picrylhydrazyl (DPPH, Sigma Aldrich) were purchased and used as-received without any further purification. Distilled-deionized water was supplied from Millipore milli-Q ultrapure water system.

### **4.2.2 Preparation of inclusion complex**

QU/ $\gamma$ -CD-IC was prepared according to the freeze-drying method at 1:1 molar ratio (QU/ $\gamma$ -CD). Firstly,  $\gamma$ -CD was dissolved in water; then QU was added to the solution. After mixing the solution 12 hours, it was freeze-dried at  $-80^{\circ}\text{C}$  for 24 hours. Then, the mixture was kept in lyophilizer for 48 hours.

### **4.2.3 Preparation of electrospinning solutions**

Zein nanofibers (zein-NF), free QU, QU/ $\gamma$ -CD-IC (1:1) incorporated zein nanofibers (zein/QU/ $\gamma$ -CD-IC-NF and zein/QU-NF) were produced via electrospinning. Firstly, 35% (w/v) zein solution in ethanol:water (8:2) mixture was electrospun. In order to produce zein/QU/ $\gamma$ -CD-IC-NF, QU/ $\gamma$ -CD-IC (5% QU, w/w, with respect to polymer) was dissolved in ethanol:water (8:2) mixture at room temperature (RT). Then, 35% zein (w/v) was added and zein/QU/ $\gamma$ -CD-IC solution was stirred for 1 hour more before electrospinning. With regards to

zein/QU-NF; QU (5% QU, w/w, with respect to polymer) was dissolved in ethanol:water (8:2) mixture at RT. Afterwards, 35% zein (w/v) was added, resulting zein/QU solution was stirred 1 hour more prior to electrospinning. Table 4 summarizes the composition of the zein, zein/QU, zein/QU/ $\gamma$ -CD-IC solutions.

**Table 4.** The composition of the solutions used for electrospinning.

Solutions	% zein <sup>a</sup> (w/v)	% $\gamma$ -CD <sup>b</sup> (w/w)	% QU <sup>b</sup> (w/w)
zein	35	-	-
zein/QU	35	-	5
zein/QU/ $\gamma$ -CD-IC	35	22	5

<sup>a</sup> with respect to solvent (ethanol:water, 8:2)

<sup>b</sup> with respect to polymer (zein).

#### 4.2.4 Electrospinning

Zein, zein/QU/ $\gamma$ -CD-IC and zein/QU solutions in 3 ml plastic syringe (needle inner diameter: 0.8 mm) were mounted on on the syringe pump (KD Scientific, KDS101) send towards the collector at 1 ml/h rate. The collector is a metal covered with a piece of aluminum foil. Distance between needle tip and collector was 12 cm. 15 kV was applied from the high voltage power supply (AU Series, Matsusada Precision Inc.). The experiments were performed at 25°C, 18% humidity.

#### 4.2.5 Characterizations and measurements

The crystalline structure of QU,  $\gamma$ -CD, and QU/ $\gamma$ -CD-IC was examined with X-ray diffraction (XRD). XRD data for the each sample were recorded using a PANalytical X'Pert powder diffractometer applying Cu K radiation in the  $2\theta$  range of 5-30°.

The thermal properties of QU,  $\gamma$ -CD, and QU/ $\gamma$ -CD-IC were analyzed by thermal gravimetric analysis (TGA, TA Q500, USA). For the measurements, the samples were heated from RT to 600°C under nitrogen atmosphere at a constant heating rate of 20°C/min.

The molar ratio of QU/ $\gamma$ -CD-IC was investigated via proton nuclear magnetic resonance ( $^1\text{H-NMR}$ ) (Bruker DPX-400 at 400 MHz). 20 mg/mL of QU,  $\gamma$ -CD, and QU/ $\gamma$ -CD-IC were dissolved in  $d_6$ -DMSO. Integration of the chemical shifts ( $\delta$ ) which is given in parts per million (ppm) was calculated via Mestrenova software.

The morphological characterization of zein-NF, zein/QU-NF and zein/QU/ $\gamma$ -CD-IC-NF was examined by using scanning electron microscopy (SEM, FEI-Quanta 200 FEG). Prior to imaging, nanofibers were coated with 5 nm Au/Pd (PECS-682). In order to determine average fiber diameter (AFD) of the nanofibers, about 100 fibers were analyzed from SEM images.

Antioxidant tests were conducted for zein/QU-NF and zein/QU/ $\gamma$ -CD-IC-NF using 2,2-diphenyl-1-picrylhydrazyl (DPPH) radical scavenging method. Around 4 mg of nanofibers having equivalent amount of QU were immersed in 3 ml of  $10^{-4}$  M DPPH solution (methanol). Then, the solutions were incubated at

RT in dark for 15 minutes. Finally, the absorbance of the each solution were analyzed by UV-Vis spectroscopy (Varian, Cary 100) at 517 nm. The absorbance of DPPH was defined as 100% and the antioxidant activities (%) were calculated based on the following equation:

$$\text{Antioxidant activity (\%)} = (A_{\text{control}} - A_{\text{sample}}) / A_{\text{control}} * 100 \quad (\text{Equation 5})$$

where  $A_{\text{control}}$  and  $A_{\text{sample}}$  represent the absorbance values of control DPPH solution and DPPH solution with nanofibers, respectively.

## **4.3 Results and discussion**

### **4.3.1 Structural characterization of inclusion complex**

In order to confirm the formation of the complex between guest and CD, XRD is one of the most widely used techniques. It is known that when a crystalline guest molecule inserted in the cavity of a CD, its molecules are separated and cannot form crystals. XRD of QU,  $\gamma$ -CD, and QU/ $\gamma$ -CD-IC are shown in Figure 28. Therefore, we do not observe the crystalline peaks of guest molecule in case of complexation [175]. Here, as-received QU exhibits crystalline peaks, but these peaks are not seen in QU/ $\gamma$ -CD-IC. In addition, transformation from cage-type packing to channel type packing occur in the crystal structure of native CDs, when they form a complexation with a guest molecule [196]. So, QU/ $\gamma$ -CD-IC exhibits the hexagonal channel type packing of  $\gamma$ -CD and the crystalline peaks of QU cannot be observed. As a result, XRD shows the successful formation of QU/ $\gamma$ -CD-IC.

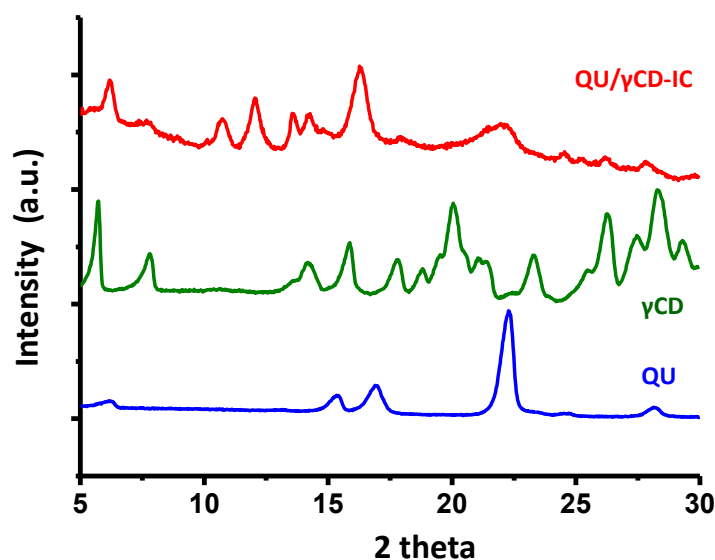


**Figure 28.** XRD patterns of QU,  $\gamma$ -CD, and QU/ $\gamma$ -CD-IC.

#### 4.3.2 Thermal analysis of inclusion complex

The thermal stability of QU,  $\gamma$ -CD, and QU/ $\gamma$ -CD-IC was determined using TGA (Figure 29). QU possesses a weight loss starting at around 275°C and going up to 400°C which is ascribed to the thermal degradation of the molecule.  $\gamma$ -CD has two weight losses corresponding to water loss in its cavity and main decomposition of  $\gamma$ -CD, respectively. As regards to QU/ $\gamma$ -CD-IC, it has two weight loss stages belonging to the water loss and degradation of QU and CD. According to TGA results IC formation did not affect the thermal stability of QU [61]. However, due to the overlapping in the degradation temperature of QU and  $\gamma$ -CD, we could not calculate the amount of QU found in QU/ $\gamma$ -CD-IC.

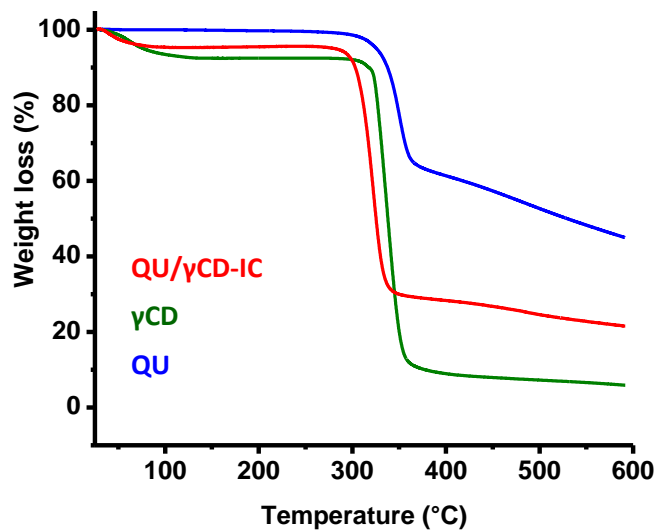


**Figure 29.** TGA thermograms of QU,  $\gamma$ -CD, and QU/ $\gamma$ -CD-IC.

### 4.3.3 The molar ratio of inclusion complex

The molar ratio in QU/ $\gamma$ -CD-IC was decided using the integration of  $^1\text{H-NMR}$  peaks and the results are given in Figure 30.  $^1\text{H-NMR}$  spectra were also taken for QU and  $\gamma$ -CD to decide the characteristic peaks of each proton. While calculating the molar ratio, the peak at 6.4 ppm for QU and the peak at 4.9 ppm for  $\gamma$ -CD was chosen to calculate the molar ratio. The molar ratio of QU/ $\gamma$ -CD-IC was found as 0.89:1.00 from  $^1\text{H-NMR}$  calculations.

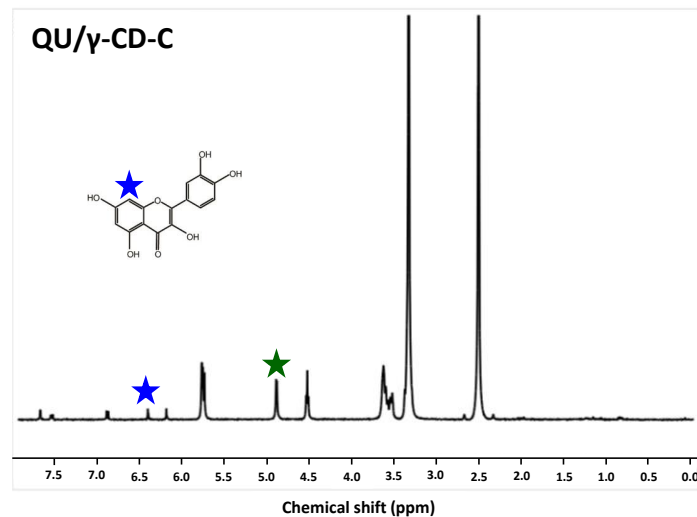


**Figure 30.** <sup>1</sup>H-NMR spectra of QU/γ-CD-IC.

#### 4.3.4 Morphology analysis of nanofibers

After the characterization of the complex, we have produced zein nanofibers (35 %, w/v) incorporating QU/γ-CD-IC (zein/QU/γ-CD-IC-NF) through electrospinning. As a control, QU containing zein nanofibers (zein/QU-NF) were also produced. The morphology of zein-NF, zein/QU-NF, and zein/QU/γ-CD-IC-NF was investigated by SEM (Figure 31). SEM images revealed that zein-NF, zein/QU-NF, and zein/QU/γ-CD-IC-NF have  $695\pm 310$  nm,  $750\pm 310$  nm, and  $750\pm 310$  nm, respectively. The slightly thinner nanofiber diameter of zein-NF as compared to zein/QU-NF and zein/QU/γ-CD-IC-NF is probably due to the viscosity and the conductivity differences in the zein/QU solution and zein/QU/γ-CD-IC solution [3]. Furthermore, the morphology of zein-NF did not change after the incorporation of QU in both free and IC form.

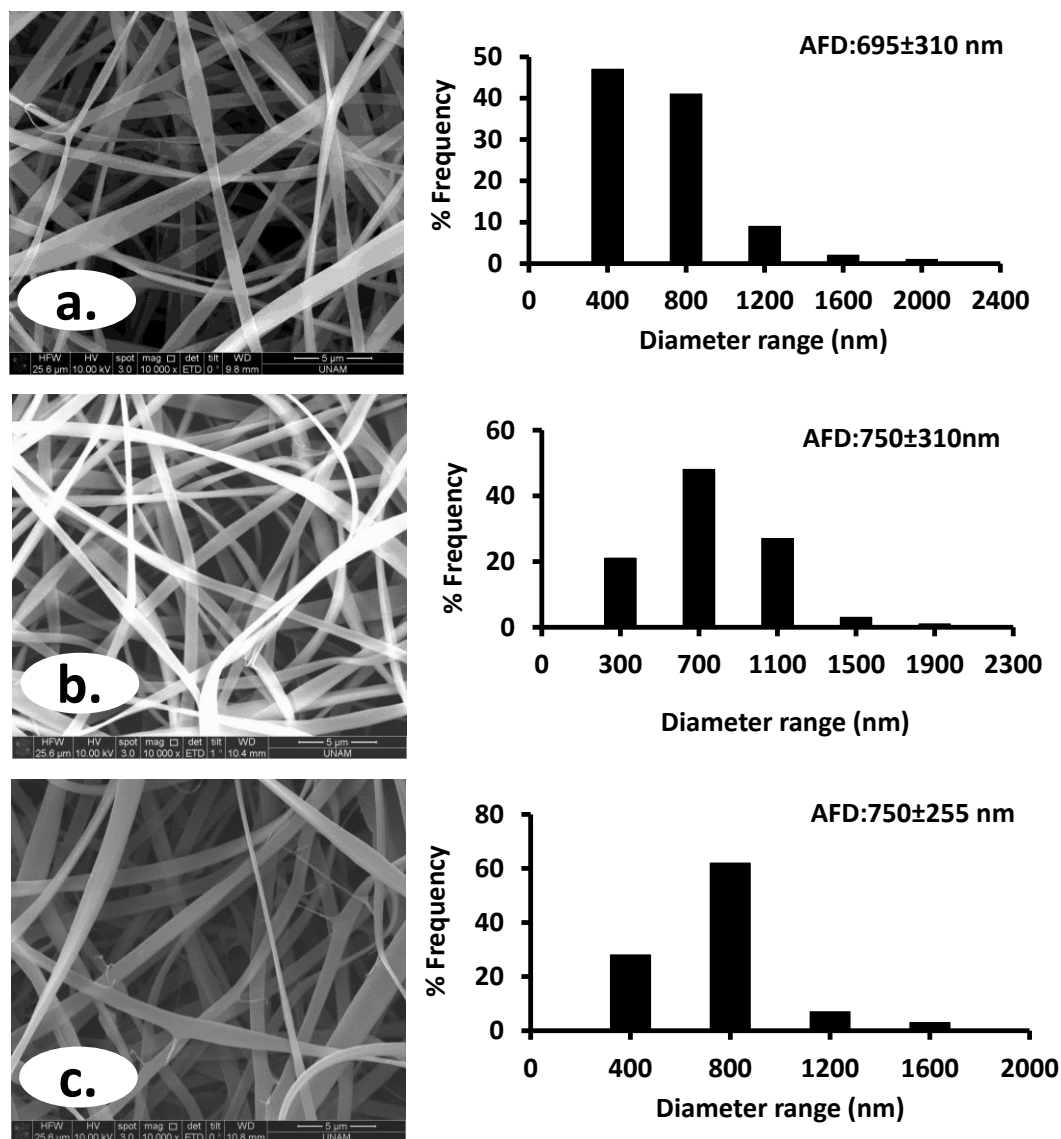


**Figure 31.** SEM images of zein-NF, zein/QU-NF, and zein/QU/γ-CD-IC-NF.

### 4.3.5 Antioxidant activity

DPPH method was used to test the antioxidant activity (%) of nanofibers and absorbance of the DPPH solutions after immersion of nanofibers were determined by UV-Vis spectroscopy. As a result, zein/QU-NF and zein/QU/γ-CD-IC-NF exhibited 84% and 90% antioxidant activity. Slightly higher antioxidant activity of zein/QU/γ-CD-IC-NF compared to zein/QU-NF could be due to the presence of CD-IC in zein-QU/γ-CD-IC-NF. The color of the solution

turn from purple to yellow as seen in Figure 32. Furthermore, electrospinning process did not affect the antioxidant property of QU in spite of the high voltage that is applied during the process.

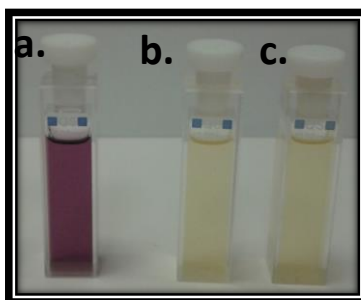


**Figure 32.** The photographs of (a) DPPH solution; DPPH solutions in which (b) zein/QU-NF, (c) zein/QU/ $\gamma$ -CD-IC-NF was immersed (after reaction).

#### 4.4 Conclusion

As a conclusion, successful formation of IC of QU with  $\gamma$ -CD was shown by XRD, TGA, and  $^1\text{H-NMR}$ . As seen from SEM images, bead-free nanofibers were produced from zein/QU and zein/QU/ $\gamma$ -CD-IC solutions. Finally, antioxidant activity of zein/QU/ $\gamma$ -CD-IC-NF were higher as compared to zein/QU-NF. Zein/QU/ $\gamma$ -CD-IC-NF could be used to prevent oxidation of many products with its quite high antioxidant activity.

## **5. Antibacterial packaging material designed by encapsulation of thymol/cyclodextrin-inclusion complex in electrospun zein nanofibers**

### **5.1 Introduction**

Incorporation of antibacterial agents into packaging material to prevent the proliferation of bacteria by releasing towards to product is one type of active food packaging. The aim of antimicrobial food packaging is preserving mostly meat, fish, poultry, fruit, vegetables, and cheese [211].

Zein is an inherently biocompatible and biodegradable polymer with low carbon dioxide and oxygen permeability and produced from renewable sources, mostly corn [198, 199]. Most of the amino acid in the structure of zein is hydrophobic; however, there are also hydrophilic amino acids. Owing to its unique properties, it can be used in biomedical [201], pharmaceutical [202] and food packaging applications [42, 203, 204].

$\gamma$ -CD (Figure 33b-c) is one of the most widely used CD type which composed of 8 glucopyranose unit. Its cavity volume, solubility and bioavailability is higher in contrast to  $\alpha$ -CD and  $\beta$ -CD. It was also stated that it has no side effects on the absorption of nutrients in food products and nutraceutical applications [188].

Thymol (THY) (Figure 33a) is essentially known as a flavour, however it is also important to prevent growth of bacteria and oxidation as an antibacterial and antioxidant compound. It is a monoterpene found in oreganos and thymes, but its delivery remains a challenge because of its hydrophobic and volatile nature. CD-IC of THY has been studied before to demonstrate its applicability in pork

meat system [212], increase the solubility and prevent oxidation by complexation [213], and show its usage as an effective larvicide [214].

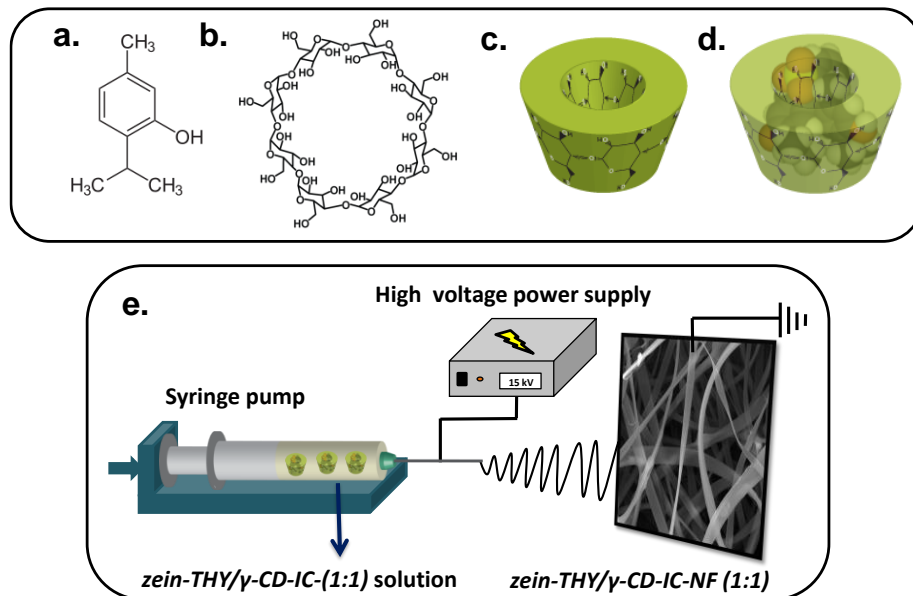


**Figure 33.** Chemical structure of (a) THY; (b)  $\gamma$ -CD; schematic representation of  $\gamma$ -CD, (d) formation of THY/ $\gamma$ -CD-IC (1:1), and (b) electrospinning of nanofibers from zein/THY/ $\gamma$ -CD-IC (1:1) solution.

In this study, CD-IC of THY was prepared at 1:1 and 2:1 (THY: $\gamma$ -CD) molar ratio (THY/ $\gamma$ -CD-IC (1:1) and THY/ $\gamma$ -CD-IC (2:1)) (Figure 33d) and then incorporated into electrospun zein nanofibers by electrospinning (Figure 33e). The characterization of CD-ICs was carried out using XRD, TGA, and  $^1\text{H-NMR}$ . Free THY, THY/ $\gamma$ -CD-IC (1:1) and THY/ $\gamma$ -CD-IC (2:1) incorporated zein nanofibers were characterized by SEM. The delivery of THY from nanofibers were investigated temperature dependently by headspace GC-MS. Colony counting method was used to evaluate the antibacterial activity of nanofibers. Finally, antibacterial activity of nanofibers against total viable counts in beef meat system was determined throughout storage.

## **5.2 Experimental**

### **5.2.1 Materials**

Zein from maize (Sigma-Aldrich), thymol (THY, 98%, Alfa Aesar), 2,2-diphenyl-1-picrylhydrazyl (DPPH, Sigma-Aldrich), dimethylformamide (DMF, >99%, Sigma Aldrich), methanol (extra pure, Sigma-Aldrich), and deuterated dimethylsulfoxide (DMSO-d<sub>6</sub>, deuteration degree min 99.8% for NMR spectroscopy, Merck) were purchased and used as received without any further purification. Gamma-cyclodextrin ( $\gamma$ -CD, Wacker Chemie AG, Germany) was kindly donated by Wacker Chemie (Germany). The water used in the experiments was distilled-deionized from a Millipore Milli-Q ultrapure water system.

### **5.2.2 Preparation of inclusion complex**

The solid THY/ $\gamma$ -CD-IC (1:1) and THY/ $\gamma$ -CD-IC (2:1) was prepared according to co-precipitation method. Initially,  $\gamma$ -CD was dissolved in aqueous solution; then THY was added to that solution. After stirring the solutions overnight, they were kept in refrigerator for 12 hours. At the end of the 12 hours, precipitate was collected by filtration.

### **5.2.3 Preparation of electrospinning solutions**

Free THY, THY/ $\gamma$ -CD-IC (1:1) and THY/ $\gamma$ -CD-IC (2:1) incorporated zein nanofibers (zein/THY-NF, zein/THY/ $\gamma$ -CD-IC-NF (1:1), and zein/THY/ $\gamma$ -CD-IC-NF (2:1)) were produced via electrospinning technique. For producing zein/THY-NF, free THY (4%, w/w, with respect to polymer) was dissolved in DMF at room temperature (RT). Then, 50% zein (w/v) was added and zein/THY

solution was stirred for 1 hours before electrospinning. With regards to zein/THY/ $\gamma$ -CD-IC-NF (1:1) and zein/THY/ $\gamma$ -CD-IC-NF (2:1); THY/ $\gamma$ -CD-IC (1:1) and THY/ $\gamma$ -CD-IC (2:1) (4% THY, w/w, with respect to polymer) was dispersed in DMF at RT. Afterwards, 50% zein (w/v) was added, resulting zein/THY/ $\gamma$ -CD-IC (1:1) and zein/THY/ $\gamma$ -CD-IC (2:1) solutions were stirred 1 hour prior to electrospinning. As a reference sample, we have also electrospun 50% (w/v) zein solution prepared in DMF (zein-NF). Table 5 summarizes the composition of the zein, zein/THY, zein/THY/ $\gamma$ -CD-IC (1:1) , and zein/THY/ $\gamma$ -CD-IC (2:1) solutions.

**Table 5.** The composition of the solutions used for electrospinning.

Solutions	% zein <sup>a</sup> (w/v)	% $\gamma$ -CD <sup>b</sup> (w/w)	% THY <sup>b</sup> (w/w)
zein	50	-	-
zein/THY	50	-	4
zein/THY/ $\gamma$ -CD-IC (1:1)	50	33	4
Zein/THY/CD-IC (2:1)	50	17	4

<sup>a</sup> with respect to solvent (DMF)

<sup>b</sup> with respect to polymer (zein).

#### 5.2.4 Electrospinning

Zein, zein/THY, zein/THY/ $\gamma$ -CD-IC (1:1) , and zein/THY/ $\gamma$ -CD-IC (2:1) solutions were loaded into a 5 mL plastic syringe with metallic needle of 0.9 mm inner diameter. Then, the solutions were pumped at a constant rate (0.5 mL/h) via syringe pump (WPI, SP 101IZ). A grounded metal covered by

aluminum foil placed at a distance of 17 cm from the needle tip was used as a collector. 17 kV electric voltage was applied from the high voltage power supply (AU Series, Matsusada Precision Inc.). All experiments were carried out in an enclosed Plexiglas box at 25°C and 18% relative humidity. Nanofibers were kept in refrigerator until the analyses.

### **5.2.5 Characterizations and measurements**

The crystalline structure of powder of THY,  $\gamma$ -CD, THY/ $\gamma$ -CD-IC (1:1), and THY/ $\gamma$ -CD-IC (2:1) were recorded via X-ray diffraction (XRD, PANalytical X'Pert powder diffractometer) applying Cu K $\alpha$  radiation in a  $2\theta$  range 5°-30°.

Thermal properties of THY,  $\gamma$ -CD, THY/ $\gamma$ -CD-IC (1:1), and THY/ $\gamma$ -CD-IC (2:1) were investigated by thermal gravimetric analysis (TGA, TA Q500, USA).

The measurements were carried out under nitrogen atmosphere, and the samples were heated up to 500°C at a constant heating rate of 20°C/min.

The proton nuclear magnetic resonance (<sup>1</sup>H-NMR) spectra were recorded for THY/ $\gamma$ -CD-IC (1:1) and THY/ $\gamma$ -CD-IC (2:1) on Bruker DPX-400. 20 mg/mL of THY/ $\gamma$ -CD-IC (1:1) and THY/ $\gamma$ -CD-IC (2:1) were dissolved in d<sub>6</sub>-DMSO to determine the molar ratio of THY/ $\gamma$ -CD-IC (1:1) and THY/ $\gamma$ -CD-IC (2:1).

Mestrenova software was used to take the integration of the chemical shifts ( $\delta$ ) given in parts per million (ppm).

The morphology of zein-NF, zein/THY-NF, zein/THY/ $\gamma$ -CD-IC-NF (1:1) and zein/THY/ $\gamma$ -CD-IC-NF (2:1) was examined via scanning electron microscopy (SEM, FEI-Quanta 200 FEG). For this purpose, samples mounted on metal stubs using a double-sided adhesive tape coated with Au/Pd layer (~5 nm) (PECS-

682). About 100 fibers were analyzed to calculate average fiber diameter (AFD) of nanofibers.

The amount of thymol released from zein/THY-NF, zein/THY/ $\gamma$ -CD-IC-NF (1:1) and zein/THY/ $\gamma$ -CD-IC-NF (2:1) was determined by headspace gas chromatography-mass spectrometry (HS GC-MS, Agilent Technologies 7890A gas chromatograph equipped with 5975C mass spectrometer) for 5 hours. The capillary column was HP-5MS (Hewlett-Packard, Avondale, PA) (30 m  $\times$  0.25 mm i.d., 0.25  $\mu$ m film thickness). Nanofibers (20 mg) were placed in 20 mL headspace glass vials and the vial was agitated at 500 rpm and 37°C, 50°C, and 75°C. The release experiments were carried out in triplicate and the results were given as average  $\pm$  standard deviation. The oven temperature was initially held at 50°C for 5 min. Then the temperature was raised with a gradient of 20°C/min until 280°C. The oven was held for 5 minute at 280°C. The instrument was operated in a splitless and selected ion monitoring mode (SIM). NIST MS Search 2.0 library was used to decide the thymol peaks.

The antibacterial properties of the zein/THY-NF and zein/THY/ $\gamma$ -CD-IC-NF (1:1) and zein/THY/ $\gamma$ -CD-IC-NF (2:1) were carried out against *Escherichia coli* (*E. coli*, ATCC 10536) and *Staphylococcus aureus* (*S. aureus*, ATCC 25923) bacteria. Bacterial cells of *E. coli* (ATCC 10536) and *S. aureus* (ATCC 25923) were grown 24 h on a shaker at 100 rpm and 37°C. Inoculum were resuspended to provide a final density of  $1 \times 10^8$  CFU/mL in phosphate buffered saline (PBS) according to 0.5 McFarland turbidity standard. UV sterilized nanofibers were then immersed in bacterial suspension in a 20 mL conical tube, and the media were shaken at 100 rpm at 37°C for 24 h. Different dilutions ( $10^1$  to  $10^9$ ) were

made by successively adding 1 mL culture into 9 mL of phosphate buffer solution. Then, 0.1 mL of the diluted culture was spreaded on a nutrient agar (NA) plate and incubated at 37°C for overnight and CFU/mL was counted.

The antibacterial capability of the powder and mats were defined as follows:

$$\text{Antibacterial activity (\%)} = \frac{A-B}{A} \times 100$$

where A and B are the number of colonies (colony forming unit, CFU/mL).  
(Equation 6)

The antibacterial tests were also conducted by packing beef meat (10 g) with zein/THY-NF, zein/THY/ $\gamma$ -CD-IC-NF (1:1) and zein/THY/ $\gamma$ -CD-IC-NF (2:1) and a storing under the conditions of 4°C was performed for 5 days. For the three treatments, the unpacked beef meat was served as blank control and one packed with zein-NF used as negative control. The bacteria enumeration in the meat samples were determined immediately after packaging with nanofibers. Meat samples (10 g) were combined with sterile PBS and vortexes for 2 min. Appropriate dilutions in PBS were plated in triplicate on plate count agar (PCA) for determination of aerobes in the samples. Colonies were counted after incubation of the plates at 35°C for 120 hours [215]. The microorganism counts were expressed in log CFU/g of beef meat sample.

## 5.3 Results and discussion

### 5.3.1 Structural characterization of inclusion complex

X-ray diffraction (XRD) was performed for THY,  $\gamma$ -CD, THY/ $\gamma$ -CD-IC (1:1), and THY/ $\gamma$ -CD-IC (2:1) patterns are displayed in Figure 34. Intense and sharp diffraction peaks of THY were observed at  $2\theta$  values of  $8.29^\circ$ ,  $17.07^\circ$ ,  $19.09^\circ$ , and  $25.84^\circ$ . In case of THY/ $\gamma$ -CD-IC (1:1) and THY/ $\gamma$ -CD-IC (2:1), the crystalline peaks of thymol were disappeared and the absence of the crystalline peaks of thymol the indication of complex formation between THY and  $\gamma$ -CD, since the guest molecules are separated from each other during inclusion complex formation [175]. In addition to that, transformation of crystalline structure of as-received  $\gamma$ -CD from cage in which cavity of each CD molecule is blocked by other CD molecules to channel with a major peak at  $2\theta$  value of  $7.5^\circ$  and minor peaks at  $2\theta$  values of  $14^\circ$ ,  $15^\circ$ ,  $16^\circ$ ,  $17^\circ$  and  $22^\circ$  is another proof of complex formation between THY and  $\gamma$ -CD [95].

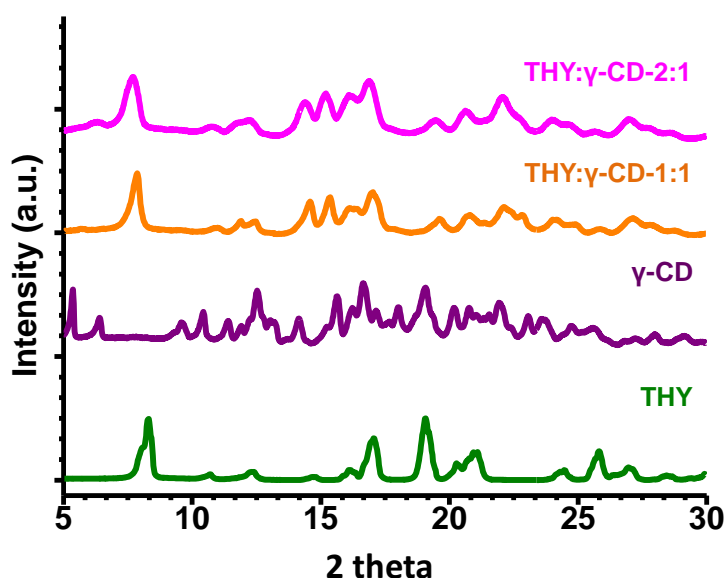


**Figure 34.** XRD patterns of THY,  $\gamma$ -CD, THY/ $\gamma$ -CD-IC (1:1), and THY/ $\gamma$ -CD-IC (2:1).

### 5.3.2 Thermal analysis of inclusion complex

The thermal stability of THY,  $\gamma$ -CD, THY/ $\gamma$ -CD-IC (1:1), and THY/ $\gamma$ -CD-IC (2:1) was investigated by thermal gravimetric analysis (TGA) (Figure 35). The thermal evaporation of THY starts from 50°C and continues up to 150°C.  $\gamma$ -CD exhibited two weight losses below 100°C and above 275°C which belong to the water loss from the cavity and main thermal degradation of CD, respectively. THY/ $\gamma$ -CD-IC (1:1) and THY/ $\gamma$ -CD-IC (2:1) lost weight in three steps. The first losses which are below 100°C were the loss of water molecules in the cavity of CDs. The second weight loss that belongs to thermal evaporation of THY observed in THY/ $\gamma$ -CD-IC (1:1) and THY/ $\gamma$ -CD-IC (2:1) was between 120-200°C and 110-270°C, respectively. Therefore, the increment in the thermal stability of THY suggested the existence of true complexation between THY and  $\gamma$ -CD in both cases. The last weight loss occurred at higher temperatures than 275°C corresponded to the main thermal degradation of  $\gamma$ -CD. In addition, the amount of THY in THY/ $\gamma$ -CD-IC (1:1) and THY/ $\gamma$ -CD-IC (2:1) was determined as ~10.4% and 18.0 %, respectively. The calculated amount of THY present in THY/ $\gamma$ -CD-IC (1:1) and THY/ $\gamma$ -CD-IC (2:1) is well agreed with the initial amount of THY (10.7% and 18.7 %) used for the preparation of the complexes. Therefore, the initial amount of THY preserved during the formation and storage in THY/ $\gamma$ -CD-IC (1:1) and THY/ $\gamma$ -CD-IC (2:1).

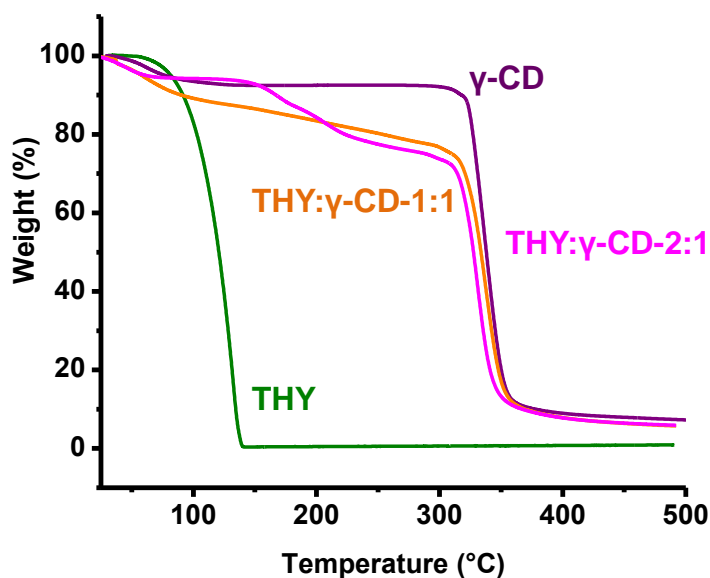


**Figure 35.** TGA thermograms of THY,  $\gamma$ -CD, THY/ $\gamma$ -CD-IC (1:1), and THY/ $\gamma$ -CD-IC (2:1).

### 5.3.3 The molar ratio of inclusion complex

Proton nuclear magnetic resonance ( $^1\text{H-NMR}$ ) spectra for THY/ $\gamma$ -CD-IC (1:1) and THY/ $\gamma$ -CD-IC (2:1) are given in Figure 36 and the molar ratio of THY/ $\gamma$ -CD-IC (1:1) and THY/ $\gamma$ -CD-IC (2:1) was calculated via  $^1\text{H-NMR}$  by taking the integration of the peak ratio of the characteristic chemical shifts of THY (9.1 ppm) and  $\gamma$ -CD (3.5-3.8 ppm). As a result, the molar ratio of THY/ $\gamma$ -CD-IC (1:1) and THY/ $\gamma$ -CD-IC (2:1) was calculated as 1.00:1.00 and 1.99:1.00, respectively. Briefly, it was revealed from  $^1\text{H-NMR}$  study that the initial molar ratio of THY/ $\gamma$ -CD-IC was preserved to a great extent by complexation.

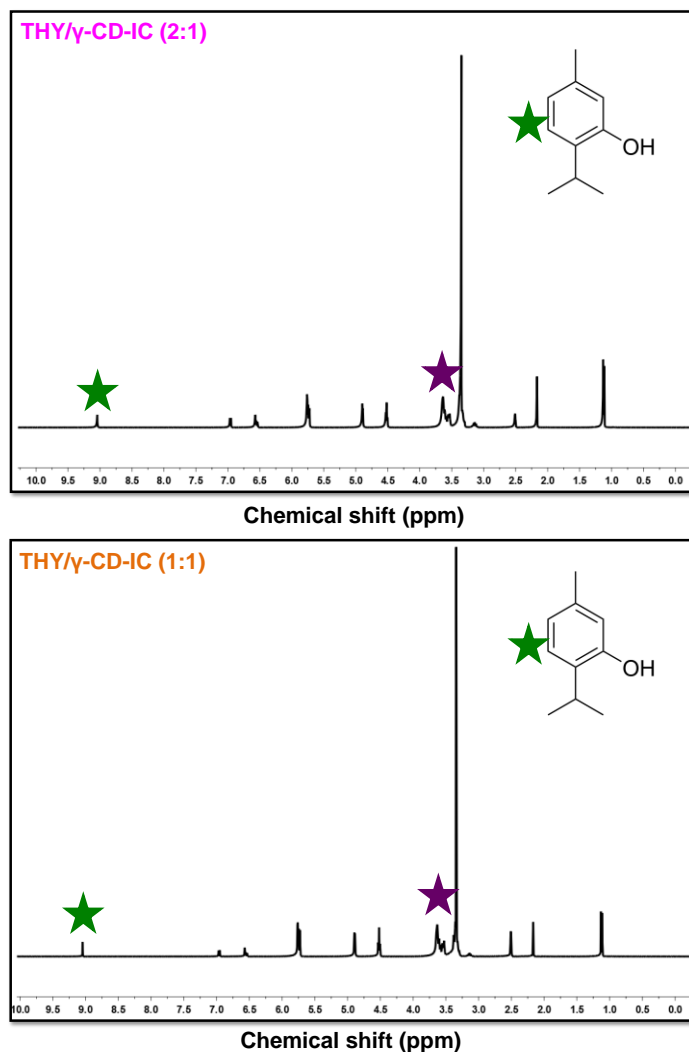


**Figure 36.**  $^1\text{H-NMR}$  spectra of THY/ $\gamma$ -CD-IC (1:1) and (d) THY/ $\gamma$ -CD-IC (2:1).

### 5.3.4 Morphology analysis of nanofibers

The morphological characterization of zein-NF, zein/THY-NF, zein/THY/ $\gamma$ -CD-IC-NF (1:1) and zein/THY/ $\gamma$ -CD-IC-NF (2:1) was carried out via scanning electron microscopy (SEM). SEM images and average fiber diameter (AFD) along with fiber distributions of the nanofibers are depicted in Figure 37. 155 $\pm$ 30 nm, 205 $\pm$ 50 nm, 245 $\pm$ 70 nm, 415 $\pm$ 100 nm, respectively. The

differences in the diameter of nanofibers could be related with the viscosity and conductivity of the solutions [3].

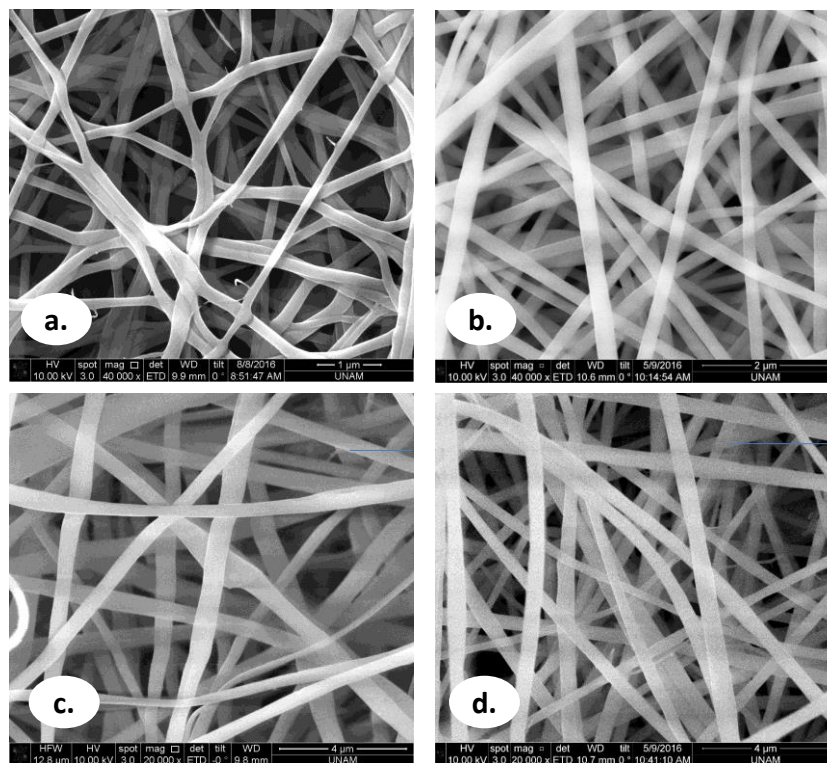


**Figure 37.** SEM images of electrospun nanofibers obtained from the solutions of (a) zein, (b) zein/THY, (c) zein/THY/ $\gamma$ -CD-IC (1:1), (d) zein/THY/ $\gamma$ -CD-IC (2:1).

### 5.3.5 Release study

The amount of THY released from zein/THY-NF, zein/THY/ $\gamma$ -CD-IC-NF (1:1), and zein/THY/ $\gamma$ -CD-IC-NF (2:1) at 37°C, 50°C, and 75°C for 5 hours are shown in Figure 38. The release of THY from the nanofibers was increased gradually by the time and became constant in the last stage. The released amount of THY was more from zein/THY/ $\gamma$ -CD-IC-NF (2:1) compared to zein/THY-NF and zein/THY/ $\gamma$ -CD-IC-NF (1:1). The reason of the less amount of release from zein/THY-NF could be due to the absence of CD-IC that preserving THY from evaporation. In case of zein/THY/ $\gamma$ -CD-IC-NF (1:1), the

stability of the complex in zein/THY/ $\gamma$ -CD-IC-NF (1:1) was lower than the complex in zein/THY/ $\gamma$ -CD-IC-NF (2:1). Therefore, the complex structure could not be preserved effectively. In addition, as the temperature increased, the amount of THY released increased as well for all nanofiber samples due to the increment in the motion of polymer chains favouring the movement of active molecules through the amorphous parts of the polymer at higher temperatures [216].

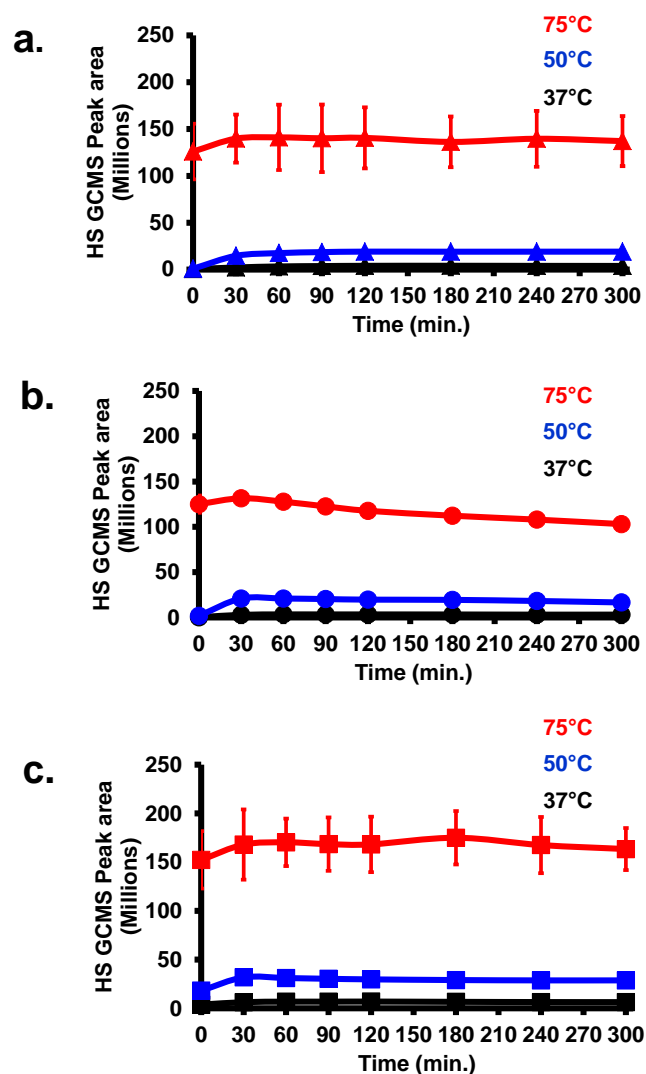


**Figure 38.** The cumulative release of thymol from (a) zein/THY-NF, (b) zein/THY/ $\gamma$ -CD-IC-NF (1:1), and (c) zein/THY/ $\gamma$ -CD-IC-NF (2:1) at 37°C, 50°C, 75°C (n = 3). The error bars in the figure represent the standard deviation (SD).

### 5.3.6 Antibacterial activity

Figure 39 shows results of the antibacterial activity of zein/THY-NF, zein/THY/ $\gamma$ -CD-IC-NF (1:1), and zein/THY/ $\gamma$ -CD-IC-NF (2:1) for *E. coli* and *S. aureus*. It is well-known that thymol, one of the major components of thyme oil with a phenolic structure, has useful antibacterial activity against various microorganisms [217]. Zein/THY/ $\gamma$ -CD-IC-NF (1:1) and zein/THY/ $\gamma$ -CD-IC-NF (2:1) showed better antibacterial effect for *E. coli* and *S. aureus* versus zein-THY-NF (*E. coli*:  $56\pm 2\%$  and *S. aureus*:  $67\pm 3\%$ ). Furthermore, when molar ratios were increased 1:1 to 2:1, nanofibers showed more effective antibacterial activity for both *E. coli* and *S. aureus*. *E. coli* has a thin peptidoglycan layer and an outer layer of lipoproteins, lipopolysaccharides and phospholipids, while the cell wall of *S. aureus* comprises peptidoglycan layer with lots of pores. The porous cell wall structure of *S. aureus* makes it easy to be permeated by thymol. It has been generally accepted that inhibition of nucleic acid synthesis, cytoplasmic membrane function and energy metabolism are three main antibacterial mechanisms of phenolics [218]. This results can also explain the strong inhibition capacity of thymol against two bacteria.

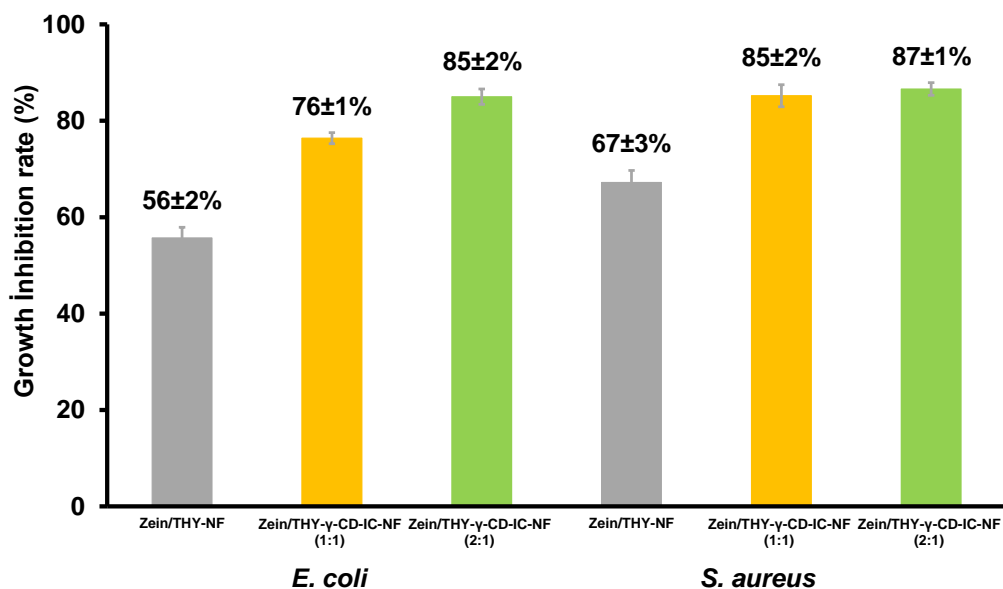


**Figure 39.** The growth inhibition rate (%) of *E. coli* and *S. aureus* colonies in zein/THY-NF, zein/THY/γ-CD-IC-NF (1:1), and zein/THY/γ-CD-IC-NF (2:1) (n = 3). The error bars in the figure represent the standard deviation (SD).

Zein/THY-NF, zein/THY/γ-CD-IC-NF (1:1), and zein/THY/γ-CD-IC-NF (2:1) were applied in the preservation of beef meat at 4°C to evaluate functionality of nanofibers in antibacterial food packaging. When the number of microorganisms on the food surface exceeds a count of  $10^7$  CFU/ml, food is considered as spoiled. The photographs of the raw meat samples; raw meat samples packed with zein/THY-NF, zein/THY/γ-CD-IC-NF (1:1), and zein/THY/γ-CD-IC-NF (2:1) and the photographs of petri dishes at the end of 1, 2, and 5 days of storage at 4°C are given in Figure 40. The initial bacteria colonies of the unpackaged beef meat was  $16 \times 10^2 \pm 0.2$  CFU/g on the first day; whereas, the viable bacteria counts in the nanofibers are less than the control. Thus, the beef meat packed with zein/THY-NF, zein/THY/γ-CD-IC-NF (1:1) and zein/THY/γ-CD-IC-NF (2:1) has  $7.5 \times 10^2 \pm 0.2$ ,  $9.1 \times 10^2 \pm 0.5$ , and  $5.6 \times 10^2 \pm 0.6$  CFU/g. So, nanofibers can prolong the shelf-life of the meat. After

2 and 5 days of storage, total bacteria counts began to increase for all samples. The meat packed with nanofibers had less bacteria counts at the end of 2 and 5 days of storage. Furthermore, zein/THY/ $\gamma$ -CD-IC-NF (2:1) showed the highest antibacterial activity at 4°C after 5 days of storage as well. Additionally, nanofibers are nontoxic thus potential in active food packaging for the concern of food security.

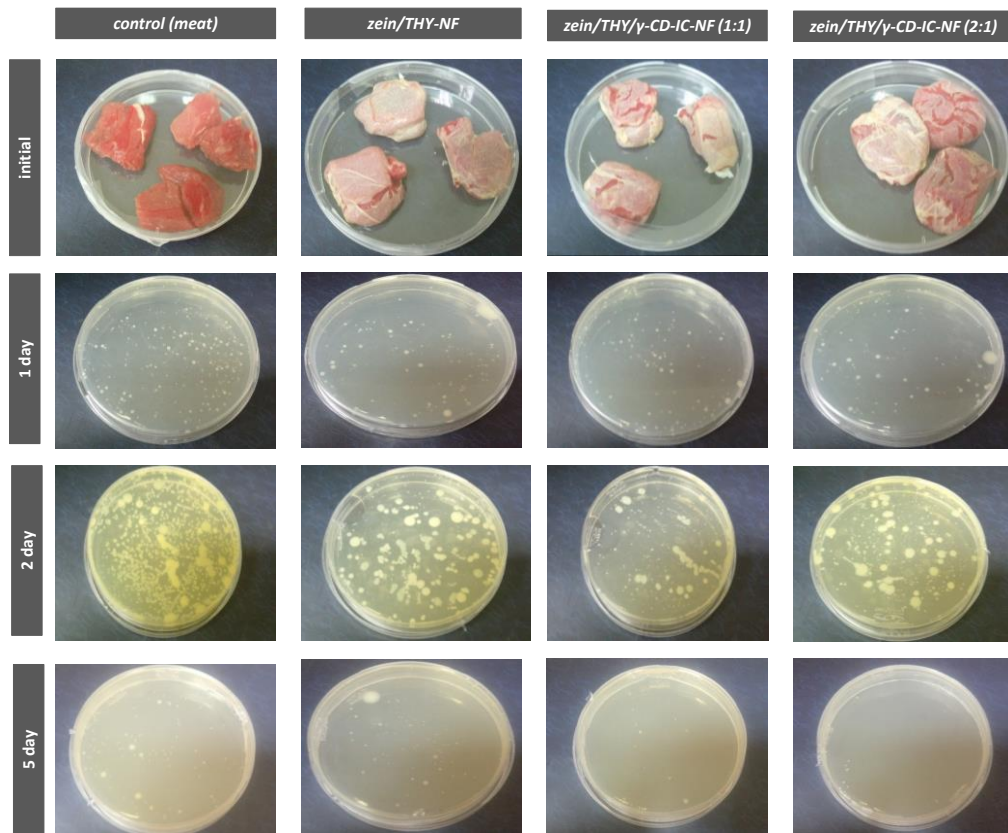


**Figure 40.** The photographs of the raw meat samples; raw meat samples packed with zein/THY-NF, zein/THY/ $\gamma$ -CD-IC-NF (1:1), and zein/THY/ $\gamma$ -CD-IC-NF (2:1) and the photographs of petri dishes at the end of 1, 2 and 5 days of storage at 4°C.

## 5.4 Conclusion

To conclude, the characterization of THY/ $\gamma$ -CD-IC (1:1) and THY/ $\gamma$ -CD-IC (2:1) which was done by XRD, TGA, and  $^1\text{H-NMR}$  indicated that CD-IC was achieved successfully. Bead-free and uniform morphology of nanofibers are seen in SEM images. The release of THY from zein/THY/ $\gamma$ -CD-IC-NF (2:1) was higher than zein/THY-NF and zein/THY/ $\gamma$ -CD-IC-NF (1:1) due to the better preservation of THY by complexation and higher stability of 2:1 complex compared to 1:1 complex, respectively. In addition, antibacterial activity of zein/THY-NF, zein/THY/ $\gamma$ -CD-IC-NF (1:1), and zein/THY/ $\gamma$ -CD-IC-NF (2:1) which was measured by colony counting method demonstrated the higher antibacterial activity of zein/THY/ $\gamma$ -CD-IC-NF (1:1) and zein/THY/ $\gamma$ -CD-IC-NF (2:1) than zein/THY-NF. However, the highest antibacterial activity values were obtained with zein/THY/ $\gamma$ -CD-IC-NF (2:1). Finally, antibacterial food packaging performance of nanofibers were analyzed by packing beef meat samples with nanofibers. As a result, it was concluded both zein/THY/ $\gamma$ -CD-IC-NF (1:1) and zein/THY/ $\gamma$ -CD-IC-NF (2:1) might be used as antibacterial food packaging for meat. However, zein/THY/ $\gamma$ -CD-IC-NF (2:1) exhibited slightly better results in comparison to zein/THY/ $\gamma$ -CD-IC-NF (1:1). This result is correlated well with the release and antibacterial test.

## Chapter 3

---

### **ELECTROSPINNING OF POLYMER-FREE CYCLODEXTRIN INCLUSION COMPLEX NANOFIBERS**

(Parts of this study was published as “Electrospinning of polymer-free cyclodextrin/geraniol-inclusion complex nanofibers: enhanced shelf-life of geraniol with antibacterial and antioxidant properties”, Zeynep Aytac, Zehra Irem Yildiz, Fatma Kayaci-Senirmak, Nalan Oya San Keskin, Turgay Tekinay and Tamer Uyar\*, RSC Advances, May 4, 2016 (Web), Reproduced (or 'Reproduced in part') from Ref. [127] with permission from Royal Society of Chemistry. DOI: 10.1039/c6ra07088d)

## **6. Electrospinning of polymer-free cyclodextrin/geraniol-inclusion complex nanofibers: enhanced shelf-life of geraniol with antibacterial and antioxidant properties**

### **6.1 Introduction**

Electrospinning is one of the most common techniques to produce polymeric nanofibers. The unique characteristics of electrospun nanofibers such as high surface-to-volume ratio, controllable fiber diameter and morphologies (core-shell, hollow, and porous) can be obtained by changing the process parameters [3, 9]. The nanofiber production through electrospinning is usually carried out by dissolving polymers in organic solvents; however, there exist some drawbacks like solvent costs and environmental hazards when organic solvents are used, especially in healthcare and food applications. So, the use of water-soluble polymers is an alternative choice to avoid such organic solvent issues by using water as a solvent for the electrospinning. The electrospinning of nanofibers from small molecules [219-222] and cyclic oligosaccharides such as CDs [119-123, 125] is quite a challenge when compared to polymeric systems due to the lack of chain entanglement and overlapping. The formation self-assembly and aggregates in highly concentrated solutions of CDs via intermolecular hydrogen bonding enables the production of nanofibers from CD solutions [119-123, 125]. Moreover, CDs are advantageous over other small molecules that are being used to produce nanofibers by electrospinning, since CDs are capable of forming CD-ICs with various compounds. In our group, we had previously produced polymeric nanofibers to incorporate CD-ICs of volatile

compounds such as menthol [94-96], vanillin [97], eugenol [99], geraniol [100], and allyl isothiocyanate [102]. However, the weight loading of volatile compound was always limited (up to 5% (w/w), with respect to polymer matrix) since the incorporation of higher amount of CD-IC disturbs the electrospinnability of the system to obtain uniform nanofibers. In our recent studies, we have also demonstrated the electrospinning of polymer-free nanofibers from triclosan/cyclodextrin inclusion complexes by using modified CDs (HP $\beta$ CD and HP $\gamma$ CD) without using polymeric carrier matrix [124, 125].

Essential oils (EOs) are an important category of hydrophobic agents synthesized in plants and they are volatile compounds characterized by a strong odour [223]. Known for their antibacterial, antioxidant, antifungal, antiseptic properties and fragrance, EOs are used in preservation and flavouring of foods and as fragrance in cosmetic and household cleaning products [223]. Because of their low water solubility and highly volatile nature, encapsulation is of great importance for EOs to be used efficiently [223].

Geraniol (Figure 41d) is a terpene alcohol found in EOs of various aromatic plants and it is used in cosmetics, shampoos, soaps, toiletries, household cleaners, and detergents [224]. Beside its characteristic rose-like odour, it also exhibits insecticidal, antimicrobial, antioxidant, antifungal and anti-inflammatory properties [224]. However, its insolubility in water reduces its efficiency as flavour/fragrance in certain applications [224]. Supramolecular host-guest complexes can be designed in order to enhance the solubility of EOs with CDs. In addition to solubility issue, administering volatile compounds for various purposes often require development of novel carrier

systems. One of the ways to achieve this goal is incorporating CD-IC of active agents into electrospun polymeric nanofibers [94-97, 99, 100, 102]. Therefore, the need for biodegradable polymers have occurred. A number of our recent studies have dealt with the use of biodegradable/biocompatible polymeric nanofibers in encapsulating EOs [96, 97, 99, 100, 102].

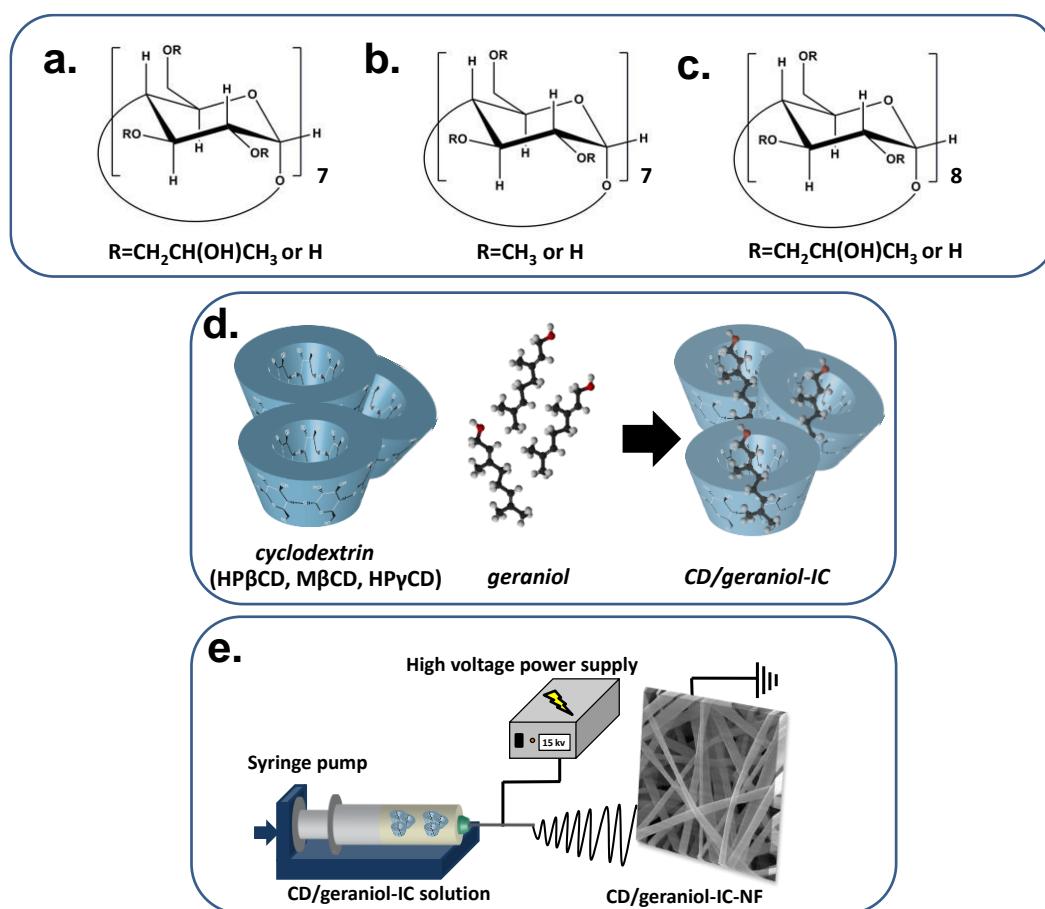


**Figure 41.** The chemical structure of (a) HPβCD, (b) MβCD, (c) HPγCD; the schematic representation of (d) CD/geraniol-IC formation, and (e) electrospinning of nanofibers from CD/geraniol-IC aqueous solution. (Copyright © 2016, Royal Society of Chemistry. Reprinted with permission from Ref. [127])

In this part, we have formed inclusion complexes of geraniol (which is a well-known volatile essential oil compound) with three modified CDs (HPβCD,

M $\beta$ CD, and HP $\gamma$ CD) (Figure 41a-c) (Figure 41d), and we have produced free-standing CD/geraniol-IC nanofibrous web via electrospinning without using polymeric carrier matrix (Figure 41e). The solubility improvement in geraniol by complexation was confirmed by phase solubility test. The uniform and bead-free morphology of the CD/geraniol-IC nanofibers was observed by SEM imaging. Further chemical, structural and thermal characterizations of CD/geraniol-IC nanofibers were performed by <sup>1</sup>H-NMR, XRD, FTIR, TGA, and DSC. The short-term temperature dependent release of geraniol from CD/geraniol-IC-NF at 37°C, 50°C, and 75°C was examined using HS GC-MS for 3 h, whereas the long term release of geraniol from nanofibers at room temperature was measured by TGA for 50 days. The antibacterial activity of CD/geraniol-IC nanofibers against model Gram-negative (*Escherichia coli* (*E. coli*)) and Gram-positive (*Staphylococcus aureus* (*S. aureus*)) bacteria was tested using colony counting method. Furthermore, antioxidant activity of nanofibers was monitored by 2,2-diphenyl-1-picrylhydrazyl (DPPH) radical scavenging assay.

## **6.2 Experimental**

### **6.2.1 Materials**

Geraniol (97%, Sigma), 2,2-diphenyl-1-picrylhydrazyl (DPPH, Sigma-Aldrich) methanol (extra pure, Sigma-Aldrich) and deuterated dimethylsulfoxide (DMSO-d<sub>6</sub>, deuteration degree min 99.8% for NMR spectroscopy, Merck), polyvinyl alcohol (PVA, Mw ~ 85.000-146.000 g/mol, Sigma Aldrich, 87-89% hydrolyzed) were purchased and used as received without any further

purification. Hydroxypropyl-beta-cyclodextrin (HP $\beta$ CD), methylated-beta-cyclodextrin (M $\beta$ CD), and hydroxypropyl-gamma-cyclodextrin (HP $\gamma$ CD) was kindly donated by Wacker Chemie (Germany). The water used in the experiments was distilled-deionized from a Millipore Milli-Q ultrapure water system.

### **6.2.2 Preparation of electrospinning solutions**

In order to prepare the CD/geraniol-IC solutions; HP $\beta$ CD, M $\beta$ CD, and HP $\gamma$ CD (200%, w/v) was dissolved in water and afterwards geraniol was added. The amount of geraniol was determined as 1:1 molar ratio with each CD type. The resulting solutions were stirred at room temperature (RT) for overnight. Finally, electrospinning was performed and HP $\beta$ CD/geraniol-IC-NF, M $\beta$ CD/geraniol-IC-NF, and HP $\gamma$ CD/geraniol-IC-NF webs were obtained. The viscosity and conductivity of CD/geraniol-IC solutions and the average fiber diameter (AFD) values of CD/geraniol-IC-NF are shown in Table 6. Electrospinning of pure CD nanofibers without geraniol (HP $\beta$ CD-NF, M $\beta$ CD-NF, and HP $\gamma$ CD-NF) were produced for comparative measurements according to our previous reports.<sup>18-19</sup> 10% (w/w, with respect to polymer) geraniol encapsulated PVA solution was prepared in aqueous solution and nanofibers (PVA/geraniol-NF) was produced via electrospinning.

### **6.2.3 Electrospinning**

CD, CD/geraniol-IC, and PVA/geraniol solutions were loaded into a 1 mL plastic syringe with metallic needle of 0.4 mm inner diameter. Then, the solutions were pumped at a constant rate (0.5 mL/h) via syringe pump (KD

Scientific, KDS-101, USA). A grounded metal covered by aluminium foil placed at a distance of 10 cm from the needle tip was used as a collector. 15-20 kV was applied from the high voltage power supply (AU Series, Matsusada Precision Inc., Japan). CD/geraniol-IC-NFs were kept in refrigerator until the analyses. All experiments were carried out in an enclosed Plexiglas box at 25°C and 18% relative humidity.

## **6.2.4 Characterizations and measurements**

Phase-solubility measurements for CDs (HP $\beta$ CD, M $\beta$ CD, and HP $\gamma$ CD) and geraniol systems were performed in aqueous solution according to the method of Higuchi and Connors [161]. An excess amount of geraniol was added to CD solutions and the suspensions were shaken at RT. After the equilibrium was achieved at the end of 24 hours, the suspensions were filtered through 0.45  $\mu$ m membrane filter and finally dilution was done with water. UV spectroscopy measurements were done at 241 nm (Varian, Cary 100). The experiments were carried out in triplicate and each data point is the average of the three determinations.

The viscosity measurements of HP $\beta$ CD/geraniol-IC, M $\beta$ CD/geraniol-IC, and HP $\gamma$ CD/geraniol-IC solutions were performed at RT via Anton Paar Physica MCR 301 rheometer equipped with a cone/plate accessory (spindle type CP 40-2) at a constant shear rate of 100 s<sup>-1</sup>. The solution conductivity for these CD/geraniol-IC systems was measured by Inolab® pH/Cond 720-WTW.

The morphological characterization of HP $\beta$ CD-NF, M $\beta$ CD-NF, HP $\gamma$ CD-NF, HP $\beta$ CD/geraniol-IC-NF, M $\beta$ CD/geraniol-IC-NF, and HP $\gamma$ CD/geraniol-IC-NF,

and PVA/geraniol-NF was examined by scanning electron microscopy (SEM, FEI - Quanta 200 FEG). The nanofibrous web samples were placed on metal stubs by using double-sided copper tape prior to taking SEM images and the samples were sputtered with 5 nm of Au/Pd (PECS-682) to minimize charging problem during SEM imaging of the samples. SEM images were also used to calculate the average fiber diameter (AFD) and fiber diameter distribution of the nanofibrous webs by measuring the diameter of about 100 fibers.

The proton nuclear magnetic resonance ( $^1\text{H-NMR}$ ) spectra were recorded at 400 MHz (Bruker DPX-400). 10 mg of HP $\beta$ CD/geraniol-IC-NF, M $\beta$ CD/geraniol-IC-NF, and HP $\gamma$ CD/geraniol-IC-NF were dissolved in 0.5 mL of d<sub>6</sub>-DMSO to calculate the molar ratio of CDs and geraniol in each system by integrating the peak ratio of the characteristic chemical shifts corresponding to CD and geraniol. Integration of the chemical shifts ( $\delta$ ) was calculated by using Mestrenova software.

Thermal gravimetric analysis (TGA, TA Q500, USA) analyses were performed for geraniol, HP $\beta$ CD-NF, M $\beta$ CD-NF, HP $\gamma$ CD-NF, HP $\beta$ CD/geraniol-IC-NF, M $\beta$ CD/geraniol-IC-NF, and HP $\gamma$ CD/geraniol-IC-NF. TGA was conducted under nitrogen atmosphere by heating the samples from 25°C to 450°C at the heating rate of 20°C/min. Differential scanning calorimetry (DSC, TA Q2000, USA) analyses were performed on HP $\beta$ CD-NF, M $\beta$ CD-NF, HP $\gamma$ CD-NF, HP $\beta$ CD/geraniol-IC-NF, M $\beta$ CD/geraniol-IC-NF, and HP $\gamma$ CD/geraniol-IC-NF with a heating rate of 20°C/min from 25°C to 200°C under nitrogen flow.

X-ray diffraction (XRD) measurements of HP $\beta$ CD-NF, M $\beta$ CD-NF, HP $\gamma$ CD-NF, HP $\beta$ CD/geraniol-IC-NF, M $\beta$ CD/geraniol-IC-NF, and HP $\gamma$ CD/geraniol-IC-NF were recorded at PANalytical X'Pert powder diffractometer using Cu K $\alpha$  radiation in powder diffraction configuration and the spectra were collected in the 5-30° 2 $\theta$  range. XRD was not carried out for geraniol since it is a liquid compound at RT.

The infrared spectra of geraniol, HP $\beta$ CD-NF, M $\beta$ CD-NF, HP $\gamma$ CD-NF, HP $\beta$ CD/geraniol-IC-NF, M $\beta$ CD/geraniol-IC-NF, and HP $\gamma$ CD/geraniol-IC-NF were obtained by using a Fourier transform infrared spectrometer (FTIR) (Bruker-VERTEX 70). The samples were mixed with potassium bromide (KBr) and pressed as pellets for the measurement. The scans (64 scans) were recorded between 4000 cm<sup>-1</sup> and 400 cm<sup>-1</sup> at resolution of 4 cm<sup>-1</sup>.

The amount of geraniol released from HP $\beta$ CD/geraniol-IC-NF, M $\beta$ CD/geraniol-IC-NF, and HP $\gamma$ CD/geraniol-IC-NF was determined through headspace gas chromatography-mass spectrometry (HS GC-MS, Agilent Technologies 7890A gas chromatograph equipped with 5975C mass spectrometer) for 3 h. The capillary column was HP-5MS (Hewlett-Packard, Avondale, PA) (30 m  $\times$  0.25 mm i.d., 0.25  $\mu$ m film thickness). CD/geraniol-IC-NFs (10 mg) were placed in 20 mL headspace glass vials and the vial was agitated at 500 rpm and 37°C, 50°C, and 75°C. The release experiments were carried out in triplicate and the results were reported as average  $\pm$  standard deviation. The syringe temperature was 37°C, 50°C, and 75°C as well. The vapour which was injected by headspace injector from vial to HS GC-MS was 250  $\mu$ L. The oven temperature was initially held at 40°C for 3 min. Then the temperature was raised with a gradient

of 10°C/min until 200°C. The oven was held for 3 minute at 200°C. The instrument was operated in a splitless and selected ion monitoring mode (SIM). NIST MS Search 2.0 library was used to decide the geraniol peak.

In order to evaluate the long term release of HPβCD/geraniol-IC-NF, MβCD/geraniol-IC-NF, HPγCD/geraniol-IC-NF, and PVA/geraniol-NF were kept separately at room temperature and 18% relative humidity for 50 days in open air in the laboratory. Then, TGA measurements were done at predetermined time intervals (1st day, 25th day, and 50th day).

The antibacterial properties of the HPβCD/geraniol-IC-NF, MβCD/geraniol-IC-NF, and HPγCD/geraniol-IC-NF were evaluated against *Escherichia coli* (*E. coli*, ATCC 10536) and *Staphylococcus aureus* (*S. aureus*, ATCC 25923) bacteria by using colony counting method. Prior to use, exponentially growing cultures of *E. coli*, and *S. aureus* were obtained by allowing each strain to grow in nutrient broth medium at 37°C for 24 h. After bacterial activation, UV sterilized nanofibers were immersed into the culture suspension and incubated at 37°C for 24 h. Finally, inocula were prepared by diluting the exponentially growing cultures with physiological solution (0.9% sodium chloride) to obtain approximately 10<sup>8</sup> colony forming unit (cfu)/ml. Different dilutions (10<sup>1</sup> to 10<sup>9</sup>) were made by successively adding 1 mL culture into 9 mL of phosphate buffer solution. Then, 0.1 mL of the diluted culture was spread on a nutrient agar plate and incubated at 37°C for 24 h. The number of the colonies was counted and three repeats were performed for each sample.

The antibacterial activity of the CD/geraniol-IC-NFs was defined as follows:

$$\text{Antibacterial activity (\%)} = (A-B)/A * 100 \quad (\text{Equation 7})$$

where A and B are the number of colonies (cfu/mL) before and after CD/geraniol-IC-NF were added, respectively.

Antioxidant activity of geraniol, HP $\beta$ CD-NF, M $\beta$ CD-NF, HP $\gamma$ CD-NF, HP $\beta$ CD/geraniol-IC-NF, M $\beta$ CD/geraniol-IC-NF, and HP $\gamma$ CD/geraniol-IC-NF were tested according to 2,2-diphenyl-1-picrylhydrazyl (DPPH) radical scavenging assay.  $10^{-4}$  M DPPH solution was prepared by dissolving DPPH in methanol:water (1:1). 40 mg HP $\beta$ CD-NF, M $\beta$ CD-NF, HP $\gamma$ CD-NF, HP $\beta$ CD/geraniol-IC-NF, M $\beta$ CD/geraniol-IC-NF, and HP $\gamma$ CD/geraniol-IC-NF and 4.76 mg geraniol (which is the maximum amount in CD/geraniol-IC-NFs) were immersed in 3 ml of DPPH solution. The resulting solutions were incubated in dark at RT for 72 h. The absorbance of the solutions was measured (24 h, 48 h, and 72 h) via UV-Vis spectroscopy (Varian, Cary 100) at 525 nm. The absorbance of DPPH solution was defined as 100% and the antioxidant activities (%) of each system were calculated with the following equation:

$$\text{Antioxidant activity (\%)} = (A_{\text{control}} - A_{\text{sample}}) / A_{\text{control}} * 100 \quad (\text{Equation 8})$$

where  $A_{\text{control}}$  and  $A_{\text{sample}}$  represent the absorbance of DPPH solution and DPPH solution with samples, respectively. The photographs of the solutions were taken after 24 hour, 48 hour, and 72 hour of the incubation. The experiments were performed in triplicate and the results were given as average values  $\pm$  standard deviation.

## **6.3 Results and discussion**

### **6.3.1 Phase solubility studies**

Phase solubility profiles of HP $\beta$ CD/geraniol, M $\beta$ CD/geraniol, and HP $\gamma$ CD/geraniol systems are given in Figure 42a-c. As seen from the diagrams, the aqueous solubility of geraniol increased linearly by complexation. CD/geraniol systems exhibited A<sub>L</sub> type diagram which is also indication of 1:1 stoichiometry between each CD and geraniol.

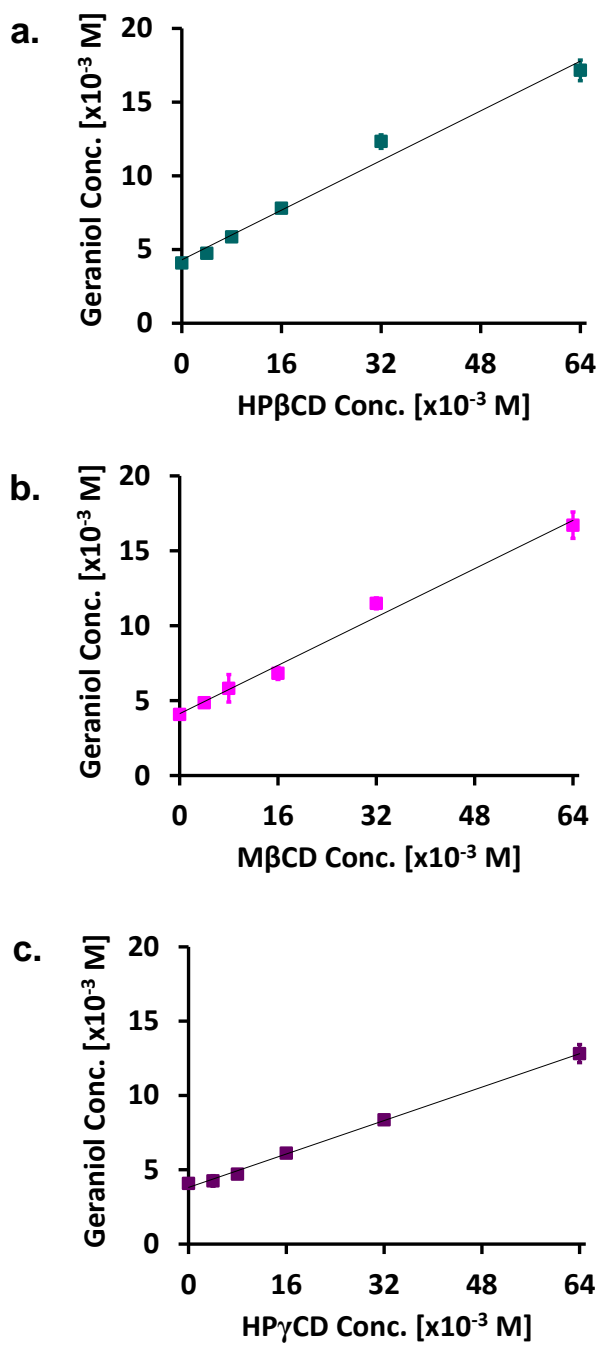


**Figure 42.** Phase solubility diagram of (a) HP $\beta$ CD/geraniol, (b) M $\beta$ CD/geraniol, (c) HP $\gamma$ CD/geraniol systems in water ( $n = 3$ ). (Copyright © 2016, Royal Society of Chemistry. Reprinted with permission from Ref. [127])

### 6.3.2 Morphology analysis of nanofibers

Figure 43a-f shows scanning electron microscopy (SEM) images of HP $\beta$ CD-NF, M $\beta$ CD-NF, HP $\gamma$ CD-NF, HP $\beta$ CD/geraniol-IC-NF, M $\beta$ CD/geraniol-IC-NF, and HP $\gamma$ CD/geraniol-IC-NF. SEM image of PVA/geraniol-NF is shown in Figure 44.

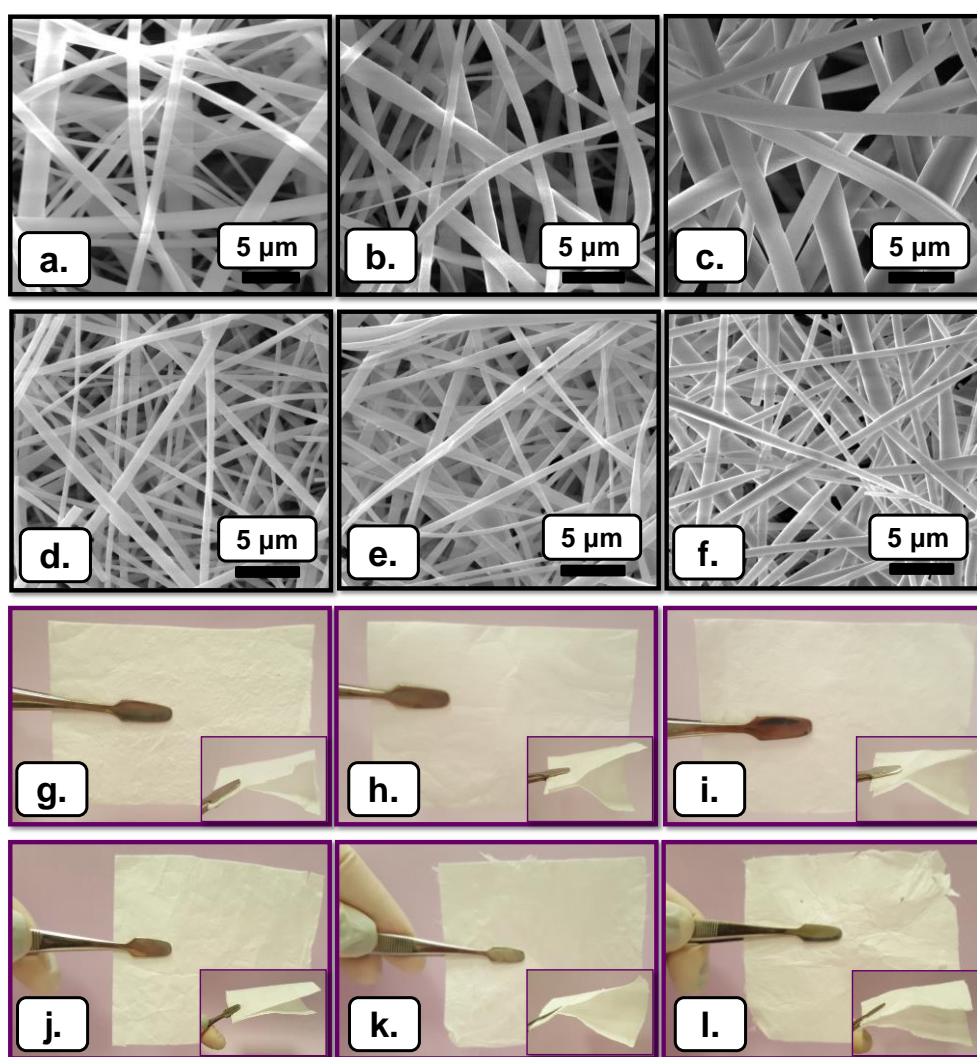


**Figure 43.** SEM images of electrospun nanofibers obtained from the aqueous solutions of (a) HP $\beta$ CD, (b) M $\beta$ CD, (c) HP $\gamma$ CD, (d) HP $\beta$ CD/geraniol-IC, (e) M $\beta$ CD/geraniol-IC, and (f) HP $\gamma$ CD/geraniol-IC; the photographs of (g) HP $\beta$ CD-NF, (h) M $\beta$ CD-NF, (i) HP $\gamma$ CD-NF, (j) HP $\beta$ CD/geraniol-IC-NF, (k) M $\beta$ CD/geraniol-IC-NF, and (l) HP $\gamma$ CD/geraniol-IC-NF webs. (Copyright © 2016, Royal Society of Chemistry. Reprinted with permission from Ref. [127])

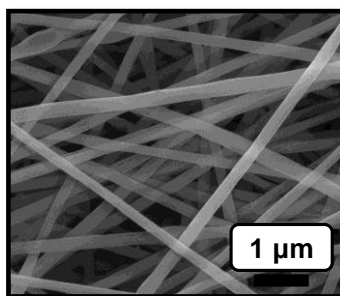


**Figure 44.** SEM image of PVA/geraniol-NF. (Copyright © 2016, Royal Society of Chemistry. Reprinted with permission from Ref. [127])

Bead-free and uniform nanofibers were obtained as seen from SEM images. The average fiber diameter (AFD) of HP $\beta$ CD-NF, M $\beta$ CD-NF, HP $\gamma$ CD-NF, HP $\beta$ CD/geraniol-IC-NF, M $\beta$ CD/geraniol-IC-NF, and HP $\gamma$ CD/geraniol-IC-NF were calculated as 910 $\pm$ 510 nm, 845 $\pm$ 425 nm, 1640 $\pm$ 545 nm, 520 $\pm$ 220 nm, 600 $\pm$ 220 nm, and 930 $\pm$ 370 nm from SEM images, respectively. There is no significant difference between AFDs of HP $\beta$ CD/geraniol-IC-NF and M $\beta$ CD/geraniol-IC-NF. The viscosity of HP $\gamma$ CD/geraniol-IC solutions was higher than HP $\beta$ CD/geraniol-IC and M $\beta$ CD/geraniol-IC solutions; whereas HP $\gamma$ CD/geraniol-IC solutions exhibited lowest conductivity among all solutions (Table 6). Therefore, AFD of HP $\gamma$ CD/geraniol-IC-NF was highest among all CD/geraniol-IC-NFs due to higher solution viscosity and much lower solution conductivity which results in less stretching of the jet during electrospinning [3, 9]. Furthermore, the photographs of free-standing HP $\beta$ CD-NF, M $\beta$ CD-NF, HP $\gamma$ CD-NF, HP $\beta$ CD/geraniol-IC-NF, M $\beta$ CD/geraniol-IC-NF, and HP $\gamma$ CD/geraniol-IC-NF webs which can be easily-handled showed that all CD/geraniol-IC-NF webs have mechanical integrity despite their main components were amorphous small molecules (Figure 43g-f).

**Table 6.** The properties of the solutions used for electrospinning and morphological characteristics of the resulting nanofibers. (Copyright © 2016, Royal Society of Chemistry. Reprinted with permission from Ref. [127])

<b>Solutions</b>	<b>% CD<sup>a</sup> (w/v)</b>	<b>%geraniol<sup>b</sup> (w/w)</b>	<b>Viscosity (Pa·s)</b>	<b>Conductivity (<math>\mu</math>S/cm)</b>	<b>Average fiber diameter (nm)</b>	<b>Fiber morphology</b>
HP $\beta$ CD/geraniol-IC-NF	200	9.502	0.522	212	520 $\pm$ 220	Bead free nanofibers
M $\beta$ CD/geraniol-IC-NF	200	11.894	0.306	768	600 $\pm$ 220	Bead free nanofibers
HP $\gamma$ CD/geraniol-IC-NF	200	8.676	0.904	4.92	930 $\pm$ 370	Bead free nanofibers

<sup>a</sup> with respect to solvent (water).

<sup>b</sup> with respect to total weight of the sample.

### 6.3.3 The molar ratio of inclusion complex

Proton nuclear magnetic resonance ( $^1\text{H-NMR}$ ) was employed to further explore the molar ratio of HP $\beta$ CD/geraniol-IC-NF, M $\beta$ CD/geraniol-IC-NF, and HP $\gamma$ CD/geraniol-IC-NF (Figure 45a-c). In order to make the molar ratio calculations, the integration of peak at 1.0 ppm (HP $\beta$ CD and HP $\gamma$ CD) and 2.0 ppm (geraniol) were used. The molar ratio was calculated as 1.00:0.60 and 1.00:0.65 for HP $\beta$ CD/geraniol-IC-NF and HP $\gamma$ CD/geraniol-IC-NF, respectively. The molar ratio of M $\beta$ CD:geraniol in M $\beta$ CD/geraniol-IC-NF was calculated as 1.00:0.64 by taking the integration of the protons of M $\beta$ CD at 3.5-3.7 ppm and geraniol at 2.0 ppm. From the  $^1\text{H-NMR}$  results, it can be concluded that the substantial amount of geraniol was preserved in HP $\beta$ CD/geraniol-IC-NF (60%, w/w), M $\beta$ CD/geraniol-IC-NF (64%, w/w), and HP $\gamma$ CD/geraniol-IC-NF (65%, w/w) during the preparation, electrospinning and storage. It is worth mentioning that, in our long term release study, we have seen that geraniol could not be preserved when electrospun with polyvinyl alcohol (PVA) polymeric matrix without cyclodextrins.

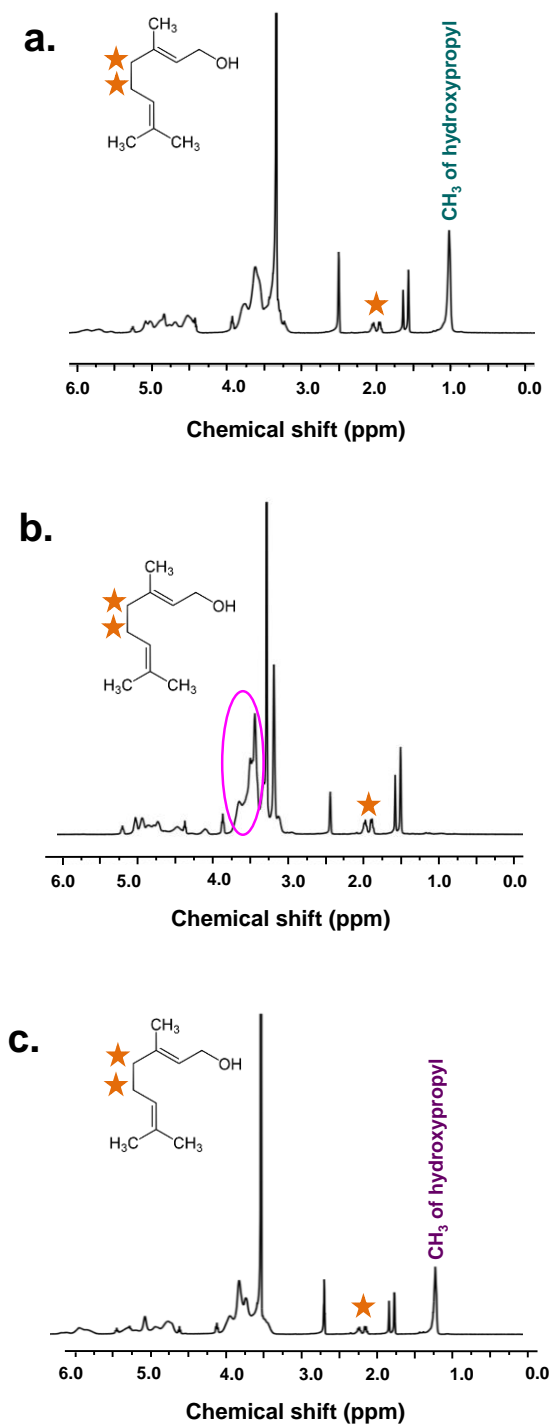


**Figure 45.** <sup>1</sup>H-NMR spectra of (a) HPβCD/geraniol-IC-NF, (b) MβCD/geraniol-IC-NF, and (c) HPγCD/geraniol-IC-NF dissolved in d<sub>6</sub>-DMSO. (Copyright © 2016, Royal Society of Chemistry. Reprinted with permission from Ref. [127])

### 6.3.4 Thermal analysis of nanofibers

The thermal stability of geraniol, HP $\beta$ CD-NF, M $\beta$ CD-NF, HP $\gamma$ CD-NF, HP $\beta$ CD/geraniol-IC-NF, M $\beta$ CD/geraniol-IC-NF, and HP $\gamma$ CD/geraniol-IC-NF were investigated by thermal gravimetric analysis (TGA) (Figure 46a-c). Pristine HP $\beta$ CD-NF, M $\beta$ CD-NF and HP $\gamma$ CD-NF exhibited two weight losses below 100°C and above 275°C which belong to the water loss and main thermal degradation of cyclodextrins (CDs), respectively [125]. The first weight loss below 100°C observed in HP $\beta$ CD/geraniol-IC-NF, M $\beta$ CD/geraniol-IC-NF, and HP $\gamma$ CD/geraniol-IC-NF attributed to water loss. In addition to water loss, two additional weight losses were seen in HP $\beta$ CD/geraniol-IC-NF and HP $\gamma$ CD/geraniol-IC-NF. The second weight loss in HP $\beta$ CD/geraniol-IC-NF was between 75°C and 240°C; whereas the second weight loss for HP $\gamma$ CD/geraniol-IC-NF started from 95°C and continued till 250°C. The shifting of thermal evaporation onset of geraniol from 70°C to higher temperature suggested the existence of inclusion complex between CDs (HP $\beta$ CD and HP $\gamma$ CD) and geraniol. The third weight loss in HP $\beta$ CD/geraniol-IC-NF and HP $\gamma$ CD/geraniol-IC-NF which is above 275°C belong to the main thermal degradation of CDs. M $\beta$ CD/geraniol-IC-NF exhibited four stages of weight loss which was below 100°C, 70°C-170°C, 170°C-290°C, and above 295°C. These stages belong to water loss, evaporation of geraniol in the complex in 2 steps, the main thermal degradation of M $\beta$ CD, respectively. There is a slight shift in the onset temperature of evaporation of geraniol as seen in the second stage and shifting to much higher temperature was observed in the third stage of TGA curve of M $\beta$ CD/geraniol-IC-NF. These results showed the presence of two types of

complexes with a stronger interaction in the third step compared to second step. In addition, thermal stability of the complex in M $\beta$ CD/geraniol-IC-NF was higher compared to the complexes in HP $\beta$ CD/geraniol-IC-NF and HP $\gamma$ CD/geraniol-IC-NF and this result suggested stronger complexation between M $\beta$ CD and geraniol. From TGA data, the calculated geraniol amount in HP $\beta$ CD/geraniol-IC-NF, M $\beta$ CD/geraniol-IC-NF, and HP $\gamma$ CD/geraniol-IC-NF was found to be 83%, 89%, and 82% of the initial amount of geraniol, respectively. Accordingly, the molar ratio of HP $\beta$ CD, M $\beta$ CD, and HP $\gamma$ CD to geraniol was calculated as 1.00:0.83, 1.00:0.89 and 1.00:0.82, respectively. The molar ratio of CD:geraniol in CD/geraniol-IC-NF samples calculated from the TGA data were not exactly same values with the data obtained from  $^1\text{H-NMR}$ , but they were comparable indicating that significant amount of geraniol was preserved in these CD based nanofibers. On the other hand, in long term release study, we observed that geraniol could not be preserved in electrospun polymeric nanofiber (PVA) without CD-IC.

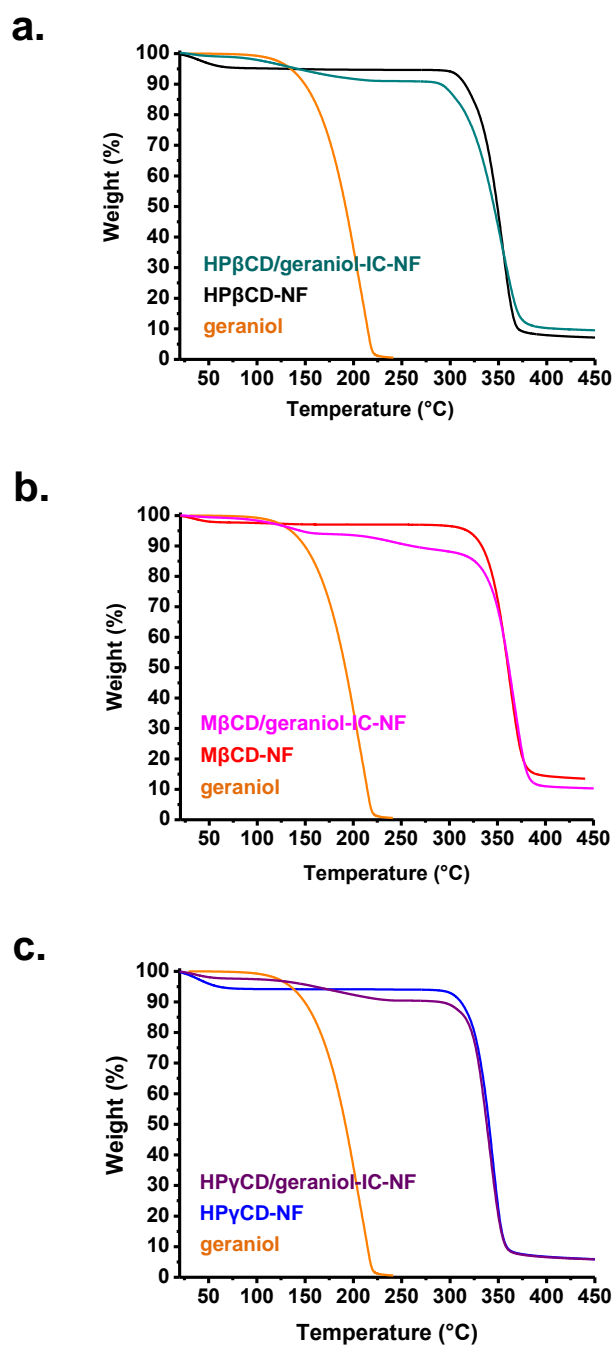


**Figure 46.** TGA thermograms of (a) geraniol, HPβCD-NF, HPβCD/geraniol-IC-NF; (b) geraniol, MβCD-NF, MβCD/geraniol-IC-NF; (c) geraniol, HPγCD-NF, HPγCD/geraniol-IC-NF. (Copyright © 2016, Royal Society of Chemistry. Reprinted with permission from Ref. [127])

Differential scanning calorimetry (DSC) curves of HPβCD-NF, MβCD-NF, HPγCD-NF, HPβCD/geraniol-IC-NF, MβCD/geraniol-IC-NF, and

HP $\gamma$ CD/geraniol-IC-NF are given in Figure 47. HP $\beta$ CD-NF, M $\beta$ CD-NF, and HP $\gamma$ CD-NF exhibited typical broad endothermic peaks between 25-160°C, 25-155°C, and 25-155°C, respectively and these peaks correspond to the dehydration of CDs. DSC curves of CD/geraniol-IC-NF indicated endothermic peaks in the range of 65-150°C, 60-150°C, and 65-170°C for HP $\beta$ CD/geraniol-IC-NF, M $\beta$ CD/geraniol-IC-NF and HP $\gamma$ CD/geraniol-IC-NF, respectively. The enthalpies of endothermic transitions of HP $\beta$ CD-NF, M $\beta$ CD-NF, and HP $\gamma$ CD-NF were 329 J/g, 99 J/g, and 255 J/g, while the enthalpies of HP $\beta$ CD/geraniol-IC-NF, M $\beta$ CD/geraniol-IC-NF, and HP $\gamma$ CD/geraniol-IC-NF were 84 J/g, 42 J/g, and 147 J/g, respectively. The reduction in the enthalpy of HP $\beta$ CD-NF, M $\beta$ CD-NF, and HP $\gamma$ CD-NF with the complexation of geraniol indicated that certain amount of water molecules in the cavity of CDs are displaced with geraniol which is an indication of complexation between CD and geraniol [225].

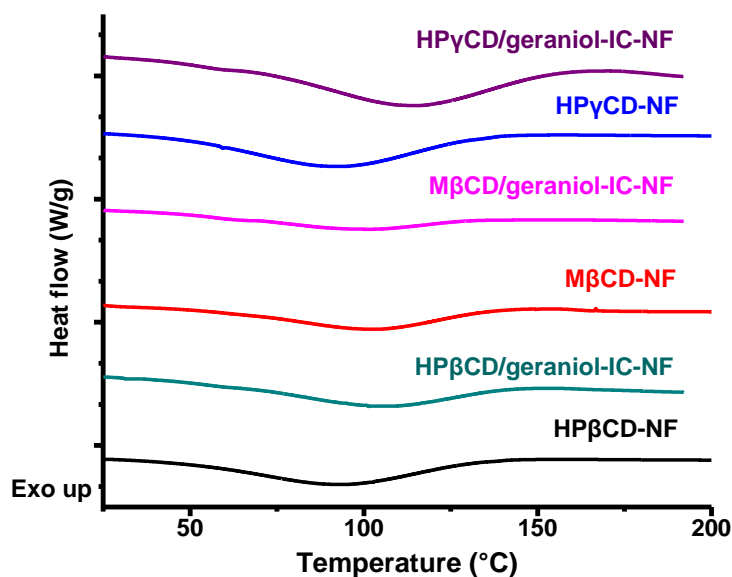


**Figure 47.** DSC thermograms of HP $\beta$ CD-NF, HP $\beta$ CD/geraniol-IC-NF, M $\beta$ CD-NF, M $\beta$ CD/geraniol-IC-NF, HP $\gamma$ CD-NF, and HP $\gamma$ CD/geraniol-IC-NF; (Copyright © 2016, Royal Society of Chemistry. Reprinted with permission from Ref. [127])

### 6.3.5 Structural characterization of nanofibers

X-ray diffraction (XRD) patterns of HP $\beta$ CD-NF, M $\beta$ CD-NF, HP $\gamma$ CD-NF, HP $\beta$ CD/geraniol-IC-NF, M $\beta$ CD/geraniol-IC-NF, and HP $\gamma$ CD/geraniol-IC-NF are shown in Figure 48. It is known that HP $\beta$ CD-NF, M $\beta$ CD-NF, and HP $\gamma$ CD-NF are amorphous like HP $\beta$ CD, M $\beta$ CD, and HP $\gamma$ CD molecules. HP $\beta$ CD/geraniol-IC-NF, M $\beta$ CD/geraniol-IC-NF, and HP $\gamma$ CD/geraniol-IC-NF were amorphous as well. Moreover, there is no crystal formation of geraniol in HP $\beta$ CD/geraniol-IC-NF, M $\beta$ CD/geraniol-IC-NF, and HP $\gamma$ CD/geraniol-IC-NF and this result confirms the formation of CD-IC.

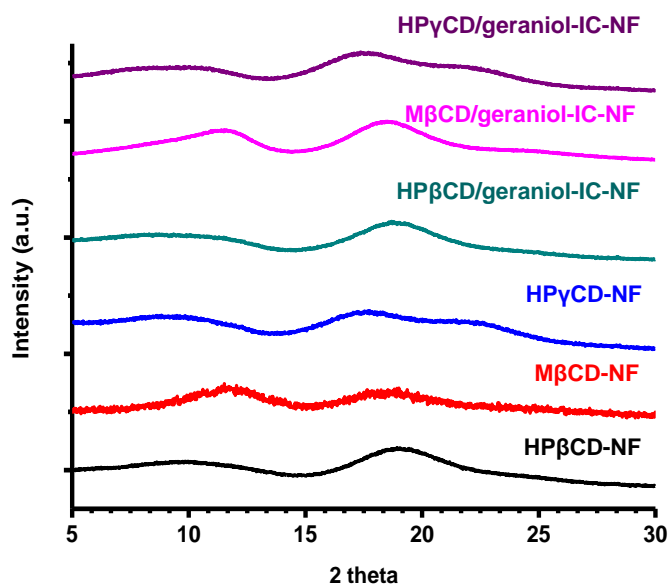


**Figure 48.** XRD patterns of HP $\beta$ CD-NF, M $\beta$ CD-NF, HP $\gamma$ CD-NF, HP $\beta$ CD/geraniol-IC-NF, M $\beta$ CD/geraniol-IC-NF, and HP $\gamma$ CD/geraniol-IC-NF. (Copyright © 2016, Royal Society of Chemistry. Reprinted with permission from Ref. [127])

The chemical structures of geraniol, HP $\beta$ CD-NF, M $\beta$ CD-NF, HP $\gamma$ CD-NF, HP $\beta$ CD/geraniol-IC-NF, M $\beta$ CD/geraniol-IC-NF, and HP $\gamma$ CD/geraniol-IC-NF was also investigated by FTIR spectroscopy (Figure 49). The FTIR spectrum of

geraniol was characterized by absorption peaks at  $3326\text{ cm}^{-1}$ ,  $1416\text{ cm}^{-1}$  (OH),  $2978\text{ cm}^{-1}$ ,  $2933\text{ cm}^{-1}$ ,  $1371\text{ cm}^{-1}$  (CH<sub>2</sub>),  $1650\text{ cm}^{-1}$ ,  $1022\text{ cm}^{-1}$ ,  $946\text{ cm}^{-1}$ ,  $863\text{ cm}^{-1}$  (C=C),  $1100\text{ cm}^{-1}$ ,  $1155\text{ cm}^{-1}$  (C-C-C) and  $1707\text{ cm}^{-1}$  (C-O) [226]. The characteristic absorption peaks of pure CDs observed at around  $1030$ ,  $1080$ , and  $1157\text{ cm}^{-1}$  due to the coupled C-C and C-O stretching vibrations and antisymmetric stretching vibration of the C-O-C glycosidic bridge,  $1638\text{ cm}^{-1}$ ,  $2925\text{ cm}^{-1}$ , and  $3401\text{ cm}^{-1}$  corresponding to H-OH bending, C-H stretching and O-H stretching, respectively overlap with the geraniol peaks [227]. Therefore, the geraniol peaks at around  $1380\text{ cm}^{-1}$  and  $1450\text{ cm}^{-1}$  in CD/geraniol-IC-NFs indicated the presence of geraniol in the nanofibers. In addition, shifting of these absorption bands toward higher frequency suggested the formation of the complex between geraniol and CDs. Similar peak shifts were also reported in the literature for geraniol/CD complexes [226].

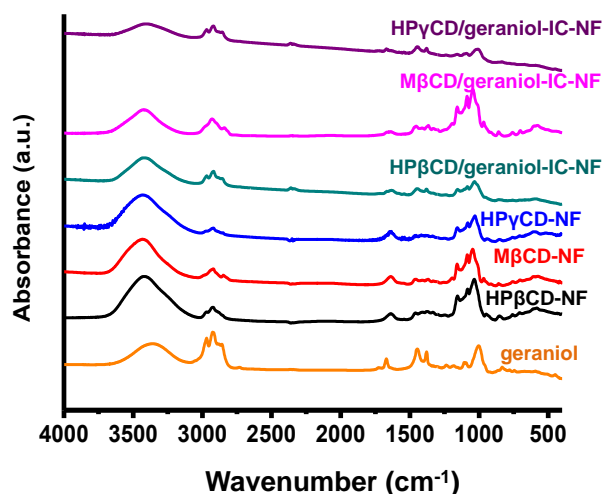


**Figure 49.** FTIR spectra of geraniol, HP $\beta$ CD-NF, M $\beta$ CD-NF, HP $\gamma$ CD-NF, HP $\beta$ CD/geraniol-IC-NF, M $\beta$ CD/geraniol-IC-NF, and HP $\gamma$ CD/geraniol-IC-NF. (a) Exemplary images of *Escherichia coli* (*E. coli*), *Staphylococcus aureus* (*S. aureus*) colonies. (Copyright © 2016, Royal Society of Chemistry. Reprinted with permission from Ref. [127])

### 6.3.6 Release study

M $\beta$ CD/geraniol-IC-NF, and HP $\gamma$ CD/geraniol-IC-NF are depicted in Figure 50a-c. When the temperature increases, the diffusion coefficient of the molecules increases [216]; so, the amount of geraniol released from HP $\beta$ CD/geraniol-IC-NF, M $\beta$ CD/geraniol-IC-NF, and HP $\gamma$ CD/geraniol-IC-NF was increased with increasing temperature from 37°C to 75°C. The total released amount of geraniol from M $\beta$ CD/geraniol-IC-NF was lower when compared to HP $\beta$ CD/geraniol-IC-NF and HP $\gamma$ CD/geraniol-IC-NF at 37°C, 50°C, and 75°C. This correlates with the higher thermal stability of M $\beta$ CD/geraniol-IC-NF as observed in TGA results (Figure 46) when compared to HP $\beta$ CD/geraniol-IC-NF and HP $\gamma$ CD/geraniol-IC-NF. In addition, although the total amount of preserved geraniol was almost same in HP $\beta$ CD/geraniol-IC-NF and HP $\gamma$ CD/geraniol-IC-NF as calculated from TGA results; the release amount of geraniol at 37°C, 50°C, and 75°C from HP $\gamma$ CD/geraniol-IC-NF was much less compared to HP $\beta$ CD/geraniol-IC-NF. The reason for the less amount of geraniol released from HP $\gamma$ CD/geraniol-IC-NF than that of HP $\beta$ CD/geraniol-IC-NF could be the higher complexation strength between HP $\gamma$ CD and geraniol.

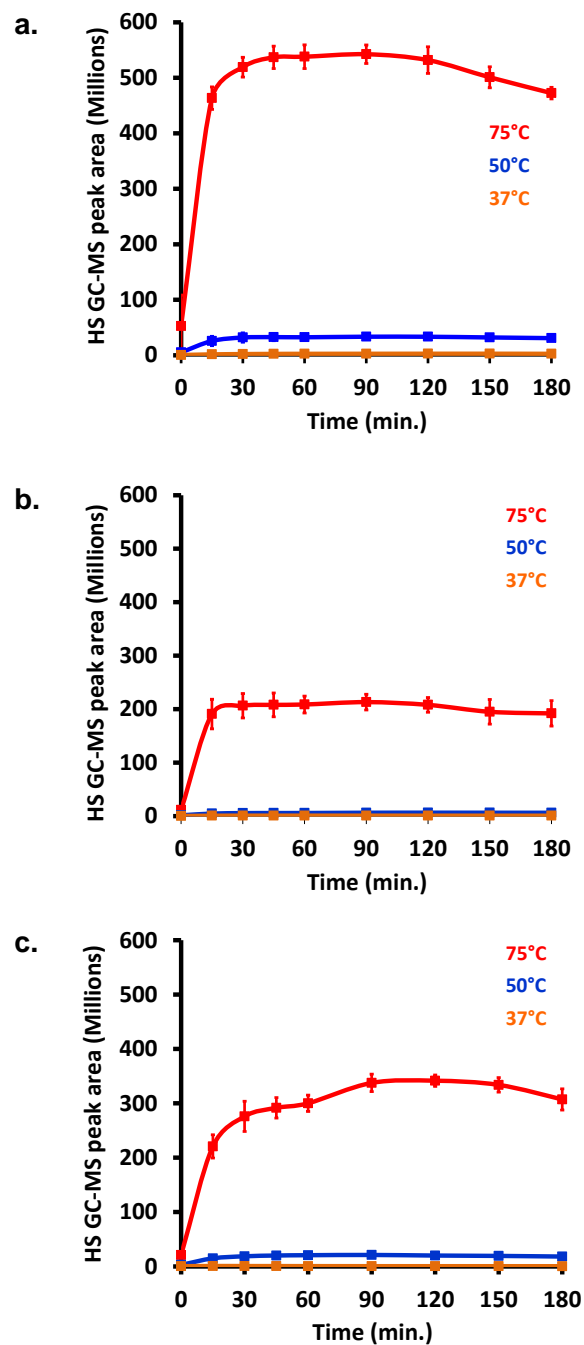


**Figure 50.** The cumulative release of geraniol from (a) HP $\beta$ CD/geraniol-IC-NF, (b) M $\beta$ CD/geraniol-IC-NF, and (c) HP $\gamma$ CD/geraniol-IC-NF at 37°C, 50°C, 75°C (n = 3). The error bars in the figure represent the standard deviation (SD). (Copyright © 2016, Royal Society of Chemistry. Reprinted with permission from Ref. [127])

TGA measurements were carried out in order to evaluate the long term release of HP $\beta$ CD/geraniol-IC-NF, M $\beta$ CD/geraniol-IC-NF, HP $\gamma$ CD/geraniol-IC-NF and geraniol encapsulated PVA nanofibers (PVA/geraniol-NF) (Figure 51). The results are given in Table 7. Most of the geraniol did not release from M $\beta$ CD/geraniol-IC-NF in parallel with the short term release experiments. This might be attributed to the high thermal stability of complex formed in M $\beta$ CD/geraniol-IC as shown in Figure 46b. Only 24% (w/w) of geraniol was released from M $\beta$ CD/geraniol-IC-NF at the end of 50 days. So, it can be concluded that M $\beta$ CD/geraniol-IC-NF is a better candidate for the long term release when compared to HP $\beta$ CD/geraniol-IC-NF and HP $\gamma$ CD/geraniol-IC-NF. The amount of released geraniol was almost same for HP $\beta$ CD/geraniol-IC-NF and HP $\gamma$ CD/geraniol-IC-NF; thus, about 50% of geraniol was released from HP $\beta$ CD/geraniol-IC-NF and HP $\gamma$ CD/geraniol-IC-NF at the end of 50 days. In our long term release study, geraniol was incorporated in PVA electrospun nanofibers for the comparative study to investigate the effect of cyclodextrin inclusion complexation for the stability of geraniol during and after electrospinning. PVA nanofiber matrix is a good comparison for CD nanofibers in terms of its electrospinnability in aqueous system and the presence of hydroxyl groups in its structure. However, we observed that geraniol could not be well preserved without CD-IC during electrospinning or during storage, and, evaporation of geraniol in PVA/geraniol-NF was unavoidable even after one day of its electrospinning. At the end of 50 days 71% of geraniol evaporated from PVA/geraniol-NF. On the contrary, here we observed that significant amount of

geraniol was preserved in nanofibrous matrix of CD/geraniol-IC-NF even after a long time of storage.

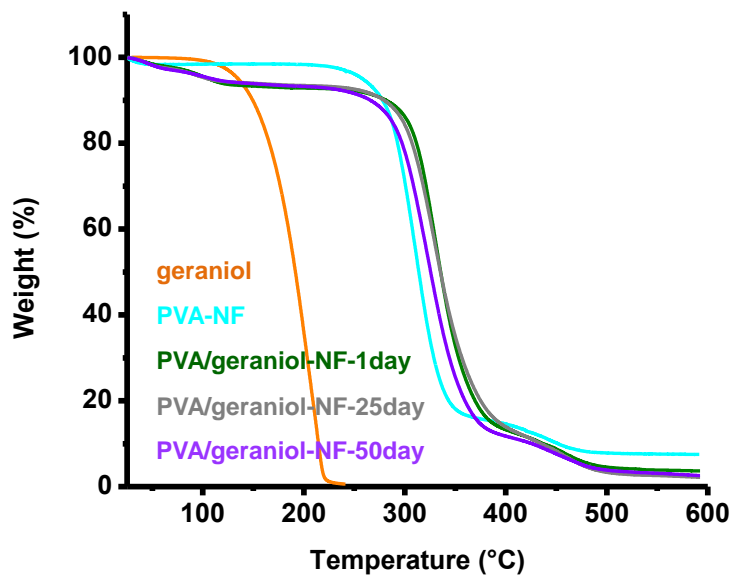


**Figure 51.** TGA of geraniol, PVA-NF, PVA/geraniol-NF-1day, PVA/geraniol-NF-25day, and PVA/geraniol-NF-50day. (Copyright © 2016, Royal Society of Chemistry. Reprinted with permission from Ref. [127])

**Table 7.** The amount of geraniol in CD/geraniol-IC-NFs and PVA/geraniol-NF at room temperature for 50 days. (Copyright © 2016, Royal Society of Chemistry. Reprinted with permission from Ref. [127])

Samples	theoretical amount		1st day		25th day		50th day	
	of geraniol <sup>a</sup> (%)		(%)	(%)	(%)	(%)	(%)	(%)
HP $\beta$ CD/geraniol-IC-NF	9.502	(100%)	7.233	(76%)	5.258	(55%)	4.228	(45%)
M $\beta$ CD/geraniol-IC-NF	11.894	(100%)	9.768	(82%)	9.381	(79%)	9.037	(76%)
HP $\gamma$ CD/geraniol-IC-NF	8.676	(100%)	5.541	(64%)	4.869	(56%)	4.289	(49%)
PVA/geraniol-NF	9.774	(100%)	4.415	(45%)	3.281	(34%)	2.866	(29%)

### 6.3.7 Antibacterial activity

There are several studies in the literature about antimicrobial effect of geraniol. For example, Friedman et al. showed that geraniol was found to be bactericidal against *E. coli* O157:H7 and *Salmonella enterica* [228]. Further, Tampieri et al. reported the antimicrobial activity of geraniol for *S.aureus* and various fungi [229]. As can be indicated from Figure 52a-d which shows the data obtained from cfu results, prepared CD/geraniol-IC-NFs possessed strong antibacterial activity against two model bacteria (*Escherichia coli* (*E. coli*) and *Staphylococcus aureus* (*S. aureus*)). Namely, HP $\beta$ CD/geraniol-IC-NF, M $\beta$ CD/geraniol-IC-NF, and HP $\gamma$ CD/geraniol-IC-NF exhibited 87 $\pm$ 0.6%, 100 $\pm$ 0.6%, and 85 $\pm$ 0.3% and 100 $\pm$ 0.3%, 100 $\pm$ 0.8%, 100 $\pm$ 0.4% antibacterial activity against *E. coli* and *S. aureus*, respectively. Antibacterial activities (%) of CD/geraniol-IC-NFs were found to be more against *S. aureus* compared to *E. coli*. Gram-negative bacteria were more resistant than Gram-positive bacteria because they have an additional protective barrier of the outer membrane [230].

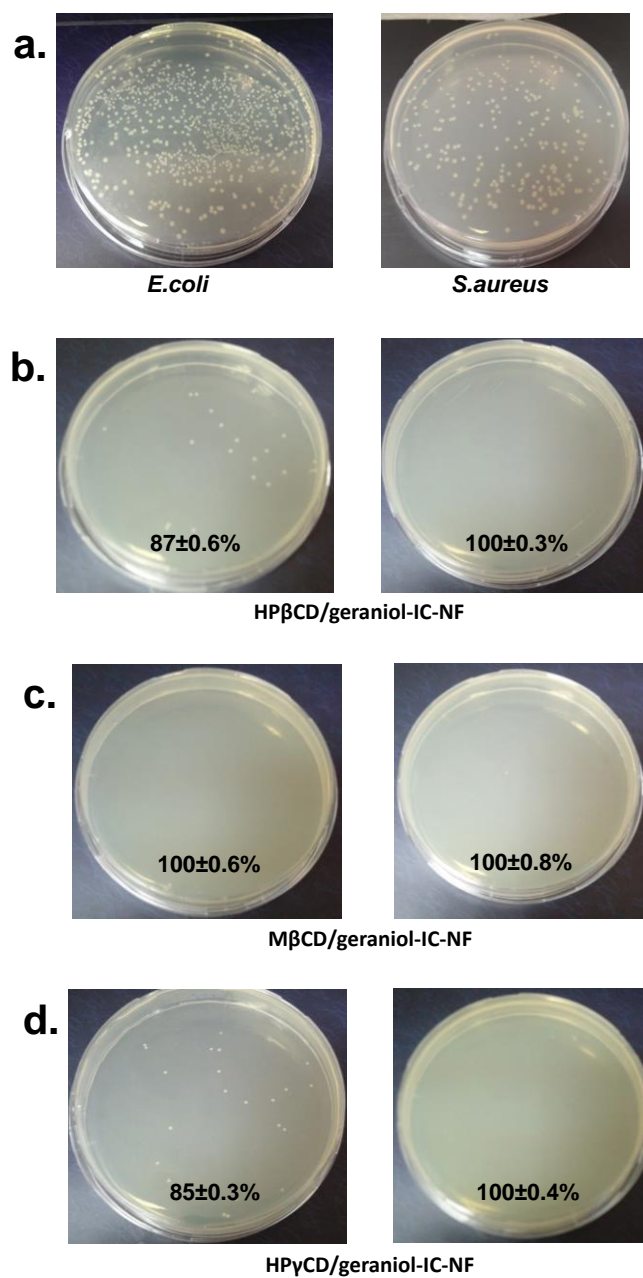


**Figure 52.** (a) Exemplary images of *Escherichia coli* (*E. coli*), *Staphylococcus aureus* (*S. aureus*) colonies. The growth inhibition rate (%) and exemplary images of *E. coli* and *S. aureus* colonies treated by (b) HPβCD/geraniol-IC-NF, (c) MβCD/geraniol-IC-NF, and (d) HPγCD/geraniol-IC-NF (n = 3). (Copyright © 2016, Royal Society of Chemistry. Reprinted with permission from Ref. [127])

### 6.3.8 Antioxidant activity

Free radicals with one or more unpaired electrons and reactive oxygen species (ROS) including superoxide radicals, hydroxyl radicals, singlet oxygen and hydrogen peroxide cause membrane damage, decreasing membrane fluidity, leading to cancer via DNA mutation and induce oxidation of lipids. Therefore, free radicals/ROS might lead to aging, cancer, Alzheimer's disease, diabetes and asthma by causing molecular alterations in the biological systems or spoiling of foods because of the oxidation in the biomolecules [231, 232]. Essential oils (EOs) might have antioxidant properties and the mechanism rely on preventing further damage of mitochondrial DNA that ultimately leading to accumulation of ROS by interacting with them [233]. It has been reported that geraniol decline the lipid peroxidation and inhibit ROS generation in the cells [224]. In order to prevent potential diseases and food spoilage, antioxidant compounds are being used in various applications; so detecting the antioxidant capacity of materials is of importance. There exist many methods to evaluate antioxidant capacity of materials [234]. However, 2,2-diphenyl-1-picrylhydrazyl (DPPH) radical scavenging assay is one of the most widely used methods to decide the potential of antioxidant molecules to scavenge free radicals. DPPH is a stable free radical in a deep purple colour. When it interacts with an antioxidant molecule purple colour of the solution turns into colour of hydrazine which is yellow [235].

The antioxidant activity of geraniol, HP $\beta$ CD-NF, M $\beta$ CD-NF, HP $\gamma$ CD-NF, HP $\beta$ CD/geraniol-IC-NF, M $\beta$ CD/geraniol-IC-NF, and HP $\gamma$ CD/geraniol-IC-NF was calculated as 55 $\pm$ 2%, 58 $\pm$ 4%, 41 $\pm$ 2%, 59 $\pm$ 1%, 75 $\pm$ 2 %, 59 $\pm$ 2%, and 57 $\pm$ 1% at the end of 72 h, respectively. The photographs of the DPPH solutions in

which geraniol, HP $\beta$ CD-NF, M $\beta$ CD-NF, HP $\gamma$ CD-NF, HP $\beta$ CD/geraniol-IC-NF, M $\beta$ CD/geraniol-IC-NF, and HP $\gamma$ CD/geraniol-IC-NF were immersed up to for 72 hour are shown in Figure 53. In a study of Stobiecka et al., antioxidant activity of geraniol comparative to geranylacetone was evaluated with DPPH assay in methanol, ethanol and toluene. It was concluded that geranylacetone exhibited higher antioxidant activity than geraniol in methanol and ethanol systems in 30 minutes. However, antioxidant activity of both geranylacetone and geraniol was quite low due to the slow kinetics of DPPH radical-scavenging caused by the steric inaccessibility [236]. In addition, it has been deduced that the reaction between DPPH and geranylacetone and geraniol was very slow irrespective of the solvent used and high amount of compound had to be applied in order to observe any measurable effects. Similarly, Zyl et al. presented that geraniol has little activity according to DPPH assay performed in methanol for 30 minute [237]. On the contrary, Choi et al. performed DPPH assay for 30 minute and claimed that geraniol had shown quite high antioxidant activity (88%, 236 mg of Trolox equiv/mL) [238]. Thus, our result in which the reaction was very slow and the activity was not high as much as observed in the study of Choi et al. is agreed with the study of Stobiecka et al. and Zyl et al. HP $\beta$ CD-NF, M $\beta$ CD-NF and HP $\gamma$ CD-NF exhibited moderate antioxidant activity due to the presence of hydroxyl groups in the structure [239]. An improvement was observed in the antioxidant activity of CD-NFs with the addition of geraniol in the system. Only HP $\gamma$ CD/geraniol-IC-NF showed similar antioxidant activity with HP $\gamma$ CD-NF, this might be due to higher strength of the complex and the position of geraniol in the cavity which is not allowing the donation of hydrogen

from the system easily. antioxidant activity (%) of HP $\beta$ CD/geraniol-IC-NF was much more as compared to antioxidant activity of geraniol, M $\beta$ CD/geraniol-IC-NF and HP $\gamma$ CD/geraniol-IC-NF. The aqueous solubility increment of geraniol as shown in phase solubility diagrams could be the reason for the better antioxidant activity of HP $\beta$ CD/geraniol-IC-NF as compared with geraniol. Moreover, higher antioxidant activity of HP $\beta$ CD/geraniol-IC-NF than M $\beta$ CD/geraniol-IC-NF and HP $\gamma$ CD/geraniol-IC-NF might be related with the higher strength of the complexes formed with M $\beta$ CD and HP $\gamma$ CD that is inhibiting the release of geraniol and the orientation of geraniol in the cavity of CDs which might make hydrogen donation difficult. The colour of the solution in which HP $\beta$ CD/geraniol-IC-NF was immersed turned from purple to yellowish at the end of 72 h. So, DPPH molecules in that solution converted into diphenyl-picrylhydrazine (DPPH-H) [240].

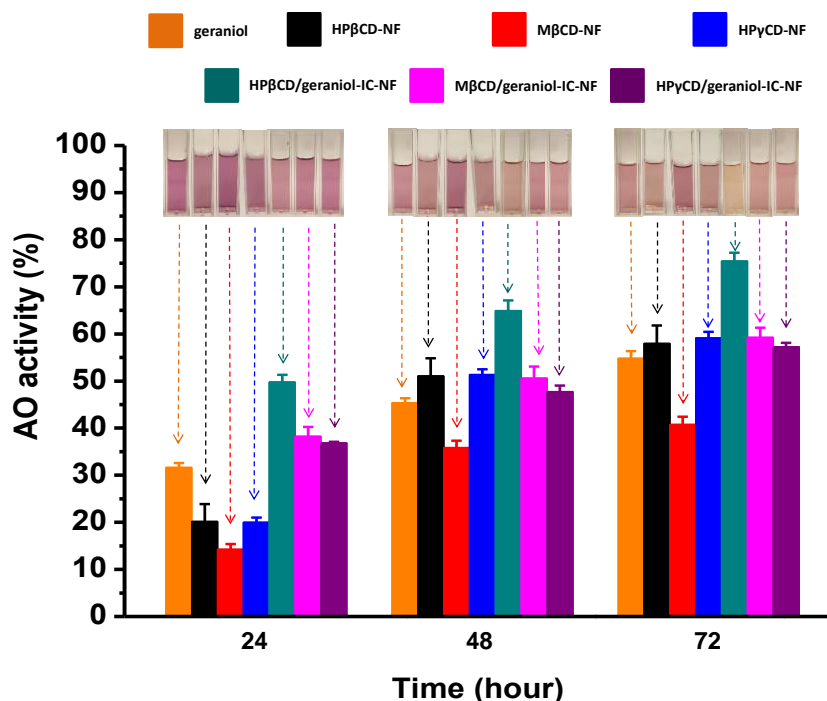


**Figure 53.** The antioxidant activity (%) of geraniol, HPβCD-NF, MβCD-NF, HPγCD-NF, HPβCD/geraniol-IC-NF, MβCD/geraniol-IC-NF, and HPγCD/geraniol-IC-NF and the photographs of DPPH solutions in which geraniol, HPβCD-NF, MβCD-NF, HPγCD-NF, HPβCD/geraniol-IC-NF, MβCD/geraniol-IC-NF, HPγCD/geraniol-IC-NF were immersed, respectively. (n = 3). The error bars in the figure represent the standard deviation (SD). (Copyright © 2016, Royal Society of Chemistry. Reprinted with permission from Ref. [127])

## 6.4 Conclusion

Free-standing nanofibrous webs of geraniol/cyclodextrin-inclusion complexes (CD/geraniol-IC-NFs) were successfully produced by electrospinning without using a polymeric carrier matrix. We have obtained bead-free and uniform nanofibers from these non-polymeric systems of CD/geraniol-ICs for three different types of CDs (HPβCD, MβCD, and HPγCD). After electrospinning, significant amount of geraniol (~ 60-90 %) was well preserved by CD/geraniol-IC-NFs due to the inclusion complexation ability of CDs. The short-term (3 h)

temperature dependent release (37°C, 50°C, and 75°C) and long-term open air (50 days, at RT) release tests for geraniol from CD/geraniol-IC-NFs were performed. Much less amount of geraniol was released from M $\beta$ CD/geraniol-IC-NF when compared to HP $\beta$ CD/geraniol-IC-NF and HP $\gamma$ CD/geraniol-IC-NF in short-term temperature release and long-term open air release tests, which indicated that M $\beta$ CD/geraniol-IC-NF was the most stable inclusion complex among the three CD/geraniol-IC-NFs web samples. The antibacterial activity test results of CD/geraniol-IC-NFs proved quite high antibacterial activity of geraniol against Gram-negative (*Escherichia coli* (*E. coli*)) and Gram-positive (*Staphylococcus aureus* (*S. aureus*)) bacteria. Moreover, CD/geraniol-IC-NFs exhibited efficient antioxidant activity when compared to pure geraniol. In brief, electrospun CD/geraniol-IC nanofibrous webs have shown enhanced shelf-life of geraniol along with antibacterial and antioxidant properties, hence, cyclodextrin inclusion complex nanofibers with variety of flavour/fragrances may have potentials to be used as prolonged releasing systems for various applications including food, cosmetic, household, cleaning products, etc.

## **7. Fast-dissolving, prolonged release and antibacterial cyclodextrin/limonene-inclusion complex nanofibrous webs via polymer-free electrospinning**

### **7.1 Introduction**

Limonene (Figure 54b), monocyclic monoterpene, is a major component of citrus oils found in orange, lemon, mandarin, and grapefruit. It is a highly volatile compound extracted from plants and widely used in perfumes, creams, soaps, as flavour additives for food applications and as a fragrance for household cleaning products [241]. Different approaches including complex formation with CDs [242-246] and encapsulating in electrospun nanofibers [31, 247] were proposed in order to protect limonene from volatilization and control its release rate. Further, Fuenmayor et al. demonstrated the encapsulation of limonene/ $\beta$ -CD-IC containing only 3.1 wt % of pullulan membrane [248].

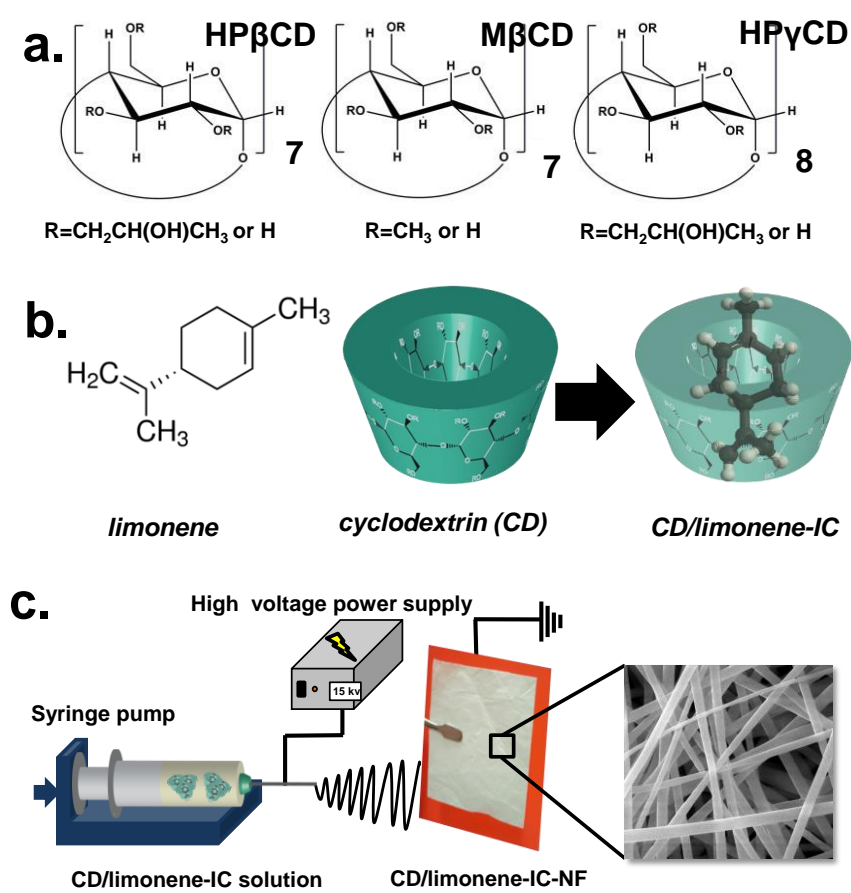


**Figure 54.** The chemical structure of (a) HPβCD, MβCD, and HPγCD, (b) the chemical structure of limonene, the schematic representation of CD and CD/limonene-IC, (c) the schematic representation of electrospinning of nanofibers from CD/limonene-IC solution.

In this study, IC of three modified CDs (HPβCD, MβCD, and HPγCD) (Figure 54a) and limonene were prepared at 1:1 molar ratio (Figure 54b) and then electrospinning was performed without using any polymer matrix to obtain CD/limonene-IC-NF (Figure 54c). Phase solubility test was used to decide the solubility change in the limonene by the addition of different CDs at various concentrations. The morphology of CD/limonene-IC-NFs was evaluated using SEM imaging. The chemical, structural and thermal characterization of CD/limonene-IC-NFs was examined by using <sup>1</sup>H-NMR, TGA, XRD, and DSC.

Computational modeling studies were carried out to investigate the stoichiometry and the most favorable orientation of the guest to form a complex with each CD. The short-term temperature dependent release (37°C, 50°C, and 75°C) of limonene from CD/limonene-IC-NFs was measured using HS GC-MS for 3 h; whereas the long term release of limonene from nanofibers at room temperature (RT) was measured by TGA for 100 days. The antibacterial activity of nanofibers was tested against *Escherichia coli* (*E. coli*) and *Staphylococcus aureus* (*S. aureus*) using colony counting method.

## **7.2 Experimental**

### **7.2.1 Materials**

Limonene (97%, Sigma) and deuterated dimethylsulfoxide (DMSO-d<sub>6</sub>, deuteration degree min 99.8% for NMR spectroscopy, Merck) were purchased and used as received without any further purification. Hydroxypropyl-beta-cyclodextrin (HPβCD), methyl-beta-cyclodextrin (MβCD), hydroxypropyl-gamma-cyclodextrin (HPγCD) were kindly donated by Wacker Chemie (Germany). The water used in the experiments was distilled-deionized from a Millipore Milli-Q ultrapure water system.

### **7.2.2 Preparation of electrospinning solutions**

CD/limonene-ICs was formed in aqueous solution by using three types of modified CD (HPβCD, MβCD, and HPγCD) at 1:1 molar ratio with limonene. First of all CDs (200%, w/v) was put in water and the solutions were stirred at room temperature (RT) until dissolving. Then, limonene was added to the solutions and the resulting solutions were stirred at RT for overnight. Finally,

CD/limonene-IC solutions which are turbid were obtained and then, clear and homogenous solutions were obtained with the dissolution of limonene after 12 h. Electrospinning was performed after 12 hours of stirring and HP $\beta$ CD/limonene-IC-NF, M $\beta$ CD/limonene-IC-NF, and HP $\gamma$ CD/limonene-IC-NF webs were produced. The viscosity, conductivity of CD/limonene-IC solutions and average fiber diameter (AFD) values of CD/limonene-IC nanofibers (CD/limonene-IC-NF) are shown in Table 9. Pure CD nanofibers without limonene (HP $\beta$ CD-NF, M $\beta$ CD-NF, and HP $\gamma$ CD-NF) were produced for comparative measurements according to our previous reports [119, 120].

### **7.2.3 Electrospinning**

CD/limonene-IC solutions were separately loaded into a 1 mL plastic syringe (metallic needle having 0.4 mm inner diameter). The solutions were pumped through a syringe pump (KD Scientific, KDS-101, USA) at 0.5 mL/h rate. A grounded metal covered with aluminum foil was used as a collector and placed at a distance of 10 cm from the needle tip. The electric field (15-20 kV) was applied from a high voltage power supply (AU Series, Matsusada Precision Inc., Japan). Electrospinning experiments were carried out in enclosed Plexiglas box at 25°C and 18% relative humidity. The nanofibers were kept in refrigerator until their usage for analysis.

### **7.2.4 Characterizations and measurements**

Phase-solubility measurements were performed in water according to the method of Higuchi and Connors [161]. An excess amount of limonene was added to 5 mL of aqueous solutions containing increasing amounts of HP $\beta$ CD,

M $\beta$ CD, and HP $\gamma$ CD. The suspensions were shaken at RT for 24 h. After equilibrium was achieved, the suspensions were filtered through 0.45  $\mu$ m membrane filter and diluted with water. In order to determine the amount of limonene dissolved, UV spectroscopy measurements were done at 235 nm (Varian, Cary 100). The phase solubility diagram was drawn by plotting the molar concentration of limonene found in the solution against the molar concentration of CDs. The experiments were carried out in triplicate and each data point is the average of three determinations.

The viscosity measurements of HP $\beta$ CD/limonene-IC, M $\beta$ CD/limonene-IC, and HP $\gamma$ CD/limonene-IC solutions were performed at RT via Anton Paar Physica MCR 301 rheometer equipped with a cone/plate accessory (spindle type CP 40-2) at a constant shear rate of 100 s<sup>-1</sup>. The solution conductivity for CD/limonene-IC solutions was measured by Inolab® pH/Cond 720-WTW.

The morphology of HP $\beta$ CD/limonene-IC-NF, M $\beta$ CD/limonene-IC-NF, and HP $\gamma$ CD/limonene-IC-NF was investigated using scanning electron microscopy (SEM, FEI - Quanta 200 FEG). Prior to taking SEM images, nanofiber samples were placed on metal stubs by using double-sided copper tape and in order to minimize charging problem during SEM examination samples were sputtered with 5 nm of Au/Pd (PECS-682). AFD and fiber diameter distribution of nanofibrous webs were calculated directly from SEM images by measuring the diameter of about 100 fibers.

The proton nuclear magnetic resonance (<sup>1</sup>H-NMR) spectra were recorded at 400 MHz (Bruker DPX-400). 20 mg/mL of HP $\beta$ CD/limonene-IC-NF,

M $\beta$ CD/limonene-IC-NF, and HP $\gamma$ CD/limonene-IC-NF were dissolved in d6-DMSO to evaluate the molar ratio of CDs and limonene in each CD/limonene-IC by integrating the peak ratio of the characteristic chemical shifts corresponding to CD and limonene. Integration of the chemical shifts ( $\delta$ ) given in parts per million (ppm) was calculated by using Mestrenova software.

Thermal gravimetric analysis (TGA, TA Q500, USA) was used to determine thermal properties of limonene, HP $\beta$ CD-NF, M $\beta$ CD-NF, HP $\gamma$ CD-NF, HP $\beta$ CD/limonene-IC-NF, M $\beta$ CD/limonene-IC-NF, and HP $\gamma$ CD/limonene-IC-NF. TGA was conducted under nitrogen atmosphere by heating the samples from 25°C to 450°C at the heating rate of 20°C/min. Differential scanning calorimetry (DSC, TA Q2000, USA) analyses were also performed on HP $\beta$ CD-NF, M $\beta$ CD-NF, HP $\gamma$ CD-NF, HP $\beta$ CD/limonene-IC-NF, M $\beta$ CD/limonene-IC-NF, and HP $\gamma$ CD/limonene-IC-NF with a heating rate of 20°C/min from 25°C to 200°C under nitrogen flow.

The crystalline structure of HP $\beta$ CD-NF, M $\beta$ CD-NF, HP $\gamma$ CD-NF, HP $\beta$ CD/limonene-IC-NF, M $\beta$ CD/limonene-IC-NF, and HP $\gamma$ CD/limonene-IC-NF were investigated at a range of  $2\theta = 5^\circ$ - $30^\circ$  via X-ray diffraction (XRD) (PANalytical X'Pert powder diffractometer) using Cu K $\alpha$  radiation in powder diffraction configuration. XRD was not carried out for limonene since it is a liquid compound at RT.

The cumulative amount of limonene released from HP $\beta$ CD/limonene-IC-NF, M $\beta$ CD/limonene-IC-NF, and HP $\gamma$ CD/limonene-IC-NF were measured using headspace gas chromatography-mass spectrometry (HS GC-MS) for 3 h. The

instrument was Agilent Technologies 7890A gas chromatograph coupled to an Agilent Technologies 5975C inert MSD combined with a triple-axis detector. The used capillary column was HP-5MS (Hewlett-Packard, Avondale, PA) (30 m × 0.25 mm i.d., 0.25 μm film thickness). 10 mg of nanofiber samples were taken from the aluminum foil and placed in 20 mL headspace glass vials. The vials including the nanofiber samples were agitated at 500 rpm at 37°C, 50°C, and 75°C. The syringe temperature was also 37°C, 50°C, and 75°C. 250 μL of vapor was injected from vials to the HS GC-MS by using a headspace injector. The oven temperature was programmed as follows: initial 40°C (held for 3 min), from 40°C to 140°C at a rate of 10°C/min (held for 3 min). HS GC-MS was operated in a splitless and selected ion monitoring mode (SIM). NIST MS Search 2.0 library was used to decide limonene peak. The release experiments were performed in triplicate and the results were reported as average ± standard deviation.

In order to evaluate the long term release of CD/limonene-IC-NFs, HPβCD/limonene-IC-NF, MβCD/limonene-IC-NF, and HPγCD/limonene-IC-NF were kept separately at RT and 18% relative humidity for 100 days in open air in the laboratory. Then, TGA measurements were done at predetermined time intervals (50th day and 100th day).

The antibacterial activity of limonene, HPβCD/limonene-IC-NF, MβCD/limonene-IC-NF, and HPγCD/limonene-IC-NF was tested against *Escherichia coli* (*E. coli*, ATCC 10536) and *Staphylococcus aureus* (*S. aureus*, ATCC 25923) according to colony counting method. *E. coli* and *S. aureus* bacteria were grown in nutrient broth medium (3 g/L of yeast extract, 15 g/L of

peptone and 6 g/L of sodium chloride) for 24 h on a shaker at 100 rpm and 37°C. UV sterilized nanofibers (20 mg) and limonene (1.6 mg) were immersed into the culture suspension which contains approximately  $10^8$  colony forming unit (cfu)/ml. In this step, nanofibers easily dissolve in the culture suspension. After 24 h incubation and shaking at 37°C, different dilutions ( $10^1$  to  $10^9$ ) were made by successively adding 1 mL culture into 9 mL of phosphate buffer solution. Then, 0.1 mL of the diluted culture was spread on a nutrient agar plate and incubated at 37°C for 24 h. The numbers of colonies were counted and three repeats were done for each sample.

The antibacterial activity (%) of limonene and CD/limonene-IC-NFs was defined as follows:

$$\text{Antibacterial activity (\%)} = (A-B)/A * 100 \text{ (Equation 9)}$$

where A and B are the numbers of colonies (cfu/mL) before and after the nanofibers were added, respectively.

## 7.2.5 Computational method

The first-principles calculations based on density functional theory (DFT) [162, 163] were performed by using the Vienna Ab initio simulation package [166, 167]. The exchange-correlation was approximated within the generalized gradient approximation [164] including Van der Waals correction [165]. The element potentials were described by projector augmented-wave method (PAW) [168] using a plane-wave basis set with a kinetic energy cutoff of 520 eV. The initial structures of HP $\beta$ CD, M $\beta$ CD, and HP $\gamma$ CD were obtained from Cambridge Structural Database [169]. In order to optimize the structure each of IC and

limonene, the conjugate gradient algorithm without any constraints have been utilized by setting convergence criteria on the total energy and force to  $10^{-4}$  eV and  $10^{-2}$  eV/Å, respectively. The solvent effect on the formation of inclusion complexation has been elucidated by using implicit solvent model, which includes dispersive interactions [170]. This model splits the system into an explicit part (solute), which is treated quantum mechanically and an implicit part (solvent), which is treated as a continuum, all combined within ab initio method [171-173] and implemented in VASP (VASPsol) [173].

## **7.3 Results and discussion**

### **7.3.1 Phase solubility studies**

The phase solubility profiles of HPβCD/limonene, MβCD/limonene, and HPγCD/limonene systems are presented in Figure 55. The obtained results clearly proves that the solubility of limonene has been increased up to 32 mM of HPβCD in HPβCD/limonene system and beyond this concentration it starts to decrease. This might be due to the formation of less water-soluble complex at higher concentration of HPβCD. However, the solubility of limonene has been increased linearly for MβCD/limonene and HPγCD/limonene. Therefore, it could be concluded that the solubility curve of HPβCD/limonene dictates  $A_n$  type; whereas MβCD/limonene and HPγCD/limonene represents  $A_L$  type solubility diagrams. In addition, the linear solubility performance of limonene in MβCD and HPγCD systems reveals the 1:1 complex formation.

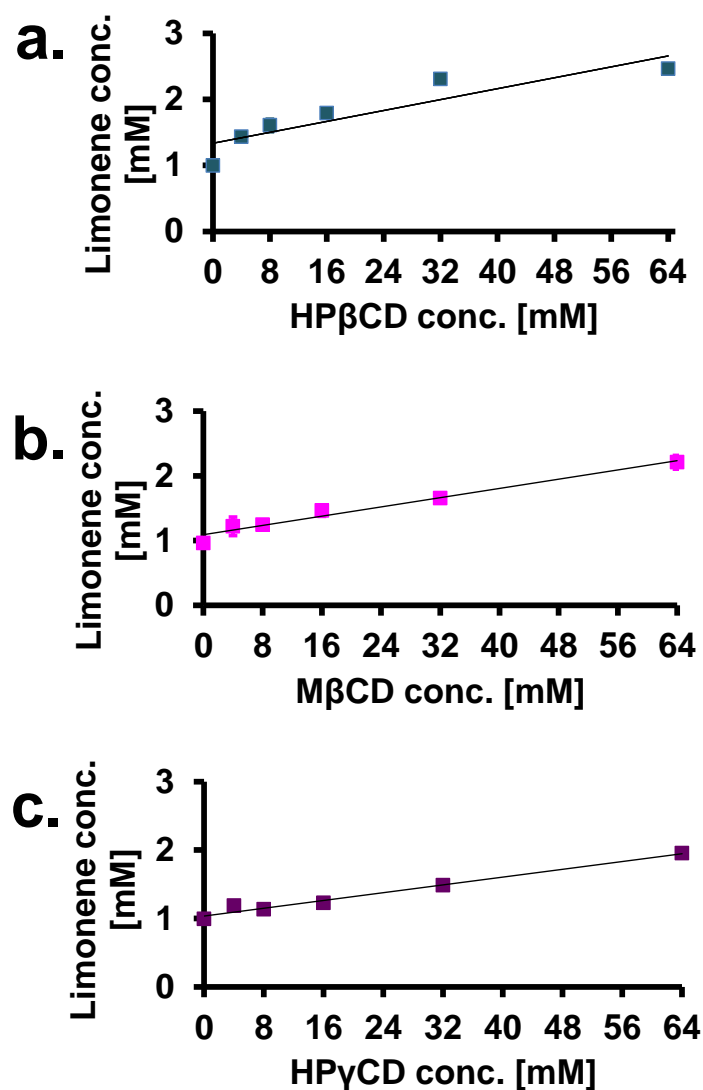


**Figure 55.** Phase solubility diagram of (a) HPβCD/limonene, (b) MβCD/limonene, (c) HPγCD/limonene systems in water (n = 3).

### 7.3.2 Molecular modeling of inclusion complex

Although thermodynamics of complexation reactions are primarily involve van der Waals and hydrophobic interactions between guest molecule and CD, this process can also induce the removal of water molecules from CD cavity, resulting in the rearrangement of the inclusion complex (IC). Therefore, we carried out structural optimization of limonene, CDs (HPβCD, MβCD, and

HP $\gamma$ CD) and their IC in vacuum, followed by optimizations in aqueous medium. The guest molecule (single limonene) is introduced into the wide rim of the cavity of HP $\beta$ CD, M $\beta$ CD, and HP $\gamma$ CD at various positions and two different orientations. These orientations include i) head: methyl group and ii) tail: ethyl group of limonene has headed inwards to the wide rim of CD cavity as shown Figure 56a-c.

The complexation energy ( $E_{\text{comp}}$ ) for the lowest energy configuration of these ICs in 1:1 stoichiometry for three possible orientations is calculated as

$$E_{\text{comp}} = E_{\text{CD}} + E_{\text{guest}} - E_{\text{IC}} \text{ (Equation 10)}$$

where  $E_{\text{CD}}$ ,  $E_{\text{guest}}$ , and  $E_{\text{IC}}$  is the total energy of CD (HP $\beta$ CD, M $\beta$ CD, and HP $\gamma$ CD); guest limonene molecule; and IC, respectively. All energies are calculated in aqueous medium. The results for 1:1 stoichiometry are summarized in Table 8. Our results indicate that limonene can form IC with all considered types of CDs with varying  $E_{\text{comp}}$  depending on the orientation of limonene and the type of CD. Due to the relatively size matching between the cavity and the limonene molecule and polarity of methyl groups, strongest binding is obtained for M $\beta$ CD with the tail orientation of limonene.

In addition, the solvation energies of bare limonene and ICs are calculated in order to rank their solubility in water. The solvation energy ( $E_{\text{solv}}$ ) in aqueous medium is calculated as

$$E_{\text{solv}} = E_{(\text{solvated})} - E_{(\text{vacuum})} \text{ (Equation 11)}$$

where  $E_{(\text{solvated})}$ , and  $E_{(\text{vacuum})}$  is the total energy of molecules in solvent and vacuum, respectively. The calculated  $E_{\text{solv}}$  of bare limonene is -0.66 kcal/mol which is very low and suggests poor solubility in water. On the other hand,  $E_{\text{solv}}$  of ICs within HP $\beta$ CD, M $\beta$ CD, and HP $\gamma$ CD in water is -74.2 kcal/mol, -29.5 kcal/mol, and -89.4 kcal/mol, respectively, asserting exothermic solvation reactions for all ICs. The IC within HP $\gamma$ CD has the highest solubility, and the IC within M $\beta$ CD shows lower solubility in water compared to the other ICs.

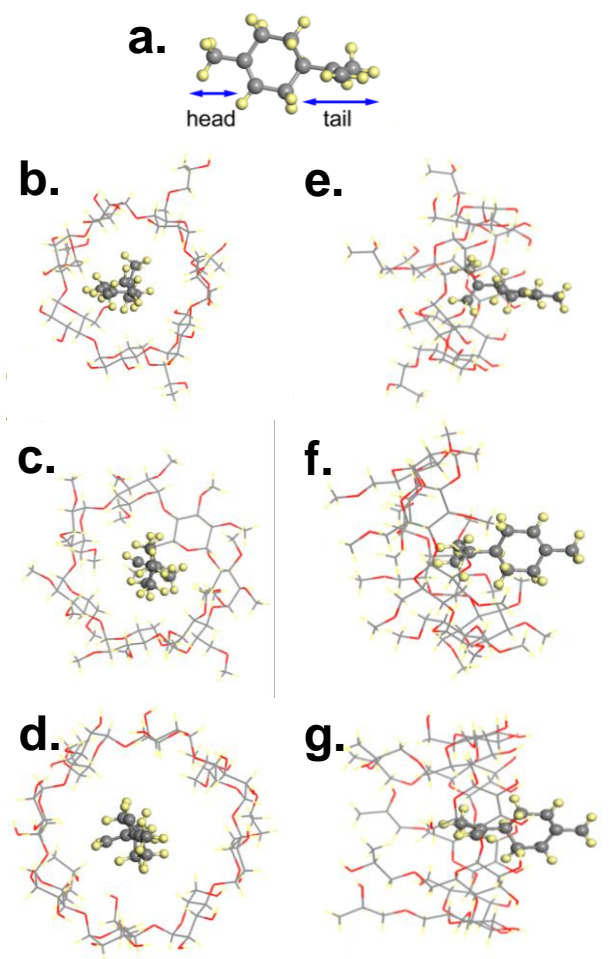


**Figure 56.** (a) The chemical structure of limonene; top view of ICs of (b) HP $\beta$ CD, (c) M $\beta$ CD, (d) HP $\gamma$ CD; side view of ICs of (e) HP $\beta$ CD, (f) M $\beta$ CD, and (g) HP $\gamma$ CD with limonene in aqueous medium. Gray and yellow spheres represent carbon and hydrogen atoms, respectively.

**Table 8.** Complexation and solvation energies of limonene within HP $\beta$ CD, M $\beta$ CD, and HP $\gamma$ CD.

Host	Guest	E <sub>comp</sub> (head) kcal/mol	E <sub>comp</sub> (tail) kcal/mol	E <sub>solv</sub> kcal/mol
-	limonene	-	-	-0.66
HP $\beta$ CD	limonene	9.7	11.7	-74.2
M $\beta$ CD	limonene	10.7	12.6	-29.5
HP $\gamma$ CD	limonene	5.9	7.1	-89.4

### 7.3.3 Morphology analysis of nanofibers

The morphological investigation clearly represents the bead-free and uniform HP $\beta$ CD/limonene-IC-NF, M $\beta$ CD/limonene-IC-NF, and HP $\gamma$ CD/limonene-IC-NF (Figure 57a-c). The average fiber diameter (AFD) of HP $\beta$ CD/limonene-IC-NF, M $\beta$ CD/limonene-IC-NF, and HP $\gamma$ CD/limonene-IC-NF were found to be 710 $\pm$ 470 nm, 405 $\pm$ 210 nm and 1450 $\pm$ 500 nm, respectively. The change in the diameter of CD/limonene-IC nanofibers (CD/limonene-IC-NF) was due to the viscosity and conductivity differences between the solutions (Table 9). The measured conductivity was in the order: M $\beta$ CD/limonene-IC solution > HP $\beta$ CD/limonene-IC solution > HP $\gamma$ CD/limonene-IC solution. Thus, it is proved that the higher conductivity of M $\beta$ CD/limonene-IC solution leads to lower diameter of M $\beta$ CD/limonene-IC-NF as compared to other nanofibers. Likewise, HP $\gamma$ CD/limonene-IC-NF have highest diameter among all CD/limonene-IC-NF due to the higher viscosity and lower conductivity of

HP $\gamma$ CD/limonene-IC solution than other solutions. The photographs of free-standing HP $\beta$ CD/limonene-IC-NF, M $\beta$ CD/limonene-IC-NF, and HP $\gamma$ CD/limonene-IC-NF webs clearly represents their flexible and easily-handled nature which indicated that all CD/limonene-IC-NF webs has excellent mechanical integrity even they were composed of CDs which are amorphous and small molecules (Figure 57d-f). The solubility of limonene, HP $\beta$ CD/limonene-IC-NF, M $\beta$ CD/limonene-IC-NF, and HP $\gamma$ CD/limonene-IC-NF is shown in Figure 58 and Supporting video 1 and 2. The observed results evidently represents that the CD/limonene-IC-NFs completely dissolve in water within seconds, however limonene is not dissolving and oily compound is easily visible on the surface.

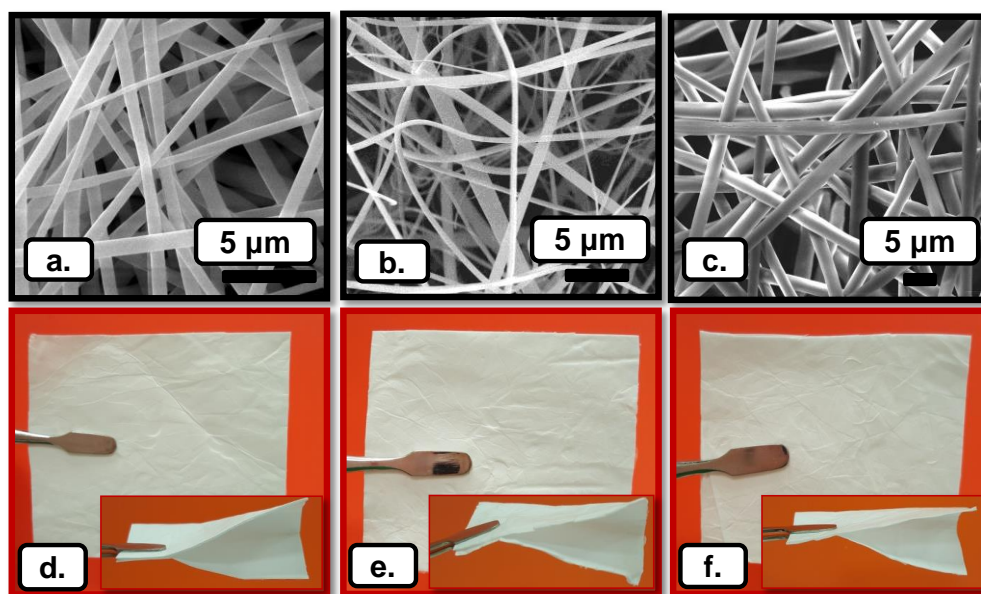


**Figure 57.** SEM images of electrospun nanofibers obtained from the solutions of (a) HP $\beta$ CD/limonene-IC, (b) M $\beta$ CD/limonene-IC (c) HP $\gamma$ CD/limonene-IC; the photographs of (d) HP $\beta$ CD/limonene-IC-NF, (e) M $\beta$ CD/limonene-IC-NF, (f) HP $\gamma$ CD/limonene-IC-NF.

**Table 9.** The properties of the solutions used for electrospinning and morphological characteristics of the resulting nanofibers.

Solutions	% CD <sup>a</sup> (w/v)	% limonene <sup>b</sup> (w/w)	Viscosity (Pa·s)	Conductivity ( $\mu$ S/cm)	Average fiber diameter (nm)	Fiber morphology
HP $\beta$ CD/limonene-IC	200	8.53	0.087	241	710 $\pm$ 470	Bead free nanofibers
M $\beta$ CD/limonene-IC	200	10.63	0.106	999	405 $\pm$ 210	Bead free nanofibers
HP $\gamma$ CD/limonene-IC	200	7.75	0.168	2.24	1450 $\pm$ 500	Bead free nanofibers

<sup>a</sup> with respect to solvent (water).

<sup>b</sup> with respect to total weight of the sample.

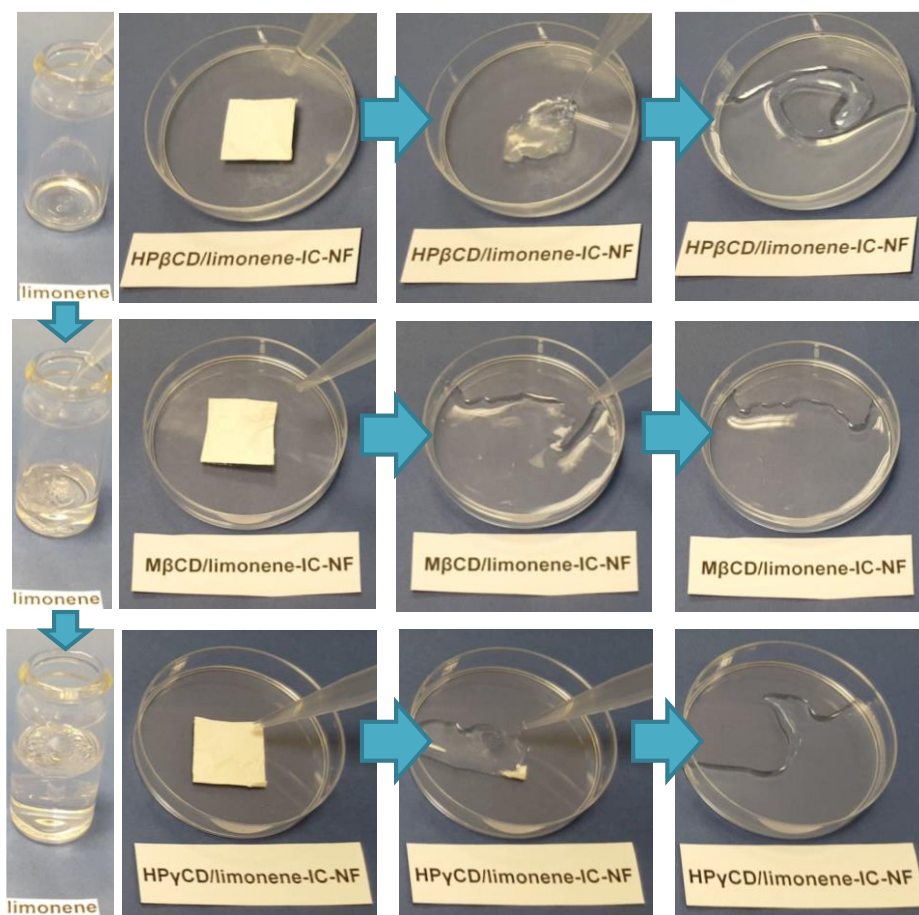


**Figure 58.** The presentation of the solubility behaviour of pure limonene and HP $\beta$ CD/limonene-IC-NF, M $\beta$ CD/limonene-IC-NF, and HP $\gamma$ CD/limonene-IC-NF in water.

### 7.3.4 The molar ratio of inclusion complex

Figure 59 shows the proton nuclear magnetic resonance ( $^1\text{H-NMR}$ ) spectra of HP $\beta$ CD/limonene-IC-NF, M $\beta$ CD/limonene-IC-NF, and HP $\gamma$ CD/limonene-IC-NF. The molar ratio between CD (HP $\beta$ CD, M $\beta$ CD, and HP $\gamma$ CD) and limonene in CD/limonene-IC-NFs was calculated from the integration of the peak ratio between the peak of HP $\beta$ CD, M $\beta$ CD, and HP $\gamma$ CD (1.029 ppm, 4.9 ppm, and 1.029 ppm) and limonene (1.616 ppm) as 1.00:0.42, 1.00:0.78, and 1.00:0.38 for HP $\beta$ CD/limonene-IC-NF, M $\beta$ CD/limonene-IC-NF, and HP $\gamma$ CD/limonene-IC-

NF, respectively. Therefore, it is concluded that 42%, 78%, and 38% of the limonene was preserved in HP $\beta$ CD/limonene-IC-NF, M $\beta$ CD/limonene-IC-NF, and HP $\gamma$ CD/limonene-IC-NF, respectively. So, the calculated amount of limonene in CD/limonene-IC-NFs suggested that significant amount of limonene was preserved in M $\beta$ CD/limonene-IC-NF. Besides, more amount of limonene was evaporated from HP $\beta$ CD/limonene-IC-NF and HP $\gamma$ CD/limonene-IC-NF during the solution preparation, electrospinning or storage.

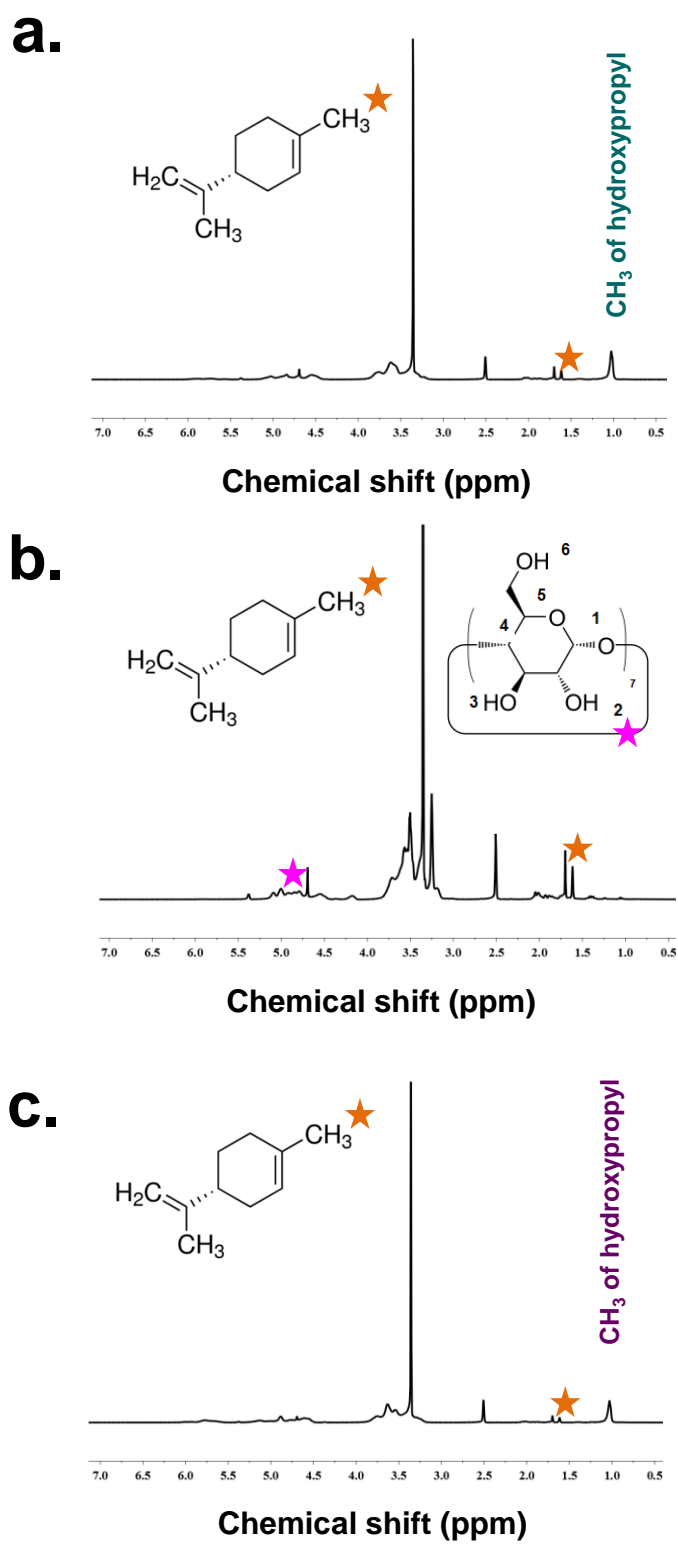


**Figure 59.**  $^1\text{H-NMR}$  spectra of (a) HP $\beta$ CD/limonene-IC-NF, (b) M $\beta$ CD/limonene-IC-NF, and (c) HP $\gamma$ CD/limonene-IC-NF.

### 7.3.5 Thermal analysis of nanofibers

Thermal gravimetric analysis (TGA) of limonene, HP $\beta$ CD-NF, M $\beta$ CD-NF, HP $\gamma$ CD-NF, HP $\beta$ CD/limonene-IC-NF, M $\beta$ CD/limonene-IC-NF, and HP $\gamma$ CD/limonene-IC-NF are given in Figure 60a-c. Thermal evaporation of pure limonene started at about 50°C and continued till 150°C. Pristine HP $\beta$ CD-NF, M $\beta$ CD-NF and HP $\gamma$ CD-NF exhibited two weight losses below 100°C and above 275°C which belongs to the water loss and main thermal degradation of each CD, respectively [125]. Three stages of weight loss were observed for HP $\beta$ CD/limonene-IC-NF. The first weight loss is below 100°C belongs to the water loss, whereas second and third weight losses between 100-230°C and above 275°C corresponds to limonene and HP $\beta$ CD, respectively. The shifting of thermal evaporation onset of limonene to higher temperature suggested the IC formation between HP $\beta$ CD and limonene. Four steps of weight loss existed in case of M $\beta$ CD/limonene-IC-NF. The initial weight loss below 100°C was due to the water loss, the second and third weight losses ranging between 120-170°C and 170-270°C were attributed to limonene. The shifting of evaporation onset of limonene up to 120°C and 170°C confirms IC formation between M $\beta$ CD and limonene. Moreover, the presence of two steps for limonene which are at higher temperature than free limonene showed that there might be two types complex formation between M $\beta$ CD and limonene. However, the second complex at the third step shows a stronger interaction with limonene compared to first complex formed in second step. The last weight loss observed in M $\beta$ CD/limonene-IC-NF is above 300°C belongs to the degradation of M $\beta$ CD. HP $\gamma$ CD/limonene-IC-NF exhibited three steps of weight loss: the initial weight loss below 100°C

belonging to the water, the second weight loss between 165°C and 245°C is due to the limonene and the third weight loss above 300°C corresponding to thermal degradation of HP $\gamma$ CD. A shift was observed in the thermal evaporation onset of limonene to higher temperature and this shift was owing to the inclusion complexation between HP $\gamma$ CD and limonene. Furthermore, the thermal stability of the second complex in M $\beta$ CD/limonene-IC-NF was higher than the complexes formed in HP $\beta$ CD/limonene-IC-NF and HP $\gamma$ CD/limonene-IC-NF. This result indicated the existence of strong and more stable complexation between M $\beta$ CD and limonene which was also confirmed with the computational modeling studies. Here, the methyl groups of M $\beta$ CD might be increase the hydrophobic interaction and provide higher stability to the system [249].

From TGA data, limonene amount in HP $\beta$ CD/limonene-IC-NF, M $\beta$ CD/limonene-IC-NF, and HP $\gamma$ CD/limonene-IC-NF was calculated to be ~ 3.66%, ~ 8.45% (2.71% and 5.74% belong to the first and second complex, respectively), and ~ 2.05% (w/w, with respect to CD) and this calculations confirmed that 43%, 80% (26% and 54%), and 26% of limonene was remained during the preparation, electrospinning processes or storage, respectively. According to TGA results, the molar ratio of HP $\beta$ CD, M $\beta$ CD, and HP $\gamma$ CD to limonene was calculated as 1.00:0.43, 1.00:0.80 and 1.00:0.27, respectively. The molar ratio of CD:limonene in CD/limonene-IC-NF samples calculated from TGA data are well agreed with the data obtained from <sup>1</sup>H-NMR. Therefore, limonene was preserved to a great extent in M $\beta$ CD/limonene-IC-NF; however certain amount of limonene presents in HP $\beta$ CD/limonene-IC-NF and HP $\gamma$ CD/limonene-IC-NF was lost during the preparation, electrospinning or

storage. Nevertheless, it is anticipated that CD-IC nanofiber matrix could preserve much higher limonene content compared to polymeric nanofiber matrix. For instance, in our previous studies, we have seen that volatile molecules such as vanillin [97], allyl isothiocyanate [102], and geraniol [100] could not be preserved at all in electrospun polyvinyl alcohol (PVA) nanofibers without CD-IC.

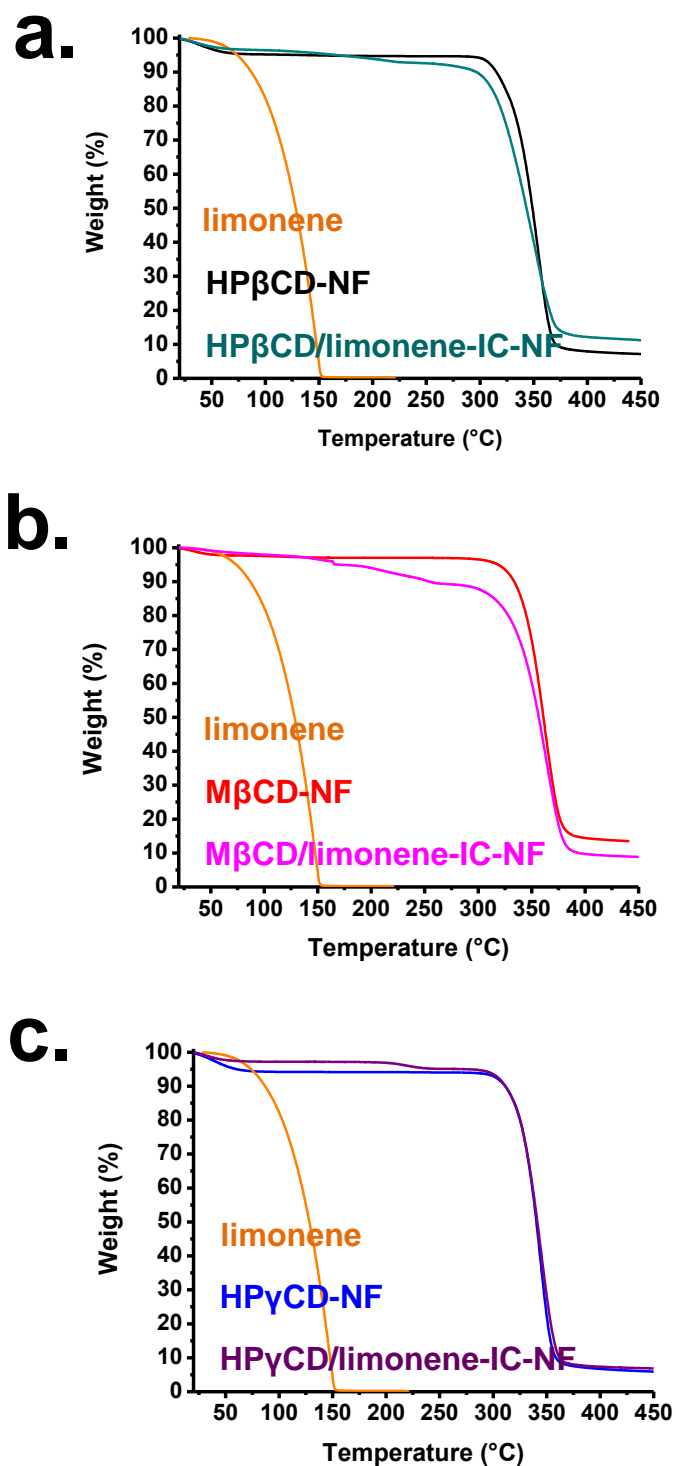


**Figure 60.** TGA thermograms of (a) limonene, HP $\beta$ CD-NF, HP $\beta$ CD/limonene-IC-NF; (b) limonene, M $\beta$ CD-NF, M $\beta$ CD/limonene-IC-NF; (c) limonene, HP $\gamma$ CD-NF, HP $\gamma$ CD/limonene-IC-NF.

Differential scanning calorimetry (DSC) curves of HP $\beta$ CD-NF, M $\beta$ CD-NF, HP $\gamma$ CD-NF, HP $\beta$ CD/limonene-IC-NF, M $\beta$ CD/limonene-IC-NF, and HP $\gamma$ CD/limonene-IC-NF are given in Figure 61. The dehydration of CDs in HP $\beta$ CD-NF, M $\beta$ CD-NF, and HP $\gamma$ CD-NF observed as typical broad endothermic peaks between 25-160°C, 25-155°C, and 25-155°C, respectively. The endothermic peaks in the DSC curves of CD/limonene-IC-NFs was in the range of 65-160°C, 70-140°C, and 50-170°C for HP $\beta$ CD/limonene-IC-NF, M $\beta$ CD/limonene-IC-NF, and HP $\gamma$ CD/limonene-IC-NF, respectively. The enthalpies of endothermic transitions in of HP $\beta$ CD-NF, M $\beta$ CD-NF, and HP $\gamma$ CD-NF were 329 J/g, 99 J/g, and 255 J/g; whereas the enthalpies of HP $\beta$ CD/limonene-IC-NF, M $\beta$ CD/limonene-IC-NF, and HP $\gamma$ CD/limonene-IC-NF were 131 J/g, 54 J/g, and 229 J/g, respectively. The reduction in the enthalpy of HP $\beta$ CD-NF, M $\beta$ CD-NF, and HP $\gamma$ CD-NF after the complexation of limonene confirmed the complexation by displacing of certain amount of water molecules in the cavity of CDs with limonene [225].

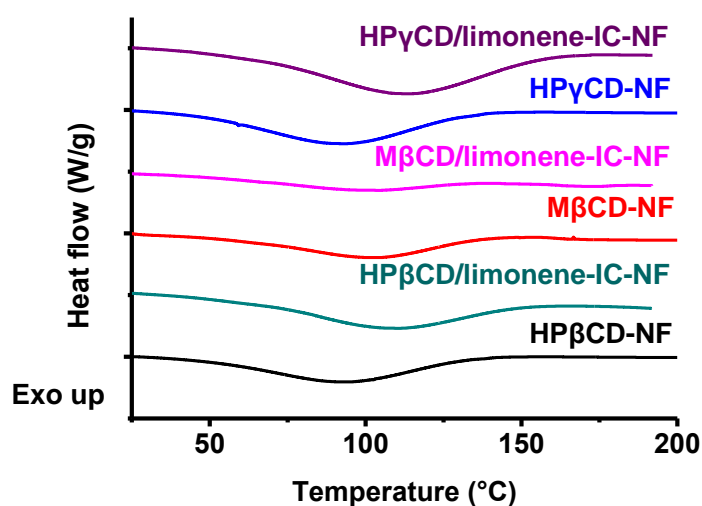


**Figure 61.** DSC thermograms of HP $\beta$ CD-NF, HP $\beta$ CD/limonene-IC-NF, M $\beta$ CD-NF, M $\beta$ CD/limonene-IC-NF, HP $\gamma$ CD-NF, and HP $\gamma$ CD/limonene-IC-NF.

### 7.3.6 Structural characterization of nanofibers

Figure 62 shows the X-ray diffraction (XRD) pattern of HP $\beta$ CD-NF, M $\beta$ CD-NF, HP $\gamma$ CD-NF, HP $\beta$ CD/limonene-IC-NF, M $\beta$ CD/limonene-IC-NF, and HP $\gamma$ CD/limonene-IC-NF. HP $\beta$ CD, M $\beta$ CD, and HP $\gamma$ CD are known to be amorphous molecules. The observed amorphous peak in HP $\beta$ CD-NF, M $\beta$ CD-NF, and HP $\gamma$ CD-NF further confirms the native amorphous nature of HP $\beta$ CD, M $\beta$ CD, and HP $\gamma$ CD molecules. Similarly, amorphous pattern was also observed for HP $\beta$ CD/limonene-IC-NF, M $\beta$ CD/limonene-IC-NF, and HP $\gamma$ CD/limonene-IC-NF. More importantly, the absence limonene peak in HP $\beta$ CD/limonene-IC-NF, M $\beta$ CD/limonene-IC-NF, and HP $\gamma$ CD/limonene-IC-NF confirmed the formation of the complex.

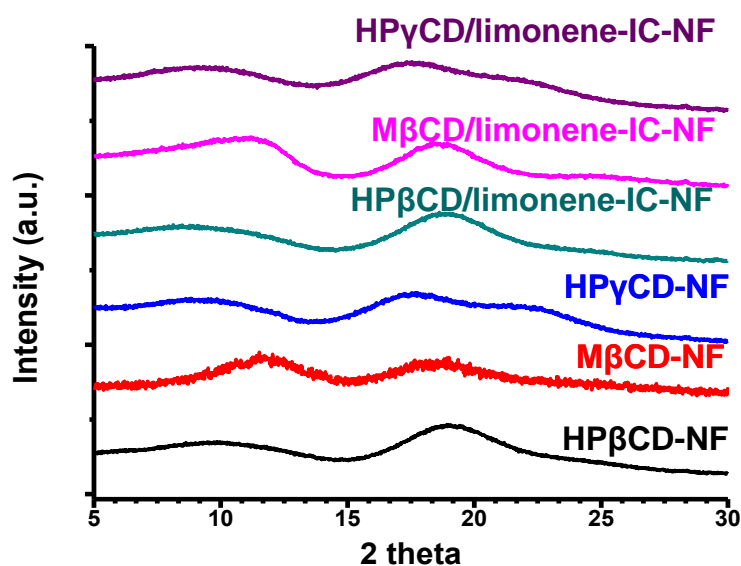


**Figure 62.** XRD patterns of HP $\beta$ CD-NF, M $\beta$ CD-NF, HP $\gamma$ CD-NF, HP $\beta$ CD/limonene-IC-NF, M $\beta$ CD/limonene-IC-NF, and HP $\gamma$ CD/limonene-IC-NF.

### 7.3.7 Release study

The release results of the limonene from CD/limonene-IC-NFs as a function of temperature over 3 hour are shown in Figure 63a-c. The release of limonene from CD/limonene-IC-NFs was increased with increasing temperature from 37°C to 75°C. Since the variations in the temperature induce the increases in the diffusion coefficient of the molecules [216]. Total amount of released limonene was in the order: M $\beta$ CD/limonene-IC-NF>HP $\gamma$ CD/limonene-IC-NF>HP $\beta$ CD/limonene-IC-NF; on the other hand, the rate of release was highest from HP $\gamma$ CD/limonene-IC-NF and lowest from M $\beta$ CD/limonene-IC-NF at 37°C, 50°C, and 75°C.

The better preservation of limonene shown in <sup>1</sup>H-NMR and TGA data might be the reason of high amount of limonene release from M $\beta$ CD/limonene-IC-NF. The higher stability of complex formed in M $\beta$ CD/limonene-IC-NF as shown in TGA results could be responsible from the slower release of limonene from the nanofibers. Moreover, superior size fit between modified  $\beta$ CDs than HP $\gamma$ CD might be another reason for the quick release of HP $\gamma$ CD/limonene-IC-NF. As discussed above, the computational modeling studies are well correlated with the experimental results where the complexation energy was calculated in the order of M $\beta$ CD/limonene-IC >HP $\beta$ CD/limonene-IC >HP $\gamma$ CD/limonene-IC.

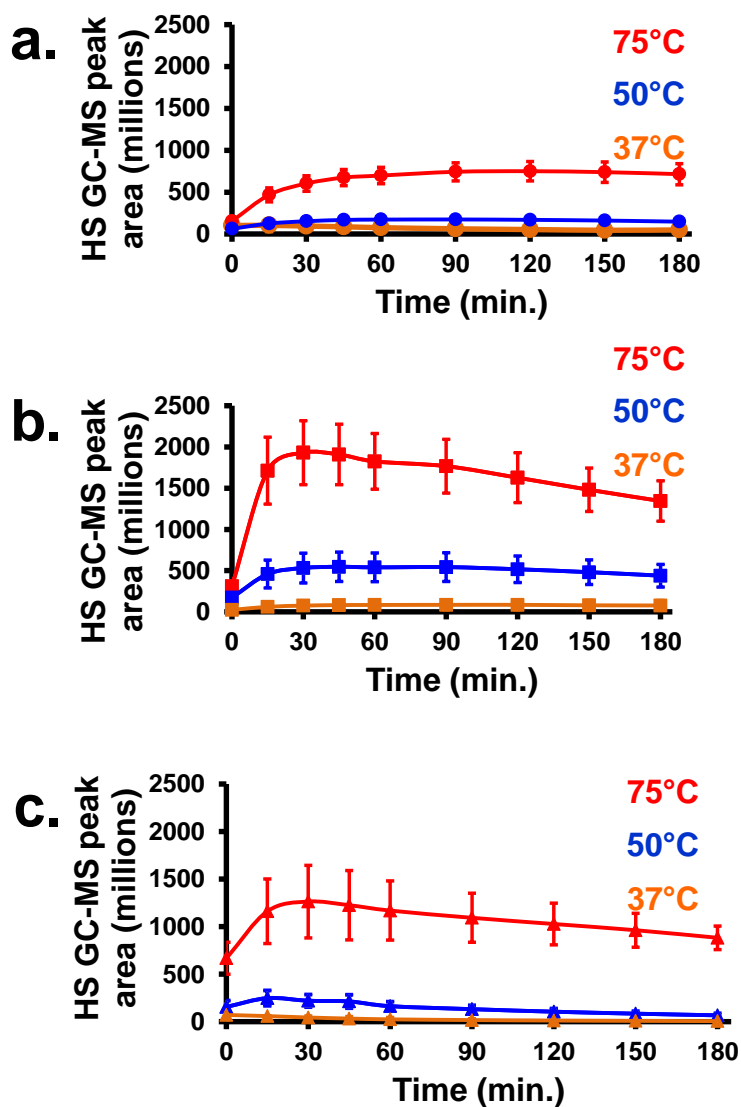


**Figure 63.** The cumulative release of limonene from (a) HPβCD/limonene-IC-NF, (b) MβCD/limonene-IC-NF, and (c) HPγCD/limonene-IC-NF at 37°C, 50°C, and 75°C (n = 3). The error bars in the figure represent the standard deviation.

TGA measurements were also performed to investigate the long term release of HPβCD/limonene-IC-NF, MβCD/limonene-IC-NF, and HPγCD/limonene-IC-NF, and the results are summarized in Figure 64. Most of the limonene present in MβCD/limonene-IC-NF did not release (remaining of 75% (w/w)) at the end of 100 days due to the high stability of MβCD/limonene-IC-NF as discussed

previously. 51% (w/w) of limonene was released from HP $\beta$ CD/limonene-IC-NF at the end of 100 days. Comparatively lower stability of the complex in HP $\beta$ CD/limonene-IC-NF could be the reason for the higher amount of limonene release than M $\beta$ CD/limonene-IC-NF. The amount of released limonene was 88% (w/w) for HP $\gamma$ CD/limonene-IC-NF at the end of 100 days. These results might be due to the excellent size fit between HP $\beta$ CD and M $\beta$ CD with limonene and correlates well with the short term release experiments in which HP $\gamma$ CD/limonene-IC-NF released limonene quickly compared to HP $\beta$ CD/limonene-IC-NF and M $\beta$ CD/limonene-IC-NF. In previous studies conducted by our group, most of the vanillin, allyl isothiocyanate, geraniol loaded was lost during electrospinning and storage without CD-IC in electrospun PVA nanofibers [97, 100, 102]. Here, we observed that considerable amount of limonene remained in the nanofibrous matrix of HP $\beta$ CD/limonene-IC-NF and M $\beta$ CD/limonene-IC-NF even after a long time of storage (100 days) on the shelf.

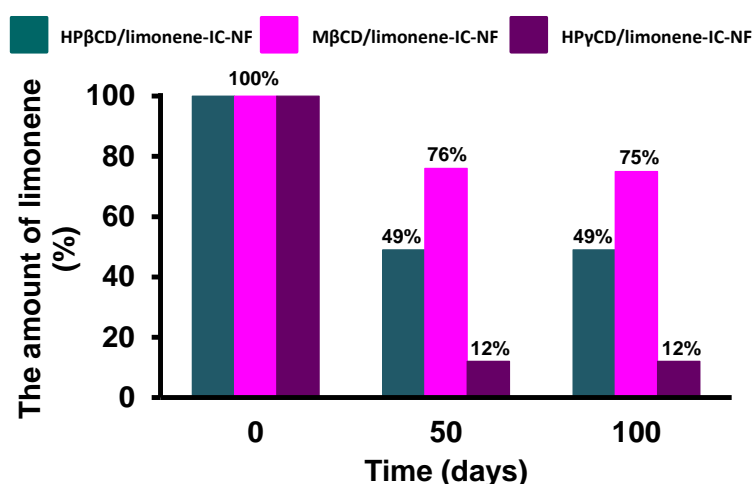


**Figure 64.** The amount of limonene in HP $\beta$ CD/limonene-IC-NF, M $\beta$ CD/limonene-IC-NF, and HP $\gamma$ CD/limonene-IC-NF at RT for 100 days.

### 7.3.8 Antibacterial activity

Essential oils are known to have antibacterial activity due to the terpene constituents disrupting the bacterial membrane in both Gram-negative and Gram-positive bacteria [250]. Figure 65 presents the effect of limonene and CD/limonene-IC-NFs on the growth inhibition rate of *Escherichia coli* (*E. coli*) and *Staphylococcus aureus* (*S. aureus*). CD/limonene-IC-NFs possessed a strong antibacterial activity against *E. coli* and *S. aureus* even higher than limonene. Higher antibacterial activity of CD/limonene-IC-NFs could be due to the higher solubility and preservation rate of limonene in CD/limonene-IC-NFs. Namely, limonene, HP $\beta$ CD/limonene-IC-NF, M $\beta$ CD/limonene-IC-NF, and HP $\gamma$ CD/limonene-IC-NF exhibited 77 $\pm$ 1.0%, 79 $\pm$ 0.9%, 93 $\pm$ 1.2%, and 90 $\pm$ 0.7% against *E. coli* and 70 $\pm$ 0.6%, 96 $\pm$ 1.3%, 97 $\pm$ 1.5%, and 85 $\pm$ 0.9% *S. aureus*, respectively. M $\beta$ CD/limonene-IC-NF had the strongest antibacterial effect for *E. coli* and *S. aureus*, this could be due to the better preservation of limonene shown in <sup>1</sup>H-NMR, TGA and HS GC-MS. Furthermore, it is known that Gram-positive bacteria have a thin layer of peptidoglycan, whereas Gram-negative bacteria have a thick lipid bilayer on the outside. So, Gram-positive bacteria are much more susceptible to antibacterial agents than Gram-negative bacteria [251]. These results clarified the higher antibacterial activity of CD/limonene-IC-NFs against *S. aureus* than *E. coli* that is expected to inhibit the growing of the bacteria in the mouth causing the bad breath as an oral care strip.

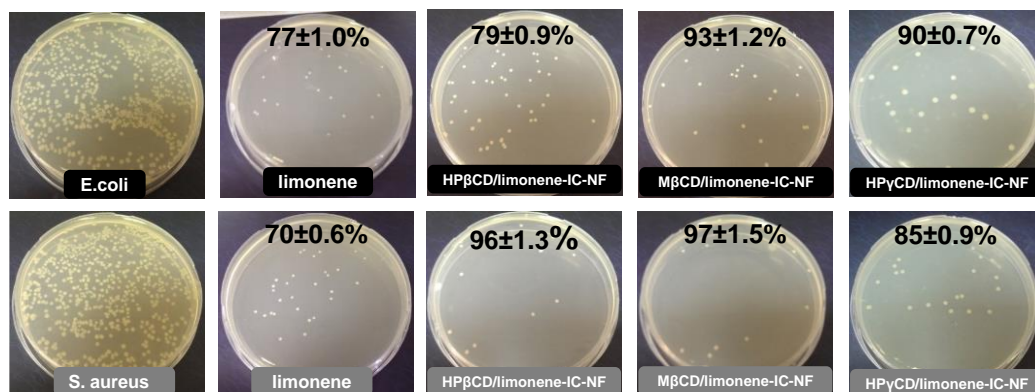


**Figure 65.** Exemplary images of *E. coli*, *S. aureus* colonies. The growth inhibition rate (%) and exemplary images of *E. coli* and *S. aureus* colonies treated by limonene, HPβCD/limonene-IC-NF, MβCD/limonene-IC-NF, and HPγCD/limonene-IC-NF (n = 3).

## 7.4 Conclusion

Here, by using electrospinning we present the production of free-standing nanofibrous webs from three modified CDs (HPβCD, MβCD, and HPγCD) and volatile essential oil, limonene, without using a polymer matrix. The solubility of limonene was increased with all CD types as seen in phase solubility diagrams. The stoichiometry of the complexes was 1:1 from the computational and experimental studies. SEM images revealed that all CD/limonene-IC-NFs had bead-free morphology. TGA, DSC, and XRD confirmed the formation of the complexes. HPβCD/limonene-IC-NF, MβCD/limonene-IC-NF, and HPγCD/limonene-IC-NF preserved up to 43%, 80%, and 38% of limonene according to <sup>1</sup>H-NMR and TGA results, respectively. The short-term (3 h) release of limonene evaluated at three different temperature (37 °C, 50 °C, and 75°C) via HS GC-MS revealed that MβCD/limonene-IC-NF released much more amount of limonene due to the better preservation compared to HPβCD/limonene-IC-NF and HPγCD/limonene-IC-NF. The long-term open air

(100 days at RT) release tests of limonene from CD/limonene-IC-NFs were performed as well. Much less amount of limonene was released from M $\beta$ CD/limonene-IC-NF when compared to HP $\beta$ CD/limonene-IC-NF and HP $\gamma$ CD/limonene-IC-NF in long-term open air release tests. These results confirm the highest stability of the complexes in M $\beta$ CD/limonene-IC-NF among the three CD/limonene-IC-NFs web sample. In addition, the rate of release in short and long-term release studies were also slow in case of M $\beta$ CD/limonene-IC-NF, this is likely due to the higher stability of limonene in M $\beta$ CD/limonene-IC-NF than HP $\beta$ CD/limonene-IC-NF and HP $\gamma$ CD/limonene-IC-NF as mentioned in TGA results. Antibacterial activity test results indicated that CD/limonene-IC-NFs presented high antibacterial activity against both Gram-negative (*E. coli*) and Gram-positive (*S. aureus*) bacteria. Finally, it was observed that CD/limonene-IC-NFs were dissolved in water in a few seconds. In conclusion, the results suggested the potential of CD/limonene-IC nanofibrous webs could be used in food or healthcare areas such as an oral care strip for supplying oral hygiene and make the breath fresh at the same time owing to the high amount of preserved limonene with enhanced solubility and high antibacterial activity.

## **8. Fast-dissolving delivery membranes produced from electrospun polymer-free cyclodextrin/linalool-inclusion complex nanofibers with prolonged release and antibacterial activity**

### **8.1 Introduction**

Linalool (3,7-dimethyl-1,6-octadien-3-ol) is an acyclic monoterpene tertiary alcohol known for its volatile and hydrophobic nature. It is found in most of the cosmetic products such as shampoos, shower gels, soaps, body lotions, hairsprays, creams, antiperspirants as well as in non-cosmetic products such as household cleaners, detergents and food products as a fragrance and flavour agent. Linalool has antimicrobial, anti-inflammatory, local anaesthetic, analgesic and antitumoral activities [252]. There are studies dealing with the IC formation with CDs aiming to overcome the limitations of linalool including low solubility and stability [89, 253]. Fast-dissolving drug delivery systems became important especially for the poorly soluble drugs administered on pediatric, geriatric and psychiatric patients since they can rapidly disintegrate in the oral cavity without the need of water. In addition, they can enhance the solubility, onset of action and bioavailability. Oral fast-dissolving membranes are included in fast-dissolving drug delivery systems and they can easily dissolve in mouth and deliver the drugs [254]. Electrospinning is a technique that is capable of producing nanofibers to increase drug release and dissolution rate of drugs owing to high specific surface area and highly porous network. In addition, amorphous state of incorporated drugs in electrospun nanofibers is very useful in enhancing the solubility and dissolution rate of drugs [255].

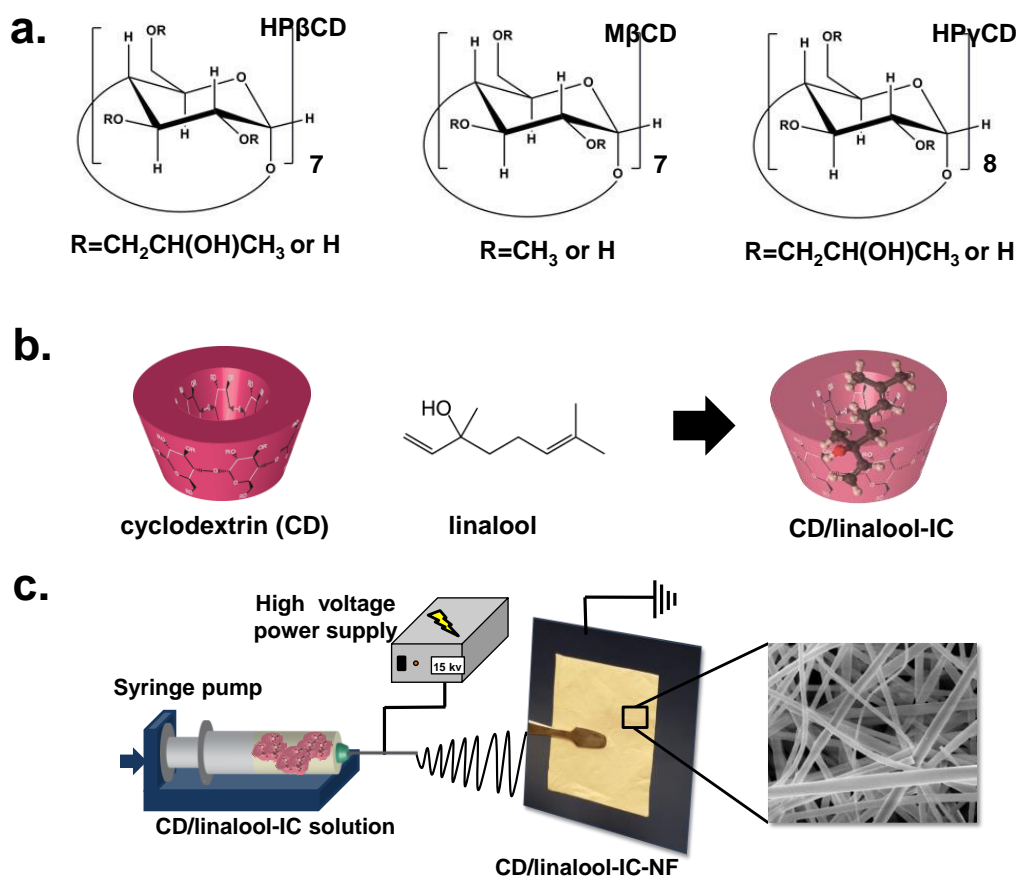


**Figure 66.** (a) The chemical structure of HPβCD, MβCD, HPγCD; (b) the schematic representation of CD/linalool-IC formation, and (c) electrospinning of nanofibers from CD/linalool-IC aqueous solution.

Here, ICs of a model volatile and hydrophobic compound, linalool with three modified CDs (HPβCD, MβCD, and HPγCD) (Figure 66a) were formed (Figure 66b) at 1:1 molar ratio, and then, free-standing CD/linalool-IC nanofibrous webs (CD/linalool-IC-NFs) were produced via electrospinning without using polymeric carrier matrix (Figure 66c). The morphological characterization of CD/linalool-IC-NFs was done by SEM; whereas chemical, structural and thermal characterizations of CD/linalool-IC-NFs were performed by <sup>1</sup>H-NMR, TGA, DSC, and XRD. The short-term temperature release of linalool (37°C, 50°C, and 75°C; for 3 h) from CD/linalool-IC-NFs was examined using HS GC-

MS, whereas the long term release of linalool (at room temperature (RT), for 50 days) from CD/linalool-IC-NFs was measured by TGA. The antibacterial activity of CD/linalool-IC-NFs against model Gram-negative (*Escherichia coli* (*E. coli*)) and Gram-positive (*Staphylococcus aureus* (*S. aureus*)) bacteria was tested using colony counting method.

## **8.2 Experimental**

### **8.2.1 Materials**

Linalool (97%, Sigma Aldrich) and deuterated dimethylsulfoxide (DMSO-d<sub>6</sub>, deuteration degree min 99.8% for NMR spectroscopy, Merck) were purchased and used as received without any further purification. Hydroxypropyl-beta-cyclodextrin (HPβCD), methyl-beta-cyclodextrin (MβCD) and hydroxypropyl-gamma-cyclodextrin (HPγCD) were kindly donated by Wacker Chemie (Germany). The water used in the experiments was distilled-deionized from a Millipore Milli-Q ultrapure water system.

### **8.2.2 Preparation of electrospinning solutions**

In order to prepare the cyclodextrin/linalool-inclusion complex (CD/linalool-IC) solutions, (CDs) (200%, w/v) were dissolved in water and then linalool was added. The amount of linalool was determined as 1:1 molar ratio with each CD (HPβCD, MβCD, and HPγCD). HPβCD/linalool-IC-NF, MβCD/linalool-IC-NF, and HPγCD/linalool-IC-NF webs were produced via electrospinning after overnight stirring the solutions at RT. The viscosity and conductivity of CD/linalool-IC solutions and the average fiber diameter (AFD) values of CD/linalool-IC-NFs are shown in Table 10. Pure CD nanofibers without linalool

(HP $\beta$ CD-NF, M $\beta$ CD-NF, and HP $\gamma$ CD-NF) were also prepared according to our previous reports for the comparative measurements [119, 120].

### **8.2.3 Electrospinning**

The solutions of CD/linalool-ICs were loaded into a plastic syringe having 0.4 mm of inner diameter and placed horizontally on a syringe pump (KD Scientific, KDS-101, USA). A grounded metal covered by aluminum foil that is 10 cm away from the needle tip was used as a collector. The CD/linalool-IC solutions were pumped at a constant rate (0.5 mL/h) via syringe pump and 15-20 kV was applied from the high voltage power supply (AU Series, Matsusada Precision Inc., Japan). CD/linalool-IC-NFs were kept in refrigerator until the analyses were done. The experiments were carried out in an enclosed Plexiglas box at 25°C and 18% relative humidity.

### **8.2.4 Characterizations and measurements**

Anton Paar Physica MCR 301 rheometer equipped with a cone/plate accessory (spindle type CP 40-2) at a constant shear rate of 100 s<sup>-1</sup> was used to measure the viscosity of HP $\beta$ CD/linalool-IC, M $\beta$ CD/linalool-IC, and HP $\gamma$ CD/linalool-IC solutions at RT. The solution conductivity of CD/linalool-IC systems was determined via Inolab® pH/Cond 720-WTW.

The morphological characterization of HP $\beta$ CD/linalool-IC-NF, M $\beta$ CD/linalool-IC-NF, and HP $\gamma$ CD/linalool-IC-NF, was performed by using scanning electron microscopy (SEM, FEI - Quanta 200 FEG). The nanofibrous web samples were sputtered with 5 nm of Au/Pd (PECS-682) to minimize the charging problem during SEM imaging. AFD and fiber diameter distribution of the nanofibrous webs were calculated from SEM images of about 100 fibers.

In order to show the solubility of linalool and nanofibers, 5 mL of water was added to linalool in a vial and HP $\beta$ CD/linalool-IC-NF, M $\beta$ CD/linalool-IC-NF, and HP $\gamma$ CD/linalool-IC-NF in petri dishes. Then, video was taken for linalool and nanofibers separately.

20 mg/mL of HP $\beta$ CD/linalool-IC-NF, M $\beta$ CD/linalool-IC-NF, and HP $\gamma$ CD/linalool-IC-NF were dissolved in d6-DMSO to calculate the molar ratio of CDs and linalool. Then, the proton nuclear magnetic resonance ( $^1\text{H-NMR}$ ) spectra were recorded at 400 MHz (Bruker DPX-400). The integration of the chemical shifts ( $\delta$ ) was calculated by using Mestrenova software.

The thermal properties of linalool, HP $\beta$ CD-NF, M $\beta$ CD-NF, HP $\gamma$ CD-NF, HP $\beta$ CD/linalool-IC-NF, M $\beta$ CD/linalool-IC-NF, and HP $\gamma$ CD/linalool-IC-NF were analyzed via thermal gravimetric analysis (TGA, TA Q500, USA) and differential scanning calorimetry (DSC, TA Q2000, USA). TGA measurements were performed under nitrogen atmosphere by heating the samples from 25°C to 450°C at the heating rate of 20°C/min. DSC analyses were carried out with a heating rate of 20°C/min from 25°C to 190°C under nitrogen flow.

The crystalline structure of HP $\beta$ CD-NF, M $\beta$ CD-NF, HP $\gamma$ CD-NF, HP $\beta$ CD/linalool-IC-NF, M $\beta$ CD/linalool-IC-NF, and HP $\gamma$ CD/linalool-IC-NF was examined with X-ray diffraction (XRD, PANalytical X'Pert powder diffractometer). XRD data were recorded applying Cu K $\alpha$  radiation in powder diffraction configuration in the  $2\theta$  range of 5-30°. Since linalool is a liquid compound at RT, XRD was not carried out for it.

The amount of linalool released from HP $\beta$ CD/linalool-IC-NF, M $\beta$ CD/linalool-IC-NF, and HP $\gamma$ CD/linalool-IC-NF was measured via headspace gas

chromatography-mass spectrometry (HS GC-MS, Agilent Technologies 7890A gas chromatograph equipped with 5975C mass spectrometer) for 3 h. The capillary column was HP-5MS (Hewlett-Packard, Avondale, PA) (30 m × 0.25 mm i.d., 0.25 μm film thickness). CD/linalool-IC-NFs (10 mg) were placed in headspace glass vials and the agitation was made at 500 rpm. The syringe temperature was 37°C, 50°C, and 75°C. The experiments were performed in triplicate and the results were reported as average ± standard deviation. The oven temperature was initially held at 40°C for 3 min. Then the temperature was increased with a gradient of 10°C/min until 175°C. The oven was held for 3 minutes at 175°C. The instrument was operated in a splitless and selected ion monitoring mode (SIM). NIST MS Search 2.0 library was used to determine the linalool peaks.

The long term release of CD/linalool-IC-NFs were investigated by keeping HPβCD/linalool-IC-NF, MβCD/linalool-IC-NF, and HPγCD/linalool-IC-NF separately at RT and 18% relative humidity for 50 days in open air in the laboratory. TGA measurements of nanofibers were done after predetermined time intervals (25th day and 50th day).

The antibacterial activity of HPβCD/linalool-IC-NF, MβCD/linalool-IC-NF, and HPγCD/linalool-IC-NF were evaluated using colony counting method. Bacterial cells of *E. coli* (ATCC 10536) and *S. aureus* (ATCC 25923) were grown 24 hours on a shaker at 100 rpm and 37°C. Inoculum was suspended to provide a final density of 1 × 10<sup>8</sup> colony forming unit (CFU)/mL in phosphate buffered saline (PBS) according to 0.5 McFarland turbidity standard (approximately 1 to 2 × 10<sup>8</sup> CFU/mL). UV sterilized nanofibers (40 mg) were then immersed in

bacterial suspension in a 20 mL conical tube, and the media were shaken at 100 rpm at 37°C for 24 h. Different dilutions ( $10^1$  to  $10^9$ ) were made by successively adding 1 mL culture into 9 mL of PBS. Then, 0.1 mL of the diluted culture was spread on a nutrient agar plate and incubated at 37°C for overnight and CFU/mL was counted. The experiments were performed in triplicate and the results are given as average $\pm$ standard deviation.

The antibacterial activity of CD/linalool-IC-NFs was defined as follows:

$$\text{Antibacterial activity (\%)} = (A-B)/A*100 \text{ (Equation 12)}$$

where A and B are the number of colonies (CFU/mL) before and after CD/linalool-IC-NFs were added, respectively.

## 8.3 Results and discussion

### 8.3.1 Morphology analysis of nanofibers

Scanning electron microscopy (SEM) images of HP $\beta$ CD/linalool-IC-NF, M $\beta$ CD/linalool-IC-NF, and HP $\gamma$ CD/linalool-IC-NF are shown in Figure 67a-c. As seen in SEM images bead-free and uniform nanofibers were obtained with all systems used. The average fiber diameter (AFD) of HP $\beta$ CD/linalool-IC-NF, M $\beta$ CD/linalool-IC-NF, and HP $\gamma$ CD/linalool-IC-NF were calculated from SEM images as  $700\pm 250$  nm,  $655\pm 195$  nm, and  $850\pm 260$  nm, respectively. AFD of M $\beta$ CD/linalool-IC-NF was lower than HP $\beta$ CD/linalool-IC-NF due to the lower viscosity and higher conductivity of M $\beta$ CD/linalool-IC solution compared to HP $\beta$ CD/linalool-IC solution (Table 10). HP $\gamma$ CD/linalool-IC-NF had the highest AFD among all CD/linalool-IC-NFs, the higher viscosity and lower conductivity of HP $\gamma$ CD/linalool-IC solution might be the reason of this situation. The

photographs of free-standing, easily-handled CD/linalool-IC-NF webs are given in (Figure 67d-f).

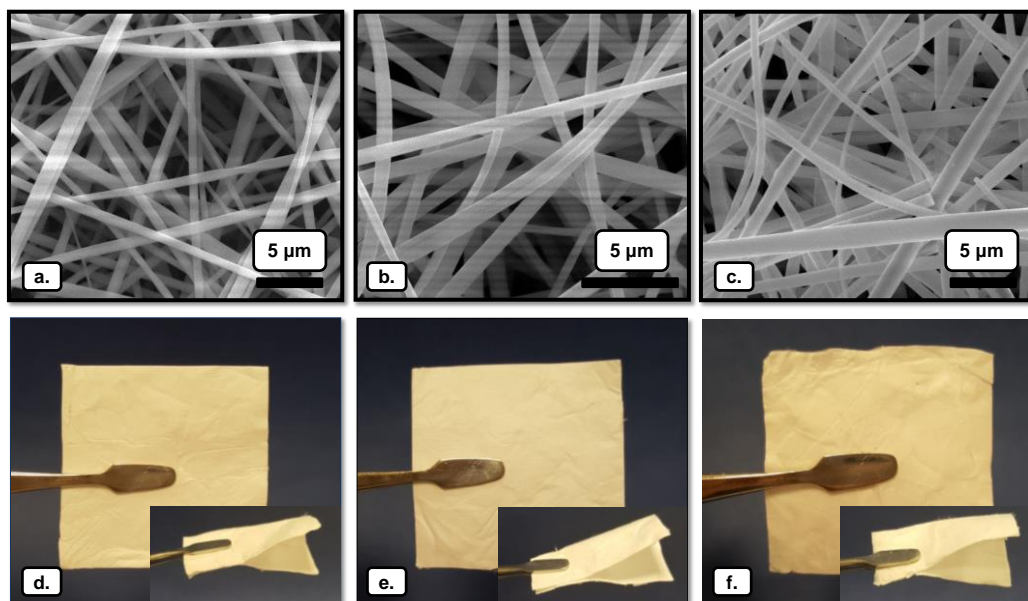


**Figure 67.** SEM images of electrospun nanofibers obtained from the aqueous solutions of (a) HP $\beta$ CD/linalool-IC, (b) M $\beta$ CD/linalool-IC, and (c) HP $\gamma$ CD/linalool-IC; the photographs of (d) HP $\beta$ CD/linalool-IC-NF, (e) M $\beta$ CD/linalool-IC-NF, and (f) HP $\gamma$ CD/linalool-IC-NF webs.

**Table 10.** The properties of the solutions used for electrospinning and morphological characteristics of the resulting nanofibers.

Solutions	% CD <sup>a</sup> (w/v)	linalool <sup>b</sup> (w/w)	Viscosity (Pa·s)	Conductivity ( $\mu$ S/cm)	Average fiber diameter (nm)	Fiber morphology
HP $\beta$ CD/linalool-IC	200	9.50	0.103	208	700 $\pm$ 250	Bead free nanofibers
M $\beta$ CD/linalool-IC	200	11.89	0.074	817	655 $\pm$ 195	Bead free nanofibers
HP $\gamma$ CD/linalool-IC	200	8.68	0.145	4.38	850 $\pm$ 260	Bead free nanofibers

It is also seen from the photographs that CD/linalool-IC-NF webs mechanical integrity despite their main components (CDs) was amorphous small molecules. Moreover, the solubility of linalool, HP $\beta$ CD/linalool-IC-NF, M $\beta$ CD/linalool-IC-NF, and HP $\gamma$ CD/linalool-IC-NF is shown in Figure 68 and Supporting video 3 and 4. As seen, linalool is not dissolving and oil molecules are easily visible on the surface; whereas CD/linalool-IC-NFs are dissolving completely in two seconds.

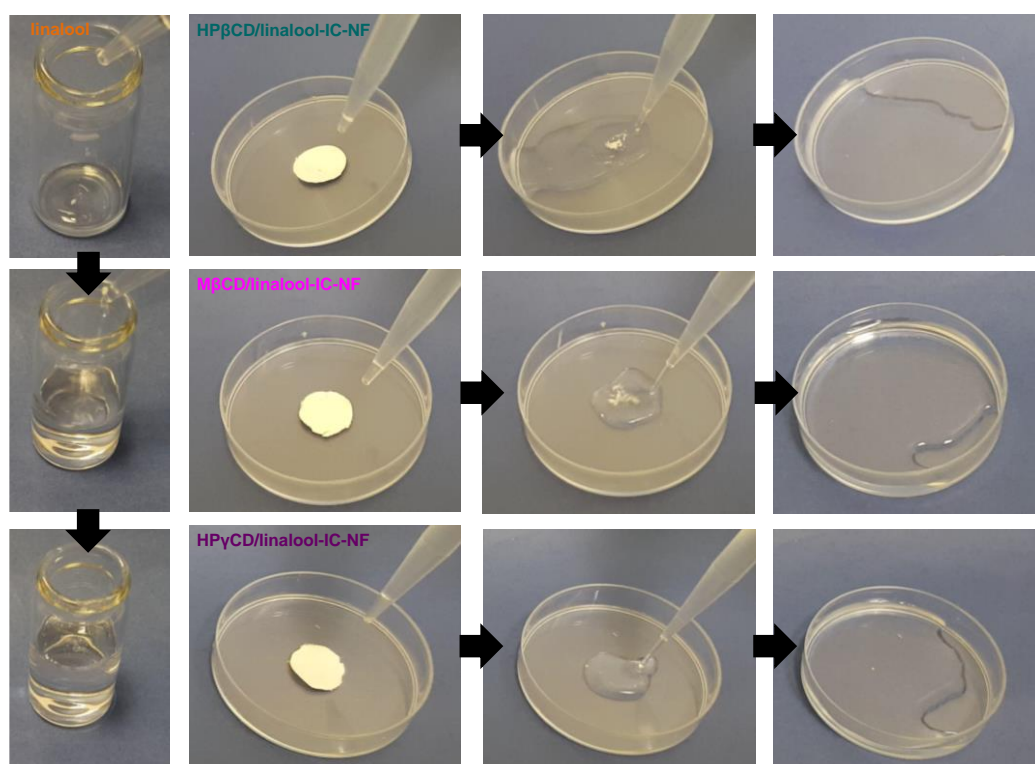


**Figure 68.** The presentation of the solubility behaviour of pure linalool and HP $\beta$ CD/linalool-IC-NF, M $\beta$ CD/linalool-IC-NF, and HP $\gamma$ CD/linalool-IC-NF in water.

### 8.3.2 The molar ratio of inclusion complex

The molar ratio of between CDs (HP $\beta$ CD, M $\beta$ CD, and HP $\gamma$ CD) and linalool in HP $\beta$ CD/linalool-IC-NF, M $\beta$ CD/linalool-IC-NF, and HP $\gamma$ CD/linalool-IC-NF were calculated from proton nuclear magnetic resonance ( $^1\text{H-NMR}$ ) spectra

(Figure 69a-c). The integration of the peaks belongs to HP $\beta$ CD, M $\beta$ CD, and HP $\gamma$ CD (1.00 ppm, 3.5-3.75 ppm, and 1.00 ppm) and linalool (1.5 and 1.6 ppm) was used to make the calculations. Therefore, the molar ratio was calculated as 1.00:0.69, 1.00:0.65, and 1.00:0.45 for HP $\beta$ CD/linalool-IC-NF, M $\beta$ CD/linalool-IC-NF, and HP $\gamma$ CD/linalool-IC-NF, respectively. It was concluded from <sup>1</sup>H-NMR results that significant amount of linalool was preserved in HP $\beta$ CD/linalool-IC-NF (69%, w/w) and M $\beta$ CD/linalool-IC-NF (65%, w/w), but HP $\gamma$ CD/linalool-IC-NF preserved 45%, w/w of linalool during the solution preparation, electrospinning and storage.

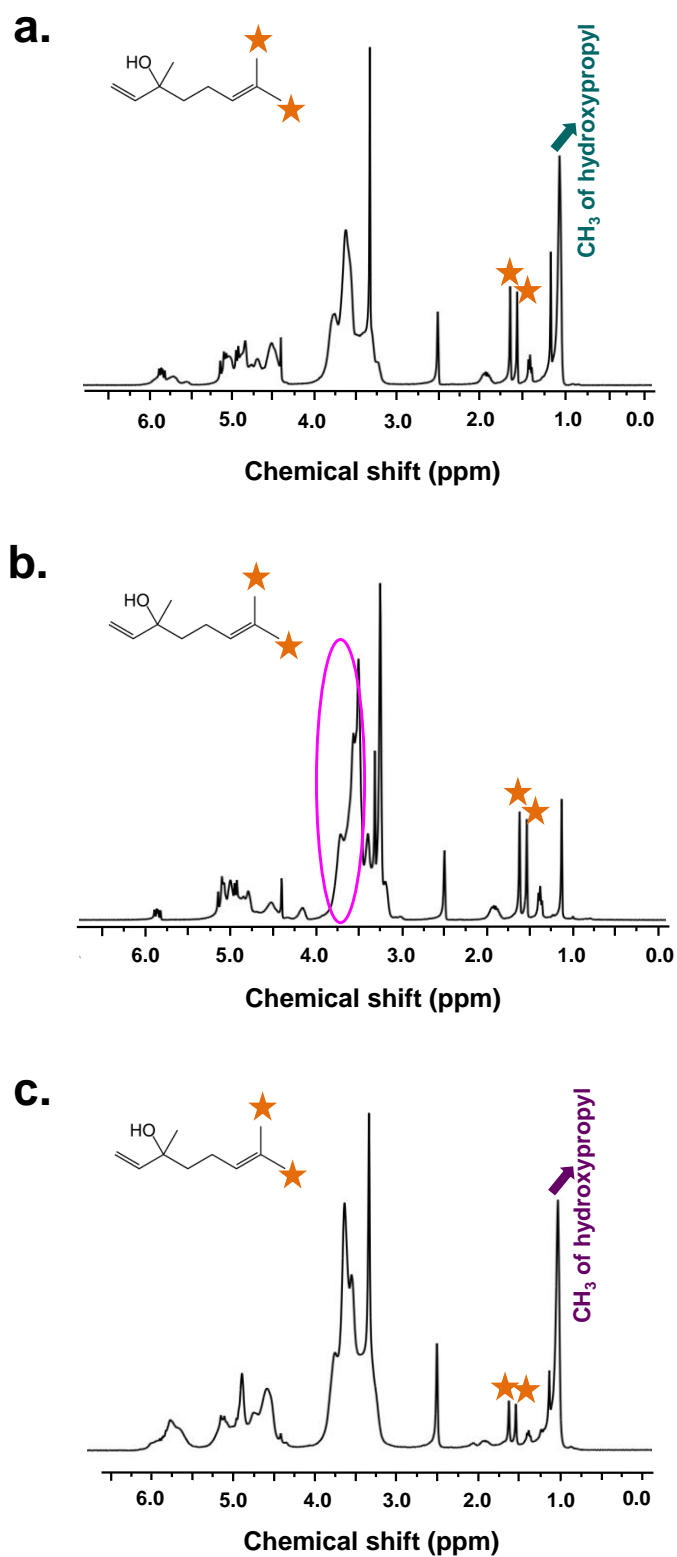


**Figure 69.**  $^1\text{H-NMR}$  spectra of (a)  $\text{HP}\beta\text{CD/linalool-IC-NF}$ , (b)  $\text{M}\beta\text{CD/linalool-IC-NF}$ , and (c)  $\text{HP}\gamma\text{CD/linalool-IC-NF}$  dissolved in  $\text{d}_6\text{-DMSO}$ .

### 8.3.3 Thermal analysis of nanofibers

The thermal stability of linalool, HP $\beta$ CD-NF, M $\beta$ CD-NF, HP $\gamma$ CD-NF, HP $\beta$ CD/linalool-IC-NF, M $\beta$ CD/linalool-IC-NF, and HP $\gamma$ CD/linalool-IC-NF were investigated by thermal gravimetric analysis (TGA) (Figure 70a-c). Two steps of weight losses were seen in TGA curves of pristine HP $\beta$ CD-NF, M $\beta$ CD-NF, and HP $\gamma$ CD-NF below 100°C and above 275°C, and these weight losses belong to the water loss and main thermal degradation of cyclodextrins (CDs), respectively [125]. The first weight loss below 100°C observed in CD/linalool-IC-NFs attributed to water loss; whereas the weight loss above 275°C, 285°C, and 275°C for HP $\beta$ CD/linalool-IC-NF, M $\beta$ CD/linalool-IC-NF, and HP $\gamma$ CD/linalool-IC-NF corresponded to the main thermal degradation of CDs, respectively. HP $\beta$ CD/linalool-IC-NF and HP $\gamma$ CD/linalool-IC-NF exhibited weight losses between 75°C-235°C and 120°C-260°C attributed to linalool. Two weight losses seen in M $\beta$ CD/linalool-IC-NF was between 65°C-170°C and 195°C-285°C and belong to evaporation of linalool in two steps. The shifting of thermal evaporation of linalool in the complexes suggested the presence of complex. However, the second complex in M $\beta$ CD/linalool-IC-NF has higher thermal stability compared to the first complex. Moreover, the thermal stability of complexes formed in M $\beta$ CD/linalool-IC-NF was higher than the complexes formed in HP $\beta$ CD/linalool-IC-NF and HP $\gamma$ CD/linalool-IC-NF.

The amount of linalool present in HP $\beta$ CD/linalool-IC-NF, M $\beta$ CD/linalool-IC-NF, and HP $\gamma$ CD/linalool-IC-NF were 84%, 89%, and 77% of the initial amount of linalool, respectively. The molar ratio of HP $\beta$ CD, M $\beta$ CD, and HP $\gamma$ CD to linalool was also calculated as 1.00:0.84, 1.00:0.89 and 1.00:0.77 based on TGA

results, respectively. The molar ratio of CD:linalool in CD/linalool-IC-NF samples calculated from the TGA data were not exactly same values with the data obtained from  $^1\text{H-NMR}$ , but they were comparable indicating that at least 45-89% of linalool was preserved in these CD based nanofibers. These results showed that great amount of linalool preserved in  $\text{HP}\beta\text{CD/linalool-IC-NF}$  and  $\text{M}\beta\text{CD/linalool-IC-NF}$ ; whereas  $\text{HP}\gamma\text{CD/linalool-IC-NF}$  preserved less amount of linalool compared to other nanofibers. On the other hand, vanillin, geraniol, and allyl isothiocyanate could not be preserved in electrospun polyvinyl alcohol (PVA) nanofibers in the absence of CD-IC during electrospinning and storage [97, 100, 102].

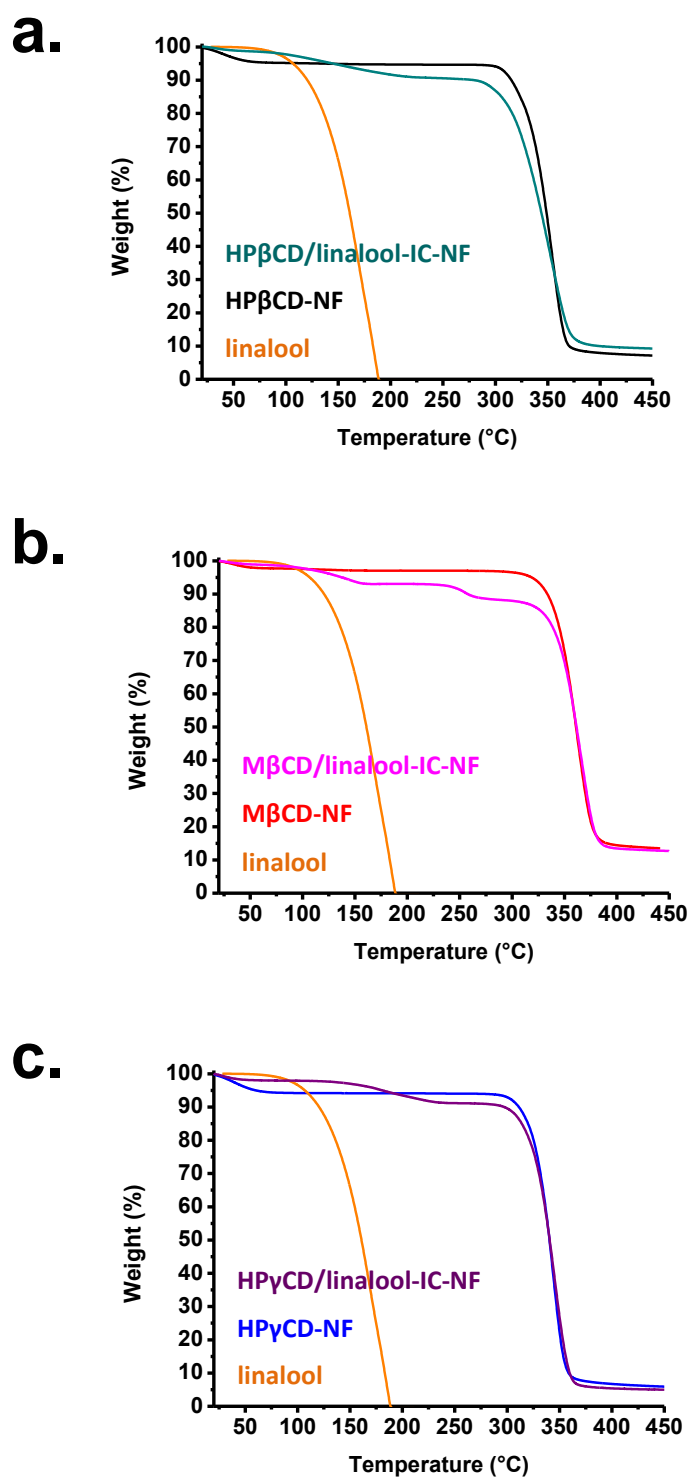


**Figure 70.** TGA thermograms of (a) linalool, HP $\beta$ CD-NF, HP $\beta$ CD/linalool-IC-NF; (b) linalool, M $\beta$ CD-NF, M $\beta$ CD/linalool-IC-NF; (c) linalool, HP $\gamma$ CD-NF, HP $\gamma$ CD/linalool-IC-NF.

Differential scanning calorimetry (DSC) curves of HP $\beta$ CD-NF, M $\beta$ CD-NF, HP $\gamma$ CD-NF, HP $\beta$ CD/linalool-IC-NF, M $\beta$ CD/linalool-IC-NF, and HP $\gamma$ CD/linalool-IC-NF are shown in Figure 71. Typical broad endothermic peaks of HP $\beta$ CD-NF, M $\beta$ CD-NF, and HP $\gamma$ CD-NF are between 25-160°C, 25-155°C, and 25-155°C and these dehydration enthalpies are 329 J/g, 99 J/g, and 255 J/g, respectively. DSC curves of HP $\beta$ CD/linalool-IC-NF, M $\beta$ CD/linalool-IC-NF and HP $\gamma$ CD/linalool-IC-NF indicated endothermic peaks between 70-160°C, 75-165°C, and 65-170°C and the enthalpies were calculated to be 88 J/g, 49 J/g, and 125 J/g, respectively. It is known that the replacement of water molecules in the cavity of CDs with the guest molecules leads to reduction in the enthalpy of CDs [225]. Therefore, the lower enthalpy values observed in CD/linalool-IC-NFs is the indication of complex formation.

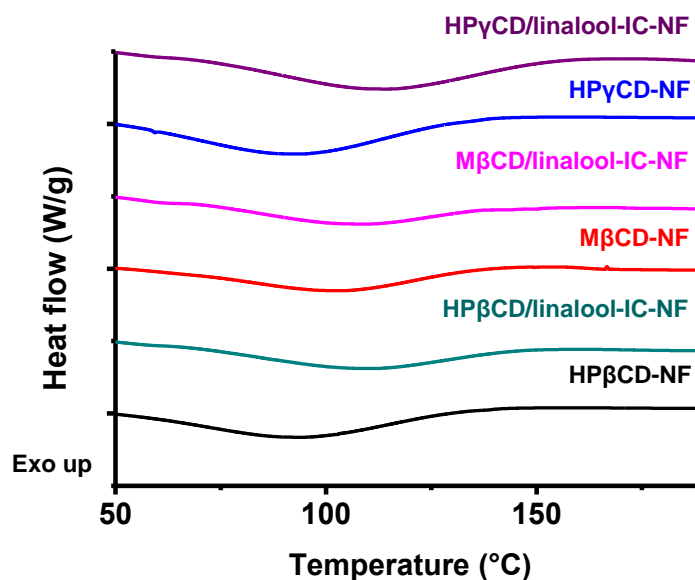


**Figure 71.** DSC thermograms of HP $\beta$ CD-NF, HP $\beta$ CD/linalool-IC-NF, M $\beta$ CD-NF, M $\beta$ CD/linalool-IC-NF, HP $\gamma$ CD-NF, and HP $\gamma$ CD/linalool-IC-NF.

### 8.3.4 Structural characterization of nanofibers

X-ray diffraction (XRD) patterns of HP $\beta$ CD-NF, M $\beta$ CD-NF, HP $\gamma$ CD-NF, HP $\beta$ CD/linalool-IC-NF, M $\beta$ CD/linalool-IC-NF, and HP $\gamma$ CD/linalool-IC-NF are given in Figure 72. It is observed that HP $\beta$ CD-NF, M $\beta$ CD-NF, and HP $\gamma$ CD-NF are amorphous like HP $\beta$ CD, M $\beta$ CD, and HP $\gamma$ CD molecules. It was found that HP $\beta$ CD/linalool-IC-NF, M $\beta$ CD/linalool-IC-NF, and HP $\gamma$ CD/linalool-IC-NF exhibited amorphous structure as well. As a conclusion, the lack of crystal formation of linalool confirmed the formation of complex in CD/linalool-IC-NFs.

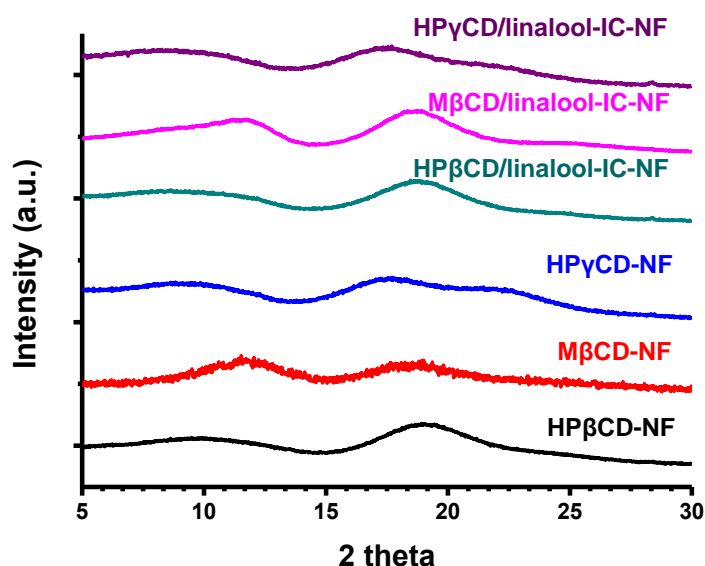


**Figure 72.** XRD patterns of HP $\beta$ CD-NF, M $\beta$ CD-NF, HP $\gamma$ CD-NF, HP $\beta$ CD/linalool-IC-NF, M $\beta$ CD/linalool-IC-NF, and HP $\gamma$ CD/linalool-IC-NF.

### 8.3.5 Release study

The release of linalool from HP $\beta$ CD/linalool-IC-NF, M $\beta$ CD/linalool-IC-NF, and HP $\gamma$ CD/linalool-IC-NF at 37°C, 50°C, and 75°C for 3 h is shown in Figure 73a-c. Firstly, the release of linalool from CD/linalool-IC-NFs increased by the

temperature increases from 37°C to 75°C. Since as the temperature increases, the diffusion coefficient of molecules becomes higher [216]. Secondly, although the preserved amount of linalool is almost same in HP $\beta$ CD/linalool-IC-NF and M $\beta$ CD/linalool-IC-NF, HP $\beta$ CD/linalool-IC-NF released much more amount of linalool in total compared to M $\beta$ CD/linalool-IC-NF. This result might be due to the lower thermal stability of HP $\beta$ CD/linalool-IC-NF shown in TGA data (Figure 70). Thirdly, since the preserved amount of linalool was less in HP $\gamma$ CD/linalool-IC-NF, the total amount of released linalool was less from HP $\gamma$ CD/linalool-IC-NF than HP $\beta$ CD/linalool-IC-NF and M $\beta$ CD/linalool-IC-NF.

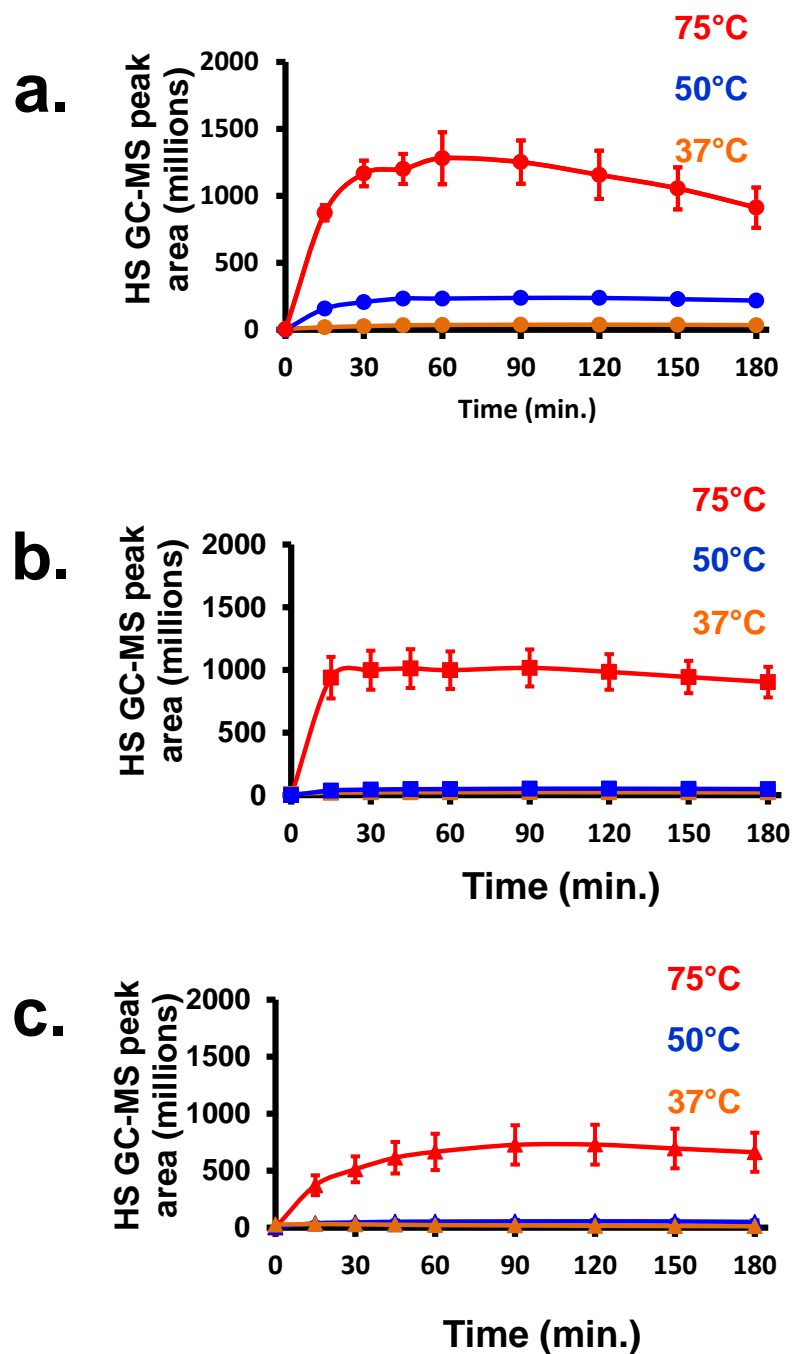


**Figure 73.** The cumulative release of linalool from (a) HP $\beta$ CD/linalool-IC-NF, (b) M $\beta$ CD/linalool-IC-NF, and (c) HP $\gamma$ CD/linalool-IC-NF at 37°C, 50°C, 75°C (n = 3). The error bars in the figure represent the standard deviation (SD).

The long term release experiments were performed for HP $\beta$ CD/linalool-IC-NF, M $\beta$ CD/linalool-IC-NF, and HP $\gamma$ CD/linalool-IC-NF at room temperature (RT).

The results are shown in Figure 74. Owing to the high thermal stability of

linalool in M $\beta$ CD/linalool-IC-NF, great amount of linalool did not release from M $\beta$ CD/linalool-IC-NF at the end of 50 days. But HP $\beta$ CD/linalool-IC-NF and HP $\gamma$ CD/linalool-IC-NF could preserve only 60% (w/w) and 69% (w/w) of linalool at the end of 50 days. Therefore, M $\beta$ CD/linalool-IC-NF is an ideal material for long term release as compared to HP $\beta$ CD/linalool-IC-NF and HP $\gamma$ CD/linalool-IC-NF. In our previous studies, significant amount vanillin, geraniol, and allyl isothiocyanate which are volatile compounds was lost from PVA nanofibers without CD-IC during electrospinning or storage even after one day of electrospinning [97, 100, 102]. However, linalool was preserved at a great extent in CD/linalool-IC-NFs even after a long time of storage.

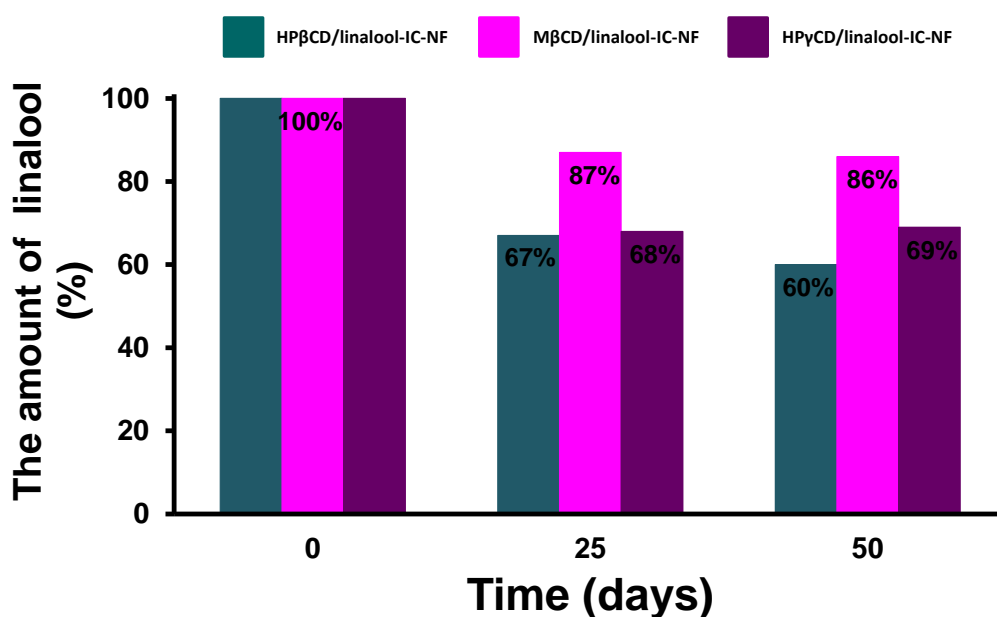


**Figure 74.** The amount of linalool in HP $\beta$ CD/linalool-IC-NF, M $\beta$ CD/linalool-IC-NF, and HP $\gamma$ CD/linalool-IC-NF at RT for 50 days.

### 8.3.6 Antibacterial activity

The terpene constituents present in essential oils disrupt the bacterial membrane in both Gram-negative and Gram-positive bacteria and therefore essential oils exhibit antibacterial activity [250]. The antibacterial activity of HP $\beta$ CD/linalool-IC-NF, M $\beta$ CD/linalool-IC-NF, and HP $\gamma$ CD/linalool-IC-NF webs against *Escherichia coli* (*E. coli*) and *Staphylococcus aureus* (*S. aureus*) was tested by using the viable cell-counting method (Figure 75). As shown in the plates that CD/linalool-IC-NF samples possessed strong antibacterial activity against *E. coli* and *S. aureus*. The antibacterial activity (%) of HP $\beta$ CD/linalool-IC-NF, M $\beta$ CD/linalool-IC-NF, and HP $\gamma$ CD/linalool-IC-NF was 84 $\pm$ 0.1%, 93 $\pm$ 0.1% and 95 $\pm$ 0.2% against *E. coli*, and 70 $\pm$ 0.3%, 79 $\pm$ 0.2%, and 88 $\pm$ 0.5% against *S. aureus*, respectively. Therefore, CD/linalool-IC-NFs are effective antibacterial materials against model Gram-negative and Gram-positive bacteria.

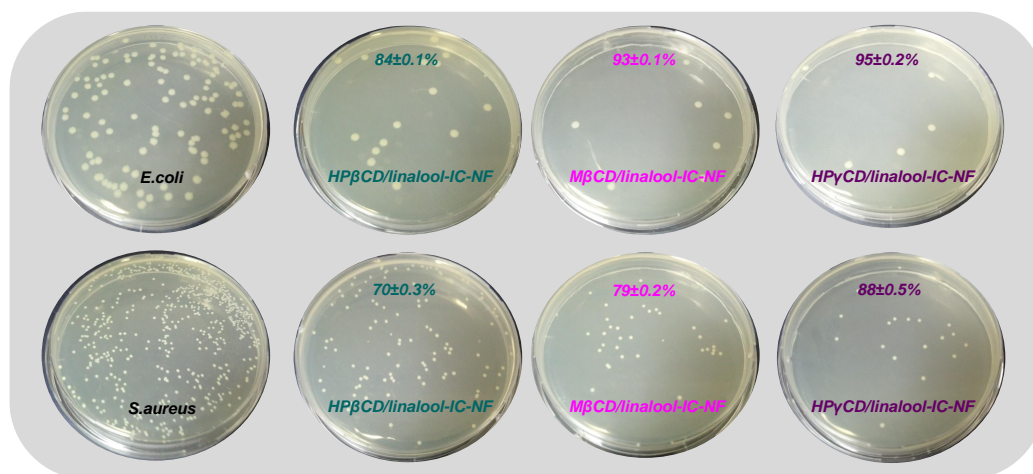


**Figure 75.** Exemplary images of *E. coli*, *S. aureus* colonies. The growth inhibition rate (%) and exemplary images of *E. coli* and *S. aureus* colonies treated by HP $\beta$ CD/linalool-IC-NF, M $\beta$ CD/linalool-IC-NF, and HP $\gamma$ CD/linalool-IC-NF (n = 3).

## 8.4 Conclusion

Free-standing nanofibrous webs were produced from non-polymeric systems of cyclodextrin/linalool-inclusion complexes (CD/linalool-ICs) by electrospinning. ~45-89% of linalool was preserved in CD/linalool-IC-NFs owing to the complexation. TGA, DSC and XRD proved the formation of inclusion complexation with HP $\beta$ CD, M $\beta$ CD, and HP $\gamma$ CD with linalool. The short-term temperature release (3h; at 37°C, 50°C, and 75°C) and long-term open air release (50 days, at RT) tests were performed for CD/linalool-IC-NFs. M $\beta$ CD/linalool-IC-NF released less amount of linalool compared to HP $\beta$ CD/linalool-IC-NF in short-term temperature release and long-term open air release tests due to its higher stability shown in TGA results. CD/linalool-IC-NFs was shown to have quite high antibacterial activity against model Gram-negative (*E. coli*) and Gram-positive (*S. aureus*) bacteria. CD/linalool-IC-NFs are shown to dissolve completely in water within two seconds. Briefly, high preservation of linalool along with antibacterial activity and controlled release was achieved by the production of CD/linalool-IC nanofibrous webs which can be used as fast dissolving oral membrane in pharmaceutical and cosmetic products.

## **Chapter 4**

---

### **ELECTROSPINNING OF CORE-SHELL NANOFIBERS FROM CYCLODEXTRIN INCLUSION COMPLEXES**

## **9. Core-shell nanofibers via electrospinning for drug delivery application**

### **9.1 Introduction**

Poly(lactic acid) (PLA) is an aliphatic biodegradable polyester and produced from lactic acid and widely used in biological application including drug delivery, wound dressing, food packaging due to its inherent properties such as biocompatibility, biodegradability; carbon dioxide, oxygen and water permeability [160].

Hydroxypropyl-beta-cyclodextrin (HP $\beta$ CD) (Figure 76b) one of the most commonly used modified CD type. The most remarkable feature of HP $\beta$ CD is its great aqueous solubility [256, 257]. So, ICs formed with HP $\beta$ CD improve dissolution and absorption of low solubility drugs [258] and oral bioavailability of drugs [259].

Curcumin (CUR) (Figure 76a) is a polyphenol and derived from turmeric [260-262]. It is composed of CUR, demethoxycurcumin, bisdemethoxycurcumin [261]. Due to its antioxidant, anticancer, and antiinflammatory activities, it finds wide application [260-262]. However, its aqueous solubility and bioavailability is low [260-262]. CDs are being used for CUR to enhance its limitations such as solubility and bioavailability [263-265]. Electrospun nanofibers were used as a carrier for CUR in the literature [201, 266-268]. Furthermore, production of CD-IC of CUR encapsulated electrospun nanofibers were also reported [106].

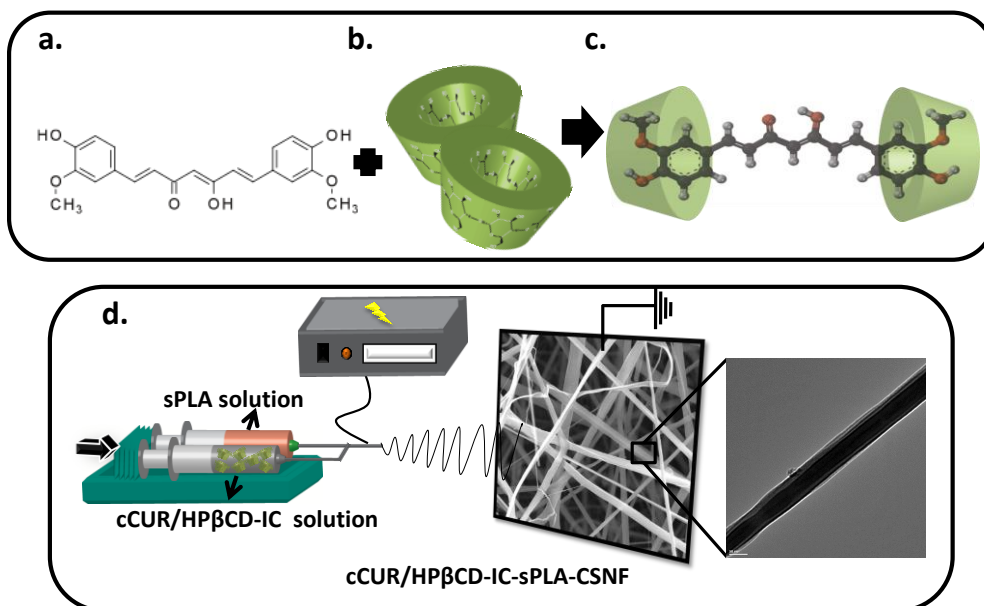


**Figure 76.** Chemical structure of (a) curcumin; schematic representation of (b) HPβCD, (c) formation of CUR/HPβCD-IC, and (d) electrospinning of nanofibers from cCUR/HPβCD-IC-sPLA solution.

In this study, core-shell nanofibers in which CD-IC of an active agent was used as a core solution for the first time. CUR was used as a model drug and its IC were prepared (CUR/HPβCD-IC) (Figure 76c) at 1:2 molar ratio (CUR:HPβCD) as core solution; PLA solution were used as shell. Then, electrospinning was applied to produce cCUR/HPβCD-IC-sPLA-CSNF (Figure 76d). The morphology of cCUR/HPβCD-IC-sPLA-CSNF were observed by scanning electron microscope (SEM), transmission electron microscopy (TEM), and confocal laser scanning microscopy (CLSM). The structural and thermal characterization of PLA-CUR-NF, PLA/CUR:HPβCD-IC-NF, and cCUR/HPβCD-IC-sPLA-CSNF were carried out by X-ray diffraction (XRD) and thermal gravimetric analysis (TGA), respectively. Antioxidant activity of PLA-CUR-NF, PLA/CUR:HPβCD-IC-NF, and cCUR/HPβCD-IC-sPLA-CSNF were tested depending of time and concentration by 2,2-diphenyl-1-

picrylhydrazyl (DPPH) radical scavenging method. The release of CUR from nanofibers into methanol was evaluated for 1 hour and measurement was done via high performance liquid chromatography (HPLC). Lastly, degradation of nanofibers were investigated by incubating nanofibers in phosphate buffered saline (PBS) for 28 days.

## **9.2 Experimental**

### **9.2.1 Materials**

Poly(lactic acid) (PLA) was donated by Natureworks (product code 6252D). Curcumin (CUR, 95%, Sigma Aldrich), hydroxypropyl-beta-cyclodextrin (HP $\beta$ CD, Wacker Chemie AG, Germany), fluorescein isothiocyanate (FITC,  $\geq 90\%$ , Sigma Aldrich), zinc acetate dihydrate (Sigma Aldrich), potassium phosphate monobasic (Riedel de Haen), disodium hydrogen phosphate dodecahydrate (Riedel de Haen), sodium chloride (99.0–100.5%, Sigma Aldrich), methanol (extra pure, Sigma Aldrich), chloroform (CHCl<sub>3</sub>, 99% Sigma Aldrich), deuterated dimethylsulfoxide (DMSO-d<sub>6</sub>, deuteration degree min 99.8% for NMR spectroscopy, Merck), 2,2-diphenyl-1-picrylhydrazyl (DPPH, Sigma Aldrich) were purchased and used as-received without any further purification. Distilled-deionized water was supplied from Millipore milli-Q ultrapure water system.

### **9.2.2 Preparation of electrospinning solutions**

Core-shell nanofibers were produced from curcumin (CUR):HP $\beta$ CD-inclusion complex (IC) (core solution) and PLA (shell solution) (cCUR:HP $\beta$ CD-IC-sPLA-CSNF). In order to prepare the core solution, HP $\beta$ CD was dissolved in

water, then CUR was added (1:2 molar ratio, CUR:HP $\beta$ CD) and the resulting solution was stirred overnight at room temperature (RT). Chloroform (CHCl<sub>3</sub>):methanol (MeOH) (2:1) system was chosen to dissolve 10% (w/v) polylactic acid (PLA) and this solution was used as shell solution. Finally, electrospinning was performed in order to obtain cCUR:HP $\beta$ CD-IC-sPLA-CSNF. Only CUR including PLA nanofibers (PLA-CUR-NF) and CUR:HP $\beta$ CD-IC (2:1 molar ratio, HP $\beta$ CD:CUR) incorporated PLA nanofibers (PLA/CUR:HP $\beta$ CD-IC-NF) were also produced as reference samples. For producing PLA-CUR-NF, firstly CUR was dissolved in methanol then 10% (w/v) PLA and CHCl<sub>3</sub> was added. After 2 hours of stirring at room temperature, electrospinning was performed. With regards to PLA/CUR:HP $\beta$ CD-IC-NF, CUR:HP $\beta$ CD-IC (2:1 molar ratio, HP $\beta$ CD:CUR) was prepared in methanol for 12 h, then 10% (w/v) PLA and CHCl<sub>3</sub> was added. PLA/CUR:HP $\beta$ CD-IC-NF was produced via electrospinning after stirring the solution 2 hours more.

### **9.2.3 Electrospinning**

cCUR:HP $\beta$ CD-IC and sPLA solutions were loaded in 3 ml plastic syringe and then placed separately on two syringe pumps (KD Scientific, KDS101). The core and shell flow rates were 1 mL/h and 3 mL/h, respectively. Core-shell nozzle was used to obtain core-shell nanofibers via electrospinning. 15 kV was applied from a high voltage power supply (AU Series, Matsusada Precision Inc.). Grounded metal collector was used to collect the nanofibers. The distance between the core-shell nozzle and the collector was 15 cm.

PLA-CUR and PLA/CUR:HP $\beta$ CD-IC solutions were loaded in 3 ml plastic syringe and then mounted on the syringe pump. The solution feed rate was 1

mL/h and the needle diameter was 0.8 mm. The grounded metal collector was placed 10 cm away from the needle tip and 15 kV was applied from a high voltage power supply. The experiments were performed at 25°C, 18% humidity.

#### **9.2.4 Characterizations and measurements**

The morphological characterization for PLA-CUR-NF, PLA/CUR/HP $\beta$ CD-IC-NF, and cCUR/HP $\beta$ CD-IC-sPLA-CSNF were carried out via scanning electron microscopy (SEM, FEI-Quanta 200 FEG). Nanofiber samples were placed on metal stubs using double-sided adhesive copper tape and then coated with 5 nm Au/Pd layer (PECS-682). Average fiber diameter (AFD) of the nanofibers was calculated from the SEM images as well. At least 100 fibers were measured for each sample, and their averages and standard deviations were reported. In addition to morphological characterization done by SEM, transmission electron microscopy (TEM, FEI-Tecnai G2F30) and confocal laser scanning microscope (CLSM, Jena, Germany) were used in order to show the core-shell structure of cCUR/HP $\beta$ CD-IC-sPLA-CSNF. For TEM imaging, zinc acetate dihydrate included core solution and PLA solution (shell) were electrospun and nanofibers were collected on grid; whereas FTIC included core solution and PLA solution (shell) were electrospun on glass substrate for CLSM imaging.

The crystalline structure of powder of CUR, HP $\beta$ CD, PLA-NF, PLA-CUR-NF, PLA/CUR/HP $\beta$ CD-IC-NF, and cCUR/HP $\beta$ CD-IC-sPLA-CSNF were investigated by X-ray diffraction (XRD, PANalytical X'Pert powder diffractometer) applying Cu K $\alpha$  radiation in a  $2\theta$  range 5°-30°.

The thermal properties of CUR, HP $\beta$ CD, PLA-NF, PLA-CUR-NF, PLA/CUR/HP $\beta$ CD-IC-NF, and cCUR/HP $\beta$ CD-IC-sPLA-CSNF were evaluated using thermal gravimetric analysis (TGA, TA Q500, USA). The TGA measurements were performed under nitrogen atmosphere, and the samples were heated up to 500°C at a constant heating rate of 20°C/min.

Antioxidant activity of PLA-CUR-NF, PLA/CUR/HP $\beta$ CD-IC-NF, and cCUR/HP $\beta$ CD-IC-sPLA-CSNF were tested via 2,2-diphenyl-1-picrylhydrazyl (DPPH) radical scavenging assay [181]. Firstly, time dependent antioxidant activity test was carried out. In order to determine time dependent antioxidant activity, nanofibers having equivalent amount of CUR were kept in methanol for 1 hour, then certain amount of that solution was added into certain amount of 10<sup>-4</sup> M DPPH solution prepared in methanol. Finally, UV absorbance of the resulting solution was measured at predetermined time intervals for 1 hour (Varian, Cary 100). With regards to concentration dependent antioxidant activity test, certain amount of nanofibers were kept in methanol for 1 hour, then 5 different concentration of these solutions were added into 10<sup>-4</sup> M DPPH solution prepared in methanol. At the end of 1 hour, UV absorbance of the solutions was measured (Varian, Cary 100).

The absorbance of DPPH was defined as 100% and the antioxidant activities (%) were calculated according to the following equation:

$$\text{Antioxidant activity (\%)} = (A_{\text{control}} - A_{\text{sample}}) / A_{\text{control}} * 100 \quad (\text{Equation 13})$$

where  $A_{\text{control}}$  and  $A_{\text{sample}}$  represent the absorbance values of control DPPH solution and DPPH solution with nanofibers, respectively.

CUR release from PLA-CUR-NF, PLA/CUR/HP $\beta$ CD-IC-NF, and cCUR/HP $\beta$ CD-IC-sPLA-CSNF were investigated as well. For this test, nanofibers were individually immersed in methanol and the solutions were stirred at RT at 50 rpm for 1 hour. 0.5 ml of sample solution was withdrawn from the solutions at pre-determined time intervals and 0.5 ml of fresh medium was refilled. Then, the amount of CUR released was measured by high performance liquid chromatography (HPLC, Agilent, 1200 series) equipped with VWD UV detector. C8 column (Agilent, column dimension: 4.6 mmx50 mm, particle size: 5  $\mu$ m.) operating at 1 ml/min with methanol eluent was used for separation. For in vitro degradation test, PLA-CUR-NF, PLA/CUR/HP $\beta$ CD-IC-NF, and cCUR/HP $\beta$ CD-IC-sPLA-CSNF were incubated in phosphate buffered saline (PBS) for 28 days at 37°C. The nanofibers were washed with distilled water after 4 and 28 days, vacuum-dried at RT, and then SEM images were taken.

## **9.3 Results and discussion**

### **9.3.1 Morphology analysis of nanofibers**

SEM images taken for PLA-CUR-NF, PLA/CUR:HP $\beta$ CD-IC-NF, and cCUR:HP $\beta$ CD-IC-sPLA-CSNF showed bead-free morphology of these nanofibers (Figure 77). The diameter of PLA-CUR-NF, PLA/CUR:HP $\beta$ CD-IC-NF, and cCUR:HP $\beta$ CD-IC-sPLA-CSNF were 465 $\pm$ 120 nm, 830 $\pm$ 275 nm, and 695 $\pm$ 280 nm, respectively. The photographs of PLA-CUR-NF, PLA/CUR:HP $\beta$ CD-IC-NF, and cCUR:HP $\beta$ CD-IC-sPLA-CSNF showed nanofibers are easily-handled (Figure 77). TEM and CLSM images showed successful production of core-shell nanofibers (Figure 78a-b).

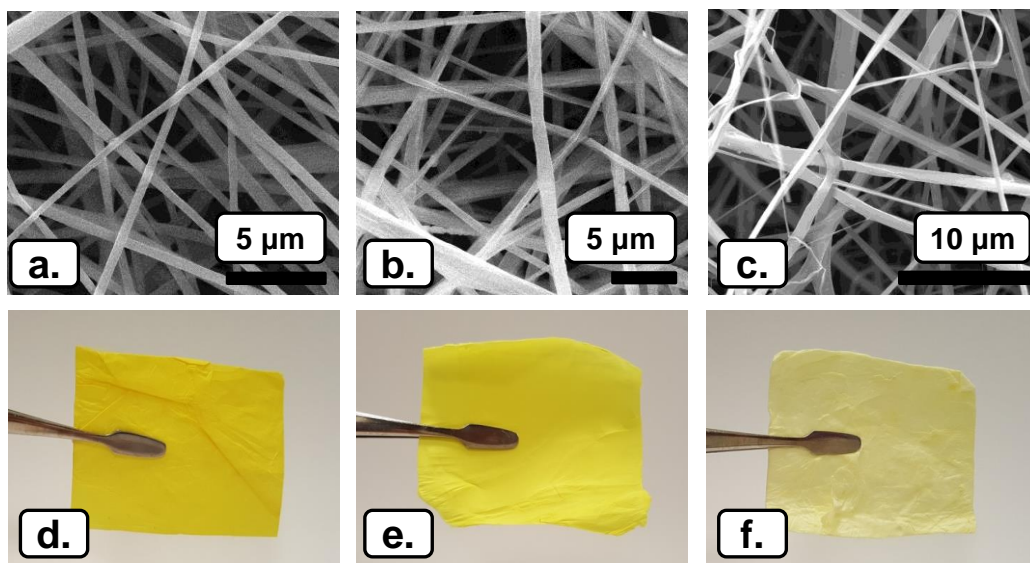


**Figure 77.** SEM images of electrospun nanofibers obtained from solutions of (a) PLA-CUR, (b) PLA/CUR-HP $\beta$ CD-IC, (c) cCUR/HP $\beta$ CD-IC-sPLA-CS; the photographs of PLA-CUR-NF, (b) PLA/CUR-HP $\beta$ CD-IC-NF, (c) cCUR/HP $\beta$ CD-IC-sPLA-CSNF.

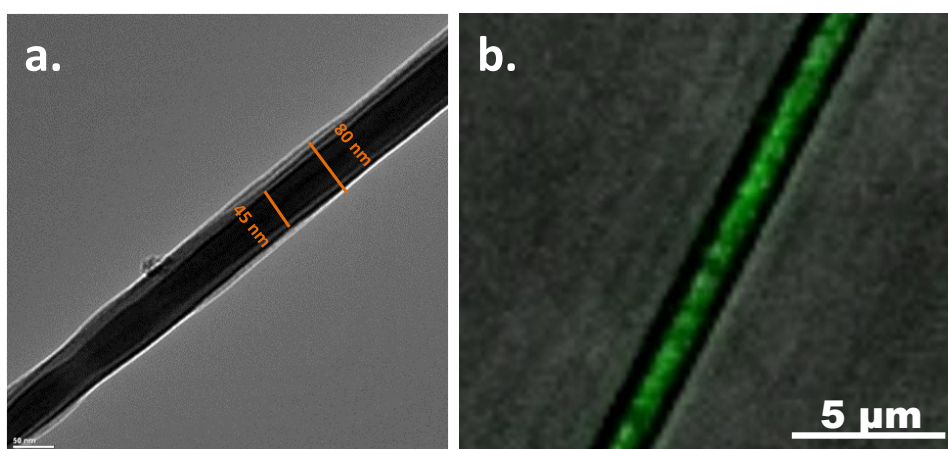


**Figure 78.** (a) TEM and (b) CLSM images of cCUR/HP $\beta$ CD-IC-sPLA-CSNF.

### 9.3.2 Structural characterization of nanofibers

XRD analysis was also performed for CUR, HP $\beta$ CD, PLA-NF, PLA-CUR-NF, PLA/CUR/HP $\beta$ CD-IC-NF, and cCUR/HP $\beta$ CD-IC-sPLA-CSNF. XRD results showed that CUR is no longer in crystalline state in PLA-CUR-NF, thus PLA-

CUR-NF exhibited amorphous structure. The reason for CUR molecules not to form crystalline aggregates is the restriction of drug mobility due to the rapid evaporation of the solvent during electrospinning. The absence of intense and sharp peaks in the XRD pattern of HP $\beta$ CD show that it has an amorphous structure. In the XRD pattern of PLA/CUR:HP $\beta$ CD-IC-NF and cCUR:HP $\beta$ CD-IC-sPLA-CSNF, the absence of crystalline diffraction peaks of CUR suggested that CUR is in amorphous state in the nanofibers [176].

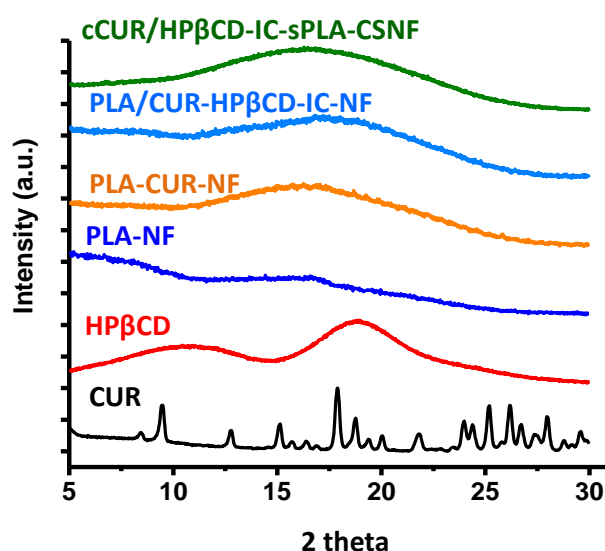


**Figure 79.** XRD patterns of CUR, HP $\beta$ CD, PLA-NF, PLA-CUR-NF, PLA/CUR-HP $\beta$ CD-IC-NF, and cCUR/HP $\beta$ CD-IC-sPLA-CSNF.

### 9.3.3 Thermal analysis of nanofibers

TGA measurements for CUR, HP $\beta$ CD, PLA-NF, PLA-CUR-NF, PLA/CUR/HP $\beta$ CD-IC-NF, and cCUR/HP $\beta$ CD-IC-sPLA-CSNF are given in Figure 80. The thermal degradation of CUR starts at around 200°C; whereas the main thermal degradation of PLA is between 225°C and 375°C. We observed that PLA-CUR-NF exhibited weight loss between 250°C and 375°C

corresponding the degradation of both CUR and PLA. HP $\beta$ CD lost weight in two steps, the first one is related with the loss of water molecules in the cavity; the second that is after 295°C is the main decomposition of HP $\beta$ CD. In the TGA graph of PLA/CUR/HP $\beta$ CD-IC-NF, there exist two distinct stage of weight loss. The first which is due to the loss of water molecules and the second weight loss is due to the thermal degradation of CUR, HP $\beta$ CD, and PLA. Two steps of weight loss seen in cCUR/HP $\beta$ CD-IC-sPLA-CSNF is attributed to the water loss and degradation of CUR, HP $\beta$ CD, and PLA, respectively. Therefore, complexation did not cause the thermal stability of CUR to change. The amount of CUR in the nanofibers could not be calculated due to the overlapping of the degradation of the molecules.

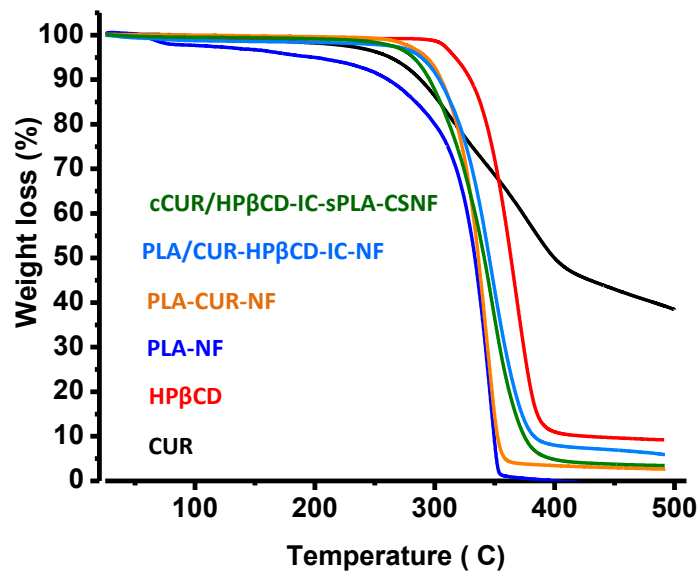


**Figure 80.** TGA thermograms of CUR, HP $\beta$ CD, PLA-NF, PLA-CUR-NF, PLA/CUR-HP $\beta$ CD-IC-NF, and cCUR/HP $\beta$ CD-IC-sPLA-CSNF.

### 9.3.4 Antioxidant activity

The antioxidant activity (%) PLA-CUR-NF, PLA/CUR:HP $\beta$ CD-IC-NF, and cCUR:HP $\beta$ CD-IC-sPLA-CSNF of were tested according to 2,2-diphenyl-1-picrylhydrazyl (DPPH) method [181]. According to the results (Figure 81), PLA-CUR-NF, PLA/CUR:HP $\beta$ CD-IC-NF, and cCUR:HP $\beta$ CD-IC-sPLA-CSNF have 96%, 93%, and 81% of antioxidant activity at the end of 1 hour. Antioxidant activity for PLA-CUR-NF is the highest starting from 1 minute of reaction, and reached 96% after 4 minutes. For PLA/CUR:HP $\beta$ CD-IC-NF, antioxidant activity was 88% after 2 minute of reaction and it increased gradually up to 93% in 20 minutes. cCUR:HP $\beta$ CD-IC-sPLA-CSNF had 61% antioxidant activity after 1 minute of reaction, and it increased slowly in 45 minutes. The photographs of the solution also showed the change in the color of DPPH solution from purple to yellow in PLA-CUR-NF and PLA/CUR:HP $\beta$ CD-IC-NF. However, the color of DPPH solution was darker in case of cCUR:HP $\beta$ CD-IC-sPLA-CSNF.

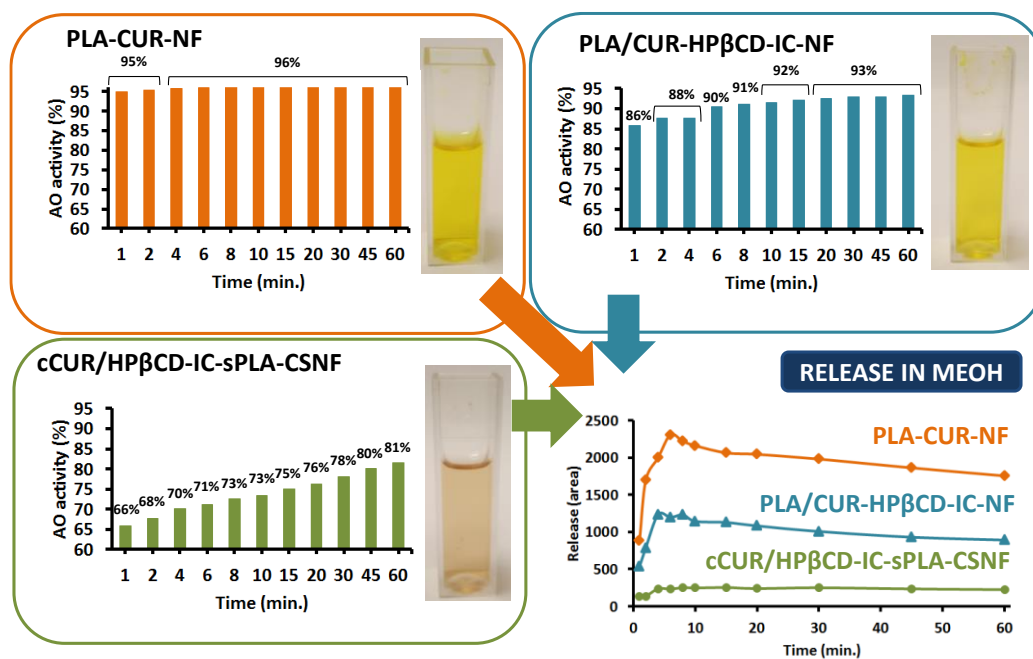


**Figure 81.** Time dependent antioxidant activity of PLA-CUR-NF, PLA/CUR-HPβCD-IC-NF, cCUR/HPβCD-IC-sPLA-CSNF and the release of CUR from PLA-CUR-NF, PLA/CUR-HPβCD-IC-NF, cCUR/HPβCD-IC-sPLA-CSNF.

Concentration dependent antioxidant activity of PLA-CUR-NF, PLA/CUR:HPβCD-IC-NF, and cCUR:HPβCD-IC-sPLA-CSNF was also decided by using DPPH method. As shown in Figure 82, when 1.03 ppm CUR including nanofibers were used PLA-CUR-NF, PLA/CUR:HPβCD-IC-NF, and cCUR:HPβCD-IC-sPLA-CSNF exhibited 58%, 48%, and 38% antioxidant activity, respectively. Antioxidant activity was increased up to 95%, 96%, and 87%, when 16.5 ppm CUR including nanofibers were used. The photographs taken for each concentration of nanofibers also confirmed these results.

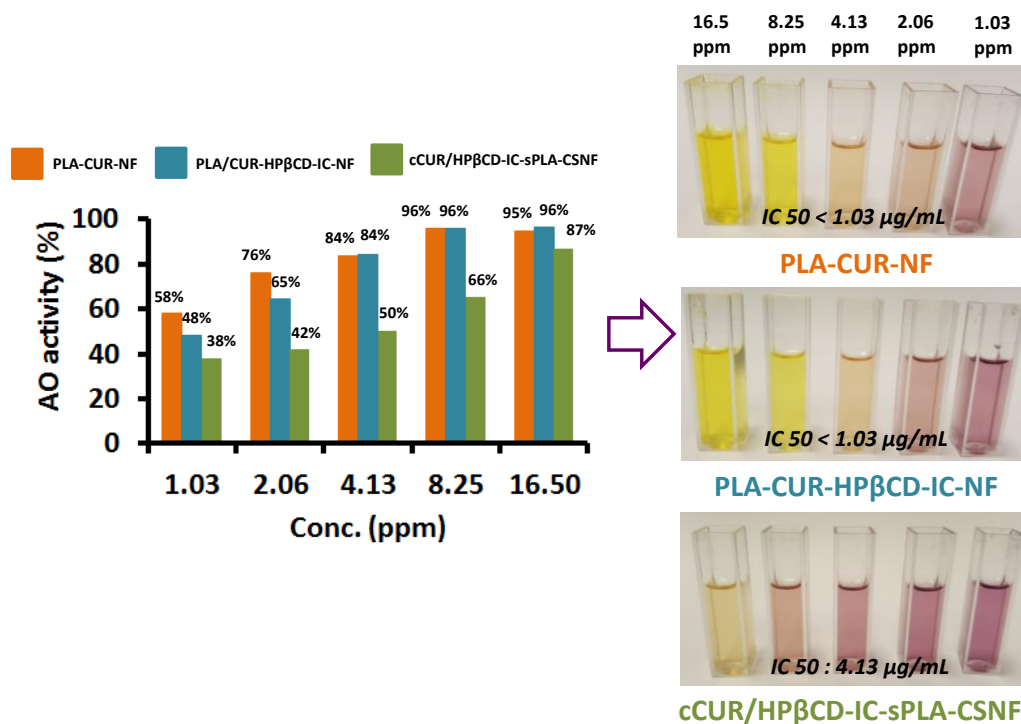


**Figure 82.** Concentration dependent antioxidant activity of PLA-CUR-NF, PLA/CUR-HPβCD-IC-NF, cCUR/HPβCD-IC-sPLA-CSNF.

### 9.3.5 In vitro release study

The release of CUR from PLA-CUR-NF, PLA/CUR:HPβCD-IC-NF, and cCUR:HPβCD-IC-sPLA-CSNF into methanol was determined by HPLC for 1 hour (Figure 81). The rate of release from PLA-CUR-NF, PLA/CUR:HPβCD-IC-NF, and cCUR:HPβCD-IC-sPLA-CSNF reached maximum in 6, 8, and 15 minutes, respectively. The amount of CUR released was highest from PLA-CUR-NF and lowest from cCUR:HPβCD-IC-sPLA-CSNF. The rate and amount of CUR release supported the time dependent antioxidant activity result.

### 9.3.6 In vitro degradation test

The degradation behaviour of materials that are intended to be used in biological applications is of vital importance. The degradation of aliphatic polyesters (e.g.

PLA) is based on the hydrolytic reaction, thus the average length of the degraded chains reduce on the chain in the presence of water molecules. Since water molecules attack to ester bonds in the polymer structure [269]. As seen in Figure 83, cCUR/HP $\beta$ CD-IC-sPLA-CSNF preserve their nanofibrous structure and integrity at the end of 28 days. This result is in good agreement with the study of Ishii et al. in which nanofibers maintained even after 12 weeks of incubation [270].

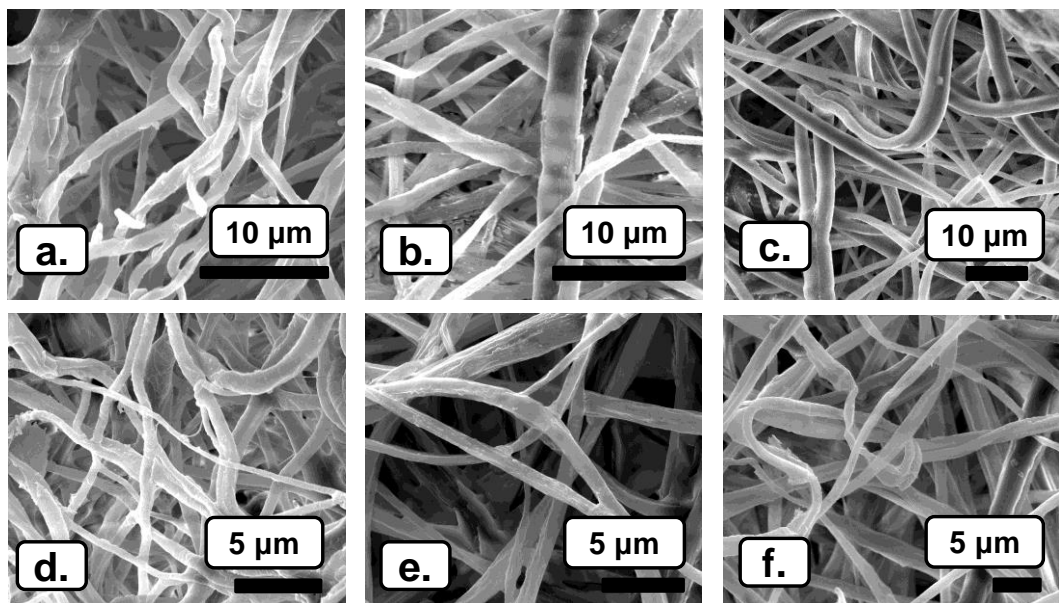


**Figure 83.** SEM images of (a, d) PLA-CUR-NF, (b, e) PLA/CUR-HP $\beta$ CD-IC-NF, (c, f) cCUR/HP $\beta$ CD-IC-sPLA-CSNF after 4 (a-c) and 28 (d-f) days in vitro degradation in PBS.

## 9.4 Conclusion

As a result, core-shell nanofibers were obtained from CUR-HP $\beta$ CD-IC and PLA solution for the first time (cCUR/HP $\beta$ CD-IC-sPLA-CSNF). The characterization of core-shell nanofibers was firstly carried out by SEM, TEM, and CLSM. Images showed the successful formation of core-shell nanofibers with bead-free morphology. XRD and TGA were also used for structural and thermal analysis

of core-shell nanofibers. Antioxidant activity of cCUR/HP $\beta$ CD-IC-sPLA-CSNF were investigated comparative to PLA-CUR-NF and PLA/CUR-HP $\beta$ CD-IC-NF depend on time and concentration. cCUR/HP $\beta$ CD-IC-sPLA-CSNF had slower and slightly less antioxidant activity than control nanofibers. The release of CUR into 95% methanol was slower as well from cCUR/HP $\beta$ CD-IC-sPLA-CSNF than other nanofibers and this result shows the applicability of these nanofibers as slow releasing material. Therefore, cCUR/HP $\beta$ CD-IC-sPLA-CSNF has potential to be used as slow release systems for bioactive molecules.

# **Chapter 5**

---

## **CONCLUSION AND FUTURE PERSPECTIVES**

In this dissertation, three different approaches were proposed to produce electrospun nanofibers from both polymeric and non-polymeric systems. As a first study, CD-ICs of four different antioxidant and antibacterial agents (GA,  $\alpha$ -TC, QU, and THY) loaded into electrospun PLA and zein nanofibers. The release of GA,  $\alpha$ -TC was investigated by HPLC; whereas since THY is a volatile compound its release was measured by HS GC-MS. As a result, PLA nanofibers containing CD-ICs of GA and  $\alpha$ -TC released much more amount of bioactive agent compared to nanofibers containing bioactive agent without CD. This is related with the increment in the concentration of diffusible species by complexation. In addition, the release of  $\alpha$ -TC from  $\alpha$ -TC/CD-IC incorporated PLA nanofibers was also slower owing to the lower diffusion rate of bioactive molecules when they are in the cavity of CDs. THY/CD-IC (2:1) incorporated zein nanofibers released much more amount of THY than only THY including nanofibers due to the better preservation of THY against evaporation. Nanofibers containing CD-IC of GA,  $\alpha$ -TC, and QU exhibited quite high antioxidant activity as well. THY/CD-IC loaded zein nanofibers exhibited much better antibacterial activity in comparison to nanofibers without CD-IC. As an aim towards investigating the potential of nanofibers as a packaging material,  $\alpha$ -TC/CD-IC and THY/CD-IC loaded nanofibers were used. As a result, it was concluded that  $\alpha$ -TC/CD-IC incorporated PLA and THY/CD-IC incorporated zein nanofibers are good candidates to be used as antioxidant and antibacterial food packaging materials, respectively.

As a second study, electrospun nanofibers were designed from a non-polymeric system, CD-ICs. For this purpose, three types of volatile flavour/fragrance

(geraniol, limonene, and linalool) was used as model bioactive agents with three types of modified CDs (HP $\beta$ CD, M $\beta$ CD, HP $\gamma$ CD). CD-IC nanofibers were proved to be superior to polymeric nanofibers in terms of the amount of bioactive agent loaded and the possibility of production in aqueous solution. The short time temperature and long time-release experiments and antibacterial studies were conducted for these nanofibers. The release of volatile flavour/fragrances from nanofibers was analyzed by HS GC-MS depending on temperature; whereas long time release of nanofibers incubated at RT was measured by TGA. As a result, the release of flavour/fragrances has increased by the increment in the temperature. However, among CD types M $\beta$ CD exhibited higher thermal stability and lower release in case of geraniol and linalool compared to hydroxypropyl derivatives. On the other hand, M $\beta$ CD/limonene-IC-NF released much more amount of limonene compared to other nanofibers. This is most likely related with the greater amount of limonene preservation by M $\beta$ CD in addition to its high thermal stability. Similar with the results obtained from HS GCMS, M $\beta$ CD-IC nanofibers did release most of the flavour/fragrance slowly. Thus, only 24%, 24%, and 14% of geraniol, limonene, and linalool were lost at the end of 50 days from M $\beta$ CD-IC nanofibers, respectively. Furthermore, the antibacterial activity of CD-IC nanofibers against Gram-negative (*E. coli*) and Gram-positive (*S. aureus*) bacteria is quite high enough to prevent the growth of microorganisms. Therefore, CD-IC nanofibers constructed from three volatile flavour/fragrance can serve as an excellent slow release materials.

As a last study, core-shell nanofibers were successfully produced for the first time from CD-IC solution of an antioxidant (CUR) and PLA solution as a carrier matrix for drug, antioxidant and antibacterial agents etc. There are many studies in the literature concerning the production of core-shell nanofibers for retarded release of drug molecules. Since, shell material is acting as an additional barrier for the release of drugs. In addition, it is also important for non-spinnable and sensitive compounds to be electrospun as core-shell nanofibers. Using CD-ICs in core instead of free bioactive molecule provides so many advantages including enhanced solubility, better preservation for volatile compounds, reduced required dose, and slow release of molecules. Therefore, cCUR/HP $\beta$ CD-IC-sPLA-CSNF has been produced via electrospinning. SEM, TEM, and CLSM confirmed the formation of core-shell nanofibers. The release and antioxidant activity of these nanofibers were also studied. The release of CUR from cCUR/HP $\beta$ CD-IC-sPLA-CSNF were slower as compared to control nanofibers which was produced without core-shell nozzle from free CUR and CUR/HP $\beta$ CD-IC. In addition, time dependent antioxidant activity results also demonstrated that cCUR/HP $\beta$ CD-IC-sPLA-CSNF released CUR slowly, because antioxidant activity of core-shell nanofibers is not as quick as controls. As a result, cCUR/HP $\beta$ CD-IC-sPLA-CSNF could hold great promise for drug delivery systems.

To conclude, as shown in the dissertation CD-IC integrated electrospun polymeric, non-polymeric (CD-IC), and core-shell nanofibers are promising materials. Namely, CD-IC encapsulated polymeric and non-polymeric nanofibers has already shown to be useful for applications including drug

delivery, food packaging and flavour/fragrance releasing. In the future, encapsulation CD-ICs of volatile and hydrophobic antifungal agents into the electrospun nanofibers could be a new type of packaging system to increase the shelf life of food products such as cheese, bread, fruit etc. in a more efficient way owing to the presence of complexation. In addition, CD-ICs of anticancer drugs, which are usually hydrophobic, could be incorporated into electrospun nanofibers in order to increase the solubility and reduce the required dose of the anticancer drug. Therefore, this system is expected to minimize the toxicity and side effects of the anticancer drugs causes in the body. Core-shell nanofibers are widely used for biological applications. For instance, they find application for the protection of drugs, which are sensitive to light. Once IC of light-sensitive hydrophobic drug with CDs used as a core solution, drug will be protected efficiently against light and its solubility will be enhanced at the same time. So, core-shell nanofibers produced from CD-IC solutions will most likely find application as a multifunctional carrier for bioactive compounds in the coming years. Additionally, core-shell nanofibers of CD-ICs can be used for targeted delivery of some drugs. Thus, polymer in the shell is dissolved in certain conditions, to release the loaded drug only in the targeted area in order to prevent the undesirable toxicity to the normal tissues. However, using too high dose because of the ineffective usage of the drug increases the toxicity as well. Therefore, using CD-ICs in the core solution instead of a free drug will enhance solubility, reduce the required dose of the drug and increase the bioavailability of the drug. Additionally, the usage of CD-IC encapsulated electrospun nanofibers will expand to several more fields in the near future.

## LIST OF PUBLICATIONS

### Publications from thesis studies

- 1) **Aytac, Z.**, Kusku, S. I., Durgun, E., & Uyar, T\*. (2016). Encapsulation of gallic acid/cyclodextrin inclusion complex in electrospun polylactic acid nanofibers: Release behavior and antioxidant activity of gallic acid. *Materials Science and Engineering: C*, 63, 231-239.
- 2) **Aytac, Z.**, Yildiz, Z. I., Kayaci-Senirmak, F., San Keskin, N. O., Tekinay, T., & Uyar, T\*. (2016). Electrospinning of polymer-free cyclodextrin/geraniol–inclusion complex nanofibers: enhanced shelf-life of geraniol with antibacterial and antioxidant properties. *RSC Advances*, 6(52), 46089-46099.
- 3) **Aytac, Z.**, San Keskin, N. O., Tekinay, T., & Uyar, T\*. Antioxidant food packaging from  $\alpha$ -tocopherol/ $\gamma$ -cyclodextrin-inclusion complex incorporated polylactic acid electrospun nanofibers (in preparation).
- 4) **Aytac, Z.**, Kusku, S. I., Durgun, E., & Uyar, T\*., Electrospun zein nanofibers incorporating quercetin/cyclodextrin-inclusion complex and their antioxidant activity (in preparation).
- 5) **Aytac, Z.**, San Keskin, N. O., Kusku, S. I., Durgun, E., Tekinay, T., & Uyar, T\*., Antibacterial packaging material designed by encapsulation of thymol/cyclodextrin-inclusion complex in electrospun zein nanofibers (in preparation).
- 6) **Aytac, Z.**, Yildiz, Z. I., Kayaci-Senirmak, F., San Keskin, N. O., Kusku, S.I., Durgun, E., Tekinay, T., & Uyar, T\*., Fast-dissolving, prolonged release and antibacterial cyclodextrin/limonene-inclusion complex nanofibrous webs via polymer-free electrospinning” (submitted).
- 7) **Aytac, Z.**, Yildiz, Z. I., Kayaci-Senirmak, F., San Keskin, N. O., Tekinay, T., & Uyar, T\*., Fast-dissolving delivery membranes produced from electrospun cyclodextrin/linalool-inclusion complex nanofibers with prolonged release and antibacterial activity (in preparation).

**8) Aytac, Z.** And Uyar, T.\*, Core-shell nanofibers from cyclodextrin inclusion complex of curcumin (in preparation).

### **Others**

**9) Arslan, O., Aytac, Z., & Uyar, T.** (2016). Superhydrophobic, Hybrid, Electrospun Cellulose Acetate Nanofibrous Mats for Oil/Water Separation by Tailored Surface Modification. *ACS Applied Materials & Interfaces*, 8 (30), 19747-19754.

**10) Anitha, S., Balusamy, B., Aytac, Z., & Uyar, T.** (2016). Grain boundary engineering in electrospun ZnO nanostructures as promising photocatalyst. *CrystEngComm*, 18, 6341-6351.

**11) Aytac, Z., & Uyar, T.** (2016). Antioxidant activity and photostability of  $\alpha$ -tocopherol/ $\beta$ -cyclodextrin inclusion complex encapsulated electrospun polycaprolactone nanofibers. *European Polymer Journal* 79, 140-149.

**12) Aytac, Z., Kusku, S. I., Durgun, E., & Uyar, T.** (2016). Quercetin/ $\beta$ -cyclodextrin inclusion complex embedded nanofibres: Slow release and high solubility. *Food Chemistry*, 197, 864-871.

**13) Senthamizhan, A., Balusamy, B., Aytac, Z., & Uyar, T.** (2016). Ultrasensitive electrospun fluorescent nanofibrous membrane for rapid visual colorimetric detection of H<sub>2</sub>O<sub>2</sub>. *Analytical and Bioanalytical Chemistry*, 408(5), 1347-1355.

**14) Aytac, Z., Sen, H. S., Durgun, E., & Uyar, T.** (2015). Sulfisoxazole/cyclodextrin inclusion complex incorporated in electrospun hydroxypropyl cellulose nanofibers as drug delivery system. *Colloids and Surfaces B: Biointerfaces*, 128, 331-338.

**15) Aytac, Z., Dogan, S. Y., Tekinay, T., & Uyar, T.** (2014). Release and antibacterial activity of allyl isothiocyanate/ $\beta$ -cyclodextrin complex encapsulated in electrospun nanofibers. *Colloids and Surfaces B: Biointerfaces*, 120, 125-131.

- 16)** Demirci, S., Celebioglu, A., **Aytac, Z.**, & Uyar, T. (2014). pH-responsive nanofibers with controlled drug release properties. *Polymer Chemistry*, 5(6), 2050-2056.
- 17)** Munteanu, B. S., **Aytac, Z.**, Pricope, G. M., Uyar, T., & Vasile, C. (2014). Polylactic acid (PLA)/Silver-NP/VitaminE bionanocomposite electrospun nanofibers with antibacterial and antioxidant activity. *Journal of Nanoparticle Research*, 16(10), 1-12.
- 18)** Celebioglu, A., **Aytac, Z.**, Umu, O. C., Dana, A., Tekinay, T., & Uyar, T. (2014). One-step synthesis of size-tunable Ag nanoparticles incorporated in electrospun PVA/cyclodextrin nanofibers. *Carbohydrate Polymers*, 99, 808-816.
- 19)** Kayaci, F., **Aytac, Z.**, & Uyar, T. (2013). Surface modification of electrospun polyester nanofibers with cyclodextrin polymer for the removal of phenanthrene from aqueous solution. *Journal of Hazardous Materials*, 261, 286-294.

## BIBLIOGRAPHY

- [1] D.H. Reneker, I. Chun, Nanometre diameter fibres of polymer, produced by electrospinning, *Nanotechnology* 7 (1996) 216.
- [2] A. Greiner, J.H. Wendorff, Electrospinning: a fascinating method for the preparation of ultrathin fibers, *Angewandte Chemie International Edition* 46 (2007) 5670-5703.
- [3] S. Ramakrishna, K. Fujihara, W.-E. Teo, T.-C. Lim, Z. Ma, *An introduction to electrospinning and nanofibers*. Vol. 90. 2005: World Scientific.
- [4] J.H. Wendorff, S. Agarwal, A. Greiner, *Electrospinning: materials, processing, and applications*. 2012: John Wiley & Sons.
- [5] A. Frenot, I.S. Chronakis, Polymer nanofibers assembled by electrospinning, *Current opinion in colloid & interface science* 8 (2003) 64-75.
- [6] S. Ramakrishna, K. Fujihara, W.-E. Teo, T. Yong, Z. Ma, R. Ramaseshan, Electrospun nanofibers: solving global issues, *Materials today* 9 (2006) 40-50.
- [7] D. Li, Y. Xia, Electrospinning of nanofibers: reinventing the wheel?, *Advanced materials* 16 (2004) 1151-1170.
- [8] D.H. Reneker, A.L. Yarin, Electrospinning jets and polymer nanofibers, *Polymer* 49 (2008) 2387-2425.
- [9] T. Uyar, F. Besenbacher, Electrospinning of uniform polystyrene fibers: The effect of solvent conductivity, *Polymer* 49 (2008) 5336-5343.
- [10] F. Yang, R. Murugan, S. Wang, S. Ramakrishna, Electrospinning of nano/micro scale poly (L-lactic acid) aligned fibers and their potential in neural tissue engineering, *Biomaterials* 26 (2005) 2603-2610.
- [11] D. Li, Y. Wang, Y. Xia, Electrospinning of polymeric and ceramic nanofibers as uniaxially aligned arrays, *Nano letters* 3 (2003) 1167-1171.
- [12] Z. Sun, E. Zussman, A.L. Yarin, J.H. Wendorff, A. Greiner, Compound core-shell polymer nanofibers by co-electrospinning, *Advanced materials* 15 (2003) 1929-1932.

- [13] Y. Zhang, X. Wang, Y. Feng, J. Li, C. Lim, S. Ramakrishna, Coaxial electrospinning of (fluorescein isothiocyanate-conjugated bovine serum albumin)-encapsulated poly ( $\epsilon$ -caprolactone) nanofibers for sustained release, *Biomacromolecules* 7 (2006) 1049-1057.
- [14] C. Ozgit-Akgun, F. Kayaci, S. Vempati, A. Haider, A. Celebioglu, E. Goldenberg, S. Kizir, T. Uyar, N. Biyikli, Fabrication of flexible polymer-GaN core-shell nanofibers by the combination of electrospinning and hollow cathode plasma-assisted atomic layer deposition, *Journal of Materials Chemistry C* 3 (2015) 5199-5206.
- [15] D. Li, Y. Xia, Direct fabrication of composite and ceramic hollow nanofibers by electrospinning, *Nano letters* 4 (2004) 933-938.
- [16] D. Li, J.T. McCann, Y. Xia, Use of electrospinning to directly fabricate hollow nanofibers with functionalized inner and outer surfaces, *Small* 1 (2005) 83-86.
- [17] A. Celebioglu, T. Uyar, Electrospun porous cellulose acetate fibers from volatile solvent mixture, *Materials Letters* 65 (2011) 2291-2294.
- [18] J. Wu, N. Wang, L. Wang, H. Dong, Y. Zhao, L. Jiang, Electrospun porous structure fibrous film with high oil adsorption capacity, *ACS applied materials & interfaces* 4 (2012) 3207-3212.
- [19] C. Xu, R. Inai, M. Kotaki, S. Ramakrishna, Aligned biodegradable nanofibrous structure: a potential scaffold for blood vessel engineering, *Biomaterials* 25 (2004) 877-886.
- [20] J.T. McCann, M. Marquez, Y. Xia, Melt coaxial electrospinning: a versatile method for the encapsulation of solid materials and fabrication of phase change nanofibers, *Nano letters* 6 (2006) 2868-2872.
- [21] A. Celebioglu, Z. Aytac, O.C. Umu, A. Dana, T. Tekinay, T. Uyar, One-step synthesis of size-tunable Ag nanoparticles incorporated in electrospun PVA/cyclodextrin nanofibers, *Carbohydrate polymers* 99 (2014) 808-816.
- [22] C.D. Saquing, J.L. Manasco, S.A. Khan, Electrospun nanoparticle-nanofiber composites via a one-step synthesis, *Small* 5 (2009) 944-951.

- [23] C. Shao, H.-Y. Kim, J. Gong, B. Ding, D.-R. Lee, S.-J. Park, Fiber mats of poly (vinyl alcohol)/silica composite via electrospinning, *Materials Letters* 57 (2003) 1579-1584.
- [24] S. Aryal, C.K. Kim, K.-W. Kim, M.S. Khil, H.Y. Kim, Multi-walled carbon nanotubes/TiO<sub>2</sub> composite nanofiber by electrospinning, *Materials Science and Engineering: C* 28 (2008) 75-79.
- [25] E.-R. Kenawy, G.L. Bowlin, K. Mansfield, J. Layman, D.G. Simpson, E.H. Sanders, G.E. Wnek, Release of tetracycline hydrochloride from electrospun poly (ethylene-co-vinylacetate), poly (lactic acid), and a blend, *Journal of controlled release* 81 (2002) 57-64.
- [26] K. Kim, Y.K. Luu, C. Chang, D. Fang, B.S. Hsiao, B. Chu, M. Hadjiargyrou, Incorporation and controlled release of a hydrophilic antibiotic using poly (lactide-co-glycolide)-based electrospun nanofibrous scaffolds, *Journal of Controlled Release* 98 (2004) 47-56.
- [27] J. Peng, Z. Qian, B. Wang, S. Fu, G. Guo, F. Luo, R. Li, D. Wu, Preparation and release characteristic of quercetin loaded poly (lactic acid) ultrafine fibers, *Journal of nanoscience and nanotechnology* 11 (2011) 3659-3668.
- [28] P. Taepaiboon, U. Rungsardthong, P. Supaphol, Vitamin-loaded electrospun cellulose acetate nanofiber mats as transdermal and dermal therapeutic agents of vitamin A acid and vitamin E, *European Journal of Pharmaceutics and Biopharmaceutics* 67 (2007) 387-397.
- [29] P.-o. Rujitanaroj, N. Pimpha, P. Supaphol, Wound-dressing materials with antibacterial activity from electrospun gelatin fiber mats containing silver nanoparticles, *Polymer* 49 (2008) 4723-4732.
- [30] R. Thakur, C. Florek, J. Kohn, B. Michniak, Electrospun nanofibrous polymeric scaffold with targeted drug release profiles for potential application as wound dressing, *International journal of pharmaceutics* 364 (2008) 87-93.
- [31] A. Camerlo, C. Vebert-Nardin, R.M. Rossi, A.-M. Popa, Fragrance encapsulation in polymeric matrices by emulsion electrospinning, *European Polymer Journal* 49 (2013) 3806-3813.

- [32] A. Rezaei, A. Nasirpour, H. Tavanai, M. Fathi, A study on the release kinetics and mechanisms of vanillin incorporated in almond gum/polyvinyl alcohol composite nanofibers in different aqueous food simulants and simulated saliva, *Flavour and Fragrance Journal* (2016).
- [33] M.A. Cerqueira, M.J. Fabra, J.L. Castro-Mayorga, A.I. Bourbon, L.M. Pastrana, A.A. Vicente, J.M. Lagaron, Use of Electrospinning to Develop Antimicrobial Biodegradable Multilayer Systems: Encapsulation of Cinnamaldehyde and Their Physicochemical Characterization, *Food and Bioprocess Technology* (2016) 1-11.
- [34] R. Gopal, S. Kaur, Z. Ma, C. Chan, S. Ramakrishna, T. Matsuura, Electrospun nanofibrous filtration membrane, *Journal of Membrane Science* 281 (2006) 581-586.
- [35] K. Yoon, K. Kim, X. Wang, D. Fang, B.S. Hsiao, B. Chu, High flux ultrafiltration membranes based on electrospun nanofibrous PAN scaffolds and chitosan coating, *Polymer* 47 (2006) 2434-2441.
- [36] Z. Ma, M. Kotaki, S. Ramakrishna, Electrospun cellulose nanofiber as affinity membrane, *Journal of membrane science* 265 (2005) 115-123.
- [37] M.S. Khil, D.I. Cha, H.Y. Kim, I.S. Kim, N. Bhattarai, Electrospun nanofibrous polyurethane membrane as wound dressing, *Journal of Biomedical Materials Research Part B: Applied Biomaterials* 67 (2003) 675-679.
- [38] Y. Zhou, D. Yang, X. Chen, Q. Xu, F. Lu, J. Nie, Electrospun water-soluble carboxyethyl chitosan/poly (vinyl alcohol) nanofibrous membrane as potential wound dressing for skin regeneration, *Biomacromolecules* 9 (2007) 349-354.
- [39] Y. Luu, K. Kim, B. Hsiao, B. Chu, M. Hadjiargyrou, Development of a nanostructured DNA delivery scaffold via electrospinning of PLGA and PLA-PEG block copolymers, *Journal of controlled release* 89 (2003) 341-353.
- [40] J. Zeng, X. Xu, X. Chen, Q. Liang, X. Bian, L. Yang, X. Jing, Biodegradable electrospun fibers for drug delivery, *Journal of Controlled Release* 92 (2003) 227-231.

- [41] E. Luong-Van, L. Grøndahl, K.N. Chua, K.W. Leong, V. Nurcombe, S.M. Cool, Controlled release of heparin from poly ( $\epsilon$ -caprolactone) electrospun fibers, *Biomaterials* 27 (2006) 2042-2050.
- [42] S. Torres-Giner, E. Gimenez, J.M. Lagarón, Characterization of the morphology and thermal properties of zein prolamine nanostructures obtained by electrospinning, *Food Hydrocolloids* 22 (2008) 601-614.
- [43] A.-C. Vega-Lugo, L.-T. Lim, Controlled release of allyl isothiocyanate using soy protein and poly (lactic acid) electrospun fibers, *Food Research International* 42 (2009) 933-940.
- [44] L. Ge, Y.-s. Zhao, T. Mo, J.-r. Li, P. Li, Immobilization of glucose oxidase in electrospun nanofibrous membranes for food preservation, *Food Control* 26 (2012) 188-193.
- [45] H. Bagheri, Z. Ayazi, A. Aghakhani, N. Alipour, Polypyrrole/polyamide electrospun-based sorbent for microextraction in packed syringe of organophosphorous pesticides from aquatic samples, *Journal of separation science* 35 (2012) 114-120.
- [46] H. Jia, G. Zhu, B. Vugrinovich, W. Kataphinan, D.H. Reneker, P. Wang, Enzyme-carrying polymeric nanofibers prepared via electrospinning for use as unique biocatalysts, *Biotechnology progress* 18 (2002) 1027-1032.
- [47] T.E. Herricks, S.-H. Kim, J. Kim, D. Li, J.H. Kwak, J.W. Grate, S.H. Kim, Y. Xia, Direct fabrication of enzyme-carrying polymer nanofibers by electrospinning, *Journal of materials chemistry* 15 (2005) 3241-3245.
- [48] J.S. Im, O. Kwon, Y.H. Kim, S.-J. Park, Y.-S. Lee, The effect of embedded vanadium catalyst on activated electrospun CFs for hydrogen storage, *Microporous and Mesoporous Materials* 115 (2008) 514-521.
- [49] M. Stasiak, A. Studer, A. Greiner, J.H. Wendorff, Polymer fibers as carriers for homogeneous catalysts, *Chemistry—A European Journal* 13 (2007) 6150-6156.
- [50] A. Senthamizhan, A. Celebioglu, S. Bayir, M. Gorur, E. Doganci, F. Yilmaz, T. Uyar, Highly fluorescent pyrene-functional polystyrene

copolymer nanofibers for enhanced sensing performance of TNT, *ACS applied materials & interfaces* 7 (2015) 21038-21046.

- [51] A. Senthamizhan, B. Balusamy, Z. Aytac, T. Uyar, Ultrasensitive electrospun fluorescent nanofibrous membrane for rapid visual colorimetric detection of H<sub>2</sub>O<sub>2</sub>, *Analytical and bioanalytical chemistry* 408 (2016) 1347-1355.
- [52] X. Wang, C. Drew, S.-H. Lee, K.J. Senecal, J. Kumar, L.A. Samuelson, Electrospun nanofibrous membranes for highly sensitive optical sensors, *Nano letters* 2 (2002) 1273-1275.
- [53] H. Wu, L. Hu, M.W. Rowell, D. Kong, J.J. Cha, J.R. McDonough, J. Zhu, Y. Yang, M.D. McGehee, Y. Cui, Electrospun metal nanofiber webs as high-performance transparent electrode, *Nano letters* 10 (2010) 4242-4248.
- [54] P. Joshi, L. Zhang, Q. Chen, D. Galipeau, H. Fong, Q. Qiao, Electrospun carbon nanofibers as low-cost counter electrode for dye-sensitized solar cells, *ACS applied materials & interfaces* 2 (2010) 3572-3577.
- [55] S. Chuangchote, T. Sagawa, S. Yoshikawa, Efficient dye-sensitized solar cells using electrospun TiO<sub>2</sub> nanofibers as a light harvesting layer, *Applied Physics Letters* 93 (2008) 33310-33310.
- [56] J. Szejtli, Introduction and general overview of cyclodextrin chemistry, *Chemical reviews* 98 (1998) 1743-1754.
- [57] E.M. Del Valle, Cyclodextrins and their uses: a review, *Process biochemistry* 39 (2004) 1033-1046.
- [58] A.R. Hedges, Industrial applications of cyclodextrins, *Chemical reviews* 98 (1998) 2035-2044.
- [59] H. Yoshii, T. Furuta, E. Okita, A. Toyomi, Y.-Y. Linko, P. Linko, The increased effect of kneading on the formation of inclusion complexes between d-limonene and  $\beta$ -cyclodextrin at low water content, *Bioscience, biotechnology, and biochemistry* 62 (1998) 464-468.
- [60] X. Li, Z. Jin, J. Wang, Complexation of allyl isothiocyanate by  $\alpha$ - and  $\beta$ -cyclodextrin and its controlled release characteristics, *Food chemistry* 103 (2007) 461-466.

- [61] J.L. Koontz, J.E. Marcy, S.F. O'Keefe, S.E. Duncan, Cyclodextrin inclusion complex formation and solid-state characterization of the natural antioxidants  $\alpha$ -tocopherol and quercetin, *Journal of agricultural and food chemistry* 57 (2009) 1162-1171.
- [62] S. Rawat, S.K. Jain, Solubility enhancement of celecoxib using  $\beta$ -cyclodextrin inclusion complexes, *European journal of pharmaceuticals and biopharmaceutics* 57 (2004) 263-267.
- [63] N. Nasongkla, A.F. Wiedmann, A. Bruening, M. Beman, D. Ray, W.G. Bornmann, D.A. Boothman, J. Gao, Enhancement of solubility and bioavailability of  $\beta$ -lapachone using cyclodextrin inclusion complexes, *Pharmaceutical research* 20 (2003) 1626-1633.
- [64] C. Samperio, R. Boyer, W.N. Eigel III, K.W. Holland, J.S. McKinney, S.F. O'Keefe, R. Smith, J.E. Marcy, Enhancement of plant essential oils' aqueous solubility and stability using alpha and beta cyclodextrin, *Journal of agricultural and food chemistry* 58 (2010) 12950-12956.
- [65] X. Liu, H.S. Lin, J. Thenmozhiyal, S.Y. Chan, P.C. Ho, Inclusion of acitretin into cyclodextrins: phase solubility, photostability, and physicochemical characterization, *Journal of pharmaceutical sciences* 92 (2003) 2449-2457.
- [66] F. Orfanou, S. Michaleas, D. Benaki, O. Galanopoulou, A. Voulgari, E. Antoniadou-Vyza, Photostabilization of oxolinic acid in hydroxypropyl- $\beta$ -cyclodextrins; implications for the effect of molecular self-assembly phenomena, *Journal of Inclusion Phenomena and Macrocyclic Chemistry* 64 (2009) 289-297.
- [67] Y. Watanabe, T. Yamashita, M. Yamashita, S. Adachi, Suppressive Effect of. ALPHA.-Tocopherol Complexed with. BETA.-Cyclodextrin on the Oxidation of Methyl Linoleate, *Food science and technology research* 15 (2009) 479-482.
- [68] S. Mallardo, V. De Vito, M. Malinconico, M.G. Volpe, G. Santagata, M.L. Di Lorenzo, Poly (butylene succinate)-based composites containing  $\beta$ -cyclodextrin/d-limonene inclusion complex, *European Polymer Journal* 79 (2016) 82-96.

- [69] R.d.C. Bergamasco, G.M. Zanin, F.F.d. Moraes, Sulfluramid volatility reduction by  $\beta$ -cyclodextrin, *Journal of agricultural and food chemistry* 53 (2005) 1139-1143.
- [70] T.L. Neoh, C. Yamamoto, S. Ikefuji, T. Furuta, H. Yoshii, Heat stability of allyl isothiocyanate and phenyl isothiocyanate complexed with randomly methylated  $\beta$ -cyclodextrin, *Food Chemistry* 131 (2012) 1123-1131.
- [71] G. Chen, B. Liu, Cellulose sulfate based film with slow-release antimicrobial properties prepared by incorporation of mustard essential oil and  $\beta$ -cyclodextrin, *Food Hydrocolloids* 55 (2016) 100-107.
- [72] M. Hoshino, M. Imamura, K. Ikehara, Y. Hama, Fluorescence enhancement of benzene derivatives by forming inclusion complexes with. beta.-cyclodextrin in aqueous solutions, *The Journal of Physical Chemistry* 85 (1981) 1820-1823.
- [73] K.N. Baglole, P.G. Boland, B.D. Wagner, Fluorescence enhancement of curcumin upon inclusion into parent and modified cyclodextrins, *Journal of Photochemistry and Photobiology A: Chemistry* 173 (2005) 230-237.
- [74] M. Arkas, R. Allabashi, D. Tsiourvas, E.-M. Mattausch, R. Perfler, Organic/inorganic hybrid filters based on dendritic and cyclodextrin “nanosponges” for the removal of organic pollutants from water, *Environmental science & technology* 40 (2006) 2771-2777.
- [75] V. Chatain, K. Hanna, C. De Brauer, R. Bayard, P. Germain, Enhanced solubilization of arsenic and 2, 3, 4, 6 tetrachlorophenol from soils by a cyclodextrin derivative, *Chemosphere* 57 (2004) 197-206.
- [76] L. Jurecska, P. Dobosy, K. Barkács, É. Fenyvesi, G. Záray, Characterization of cyclodextrin containing nanofilters for removal of pharmaceutical residues, *Journal of pharmaceutical and biomedical analysis* 98 (2014) 90-93.
- [77] L. Szente, É. Fenyvesi, J. Szejtli, Entrapment of iodine with cyclodextrins: potential application of cyclodextrins in nuclear waste

- management, *Environmental science & technology* 33 (1999) 4495-4498.
- [78] T. Badr, K. Hanna, C. De Brauer, Enhanced solubilization and removal of naphthalene and phenanthrene by cyclodextrins from two contaminated soils, *Journal of hazardous materials* 112 (2004) 215-223.
- [79] T. Miyaji, Y. Inoue, F. Acartürk, T. Imai, M. Otagiri, K. Uekama, Improvement of oral bioavailability of fenbufen by cyclodextrin complexations, *Acta pharmaceutica nordica* 4 (1991) 17-22.
- [80] F.M. Andersen, H. Bundgaard, H.B. Mengel, Formation, bioavailability and organoleptic properties of an inclusion complex of femoxetine with  $\beta$ -cyclodextrin, *International journal of pharmaceutics* 21 (1984) 51-60.
- [81] S. Sajeesh, C.P. Sharma, Cyclodextrin-insulin complex encapsulated polymethacrylic acid based nanoparticles for oral insulin delivery, *International journal of pharmaceutics* 325 (2006) 147-154.
- [82] T. Karpkird, R. Khunsakorn, C. Noptheeranuphap, J. Jettanasen, Photostability of water-soluble inclusion complexes of UV-filters and curcumin with gamma-cyclodextrin polymer, *Journal of Inclusion Phenomena and Macrocyclic Chemistry* 84 (2016) 121-128.
- [83] C. López-de-Dicastillo, M. Jordá, R. Catalá, R. Gavara, P. Hernández-Munoz, Development of active polyvinyl alcohol/ $\beta$ -cyclodextrin composites to scavenge undesirable food components, *Journal of agricultural and food chemistry* 59 (2011) 11026-11033.
- [84] N. Ono, Y. Miyamoto, T. Ishiguro, K. Motoyama, F. Hirayama, D. Iohara, H. Seo, S. Tsuruta, H. Arima, K. Uekama, Reduction of bitterness of antihistaminic drugs by complexation with  $\beta$ -cyclodextrins, *Journal of pharmaceutical sciences* 100 (2011) 1935-1943.
- [85] K. Uekama, K. Oh, M. Otagiri, H. Seo, M. Tsuruoka, Improvement of some pharmaceutical properties of clofibrate by cyclodextrin complexation, *Pharmaceutica acta Helvetiae* 58 (1983) 338.
- [86] L.E. Hill, C. Gomes, T.M. Taylor, Characterization of beta-cyclodextrin inclusion complexes containing essential oils (trans-cinnamaldehyde, eugenol, cinnamon bark, and clove bud extracts) for antimicrobial

- delivery applications, *LWT-Food Science and Technology* 51 (2013) 86-93.
- [87] T. Wu, X. Cai, S. Tan, H. Li, J. Liu, W. Yang, Adsorption characteristics of acrylonitrile, p-toluenesulfonic acid, 1-naphthalenesulfonic acid and methyl blue on graphene in aqueous solutions, *Chemical engineering journal* 173 (2011) 144-149.
- [88] L.M.M. Gomes, N. Petito, V.G. Costa, D.Q. Falcão, K.G. de Lima Araújo, Inclusion complexes of red bell pepper pigments with  $\beta$ -cyclodextrin: preparation, characterisation and application as natural colorant in yogurt, *Food chemistry* 148 (2014) 428-436.
- [89] U. Numanoglu, T. Şen, N. Tarimci, M. Kartal, O.M. Koo, H. Önyüksel, Use of cyclodextrins as a cosmetic delivery system for fragrance materials: linalool and benzyl acetate, *AAPS PharmSciTech* 8 (2007) 34-42.
- [90] C. Anselmi, M. Centini, M. Maggiore, N. Gaggelli, M. Andreassi, A. Buonocore, G. Beretta, R.M. Facino, Non-covalent inclusion of ferulic acid with  $\alpha$ -cyclodextrin improves photo-stability and delivery: NMR and modeling studies, *Journal of pharmaceutical and biomedical analysis* 46 (2008) 645-652.
- [91] A. Lopodota, A. Cutrignelli, V. Laquintana, M. Franco, D. Donelli, L. Ragni, S. Tongiani, N. Denora,  $\beta$ -cyclodextrin in personal care formulations: role on the complexation of malodours causing molecules, *International journal of cosmetic science* 37 (2015) 438-445.
- [92] V. Đorđević, B. Balanč, A. Belščak-Cvitanović, S. Lević, K. Trifković, A. Kalušević, I. Kostić, D. Komes, B. Bugarski, V. Nedović, Trends in encapsulation technologies for delivery of food bioactive compounds, *Food Engineering Reviews* 7 (2015) 452-490.
- [93] E. Pinho, M. Grootveld, G. Soares, M. Henriques, Cyclodextrins as encapsulation agents for plant bioactive compounds, *Carbohydrate polymers* 101 (2014) 121-135.
- [94] T. Uyar, J. Hacaloglu, F. Besenbacher, Electrospun polystyrene fibers containing high temperature stable volatile fragrance/flavor facilitated by

- cyclodextrin inclusion complexes, *Reactive and Functional Polymers* 69 (2009) 145-150.
- [95] T. Uyar, Y. Nur, J. Hacaloglu, F. Besenbacher, Electrospinning of functional poly (methyl methacrylate) nanofibers containing cyclodextrin-menthol inclusion complexes, *Nanotechnology* 20 (2009) 125703.
- [96] T. Uyar, J. Hacaloglu, F. Besenbacher, Electrospun polyethylene oxide (PEO) nanofibers containing cyclodextrin inclusion complex, *Journal of nanoscience and nanotechnology* 11 (2011) 3949-3958.
- [97] F. Kayaci, T. Uyar, Encapsulation of vanillin/cyclodextrin inclusion complex in electrospun polyvinyl alcohol (PVA) nanowebs: prolonged shelf-life and high temperature stability of vanillin, *Food chemistry* 133 (2012) 641-649.
- [98] F. Kayaci, O.C. Umu, T. Tekinay, T. Uyar, Antibacterial electrospun poly (lactic acid)(PLA) nanofibrous webs incorporating triclosan/cyclodextrin inclusion complexes, *Journal of agricultural and food chemistry* 61 (2013) 3901-3908.
- [99] F. Kayaci, Y. Ertas, T. Uyar, Enhanced thermal stability of eugenol by cyclodextrin inclusion complex encapsulated in electrospun polymeric nanofibers, *Journal of agricultural and food chemistry* 61 (2013) 8156-8165.
- [100] F. Kayaci, H.S. Sen, E. Durgun, T. Uyar, Functional electrospun polymeric nanofibers incorporating geraniol–cyclodextrin inclusion complexes: High thermal stability and enhanced durability of geraniol, *Food Research International* 62 (2014) 424-431.
- [101] M.F. Canbolat, A. Celebioglu, T. Uyar, Drug delivery system based on cyclodextrin-naproxen inclusion complex incorporated in electrospun polycaprolactone nanofibers, *Colloids and Surfaces B: Biointerfaces* 115 (2014) 15-21.
- [102] Z. Aytac, S.Y. Dogan, T. Tekinay, T. Uyar, Release and antibacterial activity of allyl isothiocyanate/ $\beta$ -cyclodextrin complex encapsulated in

- electrospun nanofibers, *Colloids and Surfaces B: Biointerfaces* 120 (2014) 125-131.
- [103] Z. Aytac, H.S. Sen, E. Durgun, T. Uyar, Sulfoxazole/cyclodextrin inclusion complex incorporated in electrospun hydroxypropyl cellulose nanofibers as drug delivery system, *Colloids and Surfaces B: Biointerfaces* 128 (2015) 331-338.
- [104] Z. Aytac, S.I. Kusku, E. Durgun, T. Uyar, Quercetin/ $\beta$ -cyclodextrin inclusion complex embedded nanofibres: Slow release and high solubility, *Food chemistry* 197 (2016) 864-871.
- [105] Z. Aytac, T. Uyar, Antioxidant activity and photostability of  $\alpha$ -tocopherol/ $\beta$ -cyclodextrin inclusion complex encapsulated electrospun polycaprolactone nanofibers, *European Polymer Journal* 79 (2016) 140-149.
- [106] X.-Z. Sun, G.R. Williams, X.-X. Hou, L.-M. Zhu, Electrospun curcumin-loaded fibers with potential biomedical applications, *Carbohydrate polymers* 94 (2013) 147-153.
- [107] P. Tonglairoum, T. Chuchote, T. Ngawhirunpat, T. Rojanarata, P. Opanasopit, Encapsulation of plai oil/2-hydroxypropyl- $\beta$ -cyclodextrin inclusion complexes in polyvinylpyrrolidone (PVP) electrospun nanofibers for topical application, *Pharmaceutical development and technology* 19 (2014) 430-437.
- [108] Ç. Akduman, I. Özgüney, A. Kumbasar, E. Perrin, Electrospun Thermoplastic Polyurethane Mats Containing Naproxen–Cyclodextrin Inclusion Complex, *Autex Research Journal* 14 (2014) 239-246.
- [109] J. Panichpakdee, P. Pavasant, P. Supaphol, Electrospinning of Asiaticoside/2-Hydroxypropyl- $\beta$ -cyclodextrin Inclusion Complex-loaded Cellulose Acetate Fiber Mats: Release Characteristics and Potential for Use as Wound Dressing, *Polymer Korea* 38 (2014) 338-350.
- [110] J. Liu, L. Li, S. Tang, H. Chang, D. Liang, Properties of Electrospun Composite Nanofibers of Cinnamic Aldehyde/Poly(lactic Acid), *Polymer Materials Science & Engineering* 3 (2015) 034.

- [111] S.M. Lemma, M. Scampicchio, P.J. Mahon, I. Sbarski, J. Wang, P. Kingshott, Controlled release of retinyl acetate from  $\beta$ -cyclodextrin functionalized poly (vinyl alcohol) electrospun nanofibers, *Journal of agricultural and food chemistry* 63 (2015) 3481-3488.
- [112] P.I. Siafaka, N. Üstündağ Okur, M. Mone, S. Giannakopoulou, S. Er, E. Pavlidou, E. Karavas, D.N. Bikiaris, Two Different Approaches for Oral Administration of Voriconazole Loaded Formulations: Electrospun Fibers versus  $\beta$ -Cyclodextrin Complexes, *International journal of molecular sciences* 17 (2016) 282.
- [113] P. Wen, D.-H. Zhu, K. Feng, F.-J. Liu, W.-Y. Lou, N. Li, M.-H. Zong, H. Wu, Fabrication of electrospun polylactic acid nanofilm incorporating cinnamon essential oil/ $\beta$ -cyclodextrin inclusion complex for antimicrobial packaging, *Food chemistry* 196 (2016) 996-1004.
- [114] W. Liu, Y. Wang, J. Yao, Z. Shao, X. Chen, Tamoxifen-loaded silk fibroin electrospun fibers, *Materials Letters* 178 (2016) 31-34.
- [115] T.G. Deluzio, K.I. Penev, K. Mequanint, Cyclodextrin inclusion complexes as potential oxygen delivery vehicles in tissue engineering, *Journal of Biomaterials and Tissue Engineering* 4 (2014) 957-966.
- [116] X. Luo, C. Xie, H. Wang, C. Liu, S. Yan, X. Li, Antitumor activities of emulsion electrospun fibers with core loading of hydroxycamptothecin via intratumoral implantation, *International journal of pharmaceutics* 425 (2012) 19-28.
- [117] Z. Aytac, S.I. Kusku, E. Durgun, T. Uyar, Encapsulation of gallic acid/cyclodextrin inclusion complex in electrospun polylactic acid nanofibers: Release behavior and antioxidant activity of gallic acid, *Materials Science and Engineering: C* 63 (2016) 231-239.
- [118] M.G. McKee, G.L. Wilkes, R.H. Colby, T.E. Long, Correlations of solution rheology with electrospun fiber formation of linear and branched polyesters, *Macromolecules* 37 (2004) 1760-1767.
- [119] A. Celebioglu, T. Uyar, Cyclodextrin nanofibers by electrospinning, *Chemical Communications* 46 (2010) 6903-6905.

- [120] A. Celebioglu, T. Uyar, Electrospinning of nanofibers from non-polymeric systems: polymer-free nanofibers from cyclodextrin derivatives, *Nanoscale* 4 (2012) 621-631.
- [121] A. Celebioglu, T. Uyar, Electrospinning of nanofibers from non-polymeric systems: Electrospun nanofibers from native cyclodextrins, *Journal of colloid and interface science* 404 (2013) 1-7.
- [122] A. Celebioglu, T. Uyar, Electrospun gamma-cyclodextrin ( $\gamma$ -CD) nanofibers for the entrapment of volatile organic compounds, *RSC Advances* 3 (2013) 22891-22895.
- [123] A. Celebioglu, T. Uyar, Green and one-step synthesis of gold nanoparticles incorporated into electrospun cyclodextrin nanofibers, *RSC Advances* 3 (2013) 10197-10201.
- [124] A. Celebioglu, O.C. Umu, T. Tekinay, T. Uyar, Antibacterial electrospun nanofibers from triclosan/cyclodextrin inclusion complexes, *Colloids and Surfaces B: Biointerfaces* 116 (2014) 612-619.
- [125] A. Celebioglu, T. Uyar, Electrospinning of polymer-free nanofibers from cyclodextrin inclusion complexes, *Langmuir* 27 (2011) 6218-6226.
- [126] A. Celebioglu, F. Kayaci-Senirmak, S. İpek, E. Durgun, T. Uyar, Polymer-free nanofibers from vanillin/cyclodextrin inclusion complexes: high thermal stability, enhanced solubility and antioxidant property, *Food & Function* 7 (2016) 3141-3153.
- [127] Z. Aytac, Z.I. Yildiz, F. Kayaci-Senirmak, N.O. San Keskin, T. Tekinay, T. Uyar, Electrospinning of polymer-free cyclodextrin/geraniol-inclusion complex nanofibers: enhanced shelf-life of geraniol with antibacterial and antioxidant properties, *RSC Advances* 6 (2016) 46089-46099.
- [128] I.M. Szilágyi, E. Santala, M. Heikkilä, V. Pore, M. Kemell, T. Nikitin, G. Teucher, T. Firkala, L. Khriachtchev, M. Räsänen, Photocatalytic properties of WO<sub>3</sub>/TiO<sub>2</sub> core/shell nanofibers prepared by electrospinning and atomic layer deposition, *Chemical Vapor Deposition* 19 (2013) 149-155.

- [129] S. Chakraborty, I.-C. Liao, A. Adler, K.W. Leong, Electrohydrodynamics: a facile technique to fabricate drug delivery systems, *Advanced drug delivery reviews* 61 (2009) 1043-1054.
- [130] A. Yarin, Coaxial electrospinning and emulsion electrospinning of core-shell fibers, *Polymers for Advanced Technologies* 22 (2011) 310-317.
- [131] A.V. Bazilevsky, A.L. Yarin, C.M. Megaridis, Co-electrospinning of core-shell fibers using a single-nozzle technique, *Langmuir* 23 (2007) 2311-2314.
- [132] S. Sahoo, L.T. Ang, J.C.H. Goh, S.L. Toh, Growth factor delivery through electrospun nanofibers in scaffolds for tissue engineering applications, *Journal of biomedical materials research Part A* 93 (2010) 1539-1550.
- [133] A. Saraf, L.S. Baggett, R.M. Raphael, F.K. Kasper, A.G. Mikos, Regulated non-viral gene delivery from coaxial electrospun fiber mesh scaffolds, *Journal of Controlled Release* 143 (2010) 95-103.
- [134] H. Jiang, Y. Hu, P. Zhao, Y. Li, K. Zhu, Modulation of protein release from biodegradable core-shell structured fibers prepared by coaxial electrospinning, *Journal of Biomedical Materials Research Part B: Applied Biomaterials* 79 (2006) 50-57.
- [135] A. Townsend-Nicholson, S.N. Jayasinghe, Cell electrospinning: a unique biotechnique for encapsulating living organisms for generating active biological microthreads/scaffolds, *Biomacromolecules* 7 (2006) 3364-3369.
- [136] I.-C. Liao, S. Chen, J.B. Liu, K.W. Leong, Sustained viral gene delivery through core-shell fibers, *Journal of Controlled Release* 139 (2009) 48-55.
- [137] A. López-Rubio, E. Sanchez, Y. Sanz, J.M. Lagaron, Encapsulation of living bifidobacteria in ultrathin PVOH electrospun fibers, *Biomacromolecules* 10 (2009) 2823-2829.
- [138] J. Li, H. Feng, J. He, C. Li, X. Mao, D. Xie, N. Ao, B. Chu, Coaxial electrospun zein nanofibrous membrane for sustained release, *Journal of Biomaterials Science, Polymer Edition* 24 (2013) 1923-1934.

- [139] R. Korehei, J.F. Kadla, Encapsulation of T4 bacteriophage in electrospun poly (ethylene oxide)/cellulose diacetate fibers, *Carbohydrate polymers* 100 (2014) 150-157.
- [140] S.-G. Wang, X. Jiang, P.-C. Chen, A.-G. Yu, X.-J. Huang, Preparation of coaxial-electrospun poly [bis (p-methylphenoxy)] phosphazene nanofiber membrane for enzyme immobilization, *International journal of molecular sciences* 13 (2012) 14136-14148.
- [141] H. Wang, D. Wu, D. Li, Z. Niu, Y. Chen, D. Tang, M. Wu, J. Cao, Y. Huang, Fabrication of continuous highly ordered mesoporous silica nanofibre with core/sheath structure and its application as catalyst carrier, *Nanoscale* 3 (2011) 3601-3604.
- [142] R. Haloui, E. Zussman, R. Khalfin, R. Semiat, Y. Cohen, Polymeric microtubes for water filtration by co-axial electrospinning technique, *Polymers for Advanced Technologies* (2016).
- [143] W.P. Zhang, D.Y. Wu, Y.K. Wang. *Study on Electrospun-Membrane-Based Filter to Rapidly Remove Reactive Yellow 2 from Wastewater*. in *Advanced Materials Research*. 2013: Trans Tech Publ.
- [144] J. Cao, T. Zhang, F. Li, H. Yang, S. Liu, Enhanced ethanol sensing of SnO<sub>2</sub> hollow micro/nanofibers fabricated by coaxial electrospinning, *New Journal of Chemistry* 37 (2013) 2031-2036.
- [145] R. Xue, M.T. Nelson, S.A. Teixeira, M.S. Viapiano, J.J. Lannutti, Cancer cell aggregate hypoxia visualized in vitro via biocompatible fiber sensors, *Biomaterials* 76 (2016) 208-217.
- [146] T.H. Hwang, Y.M. Lee, B.-S. Kong, J.-S. Seo, J.W. Choi, Electrospun core-shell fibers for robust silicon nanoparticle-based lithium ion battery anodes, *Nano letters* 12 (2012) 802-807.
- [147] L. Kou, T. Huang, B. Zheng, Y. Han, X. Zhao, K. Gopalsamy, H. Sun, C. Gao, Coaxial wet-spun yarn supercapacitors for high-energy density and safe wearable electronics, *Nature communications* 5 (2014).
- [148] X. Zhang, V. Thavasi, S. Mhaisalkar, S. Ramakrishna, Novel hollow mesoporous 1D TiO<sub>2</sub> nanofibers as photovoltaic and photocatalytic materials, *Nanoscale* 4 (2012) 1707-1716.

- [149] M. Leopoldini, N. Russo, M. Toscano, The molecular basis of working mechanism of natural polyphenolic antioxidants, *Food Chemistry* 125 (2011) 288-306.
- [150] A. Laura, E. Alvarez-Parrilla, G.A. Gonzalez-Aguilar, *Fruit and vegetable phytochemicals: Chemistry, nutritional value and stability*. 2009: John Wiley & Sons.
- [151] P. Manisara, P. Thawatchai, Gallic acid-loaded cellulose acetate electrospun nanofibers: thermal properties, mechanical properties, and drug release behavior, *Open Journal of Polymer Chemistry* 2012 (2012).
- [152] D. Alkan, L.Y. Aydemir, I. Arcan, H. Yavuzdurmaz, H.I. Atabay, C. Ceylan, A. Yemenicioglu, Development of flexible antimicrobial packaging materials against *Campylobacter jejuni* by incorporation of gallic acid into zein-based films, *Journal of agricultural and food chemistry* 59 (2011) 11003-11010.
- [153] Y.P. Neo, S. Ray, J. Jin, M. Gizdavic-Nikolaidis, M.K. Nieuwoudt, D. Liu, S.Y. Quek, Encapsulation of food grade antioxidant in natural biopolymer by electrospinning technique: A physicochemical study based on zein–gallic acid system, *Food chemistry* 136 (2013) 1013-1021.
- [154] Y.P. Neo, S. Swift, S. Ray, M. Gizdavic-Nikolaidis, J. Jin, C.O. Perera, Evaluation of gallic acid loaded zein sub-micron electrospun fibre mats as novel active packaging materials, *Food chemistry* 141 (2013) 3192-3200.
- [155] C.G. da Rosa, C.D. Borges, R.C. Zambiasi, M.R. Nunes, E.V. Benvenuti, S.R. da Luz, R.F. D'Avila, J.K. Rutz, Microencapsulation of gallic acid in chitosan,  $\beta$ -cyclodextrin and xanthan, *Industrial Crops and Products* 46 (2013) 138-146.
- [156] E. Pinho, G. Soares, M. Henriques, Cyclodextrin modulation of gallic acid in vitro antibacterial activity, *Journal of Inclusion Phenomena and Macrocyclic Chemistry* 81 (2015) 205-214.
- [157] P. Chuysinuan, N. Chimnoi, S. Techasakul, P. Supaphol, Gallic Acid-Loaded Electrospun Poly (L-Lactic Acid) Fiber Mats and their

Release Characteristic, *Macromolecular Chemistry and Physics* 210 (2009) 814-822.

- [158] J. Koontz, R. Moffitt, J. Marcy, S. O'Keefe, S. Duncan, T. Long, Controlled release of  $\alpha$ -tocopherol, quercetin, and their cyclodextrin inclusion complexes from linear low-density polyethylene (LLDPE) films into a coconut oil model food system, *Food additives and contaminants* 27 (2010) 1598-1607.
- [159] X.H. Hao, P. Jiang. *The Application of PVA Antibacterial Film with Clove Oil/ $\beta$ -Cyclodextrin Inclusion Complex in Fruit Packaging*. in *Advanced Materials Research*. 2013: Trans Tech Publ.
- [160] R. Auras, B. Harte, S. Selke, An overview of polylactides as packaging materials, *Macromolecular bioscience* 4 (2004) 835-864.
- [161] T. Higuchi, A. Connors, Phase-solubility techniques, (1965).
- [162] W. Kohn, L.J. Sham, Self-consistent equations including exchange and correlation effects, *Physical review* 140 (1965) A1133.
- [163] P. Hohenberg, W. Kohn, *Physical Review* 136, B864 (1964).
- [164] J.P. Perdew, J. Chevary, S. Vosko, K.A. Jackson, M.R. Pederson, D. Singh, C. Fiolhais, Atoms, molecules, solids, and surfaces: Applications of the generalized gradient approximation for exchange and correlation, *Physical Review B* 46 (1992) 6671.
- [165] S. Grimme, Semiempirical GGA-type density functional constructed with a long-range dispersion correction, *Journal of computational chemistry* 27 (2006) 1787-1799.
- [166] G. Kresse, J. Furthmüller, Efficient iterative schemes for ab initio total-energy calculations using a plane-wave basis set, *Physical review B* 54 (1996) 11169.
- [167] G. Kresse, J. Furthmüller, Efficiency of ab-initio total energy calculations for metals and semiconductors using a plane-wave basis set, *Computational Materials Science* 6 (1996) 15-50.
- [168] P.E. Blöchl, Projector augmented-wave method, *Physical Review B* 50 (1994) 17953.

- [169] F.H. Allen, The Cambridge Structural Database: a quarter of a million crystal structures and rising, *Acta Crystallographica Section B: Structural Science* 58 (2002) 380-388.
- [170] J.L. Fattebert, F. Gygi, First-principles molecular dynamics simulations in a continuum solvent, *International journal of quantum chemistry* 93 (2003) 139-147.
- [171] O. Andreussi, I. Dabo, N. Marzari, Revised self-consistent continuum solvation in electronic-structure calculations, *The Journal of chemical physics* 136 (2012) 064102.
- [172] S. Petrosyan, A. Rigos, T. Arias, Joint density-functional theory: ab initio study of Cr<sub>2</sub>O<sub>3</sub> surface chemistry in solution, *The Journal of Physical Chemistry B* 109 (2005) 15436-15444.
- [173] K. Mathew, R. Sundararaman, K. Letchworth-Weaver, T. Arias, R.G. Hennig, Implicit solvation model for density-functional study of nanocrystal surfaces and reaction pathways, *The Journal of chemical physics* 140 (2014) 084106.
- [174] V.J. Stella, V.M. Rao, E.A. Zannou, V. Zia, Mechanisms of drug release from cyclodextrin complexes, *Advanced drug delivery reviews* 36 (1999) 3-16.
- [175] F. Giordano, C. Novak, J.R. Moyano, Thermal analysis of cyclodextrins and their inclusion compounds, *Thermochimica Acta* 380 (2001) 123-151.
- [176] E.E. Eid, A.B. Abdul, F.E.O. Suliman, M.A. Sukari, A. Rasedee, S.S. Fatah, Characterization of the inclusion complex of zerumbone with hydroxypropyl- $\beta$ -cyclodextrin, *Carbohydrate Polymers* 83 (2011) 1707-1714.
- [177] J.-Y. Tsao, C.-P. Wu, H.-H. Tsai, K.-C. Peng, P.-Y. Lin, S.-Y. Su, L.-D. Chen, F.-J. Tsai, Y. Tsai, Effect of hydroxypropyl- $\beta$ -cyclodextrin complexation on the aqueous solubility, structure, thermal stability, antioxidant activity, and tyrosinase inhibition of paeonol, *Journal of Inclusion Phenomena and Macrocyclic Chemistry* 72 (2012) 405-411.

- [178] D.C. Bibby, N.M. Davies, I.G. Tucker, Mechanisms by which cyclodextrins modify drug release from polymeric drug delivery systems, *International journal of pharmaceutics* 197 (2000) 1-11.
- [179] A. Daneshfar, H.S. Ghaziaskar, N. Homayoun, Solubility of gallic acid in methanol, ethanol, water, and ethyl acetate, *Journal of Chemical & Engineering Data* 53 (2008) 776-778.
- [180] R.-E. Ghitescu, A.-M. Popa, V.I. Popa, R.M. Rossi, G. Fortunato, Encapsulation of polyphenols into pHEMA e-spun fibers and determination of their antioxidant activities, *International journal of pharmaceutics* 494 (2015) 278-287.
- [181] K. Mishra, H. Ojha, N.K. Chaudhury, Estimation of antiradical properties of antioxidants using DPPH assay: A critical review and results, *Food Chemistry* 130 (2012) 1036-1043.
- [182] S. Banerjee, J.P. Saikia, A. Kumar, B. Konwar, Antioxidant activity and haemolysis prevention efficiency of polyaniline nanofibers, *Nanotechnology* 21 (2009) 045101.
- [183] F. Tian, E.A. Decker, J.M. Goddard, Controlling lipid oxidation of food by active packaging technologies, *Food & function* 4 (2013) 669-680.
- [184] J. Gómez-Estaca, C. López-de-Dicastillo, P. Hernández-Muñoz, R. Catalá, R. Gavara, Advances in antioxidant active food packaging, *Trends in Food Science & Technology* 35 (2014) 42-51.
- [185] A.S. Badami, M.R. Kreke, M.S. Thompson, J.S. Riffle, A.S. Goldstein, Effect of fiber diameter on spreading, proliferation, and differentiation of osteoblastic cells on electrospun poly (lactic acid) substrates, *Biomaterials* 27 (2006) 596-606.
- [186] H.W. Kim, H.H. Lee, J. Knowles, Electrospinning biomedical nanocomposite fibers of hydroxyapatite/poly (lactic acid) for bone regeneration, *Journal of biomedical materials research Part A* 79 (2006) 643-649.
- [187] R. Mehta, V. Kumar, H. Bhunia, S. Upadhyay, Synthesis of poly (lactic acid): a review, *Journal of Macromolecular Science, Part C: Polymer Reviews* 45 (2005) 325-349.

- [188] Z. Li, M. Wang, F. Wang, Z. Gu, G. Du, J. Wu, J. Chen,  $\gamma$ -Cyclodextrin: a review on enzymatic production and applications, *Applied microbiology and biotechnology* 77 (2007) 245-255.
- [189] X. Sheng, L. Fan, C. He, K. Zhang, X. Mo, H. Wang, Vitamin E-loaded silk fibroin nanofibrous mats fabricated by green process for skin care application, *International journal of biological macromolecules* 56 (2013) 49-56.
- [190] P. Brantley, I. Elmadfa, A. Kafatos, F. Kelly, Y. Manios, H. Roxborough, W. Schuch, P. Sheehy, K. Wagner, Review vitamin E, *J Sci Food Agric* 80 (2000) 913-938.
- [191] S. Çelik, M. Özyürek, K. Güçlü, R. Apak, CUPRAC total antioxidant capacity assay of lipophilic antioxidants in combination with hydrophilic antioxidants using the macrocyclic oligosaccharide methyl  $\beta$ -cyclodextrin as the solubility enhancer, *Reactive and Functional Polymers* 67 (2007) 1548-1560.
- [192] Y. Sueishi, M. Hori, N. Inazumi, Characterization of inclusion complex of vitamin E compound with 2, 6-di-O-methylated  $\beta$ -cyclodextrin as the solubility enhancer and its kinetic determination for radical scavenging ability, *Journal of Inclusion Phenomena and Macrocyclic Chemistry* 72 (2012) 467-472.
- [193] I. Siró, É. Fenyvesi, L. Szente, B. De Meulenaer, F. Devlieghere, J. Orgoványi, J. Sényi, J. Barta, Release of alpha-tocopherol from antioxidative low-density polyethylene film into fatty food simulant: influence of complexation in beta-cyclodextrin, *Food additives and contaminants* 23 (2006) 845-853.
- [194] J.L. Koontz, J.E. Marcy, S.F. O'Keefe, S.E. Duncan, T.E. Long, R.D. Moffitt, Polymer processing and characterization of LLDPE films loaded with  $\alpha$ -tocopherol, quercetin, and their cyclodextrin inclusion complexes, *Journal of applied polymer science* 117 (2010) 2299-2309.
- [195] I. u Nisa, B.A. Ashwar, A. Shah, A. Gani, A. Gani, F.A. Masoodi, Development of potato starch based active packaging films loaded with

antioxidants and its effect on shelf life of beef, *Journal of Food Science and Technology* 52 (2015) 7245-7253.

- [196] T. Uyar, M.A. Hunt, H.S. Gracz, A.E. Tonelli, Crystalline cyclodextrin inclusion compounds formed with aromatic guests: guest-dependent stoichiometries and hydration-sensitive crystal structures, *Crystal growth & design* 6 (2006) 1113-1119.
- [197] J. Szejtli, *Cyclodextrin technology*. Vol. 1. 2013: Springer Science & Business Media.
- [198] E. Corradini, P.S. Curti, A.B. Meniqueti, A.F. Martins, A.F. Rubira, E.C. Muniz, Recent advances in food-packing, pharmaceutical and biomedical applications of zein and zein-based materials, *International journal of molecular sciences* 15 (2014) 22438-22470.
- [199] J.W. Lawton, Zein: A history of processing and use, *Cereal Chemistry* 79 (2002) 1-18.
- [200] R. Paliwal, S. Palakurthi, Zein in controlled drug delivery and tissue engineering, *Journal of Controlled Release* 189 (2014) 108-122.
- [201] D. Brahatheeswaran, A. Mathew, R.G. Aswathy, Y. Nagaoka, K. Venugopal, Y. Yoshida, T. Maekawa, D. Sakthikumar, Hybrid fluorescent curcumin loaded zein electrospun nanofibrous scaffold for biomedical applications, *Biomedical materials* 7 (2012) 045001.
- [202] X. Liu, Q. Sun, H. Wang, L. Zhang, J.-Y. Wang, Microspheres of corn protein, zein, for an ivermectin drug delivery system, *Biomaterials* 26 (2005) 109-115.
- [203] T. Padgett, I. Han, P. Dawson, Incorporation of food-grade antimicrobial compounds into biodegradable packaging films, *Journal of Food Protection*® 61 (1998) 1330-1335.
- [204] K. Hoffman, I. Han, P. Dawson, Antimicrobial effects of corn zein films impregnated with nisin, lauric acid, and EDTA, *Journal of Food Protection*® 64 (2001) 885-889.
- [205] X. Chen, D.S. Lee, X. Zhu, K.L. Yam, Release kinetics of tocopherol and quercetin from binary antioxidant controlled-release packaging films, *Journal of agricultural and food chemistry* 60 (2012) 3492-3497.

- [206] J. Zhou, L.-f. Wang, J.-y. Wang, N. Tang, Synthesis, characterization, antioxidative and antitumor activities of solid quercetin rare earth (III) complexes, *Journal of inorganic biochemistry* 83 (2001) 41-48.
- [207] C. Li, Z.-H. Wang, D.-G. Yu, Higher quality quercetin sustained release ethyl cellulose nanofibers fabricated using a spinneret with a Teflon nozzle, *Colloids and Surfaces B: Biointerfaces* 114 (2014) 404-409.
- [208] Z.-C. Xing, W. Meng, J. Yuan, S. Moon, Y. Jeong, I.-K. Kang, In vitro assessment of antibacterial activity and cytocompatibility of quercetin-containing PLGA nanofibrous scaffolds for tissue engineering, *Journal of Nanomaterials* 2012 (2012) 1.
- [209] M. Carlotti, S. Sapino, E. Ugazio, G. Caron, On the complexation of quercetin with methyl- $\beta$ -cyclodextrin: photostability and antioxidant studies, *Journal of Inclusion Phenomena and Macrocyclic Chemistry* 70 (2011) 81-90.
- [210] Y. Zheng, I.S. Haworth, Z. Zuo, M.S. Chow, A.H. Chow, Physicochemical and structural characterization of quercetin- $\beta$ -cyclodextrin complexes, *Journal of pharmaceutical sciences* 94 (2005) 1079-1089.
- [211] L. Vermeiren, F. Devlieghere, M. Van Beest, N. De Kruijf, J. Debevere, Developments in the active packaging of foods, *Trends in food science & technology* 10 (1999) 77-86.
- [212] F. Tao, L.E. Hill, Y. Peng, C.L. Gomes, Synthesis and characterization of  $\beta$ -cyclodextrin inclusion complexes of thymol and thyme oil for antimicrobial delivery applications, *LWT-Food Science and Technology* 59 (2014) 247-255.
- [213] I. Mourtzinou, N. Kalogeropoulos, S. Papadakis, K. Konstantinou, V. Karathanos, Encapsulation of Nutraceutical Monoterpenes in  $\beta$ -Cyclodextrin and Modified Starch, *Journal of food science* 73 (2008) S89-S94.
- [214] R.N. Marreto, E.E. Almeida, P.B. Alves, E.S. Niculau, R.S. Nunes, C.R. Matos, A.A. Araújo, Thermal analysis and gas chromatography coupled mass spectrometry analyses of hydroxypropyl- $\beta$ -cyclodextrin inclusion

complex containing *Lippia gracilis* essential oil, *Thermochimica Acta* 475 (2008) 53-58.

- [215] E. Mbandi, L. Shelef, Enhanced antimicrobial effects of combination of lactate and diacetate on *Listeria monocytogenes* and *Salmonella* spp. in beef bologna, *International Journal of Food Microbiology* 76 (2002) 191-198.
- [216] C.Y. Hu, M. Chen, Z.W. Wang, Release of thymol, cinnamaldehyde and vanillin from soy protein isolate films into olive oil, *Packaging Technology and Science* 25 (2012) 97-106.
- [217] B. Bozin, N. Mimica-Dukic, N. Simin, G. Anackov, Characterization of the volatile composition of essential oils of some Lamiaceae spices and the antimicrobial and antioxidant activities of the entire oils, *Journal of agricultural and food chemistry* 54 (2006) 1822-1828.
- [218] T.T. Cushnie, A.J. Lamb, Antimicrobial activity of flavonoids, *International journal of antimicrobial agents* 26 (2005) 343-356.
- [219] M.G. McKee, J.M. Layman, M.P. Cashion, T.E. Long, Phospholipid nonwoven electrospun membranes, *Science* 311 (2006) 353-355.
- [220] G. Singh, A.M. Bittner, S. Loscher, N. Malinowski, K. Kern, Electrospinning of diphenylalanine nanotubes, *Advanced Materials* 20 (2008) 2332-2336.
- [221] M.P. Cashion, X. Li, Y. Geng, M.T. Hunley, T.E. Long, Gemini surfactant electrospun membranes, *Langmuir* 26 (2009) 678-683.
- [222] X. Yan, M. Zhou, J. Chen, X. Chi, S. Dong, M. Zhang, X. Ding, Y. Yu, S. Shao, F. Huang, Supramolecular polymer nanofibers via electrospinning of a heteroditopic monomer, *Chemical Communications* 47 (2011) 7086-7088.
- [223] F. Bakkali, S. Averbeck, D. Averbeck, M. Idaomar, Biological effects of essential oils—a review, *Food and chemical toxicology* 46 (2008) 446-475.
- [224] W. Chen, A. Viljoen, Geraniol—a review of a commercially important fragrance material, *South African Journal of Botany* 76 (2010) 643-651.

- [225] V. Kadam, G. Bamane, G. Raut, Research Article Solubility Enhancement of Nebivolol Hydrochloride using  $\beta$ -CD Complexation Technique, (2014).
- [226] P.P. Menezes, M.R. Serafini, B.V. Santana, R.S. Nunes, L.J. Quintans, G.F. Silva, I.A. Medeiros, M. Marchioro, B.P. Fraga, M.R. Santos, Solid-state  $\beta$ -cyclodextrin complexes containing geraniol, *Thermochimica acta* 548 (2012) 45-50.
- [227] L.-F. Chen, Q. Shen, J.-P. Shen, D.-T. Shi, T. Chen, H.-R. Yu, Studies and comparison of the liquid adsorption and surface properties of  $\alpha$ -,  $\beta$ - and  $\gamma$ -cyclodextrins by FTIR and capillary rise method, *Colloids and Surfaces A: Physicochemical and Engineering Aspects* 411 (2012) 69-73.
- [228] M. Friedman, P.R. Henika, C.E. Levin, R.E. Mandrell, Antibacterial activities of plant essential oils and their components against *Escherichia coli* O157: H7 and *Salmonella enterica* in apple juice, *Journal of agricultural and food chemistry* 52 (2004) 6042-6048.
- [229] M.P. Tampieri, R. Galuppi, F. Macchioni, M.S. Carelle, L. Falcioni, P.L. Cioni, I. Morelli, The inhibition of *Candida albicans* by selected essential oils and their major components, *Mycopathologia* 159 (2005) 339-345.
- [230] P.L. Yeagle, *The structure of biological membranes*. 2004: CRC press.
- [231] A.E. Edris, Pharmaceutical and therapeutic potentials of essential oils and their individual volatile constituents: a review, *Phytotherapy research* 21 (2007) 308-323.
- [232] B. Prakash, A. Kedia, P.K. Mishra, N. Dubey, Plant essential oils as food preservatives to control moulds, mycotoxin contamination and oxidative deterioration of agri-food commodities–Potentials and challenges, *Food Control* 47 (2015) 381-391.
- [233] Y. Bhalla, V.K. Gupta, V. Jaitak, Anticancer activity of essential oils: a review, *Journal of the Science of Food and Agriculture* 93 (2013) 3643-3653.

- [234] D. Huang, B. Ou, R.L. Prior, The chemistry behind antioxidant capacity assays, *Journal of agricultural and food chemistry* 53 (2005) 1841-1856.
- [235] K. Pyrzyńska, A. Pękał, Application of free radical diphenylpicrylhydrazyl (DPPH) to estimate the antioxidant capacity of food samples, *Analytical Methods* 5 (2013) 4288-4295.
- [236] A. Stobiecka, Comparative study on the free radical scavenging mechanism exerted by geraniol and geranylacetone using the combined experimental and theoretical approach, *Flavour and Fragrance Journal* 30 (2015) 399-409.
- [237] R.L. Van Zyl, S.T. Seatholo, S.F. Van Vuuren, A.M. Viljoen, The Biological Activities of 20 Nature Identical Essential Oil Constituents, *Journal of Essential Oil Research* 18 (2006) 129.
- [238] H.-S. Choi, H.S. Song, H. Ukeda, M. Sawamura, Radical-scavenging activities of citrus essential oils and their components: detection using 1, 1-diphenyl-2-picrylhydrazyl, *Journal of agricultural and food chemistry* 48 (2000) 4156-4161.
- [239] A. Corciova, C. Ciobanu, A. Poiata, C. Mircea, A. Nicolescu, M. Droboata, C.-D. Varganici, T. Pinteala, N. Marangoci, Antibacterial and antioxidant properties of hesperidin:  $\beta$ -cyclodextrin complexes obtained by different techniques, *Journal of Inclusion Phenomena and Macrocyclic Chemistry* 81 (2015) 71-84.
- [240] I. Gülçin, Antioxidant activity of food constituents: an overview, *Archives of toxicology* 86 (2012) 345-391.
- [241] J. Sun, D-Limonene: safety and clinical applications, *Alternative Medicine Review* 12 (2007) 259.
- [242] R. Partanen, M. Ahro, M. Hakala, H. Kallio, P. Forssell, Microencapsulation of caraway extract in  $\beta$ -cyclodextrin and modified starches, *European Food Research and Technology* 214 (2002) 242-247.
- [243] H. Shiga, H. Yoshii, T. Nishiyama, T. Furuta, P. Forssele, K. Poutanen, P. Linko, Flavor encapsulation and release characteristics of spray-dried

powder by the blended encapsulant of cyclodextrin and gum arabic, *Drying Technology* 19 (2001) 1385-1395.

- [244] M. Kfoury, L. Auezova, S. Fourmentin, H. Greige-Gerges, Investigation of monoterpenes complexation with hydroxypropyl- $\beta$ -cyclodextrin, *Journal of Inclusion Phenomena and Macrocyclic Chemistry* 80 (2014) 51-60.
- [245] A. Ciobanu, D. Landy, S. Fourmentin, Complexation efficiency of cyclodextrins for volatile flavor compounds, *Food research international* 53 (2013) 110-114.
- [246] H. Yoshii, T.-L. Neoh, S.-H. Beak, T. Furuta, Release behavior of flavor encapsulated CD in slurry solution under boiling conditions, *Journal of inclusion phenomena and macrocyclic chemistry* 56 (2006) 113-116.
- [247] A. Camerlo, A.-M. Bühlmann-Popa, C. Vebert-Nardin, R.M. Rossi, G. Fortunato, Environmentally controlled emulsion electrospinning for the encapsulation of temperature-sensitive compounds, *Journal of Materials Science* 49 (2014) 8154-8162.
- [248] C.A. Fuenmayor, E. Mascheroni, M.S. Cosio, L. Piergiovanni, S. Benedetti, M. Ortenzi, A. Schiraldi, S. Mannino, *Encapsulation of R-(+)-Limonene in Edible Electrospun Nanofibers*, in *Icheap-11: 11th International Conference on Chemical and Process Engineering, Pts 1-4*, S. Pierucci and J.J. Klemes, Editors. 2013. p. 1771-1776.
- [249] P. Mura, G. Bettinetti, A. Manderioli, M. Faucci, G. Bramanti, M. Sorrenti, Interactions of ketoprofen and ibuprofen with  $\beta$ -cyclodextrins in solution and in the solid state, *International Journal of Pharmaceutics* 166 (1998) 189-203.
- [250] P.J. Delaquis, K. Stanich, B. Girard, G. Mazza, Antimicrobial activity of individual and mixed fractions of dill, cilantro, coriander and eucalyptus essential oils, *International journal of food microbiology* 74 (2002) 101-109.
- [251] M.T. Madigan, D.P. Clark, D. Stahl, J.M. Martinko, *Brock Biology of Microorganisms 13th edition*. 2010: Benjamin Cummings.

- [252] A.C. Aprotosoai, M. Hăncianu, I.I. Costache, A. Miron, Linalool: a review on a key odorant molecule with valuable biological properties, *Flavour and fragrance journal* 29 (2014) 193-219.
- [253] P. Bonetti, F.F. de Moraes, G.M. Zanin, R. de Cássia Bergamasco, Thermal behavior study and decomposition kinetics of linalool/ $\beta$ -cyclodextrin inclusion complex, *Polymer Bulletin* 73 (2016) 279-291.
- [254] D.-G. Yu, X.-X. Shen, C. Branford-White, K. White, L.-M. Zhu, S.A. Bligh, Oral fast-dissolving drug delivery membranes prepared from electrospun polyvinylpyrrolidone ultrafine fibers, *Nanotechnology* 20 (2009) 055104.
- [255] J. Quan, Y. Yu, C. Branford-White, G.R. Williams, D.-G. Yu, W. Nie, L.-M. Zhu, Preparation of ultrafine fast-dissolving feruloyl-oleyl-glycerol-loaded polyvinylpyrrolidone fiber mats via electrospinning, *Colloids and Surfaces B: Biointerfaces* 88 (2011) 304-309.
- [256] V.J. Stella, R.A. Rajewski, Cyclodextrins: their future in drug formulation and delivery, *Pharmaceutical research* 14 (1997) 556-567.
- [257] F. Hirayama, K. Uekama, Cyclodextrin-based controlled drug release system, *Advanced drug delivery reviews* 36 (1999) 125-141.
- [258] S.M. Badr-Eldin, S.A. Elkheshen, M.M. Ghorab, Inclusion complexes of tadalafil with natural and chemically modified  $\beta$ -cyclodextrins. I: Preparation and in-vitro evaluation, *European Journal of Pharmaceutics and Biopharmaceutics* 70 (2008) 819-827.
- [259] T. Järvinen, K. Järvinen, N. Schwarting, V.J. Stella,  $\beta$ -cyclodextrin derivatives, SBE4- $\beta$ -CD and HP- $\beta$ -CD, increase the oral bioavailability of cinnarizine in beagle dogs, *Journal of pharmaceutical sciences* 84 (1995) 295-299.
- [260] R. Sharma, A. Gescher, W. Steward, Curcumin: the story so far, *European journal of cancer* 41 (2005) 1955-1968.
- [261] B.B. Aggarwal, A. Kumar, A.C. Bharti, Anticancer potential of curcumin: preclinical and clinical studies, *Anticancer res* 23 (2003) 363-398.

- [262] H. Hatcher, R. Planalp, J. Cho, F. Torti, S. Torti, Curcumin: from ancient medicine to current clinical trials, *Cellular and Molecular Life Sciences* 65 (2008) 1631-1652.
- [263] C.S. Mangolim, C. Moriwaki, A.C. Nogueira, F. Sato, M.L. Baesso, A.M. Neto, G. Matioli, Curcumin- $\beta$ -cyclodextrin inclusion complex: Stability, solubility, characterisation by FT-IR, FT-Raman, X-ray diffraction and photoacoustic spectroscopy, and food application, *Food chemistry* 153 (2014) 361-370.
- [264] M.M. Yallapu, M. Jaggi, S.C. Chauhan,  $\beta$ -Cyclodextrin-curcumin self-assembly enhances curcumin delivery in prostate cancer cells, *Colloids and surfaces B: Biointerfaces* 79 (2010) 113-125.
- [265] V.R. Yadav, S. Suresh, K. Devi, S. Yadav, Effect of cyclodextrin complexation of curcumin on its solubility and antiangiogenic and anti-inflammatory activity in rat colitis model, *Aaps Pharmscitech* 10 (2009) 752-762.
- [266] O. Suwantong, P. Opanasopit, U. Ruktanonchai, P. Supaphol, Electrospun cellulose acetate fiber mats containing curcumin and release characteristic of the herbal substance, *Polymer* 48 (2007) 7546-7557.
- [267] J.G. Merrell, S.W. McLaughlin, L. Tie, C.T. Laurencin, A.F. Chen, L.S. Nair, Curcumin-loaded poly ( $\epsilon$ -caprolactone) nanofibres: Diabetic wound dressing with anti-oxidant and anti-inflammatory properties, *Clinical and Experimental Pharmacology and Physiology* 36 (2009) 1149-1156.
- [268] G. Guo, S. Fu, L. Zhou, H. Liang, M. Fan, F. Luo, Z. Qian, Y. Wei, Preparation of curcumin loaded poly ( $\epsilon$ -caprolactone)-poly (ethylene glycol)-poly ( $\epsilon$ -caprolactone) nanofibers and their in vitro antitumor activity against Glioma 9L cells, *Nanoscale* 3 (2011) 3825-3832.
- [269] Y. Dong, S. Liao, M. Ngiam, C.K. Chan, S. Ramakrishna, Degradation behaviors of electrospun resorbable polyester nanofibers, *Tissue Engineering Part B: Reviews* 15 (2009) 333-351.
- [270] D. Ishii, T.H. Ying, A. Mahara, S. Murakami, T. Yamaoka, W.-k. Lee, T. Iwata, In vivo tissue response and degradation behavior of PLLA and

stereocomplexed PLA nanofibers, *Biomacromolecules* 10 (2008) 237-242.